Low temperature sequestration of photosynthetic pigments: Model studies and natural aquatic environments

By

Matthew David Pickering

A thesis submitted in partial fulfilment of the requirements for the degree of Doctor of Philosophy at the University of York

University of York
Department of Chemistry

August 2009

Abstract

A series of synthetic C-3[1] alkylthioether chlorophyll derivatives, analogous to those found to occur naturally in sediment from Pup Lagoon, Antarctica, have been formed in laboratory reactions that simulate conditions that occur in many natural anoxic aquatic environments (low temperature, moderate pH, presence of H_2S and limitation of oxygen). This has enabled a mechanism to be proposed to explain the formation of these derivatives in nature and provided valuable insight into their environmental significance and the potential of chlorophylls to form sulfur-crosslinks with macromolecular organic matter. Reaction of the chlorophyll *a* derivative, pyrophaeophorbide *a*, with H_2S under simulation conditions led to its partial conversion to mesopyrophaeophorbide *a*. The transformation, which involves reduction of the C-3 vinyl group to an ethyl substituent, is a key event in the diagenetic pathway linking chlorophylls to many sedimentary alkyl porphyrins and provides evidence for the importance of low temperature abiotic reactions, involving H_2S, in the geochemical reduction of organic matter. The reaction of pyrophaeophorbide *a* with H_2S, in the presence of molecular oxygen, led to its near quantitative conversion into pyrophaeophorbide *d* via oxidative cleavage of the C-3 vinyl group to afford a formyl group at C-3. Such a transformation could represent a key intermediate step in the formation of C-3 β-H and β-CH_3 fossil porphyrins.

Sediment samples from an Antarctic marine core were submitted to extraction by acetone and acid methanolysis and extracts analysed by LC-MS^n. Acid extraction liberated appreciable amounts of tetrapyrroles believed to have been bound via ester linkages to components of the sediment matrix. In some cases the amount of acid-extracted tetrapyrroles was over double that extracted by acetone. Significant distributional differences existed between the acetone and acid extracted components, the latter being enriched in deesterified and oxidised transformation products of chlorophyll. Acid methanolysis also revealed the presence of derivatives of chlorophylls *b* and *c*, which were lacking from acetone extracts, as well as protoporphyrin-IX, believed to originate from heme-type precursors. These findings have implications for the use of sedimentary tetrapyrroles for palaeoenvironmental reconstruction.

Contents

List of tables

List of figures

List of schemes

List of definitions and abbreviations

α-cleavage	Cleavage of a bond adjacent to the aromatic macrocycle
APCI	Atmospheric pressure chemical ionisation
β-cleavage	Cleavage of a bond one bond away from the aromatic macrocycle
Bchl	Bacteriochlorophyll
Bphe	Bacteriophaeophytin
Bphorb	Bacteriophaeophorbide
CID	Collision induced dissociation
Chl	Chlorophyll
Chlone	Chlorophyllone
d	Days
Da	Daltons
DC	Direct current
DMS	Dimethyl sulfide
DMSP	Dimethylsulfoniopropionate
DMF	Dimethylformamide
DPEP	Desoxophylloerythroetioporphyrin
ESI	Electrospray ionisation
GC	Gas chromatography
h	Hours
HPLC	High performance liquid chromatography
i.d.	Internal diameter
LC	Liquid chromatography
λ_{max}	Wavelength of maximum absorbance
$[M+H]^+$	Protonated molecule
Mpphorb	Mesopyrophaeophorbide
MS	Mass spectrometry
MS/MS	Tandem mass spectrometry
MS^n	Multistage tandem mass spectrometry
m/z	Mass-to-charge ratio
PDA	Photodiode array
PDT	Photodynamic therapy

Phe	Phaeophytin
Phorb	Phaeophorbide
Pphe	Pyrophaeophytin
Pphorb	Pyrophaeophorbide
PTC	Phase transfer catalyst
NMR	Nuclear magnetic resonance
rf	Radio frequency
RP	Reversed phase
RT	Room temperature
SET	Single electron transfer
SDS	Sodium dodecyl sulfate
TOF MS	Time of flight mass spectrometry
t_R	Retention time
UV/vis	Ultraviolet/visible

Acknowledgments

I would like to thank the University of York and British Antarctic Survey (BAS) for funding this research. I am extremely grateful to Brendan Keely for his guidance and advice throughout his supervision of this project. Dominic Hodgson and Claire Allen at BAS are both thanked for the provision of sediment samples and core descriptions.

I would like to thank the many members of the Keely group past and present; Deborah, Jayne, Phil, Chris, Haslina, Suleman, Neung, Angela, Andy and Denize for making the past three years of my research an enjoyable and stimulating experience and for tolerating the “interesting” smells that have accompanied my work with thiols.

Special thanks go to Deborah Mawson for instructing me in the ways of chlorophyll chemistry, Trevor Dransfield for training me on the Ion Trap mass spectrometer and to Chris Knappy for helpful ideas ventured over many a pint in the pub, proof reading and for waiting until I had finished my instrumental work before breaking the Ion Trap.

Finally, I would like to thank my Mum and Dad for supporting me in this Ph.D. and Hannah for her unwavering support during my writing up and for putting up with the stacks of research papers and spectra that cluttered up the house.

Author’s declaration

I hereby declare that the work described in this thesis is my own, except where otherwise acknowledged, and has not been submitted previously for a degree at this or any other university.

……..

Matthew Pickering

Chapter 1:

Introduction

1.1 Chlorophyll structure

Chlorophylls are cyclic tetrapyrroles of the porphyrin (**1**), chlorin (dihydroporphyrin, **2**) or bacteriochlorin (tetrahydroporphyrin, **3**) oxidation state characterised by a unique 5-membered exocyclic ring (ring E) conjoint with ring C, e.g. chlorophyll *a* (chl *a*, **4**) (Sheer, 1991). Despite the reduction of one and two pyrrole rings in chlorin and bacteriochlorin macrocycles, relative to porphyrins, all possess an extended aromatic 18 electron π-system.

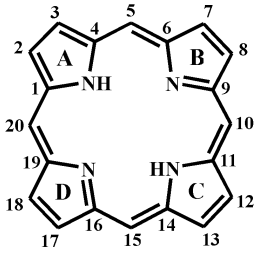

Porphyrin

1

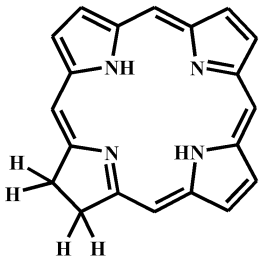

Chlorin

2

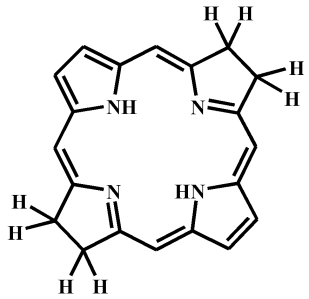

Bacteriochlorin

3

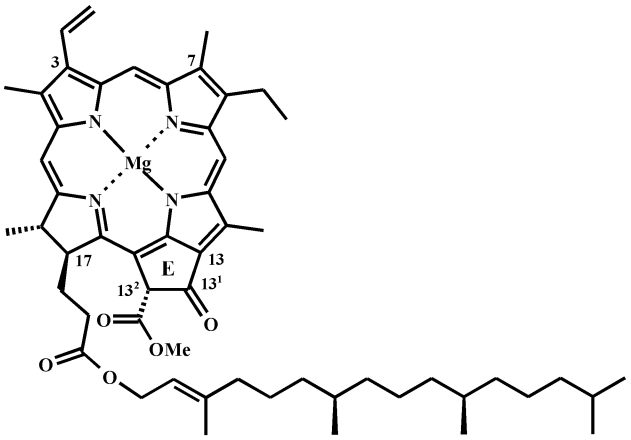

Chlorophyll *a*

4

Many different chlorophyll structures are known, varying in the nature of the structural elements embellishing the periphery of the tetrapyrrole macrocycle (Sheer, 1991). Chl *a* (**4**) is the most widely distributed chlorophyll in nature. Notable structural features include; a chelated Mg(II) ion, a vinyl group at C-3, a ketone at

C-13[1], a carbomethoxy group at C-13[2], and a propionic acid moiety at C-17 esterified with phytol.

1.2. Optical absorption spectra of chlorophylls

By virtue of the chromophore created by the tetrapyrrole extended π-system, chlorophylls interact strongly with light and exhibit characteristic UV/vis absorption spectra (Hendry et al., 1987). All cyclic tetrapyrroles exhibit a strong absorption band in the blue region of the visible light spectrum around 400 nm, termed the Soret band (e.g. Fig. 1.1). In addition to the Soret band, chlorins possess a strong red absorption around 660 nm, termed the Q_y band (e.g. Fig. 1.1), arising from $\pi \rightarrow \pi^*$ transitions centred on the reduced pyrrole ring D (Falkowski and Raven, 1997). These spectral characteristics are responsible for chlorophyll's green pigmentation. The ratio of the Soret band to the Q_y band and the wavelengths of their maximal absorbances may be used diagnostically to distinguish between different chlorophylls (Hendry et al., 1987). Bacteriochlorins lack an absorption band at 650 nm, owing to the presence of two reduced pyrrole rings, and instead exhibit a strong absorption band at 770 nm, which is beyond the limits of human vision (Hendry et al., 1987).

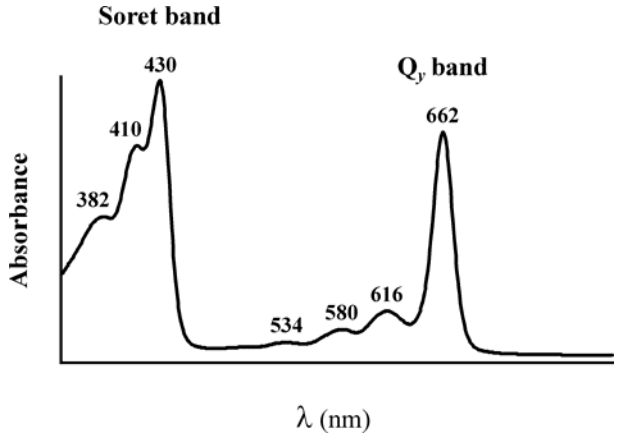

Figure 1.1. UV/vis spectrum of chlorophyll *a* (**4**) in acetone.

1.3. Occurrence of chlorophylls

Chlorophyll pigments are biosynthesised exclusively by photoautotrophic organisms where their unique photochemical properties enable the organism to perform photosynthesis: the light-driven conversion of inorganic carbon (typically CO_2 from the environment) that contains no biologically usable energy, into organic molecules (such as carbohydrates) that the organism can use for growth and as energy stores, energy being released through respiration. In addition to photoautotrophic organisms, chemoautotrophic organisms are capable of fixing carbon from inorganic sources, utilising chemical energy liberated by inorganic redox reactions (Killops and Killops, 2004). Notably, however, the chemosynthesis of organic matter is minor compared with that produced by photosynthesis. All other organisms are incapable of fixing inorganic carbon and must depend upon preformed organic materials obtained via herbivory and/or carnivory (Hall and Rao, 1999). Thus, the vast majority of life is directly or indirectly reliant upon primary production from photosynthesis.

Chl *a* is ubiquitous in oxygenic photoautotrophs, including higher plants, photosynthetic algae and cyanobacteria, where it fulfils both reaction centre and light-harvesting roles within eukaryotic chloroplasts (Table 1.1; Sheer, 1991). The aforementioned organisms perform photosynthesis aerobically, according to Equation 1.1 (Falkowski and Raven, 1997). They require H_2O, which is used as an electron donor, and evolve molecular oxygen as a byproduct.

$$nH_2O + nCO_2 + \text{light} \rightarrow C_nH_{2n}O_n + nO_2 \qquad (1.1)$$

Table 1.1. Occurrence and role of chlorophylls and bacteriochlorophylls (adapted from Sheer, 1991). A = antenna or light-harvesting pigment, RC = reaction centre pigment.

Pigment	Occurrence	Function	Type of photosynthesis
Chl *a*	All oxygenic photoautotrophs	A+RC	Oxygenic
Chl *b*	Higher plants, Chlorophyta (Green algae), Prochlorophytes	A	Oxygenic
Chl *c*	Pheophyta (Brown algae); Pyrrophyta (Dinoflagellates); Cryptophyta, Chrysophyta, Bacillariophyta (Diatoms)	A	Oxygenic
Chl *d*	Certain cyanobacteria	A+RC	Oxygenic
Bchl *a*	Photosynthetic bacteria	A+RC	Anaerobic
Bchls *c*, *d* and *e*	Chlorobiaceae, Chloroflexaceae (Green sulfur bacteria)	A	Anaerobic

With some exceptions, chl *a* occurs as the sole chlorophyll in cyanobacteria. In the majority of oxygenic photoautotrophs chl *a* is accompanied by smaller amounts of an additional chlorophyll, such as chl *b* (**5**) or chl *c* (**6**, **7**). These accessory pigments aid light capture and serve to extend the wavelength range of light absorbed (Lawlor, 1987; Stolp, 1988). In higher plants and green algae, chl *a* co-occurs with chl *b* (**5**) in ratios of approximately 3:1 (Table 1.1; Sheer 1991). The structure of chl *b* differs from that of chl *a* by the presence of a formyl group instead of a methyl group at C-7. Chl *c* occurs alongside chl *a* in a limited range of photoautotrophs including brown algae, dinoflagellates and diatoms (Table 1.1; Sheer 1991) with chl *a*:*c* ratios reported to range between 1.65-7.25 (Stauber and Jeffrey, 1988). Chl *c* is the collective term for an increasing number of pigment structures, including chl c_1 (**6**), chl c_2 (**7**) and chl c_3 (**8**), which possess a porphyrin macrocycle, various modifications at positions C-7 and C-8, an acrylic acid side chain at C-17 and typically lack an esterifying alcohol. The unique cyanobacterium, *Acaryochloris marina* (*A. marina*), contains chl *d* (**9**) as its major chlorophyll (>90% chl *d*, the remainder being chl *a*; Miyashita et al., 1996). In the structure of chl *d*, the C-3 vinyl substituent of chl *a* is replaced with a formyl group. In addition to chlorophylls, a wide variety of non-chlorophyll accessory pigments are present in photoautotrophic organisms, including carotenoids which

augment light capture and provide a photoprotective element, dissipating excess energy (Lawlor, 1987).

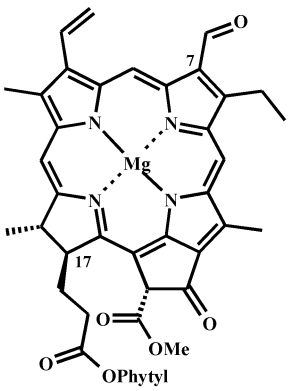

Chlorophyll *b*

5

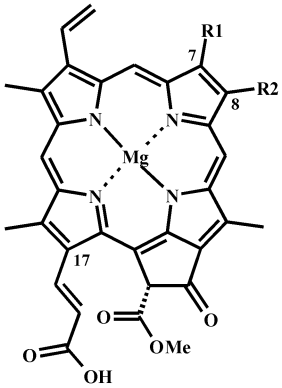

Chlorophyll *c*

6: Chl c_1, R1 = Me, R2 = Et

7: Chl c_2, R1 = Me, R2 = Vinyl

8: Chl c_3, R1 =CO_2Me, R2 = Vinyl

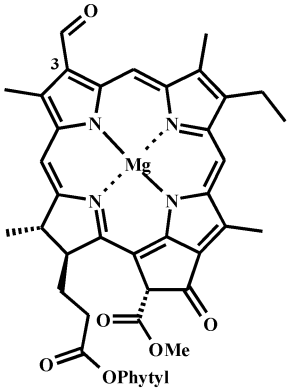

Chlorophyll *d*

9

With the notable exception of cyanobacteria (mentioned above) all photosynthetic bacteria are obligate anaerobes and perform photosynthesis anaerobically, according to Equation 1.2 (Falkowski and Raven, 1997). They lack the ability to use H_2O as an electron source and instead use H_2S, which has a lower redox potential, for this purpose. Sources of H_2S in the natural environment include both volcanic and microbial inputs. Photosynthetic sulfur bacteria often associate with colonies of sulfate reducing bacteria, which produce H_2S as a byproduct of their metabolic functions (Parkin and Brock, 1980).

$$2nH_2S + nCO_2 + \text{light} \rightarrow C_nH_{2n}O_n + nH_2O + 2nS^o \qquad (1.2)$$

Anaerobic photoautotrophs are divided into two main groups, the purple bacteria and the green bacteria, and contain bacteriochlorophylls as their major pigments (Table 1.1; Sheer 1991). Bacteriochlorophyll *a* (Bchl *a*, **10**) is the major pigment in purple bacteria and possesses a bacteriochlorin macrocycle. Bchls *c*-*e*, despite their names, are in fact chlorins (e.g. bchl *d*, **11**) and occur in Green sulfur bacteria.

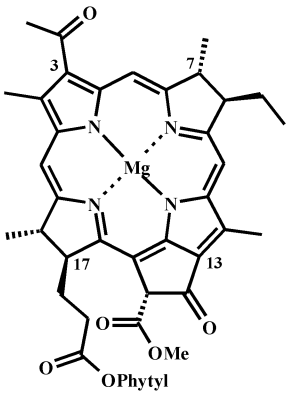

Bacteriochlorophyll *a*

(**10**)

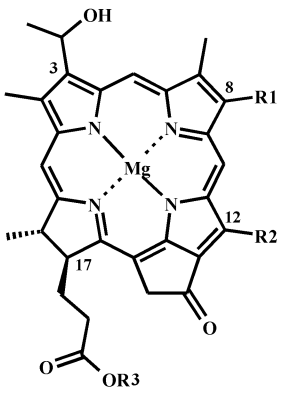

Bacteriochlorophyll *d* (11)

R1 = Et, *n*-Pr, *i*-Bu, *neo*-Pent

R2 = Me, Et

R3 = Alkyl (various)

In the strict biological context, the term chlorophyll applies only to tetrapyrroles directly involved in photosynthesis either as part of the organism's light-harvesting apparatus or embedded within photosynthetic reactions centres (Sheer, 1991). In the geochemical sense (used here), this appellation is somewhat broader and also extends to include the transformation products of chlorophyll.

1.4. Geochemistry of chlorophylls

The German chemist, Alfred Treibs, is credited as being the founding father of organic geochemistry: the study of the fate of organic matter in the geosphere from its biosynthesis to its eventual destruction. In the early 1930s, Treibs recognised the structural similarity between alkyl porphyrins, contained within petroleum and shales, and contemporary chlorophylls (Treibs, 1936). In his landmark paper, Treibs proposed a sequence of transformation reactions linking the sedimentary porphyrin, desoxophylloerythroetioporphyrin (DPEP, **12**), to an origin from chlorophylls (Treibs Scheme; Fig. 1.2). This precursor-product relationship laid the foundations for modern organic geochemistry and pioneered the concept of the biological marker, a compound whose structure provides an unambiguous link with a known biological precursor. Since its first inception, the Treibs hypothesis has been reinforced by isotopic evidence (e.g. Hayes et al., 1987) and the isolation and characterisation of the minimum number of sedimentary intermediates necessary to fulfil conversion of chl *a* into DPEP (Keely et al., 1990). The reactions outlined in the Treibs Scheme (Fig. 1.2) provide a valuable basis for understanding the provenance of tetrapyrroles contained within the sedimentary record and, over the years, the scheme has received periodic review, reevaluation and modification (Baker and Palmer, 1978; Keely et al., 1990; Callot, 1991; Keely, 2006).

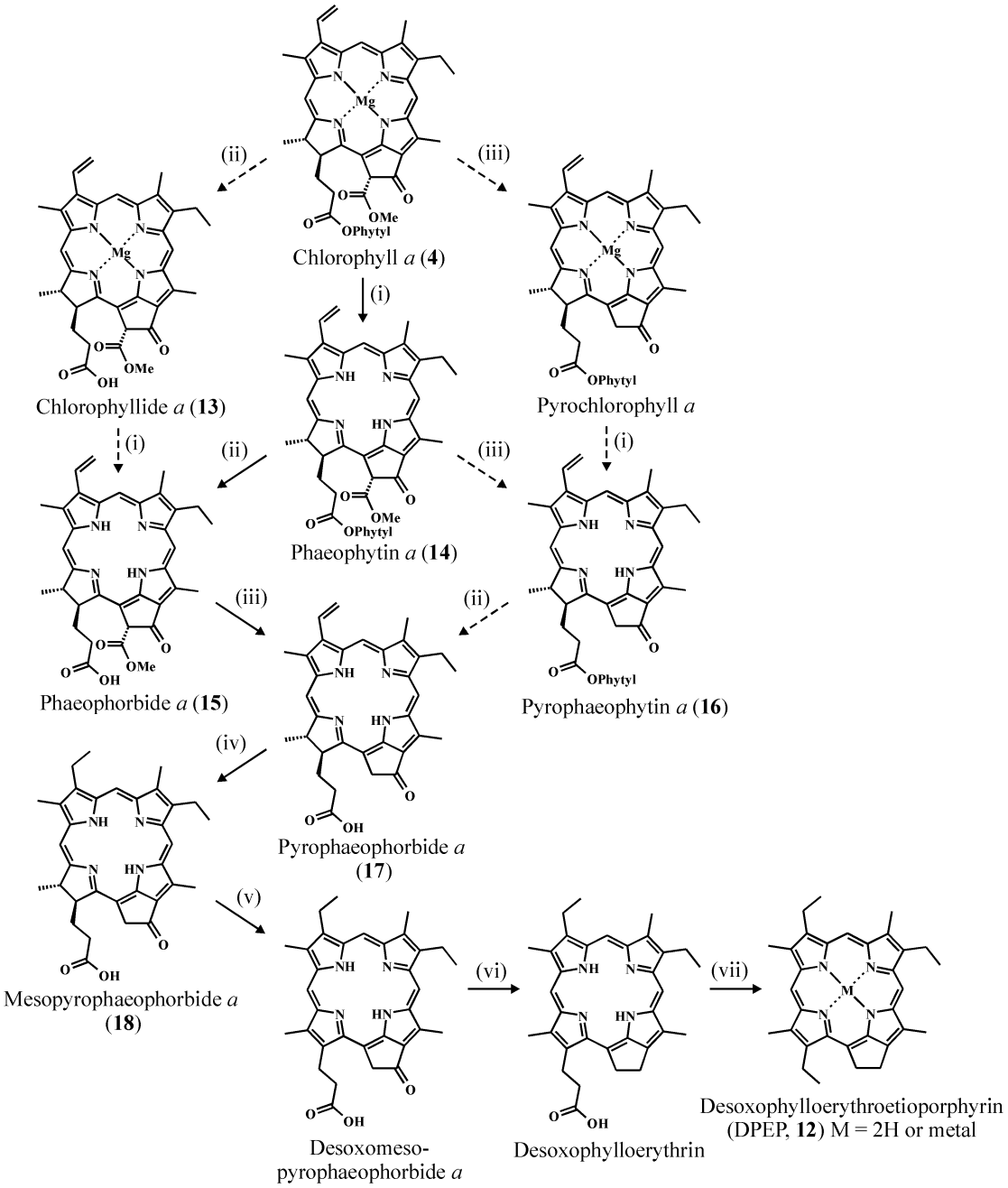

Figure 1.2. Pictorial representation of the Treibs Scheme linking chlorophyll *a* (**4**) to sedimentary DPEP (**12**), adapted from Keely et al. (1990). The reaction pathway delineated with solid arrows indicates the minimum number of intermediates required for conversion of chlorophyll *a* into DPEP. Dashed arrows indicate common variations in the reaction sequence; many other transformations are known. Reactions shown include: i) demetallation, ii) deesterification, iii) decarbomethoxylation, iv) vinyl reduction, v) aromatisation, vi) ketone reduction, vii) decarboxylation (and metal insertion).

1.5. The fate of chlorophyll pigments in the natural environment

The degradative processes which affect chlorophyll pigments in the natural environment may be divided into two main groups (Hendry et al., 1987; Brown et al., 1991); those which modify the periphery of the molecule while leaving the macrocycle intact (termed Type I reactions) and those which lead to rupture of the macrocyclic ring and consequently loss of pigment character (termed Type II reactions).

1.5.1. Type II reactions

Photo-oxidation is the primary fate of chlorophylls in oxic, well illuminated environments (Brown et al., 1991) and involves oxygenolytic cleavage of the C-5 methine bridge by singlet oxygen ($^1O_2$) (Mühlecker et al., 1993). The resulting linear tetrapyrroles degrade further to monopyrrolic units (maleimides), which in turn degrade to simpler molecules. A similar cleavage of the macrocyclic ring is considered to occur via the operation of an oxygenase enzyme during senescence, initiated by the breakdown of cellular order that accompanies the cessation of photosynthetic activity prior to death (Mühlecker et al., 1993; Matile et al., 1996; Moser et al., 2009).

1.5.2. Type I reactions

1.5.2.1. Regular transformation products

The early transformation products outlined in the Treibs Scheme (Fig. 1.2), notably, phaeophytin *a*, (phe *a*, **14**), phaeophorbide *a* (phorb *a*, **15**) and their pyro derivatives, pyrophaeophytin *a* (pphe *a*, **16**) and pyrophaeophorbide *a* (pphorb *a*, **17**), are typically amongst the most abundant products in immature sediments (Keely et al., 1990; Airs et al., 2001; Squier et al., 2002; Airs and Keely, 2003; Squier et al., 2004). Laboratory studies have shown that these compounds form during senescence, largely through the action of endogenous algal enzymes (Schoch et al., 1981; Owens and Falkowski, 1982; Jeffrey and Hallegraeff, 1987; Spooner et al., 1994a; Louda et al.,

1998; Louda et al., 2002). While the transformation pathways and products appear to vary for different algal species and environmental conditions (Louda et al., 2002 and references therein), they involve the same principal reactions: loss of the chelated Mg (II) mediated either by the enzyme Mg-dechelatase (Owens and Falkowski, 1982; Hendry et al., 1987; Brown et al., 1991) or acid catalysis (Hynninen, 1991), ester hydrolysis from the C-17[3] position mediated by the enzyme chlorophyllase to form chlorophyllide (**13**) (Jeffrey and Hallegraeff, 1987) or phaeophorbides (Louda et al., 1998), and decarbomethoxylation at position C-13[2] to form pyro derivatives e.g. pphorb *a* (Spooner et al., 1994a). The latter transformation can be facilitated in the laboratory by heating chlorophyll in degassed pyridine at 100 ºC for 24 h (Hynninen, 1991), although this reaction is not likely to have any bio-geochemical relevance.

Phaeopigments are commonly observed in the faecal pellets of heterotrophic organisms (Currie, 1962; Shuman and Lorenzen, 1975; Hurley and Armstrong, 1990; Head and Harris, 1992; Talbot et al., 1999). The high abundances of "phaeophorbide", later revealed to comprise a significant if not prevailing proportion of pphorb *a* (Head and Harris, 1992), in zooplankton faecal pellets has led to suggestions of their being possible grazing indicators (Shuman and Lorenzen, 1975). This interpretation must be treated with caution given that the physical disruption of cell structure, associated with the action of grazing, can itself elicit senescence reactions that also form phaeopigments, complicating any attempts to differentiate products arising from the two processes.

Other transformations associated with heterotrophic processing include steryl chlorin esters (e.g. **19**), formed in the alimentary canals of the grazing organism from (trans)esterification of a chlorin nucleus, typically pphorb *a*, with a variety of sterols derived from both the algal substrate and the grazer (Harradine et al., 1996; Talbot et al., 1999). Steryl chlorin esters are widely distributed in sediments (King and Repeta, 1991; Prowse and Maxwell, 1991; Pearce et al., 1998; Airs et al., 2001; Squier et al., 2002) and, by contrast with phaeophorbides, are considered to be clear markers of grazing processes. In addition, the distributions of esterified sterols are thought to reflect those of the original source organisms (Talbot et al., 1999). In some circumstances, however, such as when the diet of the grazing organism is

impoverished in cholesterol, modification of the sterol distribution can occur prior to esterification (Talbot et al., 1999).

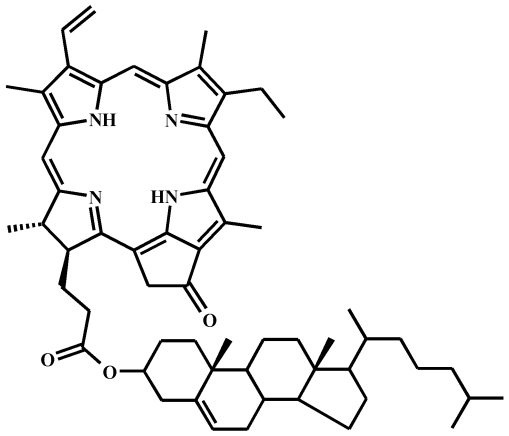

19

Bacteria play a key role in the transformation and degradation of organic matter in the natural environment. Algal degradation studies conducted under aerobic bacterial conditions have shown the formation of phe *a*, phorb *a* and pphorb *a* (Spooner et al., 1994b), although these could equally have arisen through senescence. The anaerobic bacterial degradation of algal cells (Spooner et al., 1995) showed an additional product, mesopyrophaephorbide *a* (mpphorb *a*, **18**, Fig. 1.2), resulting from the reduction of the C-3 vinyl group of pphorb *a* to afford an ethyl substituent, which has not been identified in other chlorophyll defunctionalisation studies. Thus, it appears that this transformation, responsible for the formation of mpphorb *a* and other C-3 ethyl-bearing tetrapyrroles in sediments (Keely et al., 1990; Prowse et al., 1990), is one involving anaerobic bacterial communities.

1.5.2.2. Oxidised transformation products

With the exception of pyro derivatives and some bacteriochlorophylls, all chlorophylls possess an enolisable β-ketoester group on the exocyclic ring E. The labile proton at C-13^2, created by this structural arrangement, makes the C-13^2 position particularly susceptible to reaction with triplet molecular oxygen ($^3O_2$), according to the mechanisms proposed by Hynninen (1991), to yield a variety of ring E-modified structures (e.g. Fig. 1.3). Autoxidation reactions of chlorophyll have long

been known to occur in alcoholic solutions that contain trace amounts of metal ions or base (Hynninen, 1991 and references therein) and complicate the processes of their isolation and handling. Related structures occur widely in natural water columns (Walker and Keely, 2004) and sediments (Naylor and Keely, 1998; Airs et al., 2000; Louda et al., 2000; Squier et al., 2002; Walker et al., 2002). The involvement of oxygen in this transformation, implicated by the proposed mechanism of chlorophyll autoxidation (Hynninen, 1991), has led to suggestions that these compounds are potential indicators of oxidative processes in the depositional environment (Walker et al., 2002).

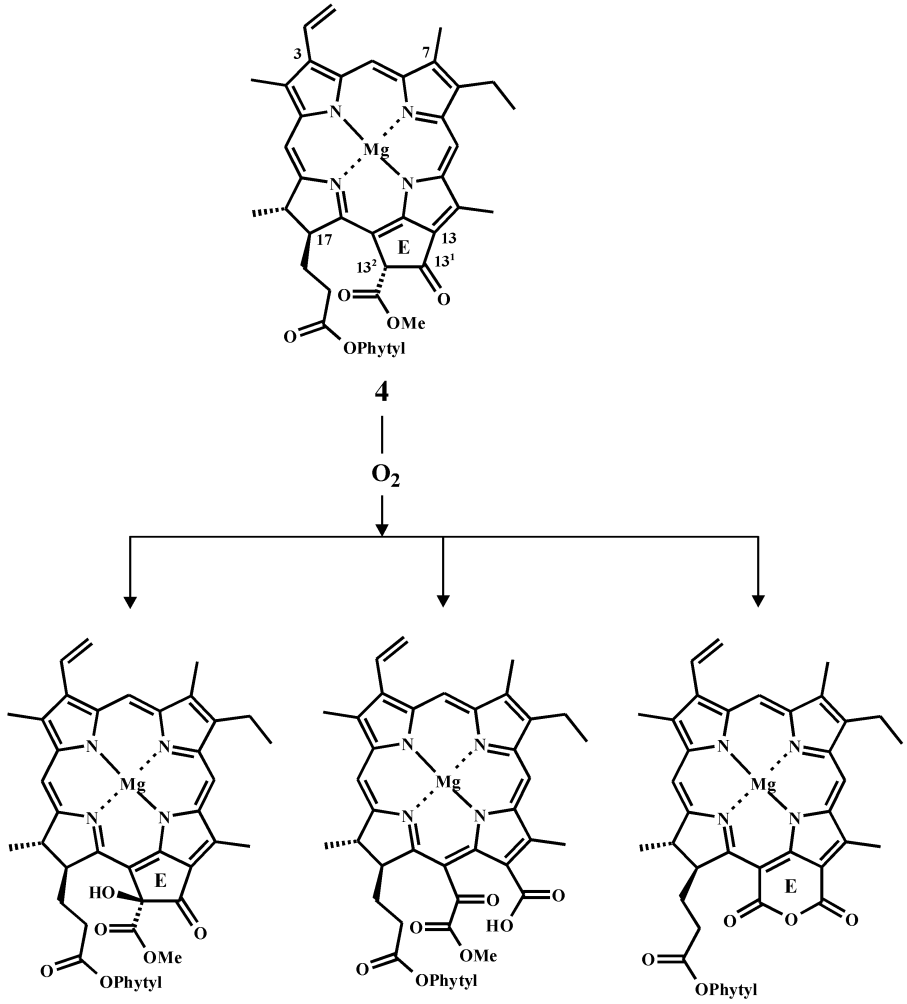

Figure 1.3. Various transformation products resulting from oxidation of ring E by molecular oxygen.

1.5.2.3. Sulfur-containing chlorophyll transformation products

Chemical desulfurisation (with nickel boride) of the organic matter contained within an ancient sediment liberated appreciable amounts of chlorophyll-derived porphyrins, suggested to have been bound via sulfide linkages (e.g. **20**) to macromolecular structures (Schaeffer et al., 1993; 1994). Notably, in addition to cleaving C-S bonds, nickel boride has been demonstrated to cleave alcohol and ester functionalities when situated adjacent to double bonds (Hartgers et al., 1996). This raises the additional possibility that some or all of the liberated porphyrins could have been bound via oxygen-containing linkages such as esters (cf. Huseby and Ocampo, 1997).

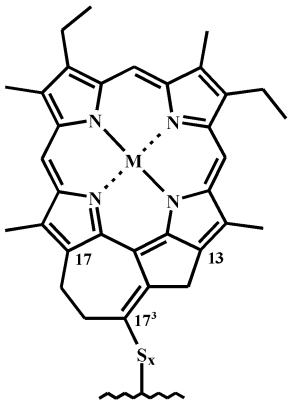

20: M = 2H, Ni, VO, Cu

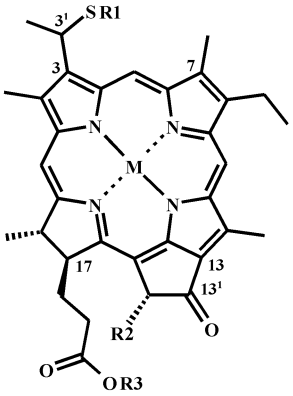

21: R1 = Me (**a**), Et (**b**), *n*-Pr (**c**), *n*-Bu (**d**), *n*-Pent (**e**); R2 = CO_2Me; R3 = Phytyl; M = Mg

22: R1 = Me (**a**), Et (**b**), *n*-Pr (**c**), *n*-Bu (**d**), *n*-Pent (**e**); R2 = CO_2Me; R3 = Phytyl; M = 2H

23: R1 = Me (**a**), Et (**b**), *n*-Pr (**c**), *n*-Bu (**d**), *n*-Pent (**e**); R2 = H; R3 = Phytyl; M = 2H

More recently, a unique series of sulfur-containing chlorophyll derivatives has been identified in the immature lake sediment from Pup Lagoon, Antarctica (Squier et al., 2003; 2004). Derivatives of chl *a*, phe *a* and pphe *a* were identified, each present as a series of homologues bearing alkylthioether groups, containing between one and five carbons, attached to the C-3^1 position (alkylS-chl *a*, **21a-e**; alkylS-phe *a*, **22a-e** and alkylS-pphe *a*, **23a-e**). The structures of these compounds do not match any chlorin structures known to be biosynthesised by photosynthetic organisms and are, therefore, believed to represent genuine early diagenetic transformation products of chl *a*. Their

occurrence provides the strongest evidence to date for the incorporation of sulfur into chlorophyll and a rationale for the formation of sulfur-bound porphyrins (Schaeffer et al., 1993; 1994), although the mechanism of their formation and the environmental significance of their occurrence remain unclear.

1.6. The sulfurisation of organic matter in the natural environment

The abiogenic incorporation of sulfur into functionalised organic molecules (sulfurisation) is a widespread phenomenon that plays a key role in the formation and preservation of sedimentary organic matter (Sinninghe Damsté and de Leeuw, 1990 and references therein). It involves reaction(s) of functionalised organic molecules with reduced inorganic sulfur species such as H_2S, and polysulfides derived therefrom, and may be broadly divided into two principle modes of incorporation: i) intramolecular sulfur incorporation, leading to the formation of low molecular weight organosulfur compounds and ii) intermolecular sulfur crosslinking, leading to the formation of oligo-polymeric structures that comprise bound moieties reticulated by catenated sulfur-sulfur bonds. Hence, the reaction of sulfur with organic matter can lead to its fractionation into both solvent extractable and solvent insoluble macromolecular forms.

The products of sulfurisation are often more resistant to chemical and biological degradation than their precursors, leading to an increased potential for the preservation of biomarker compounds (Sinninghe Damsté et al., 1989). In addition, the site of sulfur incorporation marks the location of the original functionality, often preserving the link to a specific biological or diagenetic precursor. Indeed, sulfur-bound forms of many different compound classes have been recognised in sediments (for an overview see Sinninghe Damsté and de Leeuw, 1990). The differing susceptibilities of various functional groups to reaction with reduced sulfur species may lead to selective sequestration of more reactive compounds in the sulfur-bound fraction, and has been suggested to bias the distribution of free components in sediments (Kohnen et al., 1991a). Clearly, care must be taken to account for sulfur-bound components during the interpretation of sedimentary biomarker distributions for palaeoenvironmental reconstruction.

Anoxic, non-clastic depositional environments are considered to be ideal for the formation of organosulfur compounds (Sinninghe Damsté and de Leeuw, 1990; Schaeffer et al., 1995; Hartgers et al., 1997; Adam et al., 2000). Anoxic conditions are favourable for the development of sulfate reducing bacterial communities and are, therefore, likely to contain reduced sulfur species. The availability of sulfide for reaction with organic matter depends largely on the intensity of its production and the concentration of detrital iron minerals, which are believed to compete more successfully for reaction with sulfide and lead to the formation of insoluble pyrite (Hartgers et al., 1997). Consequently, organosulfur compounds are found in abundance in non-clastic, iron-depleted depositional environments such as evaporitic basins and carbonate platforms where anoxic conditions are present (Sinninghe Damsté and de Leeuw, 1990 and references therein; Kohnen et al., 1991b; Schaeffer et al., 1995; Adam et al., 2000).

The occurrence of low molecular weight organosulfur compounds and sulfur crosslinked organic matter in Recent and immature sediments, of various origins, demonstrates that the sulfurisation of organic matter can operate from early diagenesis (Sinninghe Damsté et al., 1989; Wakeham et al., 1995; Hartgers et al., 1997; Adam et al., 2000; Werne et al., 2000; Squier et al., 2004; Sinninghe Damsté et al., 2007) and implies that the sulfurisation of organic matter can operate under mild conditions without the need for elevated temperatures or extreme pH.

The timing and processes underlying the sulfurisation of organic matter have been studied by several different approaches. Detailed molecular studies have been conducted of the low molecular weight, solvent extractable organosulfur compounds contained within sediments (Kohnen et al., 1989; Sinninghe Damsté et al., 1989; Kohnen et al., 1990; Schaeffer et al., 1995; Wakeham et al., 1995; Hartgers et al., 1997; Werne et al., 2000). Often such studies are combined with chemical degradation techniques such as treatment with Raney nickel or nickel boride (which cleave C-S and S-S bonds) and MeLi/MeI (which selectively cleaves S-S bonds and liberates bound moieties as methylthioethers) providing information regarding the subunit constituents of sulfur crosslinked organic matter (e.g. Schaeffer et al., 1995; Wakeham et al., 1995; Hartgers et al., 1997; Adam et al., 2000; Werne et al., 2000). In addition, the sulfurisation of numerous geochemically relevant compounds have

been studied experimentally in laboratory model reactions to examine the mechanisms of sulfur incorporation into organic matter within controlled systems (Vairavamurthy and Mopper, 1987; de Graaf et al., 1992; Fukushima et al., 1992; Rowland et al., 1993; Schouten et al., 1993; Krein and Aizenshtat, 1994; Schouten et al., 1994; Adam et al., 1998; Schneckenburger et al., 1998; van Dongen et al., 2003; Amrani and Aizenshtat, 2004a; 2004b; Amrani et al., 2007). Laboratory studies have revealed that functional groups such as aldehydes, ketones and alkenes are particularly susceptible to reaction with reduced sulfur species, especially when present in conjugated arrangements, whereas alcohols and carboxylic acids are relatively inert. The principle mechanisms of sulfur incorporation into organic matter can be broadly divided into three types: i) electrophilic addition, ii) nucleophilic addition and iii) radical addition.

1.6.1. Electrophilic addition

Under non-radical inducing conditions, reduced sulfur species such as H_2S or polysulfides react with alkenes according to Markovnikov's rule via an apparent electrophilic mechanism. The mechanism involves an initial protonation step to form the most stable carbocation followed by addition of the sulfur species to selectively form the most substituted product (Scheme 1.1a). The reaction of hydrogen polysulfides ($^{-}S_xH$) with various mono alkenes in laboratory simulation reactions (ethyl acetate:water 1:1, 50ºC) leads to the formation of (poly)sulfide crosslinked dimers (2-65% yield) and smaller amounts of thiols (Scheme 1.1a) (de Graaf et al., 1992; Schouten et al., 1994; de Graaf et al., 1995). The products obtained from the reaction of hydrogen polysulfides with dienes depend upon the number of methylene units (n) separating the two double bonds (Scheme 1.1b) (Schouten et al., 1994; de Graaf et al., 1995). When $n \geq 4$, dienes are converted, via intermolecular sulfurisation reactions, into (poly)sulfide crosslinked oligomeric substances (90-95% yield; Schouten et al., 1994; de Graaf et al., 1995). When $n < 4$, intramolecular addition reactions prevail leading to the formation monomeric cyclic sulfides (15-46% yield; Schouten et al., 1994; de Graaf et al., 1995).

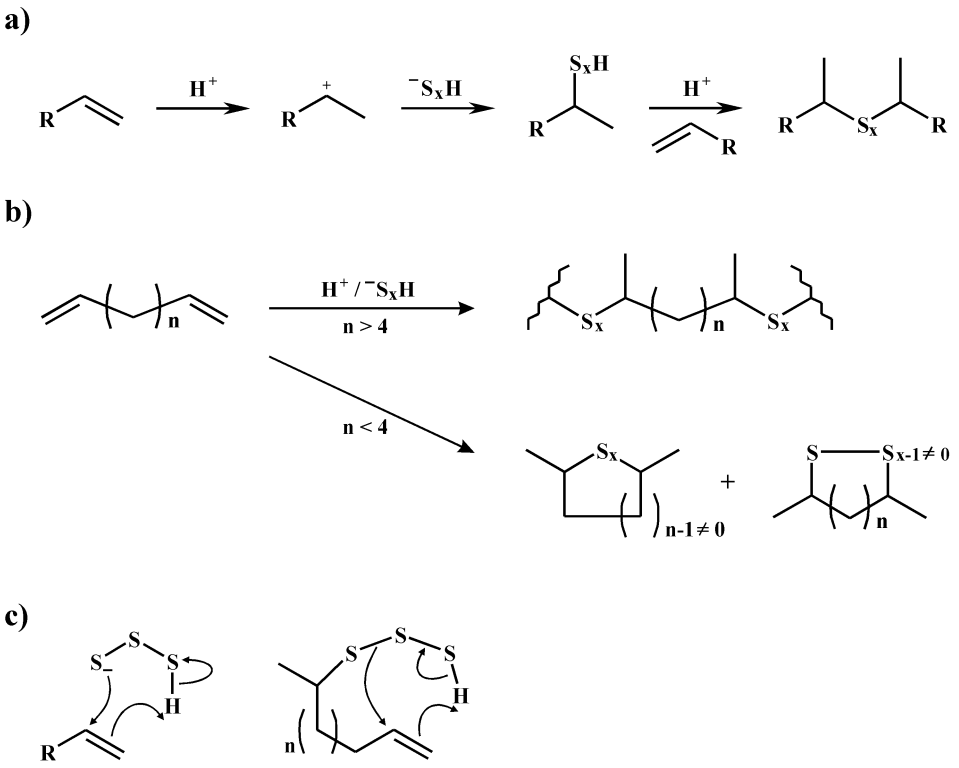

Scheme 1.1. Markovnikov addition of reduced sulfur species to a) mono alkenes (via an electrophilic mechanism) and b) non-conjugated dienes. c) Shows the proposed cyclic addition of hydrogen trisulfide to double bonds and formation of cyclic products (modified from de Graaf et al., 1995).

Although the apparent adherence to Markovnikov's rule supports an electrophilic mechanism of sulfur addition, experimental results have not been entirely consistent with this view. Firstly, the addition of H_2S to isolated double bonds is usually slow unless high temperatures or an acid catalyst are used (March, 1992). By contrast, the addition of hydrogen polysulfides to non-activated double bonds has been shown to occur over short timescales (1-10 d) at relatively low temperatures (50ºC) and without acid catalysis (de Graaf et al., 1995). In addition, 2-methylundec-1-ene, which should be an ideal substrate for an acid catalysed addition, and mid-chain alkenes were found to be much less reactive than the linear terminal alkene (hexadec-1-ene; de Graaf et al., 1995). These observations are at variance with an electrophilic addition mechanism which would be expected to give higher yields for more substituted alkenes. The authors proposed an alternative mechanism for addition involving the formation of a cyclic transition state and a hydrogen polysulfide ion

($^{-}S_xH$) of which the trisulfide (x = 3) was suggested to be the most favourable (illustrated in Scheme 1.1c; de Graaf et al., 1995). It is perhaps worth noting that in other studies, conducted at lower temperature (room temperature) in a variety of media, non-conjugated double bonds were found to be unreactive towards hydrogen polysulfides (Krein and Aizenshtat, 1994; Amrani and Aizenshtat, 2004a).

1.6.2. Nucleophilic addition

Under mildly basic conditions, nucleophilic addition mechanisms of sulfide to unsaturated molecules are favoured. H_2S and polysulfides react with aldehydes or ketones via direct, 1,2-addition at the carbonyl carbon forming gem-di(poly)sulfides (Scheme 1.2a) or mono-(poly)sulfides (Scheme 1.2b). The mechanism of formation of the latter is unclear. It has been proposed to occur via initial addition of HS^- followed by elimination of water to form a thioketone. Reduction of the thioketone is suggested to occur via single electron transfer (SET) from HS^- to form a radical anion that is subsequently quenched by hydrogen abstraction from H_2S (Schneckenburger et al., 1998). Notably, the reaction conditions used by these authors (NaSH, 0.18 M H_2SO_4, at 100ºC for periods of up to several months) differ considerably from those that occur in most natural environments and could promote the formation of radicals. Mono-(poly)sulfides have been formed in simulation reactions conducted under much milder conditions (HS_x^-, 25ºC, 5-7 d) and have been suggested to arise from the gem-disulfide (formed in the pathway illustrated in Scheme 1.2a) through an unknown reductive mechanism, possibly involving hydrogen polysulfides (Amrani and Aizenshtat, 2004a). Precedent for this pathway is provided by the reductive desulfurisation of phytenethiol in the presence of H_2S (Hebting et al., 2003). The reaction of H_2S and polysulfides with α,β-unsaturated aldehydes proceeds via initial 1,4-conjugate addition in a Michael fashion (Scheme 1.2c) followed by further nucleophilic addition(s) of sulfur to the aldehyde (as for Scheme 1.2a) to produce sulfur-crosslinked oligomers in high yields (Krein and Aizenshtat, 1994; Amrani and Aizenshtat, 2004a).

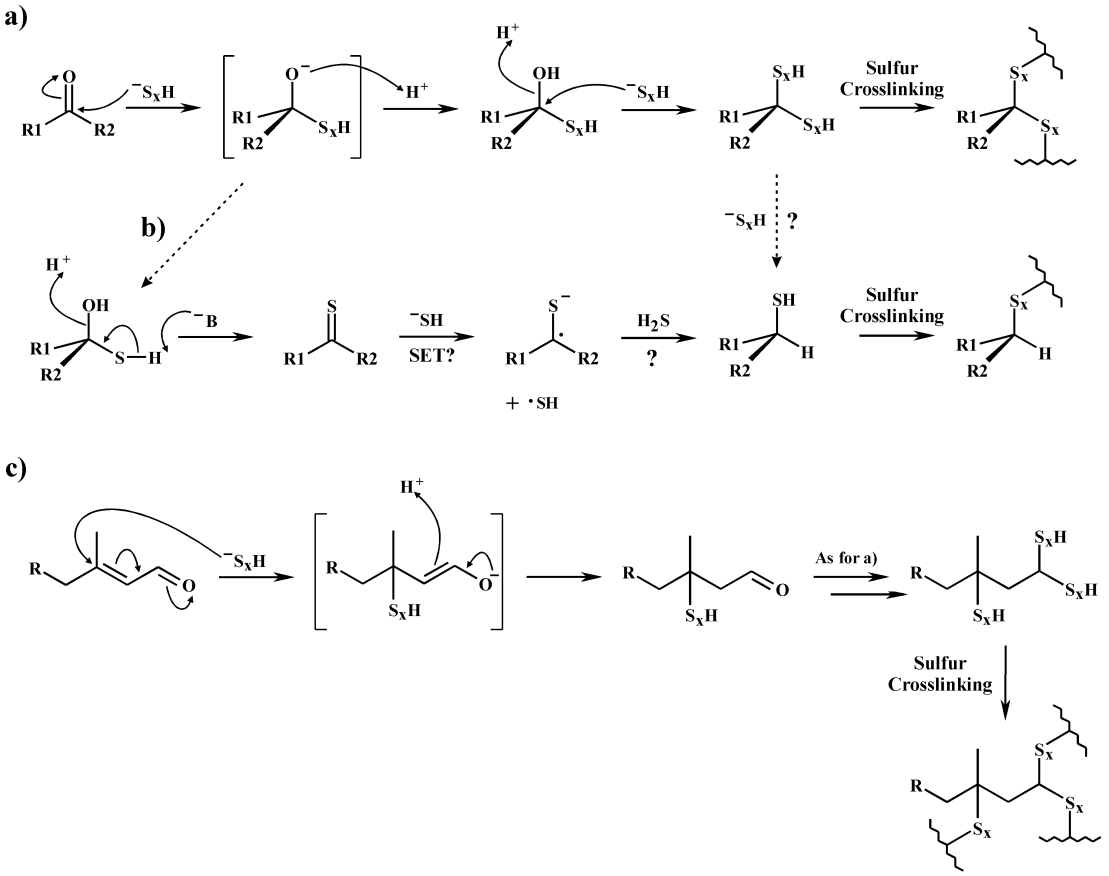

Scheme 1.2. Nucleophilic 1,2-addition of reduced sulfur species to aldehydes (R1/R2 = H/alkyl) or ketones (R1 and R2 = alkyl) to form a) gem-di(poly)sulfides (Krein and Aizenshtat, 1994) and b) mono-(poly)sulfides (Schneckenburger et al., 1998). c) Nucleophilic 1,4-(Michael-type)-addition of reduced sulfur species to α,β–unsaturated aldehydes (e.g phytenal) followed by two subsequent 1,2-additions to the aldehyde (Krein and Aizenshtat, 1994). $x \geq 1$.

1.6.3. Radical Addition

The addition of radical species to carbon-carbon double bonds is characterised by the formation of anti-Markovnikov products (March, 1992). Photochemically induced radical additions of H_2S and polysulfides to various alkenes have been demonstrated in laboratory experiments, designed to simulate environments where the sulfide rich waters impinge upon the photic zone (Adam et al., 1998). The light induced reaction of mono alkenes with H_2S, aided by the presence of a ketone sensitiser, yielded sulfide crosslinked dimers and monomeric thiols (ca. 95%) (Scheme 1.3a; Adam et al., 1998). Polysulfide linkages were formed when the reaction was conducted with

H_2S and elemental sulfur. Although not demonstrated experimentally, this process can be extended to non-conjugated di- or poly-enes and would be expected to form polymeric substances (e.g. Scheme 1.3b). Light-induced reactions of H_2S and elemental sulfur with conjugated dienes (such as phytadiene) yielded polysulfide crosslinked oligomers and a range of cyclised products, such as thiolanes and thiophenes (25-85% yield) (Scheme 1.3c; Adam et al. 1998), some of which have been found to occur naturally.

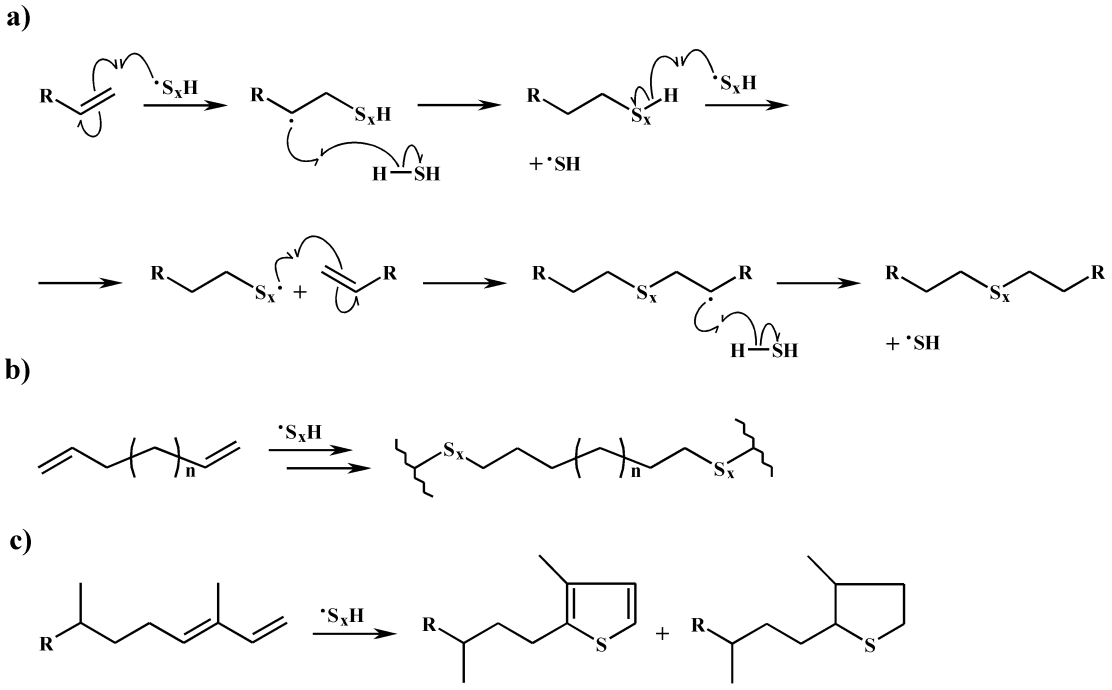

Scheme 1.3. Photochemically initiated radical addition of H_2S and polysulfides to a) mono alkenes, b) non-conjugated dienes and c) conjugated dienes (e.g. phytadienes). (Adapted from Adam et al., 1998). $x \geq 1$.

1.6.4. Summary

Despite extensive research, the processes underpinning the sulfur enrichment of organic matter are still far from being fully understood. With regard to the sulfur-containing chlorophyll derivatives (**21-23**), their occurrence raises many unanswered questions including; the manner of their formation, their environmental significance, and the potential of chlorophylls to become incorporated into sulfur-crosslinked

macromolecular structures. All of these issues are relevant to the use of sedimentary tetrapyrroles for palaeoenvironmental reconstruction.

1.7. Methods for the analysis of photosynthetic pigments

1.7.1. High performance liquid chromatography

Aptly, chromatographic separation was first demonstrated by the Russian botanist, Tswett, in 1906 for the separation of plant pigments on a column packed with powdered sugar (Hall and Rao, 1999). Modern high performance liquid chromatography (HPLC) is a powerful tool for the separation of complex mixtures of analytes. An HPLC column comprises a stainless steel tube packed with adsorbant (stationary phase), usually modified silica, consisting of highly uniform particles in sizes ranging between 3-10 μm in diameter. During analysis, solvent (the mobile phase) is pumped through the column under high pressure (flow rates 0.5-2 ml min^{-1}, pressure ~500-4000 psi) and a small volume of the sample to be analysed (10-40 μl) is injected onto the front of the column. Analytes travel through the column and separate according to differences in their chromatographic mobilities before emerging from the end of the column as distinct bands and proceeding to the detector (see Section 1.7.1.2).

1.7.1.1. Reversed phase HPLC

Reversed phase HPLC (RP-HPLC) is the most commonly used form of HPLC, characterised by utilisation of a non-polar stationary phase, typically a silica support modified with C_8 or C_{18} hydrocarbon chains, and a polar mobile phase such as water or methanol. The column can be developed with a solvent composition that remains constant over the course of the chromatographic run (isocratic elution) or with a solvent composition that changes with time (gradient elution), typically progressing from a polar starting composition through to a less polar one. Analytes are separated on the basis of the strength of their interactions with both the stationary and mobile phases, determined by their hydrophobicity. Two principle models have been proposed to govern the mechanisms by which analytes are retained by the stationary phase: the partition model and the absorption model (Vailaya and Horvath, 1998;

Nikitas et al., 2004; Nikitas and Pappa-Louisi, 2009). In the case of the former, the hydrocarbon chains bonded to the stationary phase are suggested to behave like a homogeneous hydrophobic liquid. Analytes are retained through liquid-liquid partitions between the mobile phase and the stationary phase with the strength of the retention dependant upon their solubility in each. Thus, relatively non-polar analytes, which have a greater affinity for the hydrocarbon chains of the stationary phase, are retained more strongly. By contrast, the absorption model describes retention through physisorption of analyte and organic solvent molecules to the tips and stems of the bonded hydrocarbon chains, suggested to act as a hydrophobic surface. Neither of these models is capable of describing the retention mechanism in RP-HPLC fully, and it is believed that both mechanisms operate simultaneously to varying extents, dependant upon the alkyl chain length of the stationary phase, the composition of the mobile phase (organic modifier) and the physicochemical properties of the analyte.

RP-HPLC is an extremely versatile technique, enabling the utilisation of a variety of different stationary phases, mobile phase compositions and gradients to suit a range of different applications. The capability of this technique to resolve a wide variety of compounds, spanning a broad spectrum of polarities, makes it ideally suited to the analysis of environmental samples. RP-HPLC has been used extensively for the analysis of chlorophylls (Shioi, 1991) contained in water column particulates (Walker and Keely, 2004), sediment extracts from lacustrine (Airs et al., 2001) and marine environments as well as alkyl porphyrins contained within ancient sediments (Mawson and Keely, 2008).

1.7.1.2. Photodiode array detection

Common detectors used in conjunction with HPLC include UV/vis absorption detectors such as photodiode array (PDA), fluorescence detectors and mass spectrometry (MS) (Skoog et al., 1998 and references therein). PDA detectors are capable of recording UV/vis absorbance spectra over a range of wavelengths. This is particularly useful for the detection and analysis of chlorophyll pigments, which possess distinctive UV/vis absorption spectra (e.g chl *a*, **4**, Fig. 1.1). The absorption maxima and ratios of the Soret and Q absorption bands can be used diagnostically to distinguish between different chlorophylls. During HPLC-PDA analysis of simple

mixtures of chlorophylls, the information provided by their online UV/vis spectra in combination with their chromatographic retention time is often sufficient to allow identification. Complex distributions, such as those present in sediments (Airs et al., 2001; Squier et al., 2002; Wilson et al., 2004a; 2005) and microbial mats (Airs and Keely, 2003), often require additional information provided by a more discriminating technique such as MS.

1.7.2. Mass spectrometry

Sir J.J. Thomson developed the first mass spectrometer (originally called a parabola spectrograph) in the early 20th century (Thomson, 1913). Since then mass spectrometry has burgeoned into a leading analytical technique with applications in many different subject areas (de Hoffmann and Stroobant, 2002).

In simplest terms MS involves measurement of the mass-to-charge ratio (*m/z*) and relative abundance of gas-phase ions. A mass spectrometer consists of five major elements: i) a device for sample introduction; ii) an ion source, which converts the analyte into gas phase ions; iii) a mass analyser, which separates ions according to their *m/z* ratio; iv) a detector, to count the ions emerging from the mass analyser and v) a computer for instrument control and data processing. MS provides structural information regarding the analyte including; its *m/z* ratio, isotopic pattern (characteristic of its elemental composition) and fragmentations, in addition to quantitative information provided by signal intensity (which is proportional to ion abundance).

MS can be interfaced with separation techniques such as HPLC, gas chromatography (GC), or capillary electrophoresis, enabling the analysis of complex mixture such as those present in natural samples (de Hoffmann and Stroobant, 2002).

1.7.2.1. Liquid chromatography-mass spectrometry

The online coupling of HPLC to MS (LC-MS) presents several technical challenges. Firstly it requires a method capable of converting solution phase analytes into gas phase ions, a task that is made more difficult given that the compounds analysed by HPLC are typically non-volatile molecules that are not amenable to analysis by GC. Furthermore, it requires an interface which can tolerate the high solvent flow rates employed for HPLC. The elution solvent must be eliminated prior to MS, a problem that is exacerbated further in case of RP-HPLC where a proportion of the solvent is likely to be water. Several interfaces have been developed which overcome these challenges, including electrospray ionisation (ESI) and atmospheric pressure chemical ionisation (APCI).

1.7.2.2. Atmospheric pressure chemical ionisation

APCI is a 'soft' ionisation technique, so called because it produces ions with very little excess energy and, thus, limited fragmentation. It can be operated in both positive and negative ion mode and produces predominantly singly charged species. APCI is suited to the analysis of non-volatile, thermodynamically stable, polar and moderately polar analytes.

In a typical APCI source (Fig. 1.4), the liquid containing the analyte (e.g. HPLC eluent) is introduced into to a pneumatic nebuliser inlet where it is converted into a fine mist by a stream of nitrogen. The flow of nitrogen displaces the droplets along a heated quartz tube where vaporisation of the solvent and analyte occurs. Solvent evaporation prevents thermal decomposition of the analyte molecules, although this technique is not suitable for thermally labile compounds. The hot gases, including the analyte, leave the tube and are carried past a corona discharge needle where ionisation occurs.

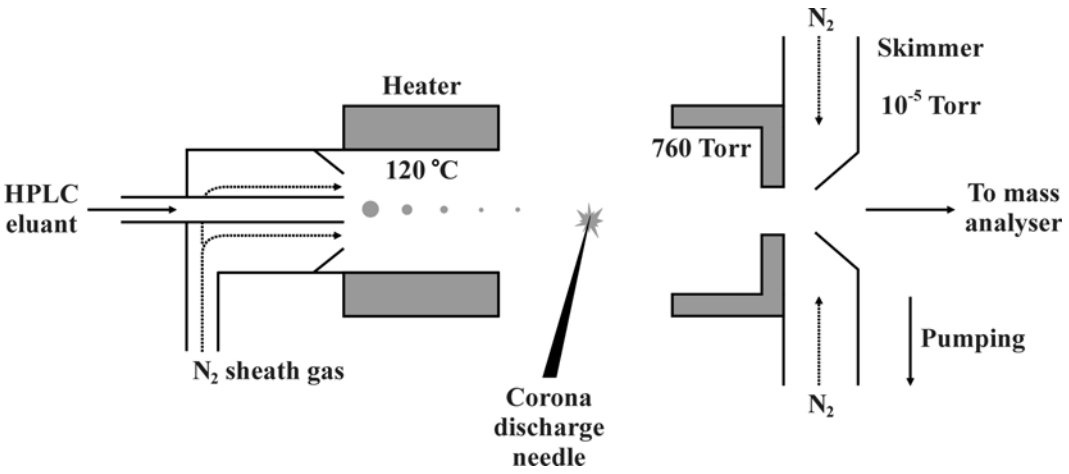

Figure 1.4. Diagram of an APCI source (modified from de Hoffmann and Stroobant, 2002).

In positive ion mode the needle is held at a potential of approximately +5-6 kV which ionises nearby gas molecules via electron ionisation, producing primary ions such as $N_2^{+\cdot}$ and $N_4^{+\cdot}$ (Equations 1.3 and 1.4). These primary ions collide with vaporised solvent molecules (such as H_2O) forming secondary reagent gas ions e.g H_3O^+ and $H^+(H_2O)_2$ (Equations 1.5-1.8). These then undergo collisions with analyte molecules to form protonated molecules ($[M+H]^+$) via proton transfer and solvent-analyte adducts. In negative ion mode the potential on the corona discharge electrode is reversed and analyte ions are formed by proton abstraction, forming deprotonated molecules ($[M-H]^-$), and adduct formation. As this process occurs at atmospheric pressure, collisions are frequent and afford efficient ionisation.

$$N_2 + e^- \rightarrow N_2^{+\cdot} + 2e^- \quad (1.3)$$

$$N_2^{+\cdot} + 2N_2 \rightarrow N_4^{+\cdot} + N_2 \quad (1.4)$$

$$N_4^{+\cdot} + H_2O \rightarrow H_2O^{+\cdot} + 2N_2 \quad (1.5)$$

$$H_2O^{+\cdot} + H_2O \rightarrow H_3O^+ + {}^{\cdot}OH \quad (1.6)$$

$$H_3O^+ + H_2O + N_2 \rightarrow H^+(H_2O)_2 + N_2 \quad (1.7)$$

$$H^+(H_2O)_{n-1} + H_2O + N_2 \rightarrow H^+(H_2O)_n + N_2 \quad (1.8)$$

The expansion and cooling of the gases in the source promotes the formation of ion-solvent clusters, which lead to loss of sensitivity. To prevent this, the source is typically heated and a curtain of drying gas employed to strip any solvent molecules from the analyte ions as they are extracted towards the mass analyser by application

of an attracting potential. A combination of differential pumping and skimmer cones efficiently removes any gases while establishing the high vacuum needed for mass spectrometry.

1.7.2.3. Ion trap mass spectrometry

The quadrupole ion trap (QIT) was invented as an ion storage device by Wolfgang Paul (Paul and Steinwedel, 1960) and was later developed into a commercial mass spectrometer by George Stafford and co-workers of the Finnigan Corporation (Stafford et al., 1984). It consists of 3 electrodes: a ring electrode flanked by two ellipsoid end-cap electrodes, all of hyperboloidal geometry arranged as shown in Fig. 1.5.

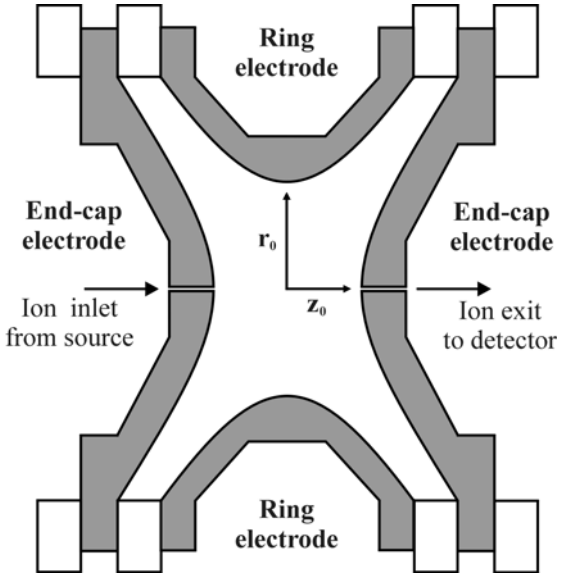

Figure 1.5. Diagram of the quadrupole ion trap (adapted from March, 1998) showing the radial and axial dimensions r_0 and z_0, respectively.

Each end-cap electrode has a single central perforation; one for the introduction of ions from the external ion source and the other allowing ejected ions passage to the detector, typically an electron multiplier. During operation, the end-cap electrodes are held at ground potential and an oscillating fundamental rf potential is applied to the ring electrode. The potential difference between the end-caps and the oscillating rf applied to the ring electrode generates a parabolic (saddle shaped) quadrupolar field

inside the chamber of the trap (e.g. Fig. 1.6a). Ions, admitted through the inlet end-cap, enter the quadrupolar field and collapse into stable trajectories within the trapping volume. For example, consider a positive ion in the quadrupolar field. When a positive (repulsive) rf potential is applied to the ring electrode a potential well is created in the radial direction (r) and the ion is focussed towards the centre of the trap (Fig. 1.6a). Simultaneously, the ion occupies a peak in the axial (z) direction and is defocused towards one of the grounded end caps. Upon reversal of the field the opposite situation prevails and the ion is defocused radially and focussed axially (Fig. 1.6b). Provided the frequency of the oscillating rf is sufficient, focussing and defocusing forces balance and the ion maintains a stable three-dimensional trajectory in the trap. Trapped ions oscillate in a figure of eight (Lissajous) motion, in a plane parallel to the z axis, at a frequency termed the ion's secular frequency which is proportional to the frequency of the rf potential applied to the ring electrode.

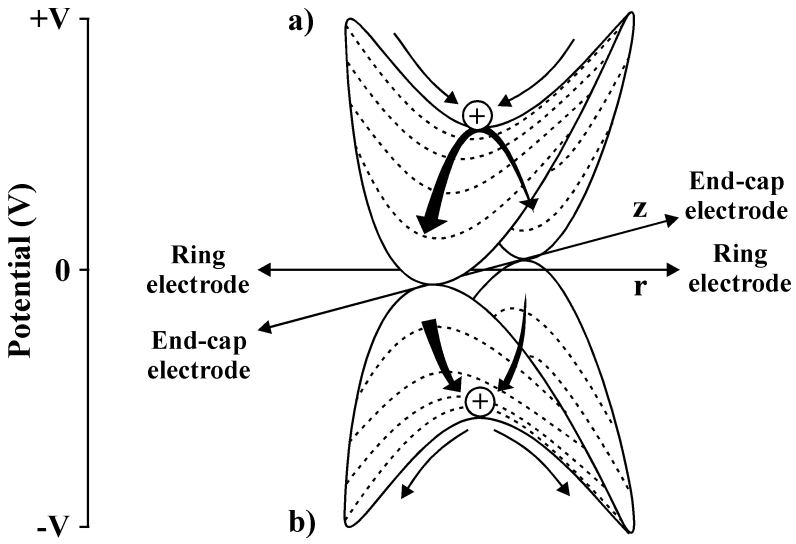

Figure 1.6. a) Representation of a positive ion on the instantaneous potential surface for a quadrupolar field when the oscillating rf applied to the ring electrode the ring electode is at its a) positive voltage excursion (+V), b) negative voltage excursion (–V). End cap electrodes are grounded (0 V). Arrows show the focussing and defocusing forces (Adapted from McLuckey et al., 1994; de Hoffmann and Stroobant, 2002).

As the confined ions possess the charges of the same sign, ion-ion repulsions cause expansion of ion trajectories with time that would eventually lead to their collision with the walls of the trap and loss. To alleviate this a constant pressure of helium buffer gas (10^{-3} Torr) is maintained within the trap and ions are focussed towards the centre of the trap by a series of ion-molecule collisions that dissipate excess energy.

The trajectory of an ion and its stability in the quadrupolar field are described mathematically by solutions to the Mathieu equation, from which the dimensionless trapping parameters q_z and a_z can be derived (Equations 1.9 and 1.10, from March 1998). These solutions can be used to construct stability diagrams that delineate regions of axial and radial stability. Fig. 1.7 shows one of the most useful regions where both axial and radial stability are satisfied simultaneously. The values of a_z and q_z (termed the working points) for an ion of given *m/z*, and hence its position in the stability region, can be altered by changing the amplitudes of the applied DC and rf potentials, respectively. In practice, the DC potential is held at zero and consequently all trapped ions arrange themselves along the q_z axis in order of decreasing *m/z*. This affords the greatest range of *m/z* values that may be stably trapped (Fig. 1.7)

$$a_z = \frac{-16zeU}{m(r_0^2 + 2z_0^2)\omega^2} \tag{1.9}$$

$$q_z = \frac{8zeV}{m(r_0^2 + 2z_0^2)\omega^2} \tag{1.10}$$

a_z, q_z	=	Trapping or stability parameters with respect to the axial (z) dimension
e	=	Elementary charge
z	=	Charge number of the ion
m	=	Mass of the ion
U	=	Amplitude of the applied DC potential
V	=	Amplitude of the fundamental rf potential
ω	=	Oscillating frequency of the fundamental rf
r_0	=	Internal radius of the ring electrode
z_0	=	Half the axial distance between end-cap electrodes

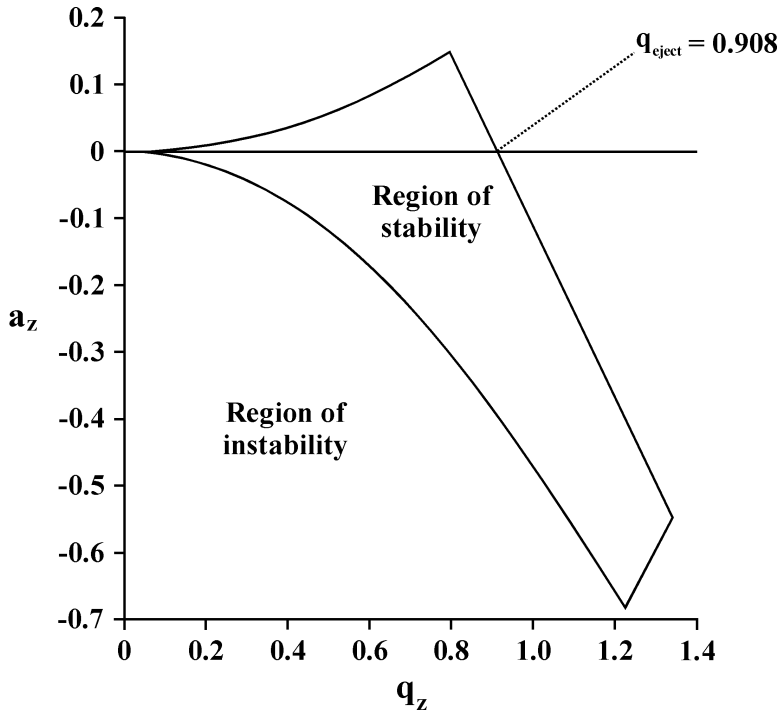

Figure 1.7. Stability diagram for positive ions in a quadrupolar field (modified from March, 1998). The stability region for negative ions is the mirror image reflected about the q_z axis.

Mass scanning is performed utilising the mass-selective instability mode for ion ejection. The amplitude of the fundamental rf potential is ramped causing the q_z value of each ion to increase. When the q_z value of the ion reaches a critical value (q_z = 0.908, termed q_{eject}, Fig. 1.7) the amplitude of the ion's oscillation in the axial direction exceeds the physical dimensions of the trap and the ions are ejected axially through the apertures in the end-cap electrodes, in order of increasing *m/z*. As ions are ejected through both end-caps only 50% of the ions ejected impinge upon the detector.

There is a maximum amplitude of the fundamental rf which can be applied before arcing occurs. This imposes a high *m/z* threshold on the ions that can be ejected from the trap by ramping the amplitude of the rf potential. The *m/z* range of the ion trap can be extended by resonance ejection which involves application of a small supplementary rf potential to the end cap electrodes, with a frequency corresponding to the axial secular frequency of a particular ion. This causes the ion to come into resonance and gain energy from the applied field, leading to a linear increase in the

amplitude of its oscillations in the axial direction until it is ejected through the end cap electrodes.

1.7.2.4. Tandem and multistage tandem mass spectrometry

Tandem mass spectrometry (MS/MS) involves the following principal operations; i) initial mass analysis, ii) isolation of a precursor ion, iii) fragmentation of the precursor ion and iv) mass analysis of the product ions. Triple quadruple instruments perform MS/MS experiments in space; where the precursor is selected by the first quadrupole, dissociated in a second quadrupole (functioning as a collision cell) and the product ions analysed with the third quadrupole. By contrast, ion trap instruments perform MS/MS temporally with scanning, precursor ion selection and dissociation operations conducted sequentially within the same space.

Isolation of the precursor ions is achieved by applying a notched waveform to the end cap electrodes leading to resonance ejection of all unwanted ions (as described above). Following isolation, resonance enhanced collision induced dissociation (CID) of the precursor ion is performed by applying an oscillating supplementary rf potential (sometimes referred to as the 'tickle' voltage) to the end cap electrodes, with a frequency matching that of the ion's secular frequency. The amplitude of the rf potential is judiciously selected so as to cause the ion to gain kinetic energy without leading to its ejection from the trap. Collisions of the precursor ions with the helium buffer gas convert some of its kinetic energy into internal energy. The energy converted with each collision is small, thus, as soon as the internal energy reaches a certain threshold the ion dissociates, almost exclusively by the lowest energy dissociations (March, 2000). In addition, because the nascent product ions possess different secular frequencies from that of the precursor ion, they are unaffected by the supplementary rf and are collisionally focussed into stable trajectories within the ion trap without dissociating further. Some of the product ions formed, however, may have q_z values greater than ($q_{eject} = 0.908$) and are therefore not stably confined by the field conditions used for CID of the precursor ion. In general, product ions that have *m/z* values less than 20% that of the precursor ion are lost from the trap. Product ions formed from CID of the selected precursor can be ejected sequentially from the trap (as described above) to produce the MS/MS (or MS^2) spectrum. Alternatively a

product ion can be isolated and subjected to CID to produce the MS/MS/MS (MS^3) spectrum. This procedure can be repeated until the prospective precursor ion ceases to dissociate further or the signal strength becomes insufficient. Thus, ion traps have the valuable capability to perform multistage tandem mass spectrometry (MS^n) experiments.

APCI LC-MS^n has been used extensively for the analysis of the pigment distributions contained within environmental samples (Airs et al., 2001; Squier et al., 2002; Walker et al., 2002; Airs and Keely, 2003; Squier et al., 2004; Wilson et al., 2004a). The combination of online PDA detection and the wealth of structural information provided by MS^n makes this technique a powerful diagnostic tool for the structural assignment of unknown components in complex mixtures.

1.8. Summary and aims

By virtue of their having a sole origin from photoautotrophic organisms, sedimentary chlorophylls and their diagenetic congeners are ideal biomarkers to assess the composition and extent of the primary producer community in times past. Moreover, some chlorophyll transformation products can be used as indicators for certain environmental parameters. In order for the information obtained from the interpretation of biomarker distributions to be of the greatest value, an appreciation is required of all possible sources, degradative processes and preservational sinks of these compounds in the natural environment. Sulfurisation plays a key role in the preservation and sequestration of organic matter in the natural environment. Thus, the recognition of alkylthioether chlorophyll derivatives in the sediment of Pup Lagoon, Antarctica (Squier et al., 2003; 2004), has potentially far reaching implications for the preservation of chlorophyll. The precise mechanism of their formation remains uncertain and their discovery is, as yet, an isolated case

The main aim of the work presented in this thesis was to develop a clearer understanding of the factors and environments conducive to the formation of alkylthioether chlorophylls in nature and the environmental significance of their occurrence. Of the Antarctic lakes studied by Squier (2003), alkylthioether

chlorophyll derivatives were only identified in Pup Lagoon, a low lying coastal lake that has, in the past, been subject to significant marine influence (Squier et al., 2003; 2004). This could indicate that the marine connection was an important factor in the formation of these derivatives. Accordingly, Chapter 2 focuses on the APCI LC-MS^n analysis and interpretation of pigment biomarkers contained within an Antarctic marine core, with the broad objective to reveal changes in the primary producer community and depositional environment, and the additional aim to try and locate other sulfur-containing chlorophylls and relate them to those identified in Pup Lagoon. Chapters 3 and 4 focus on establishing the mechanism of formation of alkylthioether chlorophylls in the natural environment through conducting detailed laboratory simulation reactions that employ geochemically relevant reagents and conditions.

Chapter 2:

Pigment analysis of a marine sediment core

2.1. Introduction

Sedimentary tetrapyrroles serve to provide valuable information regarding the photoautotrophic organisms and environmental conditions prevailing at the time of deposition. Changes in total chlorophyll abundance have been suggested to reveal variations in past productivity (Harris et al., 1996), although the abundance of pigments in sediments is also largely influenced by the extent of preservation. Recognition of pigment distributions specific to particular groups of photoautotrophs can be used to assess the composition and structure of the primary producer community (Bidigare and Ondrusek, 1996; Squier et al., 2002). As various photoautotrophs have different requirements and tolerances for light, oxygen and sulfide the presence of certain organisms can be used to infer particular palaeoenvironmental conditions. For example, the identification of bchls *d* and *e*, specific to the obligate anaerobes Chlorobiaceae, provides evidence for photic zone anoxia (Squier et al., 2002). Further information can be gleaned from the nature of the chlorophyll transformation products. Phaeophorbides and steryl chlorin esters have been linked with zooplankton herbivory (Shuman and Lorenzen, 1975; Harradine et al., 1996; Talbot et al., 1999), the latter of which are considered to be clear indicators of grazing (Harradine et al., 1996; Talbot et al., 1999). Owing to the increased environmental stability of steryl chlorin esters relative to free sterols, the regular sterol distributions (i.e. excluding 4-methyl sterols; Talbot et al., 2000) of the former are thought to more accurately reflect those of original phytoplankton substrate (Talbot et al., 1999; 2000). Oxidative transformation products of chlorophyll, in which oxygen has been incorporated into ring E, have been proposed as indicators of oxidative processes and oxygen availability in the depositional environment (Walker et al., 2002). Thus, the interpretation of sedimentary pigment distributions is a powerful tool for palaeoenvironmental reconstruction.

It has been suggested that more than 90% of the organic matter in sediments is intimately associated with components of the sediment matrix in a non-solvent extractable form (Hedges and Keil 1995; Keil et al., 1994). Solvent extractable tetrapyrroles are, therefore, only likely to represent a fraction of the chlorophyll-derived pigments present in sediments. Many biomolecules deposited in sediments

become incorporated into macromolecular structures through processes such as condensation reactions (Vandenbroucke and Largeau, 2007) and sulfurisation (Sinninghe Damsté and de Leeuw, 1990) which ultimately contribute to the formation of geopolymeric material (e.g. kerogen). The presence of an absorption band reminiscent of chlorin and porphyrin Soret bands has been noted in the UV/vis spectra of humic substances extracted from immature sediments and provides an indication for the incorporation of tetrapyrroles into macromolecular structures during early diagenesis (King and Repeta, 1994 and references therein). More reliable evidence has been provided through use of chemical degradation techniques, such as desulfurisation and acid or base hydrolysis, to selectively release components from macromolecular organic matter. Thus, chlorophyll-derived porphyrins bound by sulfide bridges have been liberated following chemical desulfurisation of the organic matter contained within the Gibellina marl, Sicily (Schaeffer et al., 1993). Acid methanolysis of high molecular weight organic matter, contained within surface sediment from the Black Sea, has been demonstrated to liberate significant amounts of porphyrins and chlorins, suggested to have been bound via ester linkages (King and Repeta, 1994). The amount of these liberated tetrapyrroles was found to represent approximately half that of the solvent extractable tetrapyrroles and contain two readily identifiable components, phorb *a* and pphorb *a*, released as their methyl esters. (King and Repeta, 1994). Similarly acid and base hydrolysis has liberated chlorophyll and heme-derived porphyrins, proposed to have been bound via ester bonds, from organic matter contained within the Messel oil shale (Huseby and Ocampo, 1997). In addition, the liberation of macromolecularly bound tetrapyrroles in hydrous pyrolysis experiments of previously extracted sediment from the Messel oil shale, conducted at a range of different temperatures (225-350ºC), revealed differences in porphyrins released at different temperatures (Huseby et al., 1996). While the porphyrins liberated at low temperature were predominantly chlorophyll-derived DPEPs (e.g. **12**), the distributions of porphyrins released at higher temperatures were dominated by aetioporphyrins (which lack any exocyclic rings), suggested to arise from heme precursors. The release of aetioporphrins at higher temperatures, compared to DPEP's, was proposed to indicate a stronger attachment of these compounds to the macromolecular network, possibly through differences in the nature/number of bonds. In addition, a decrease in the average molecular weight of the liberated porphyrins was observed with increasing temperature which the authors attributed to the

operation of dealkylation reactions initiated by the elevated temperatures (Huseby et al., 1996). An alternative explanation of these findings is that the aetioporphyrins observed derive, at least in part, from ring E-opened chlorophyll transformation products (Naylor and Keely, 1998; 1999; Airs et al., 2000). Such compounds could potentially form multiple linkages with macromolecular organic matter and, thus, the higher temperatures required for the release of aetioporpyrins, and lower molecular weights observed for the liberated molecules with increasing temperature, could reflect the cleavage of multiple bonds (and associated decarboxylations etc.).

While the precise timing and mechanisms of incorporation remain unclear, it is evident that chlorophyll-derived tetrapyrroles may become sequestered into non-solvent extractable forms relatively early during diagenesis. This raises questions as to how these sequestration reactions might affect the distributions of solvent extractable tetrapyrroles and hence any palaeoenvironmental reconstructions based on the interpretation of these pigment signatures.

The work in this chapter focuses on the pigment analysis of an Antarctic marine sediment core in order to examine variations in the total primary producer community.

2.2. Results and Discussion

2.2.1. Marine core PC461

The marine core PC641 was collected by British Antarctic Survey during the R.R.S. James Clark Ross cruise J149 (26th February 2006 – 17th April 2006; Allen et al., 2006). The core was recovered using a piston corer, activated with a trigger corer, from a site (latitude -60.81525, longitude -51.98505, water depth 2519 m) located off the Antarctic Peninsula (Fig. 2.1).

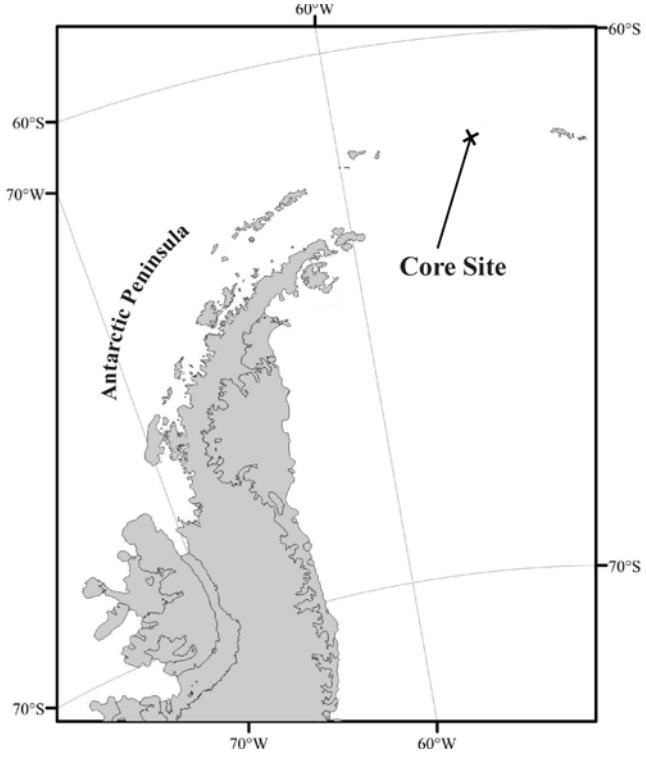

Figure 2.1. Location of the core site for PC461.

The sediments date back to approximately 43 ka (raw radiocarbon ages, Fig. 2.2) and show a roughly linear sedimentation rate with the notable exception of a hiatus between 440 cm and 540 cm depth. The core is rich in diatom remains with variable amounts of clay minerals and occasional horizons of terrigenous material. This includes a conspicuous ash layer between ~348 and 355 cm depth, most likely corresponding to material evacuated from Deception Island during a violent volcanic eruption ca. 10 ka BP (Riffenburgh, 2006). The sediment is predominantly olive green in appearance and broadly consists of several sections of faintly laminated deposits alternating with homogeneous and moderately bioturbated sediments.

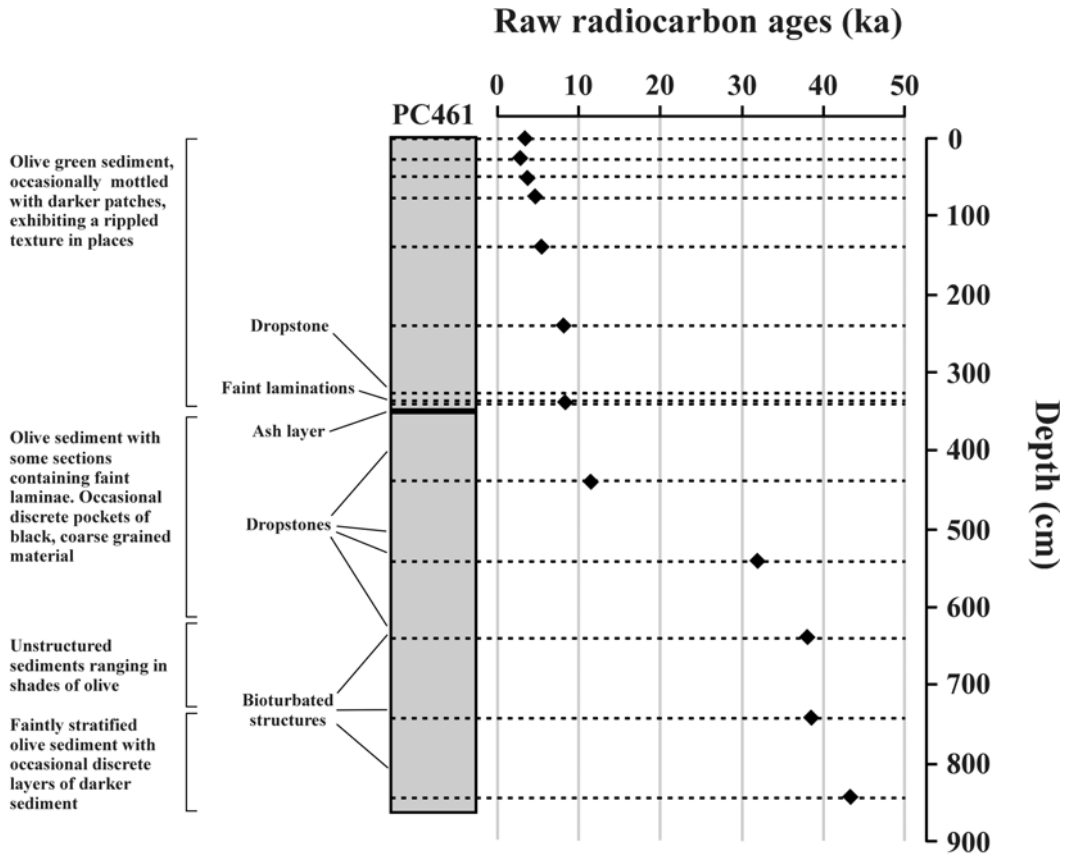

Figure 2.2. Brief core description, sample depths and age plot for marine core PC461. Diamonds show the raw (uncorrected) ^{14}C ages for horizons taken at various depths down the core. Dashed lines show the depths sampled for pigment analysis taken from horizons at or as near as possible to those measured by radiocarbon dating.

2.2.2. Preliminary analysis

An initial sediment sample from marine core PC461, taken from a horizon corresponding to 327-328 cm depth, was extracted into acetone and the extract analysed by RP-HPLC and APCI LC-MS^n utilising the methods described previously (Airs et al., 2001). Components were identified on the basis of their retention times (t_R), online UV/vis spectra, and MS^n spectra (analytical data collected in Table 2.1). The HPLC-PDA maxplot chromatogram of the extract was dominated by carotenoids with surprisingly few chlorophyll-derived components (Fig. 2.3a).

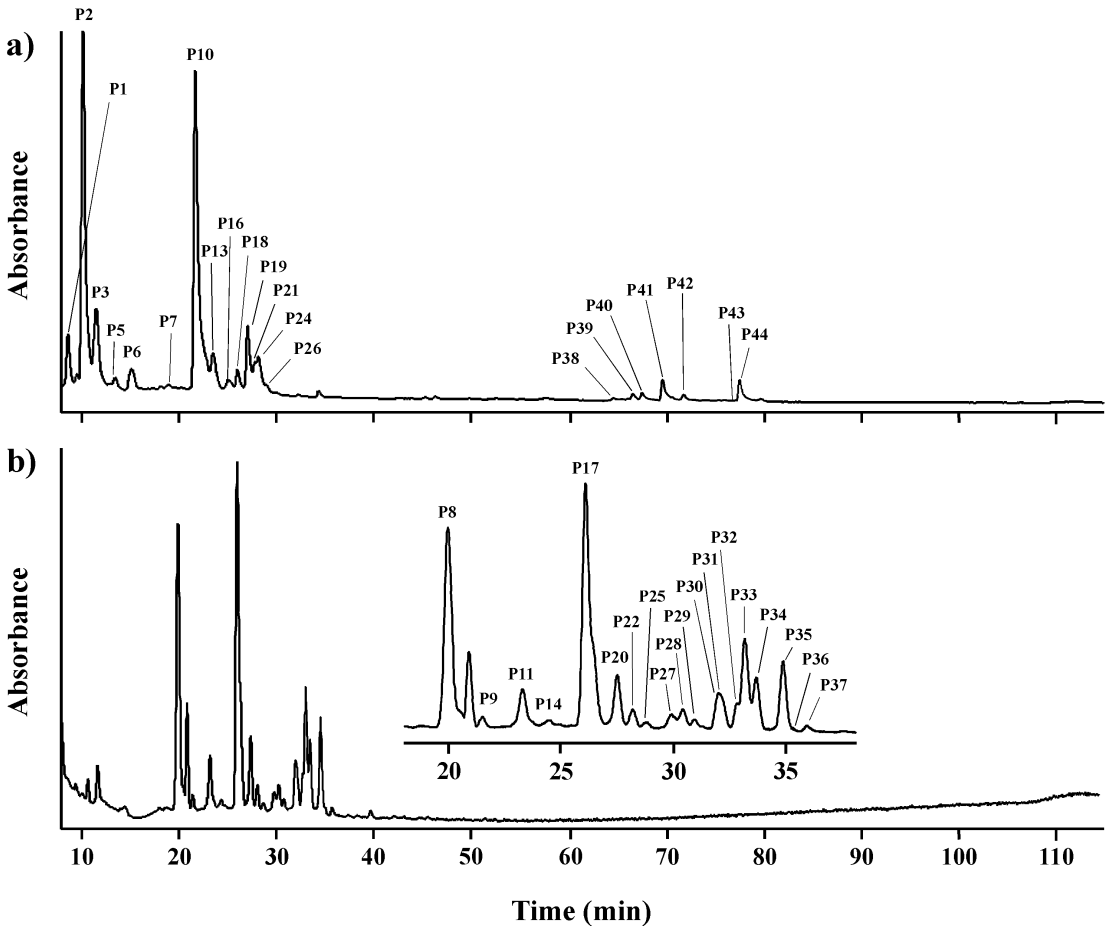

Figure 2.3. RP-HPLC-PDA maxplot chromatograms (300-800 nm) from 327-328 cm depth extracted by a) acetone, b) methanolysis. Insert shows an expansion of the region 18-38 min. For peak assignments see Table 2.1.

Table 2.1. Analytical data and assignments for the compounds identified in the marine sediment extracts.

Peak	Main UV/vis absorption bands (nm)	$[M+H]^+$ (*m/z*)[a]	Prominent ions in MS^n (*m/z*)[b]	Assignment
P1	456	641		Dehydrofucoxanthin[c]
P2	449	659	641, 623, 581, 505	Fucoxanthin[c] (**24**)
P3	333, 448	659		*cis*-Fucoxanthin[c]
P4	482			Unidentified carotenoid
P5	335, 446	659		*cis*-Fucoxanthin[c]
P6	332, 445	659		*cis*-Fucoxanthin[c]
P7	409, 665	533	515, 505, 500	Chlone (**31**)
P8	407, 665	623	605, 545, 485	C-13[2] HO-phorb *a* (**35**)
P9	397, 662	581	508, 421, 392	C-13 β-H chlorin e_6 (**44**) [c]
P10	427, 450, 479	567	549, 534	Diatoxanthin[c] (**25**)
P11	401, 668	653	566, 479, 447	Purpurin-7 trimethyl ester (**38**)
P12	434, 652	621		Phorb *b*[c] (**51**)
P13	445			Unidentified carotenoid
P14	401			Unidentified porphyrin
P15	434, 650	621		Phorb *b* epimer[c] (**51**)
P16	340, 427, 447, 473			Unidentified carotenoid
P17	408, 665	607	547, 461, 433	Phorb *a* (**32**)
P18	341, 425, 447, 473			Unidentified carotenoid
P19	342, 426, 447, 475			*cis*-diatoxanthin[c]
P20	408, 665	607	547, 461, 433	Phorb *a* epimer (**32**)
P21	341, 424, 446, 473			Unidentified carotenoid
P22	399, 670	653	621, 561, 501	C-15[1] MeO-lact-phorb *a* (**43**)
P23	447, 475			Unidentified carotenoid
P24	341, 426, 445, 473			Unidentified carotenoid
P25		635	603, 543, 483	Rearranged chl c_1 derivative (**50**)
P26	341, 426, 448, 474			Unidentified carotenoid
P27	409	595	563, 476, 420	Unidentified porphyrin
P28	411, 661	547	519, 476, 461	C-15[1]-MeO chlone (**37**) [c]
P29	398, 667	563	504, 475, 460	Chlorophyllonic acid methyl ester (**45**)
P30	408, 664	647	560, 500, 485	Unidentified chlorin
P31	409, 655	579	547, 461, 433	C-13[2] MeO-pphorb *a* (**36**) [c]
P32	399, 666	609	577, 475, 447	Unidentified ring E-disrupted chlorin
P33	413	633	601, 541, 481	Rearranged chl c_2 derivative (**49**)
P34	400	591	518, 445, 415	Protoporphyrin-IX (**47**)
P35	409, 666	549	521, 435, 420	Pphorb *a* (**33**)
P36	413	615		Unidentified porphyrin
P37	406, 544, 696	579	535, 503, 488	Purpurin-18 methyl ester (**46**)
P38	409, 665	887	609, 591, 531	C-13[2] HO-phe *a* (**26**)
P39	400, 665	903	625, 565, 533	Chlorin e_6 dimethyl phytyl ester (**29**)
P40	401, 670	917	639, 552, 537	Purpurin-7 phytyl ester (**27**)
P41	409, 665	871	593, 533, 461	Phe *a* (**14**)
P42	409, 666	871	593, 533, 461	Phe *a* epimer (**14**)
P43	408, 546, 698	843	565, 503, 488	Purpurin-18 phytyl ester (**30**)
P44	409, 666	813	535, 507, 435	Pphe *a* (**16**)
P45	410, 667	901	535	Pphorb *a* steryl ester ($C_{27:2}$)
P46	410, 667	915	535	Pphorb *a* steryl ester ($C_{28:2}$)
P47	410, 667	903	535	Pphorb *a* steryl ester ($C_{27:1}$)
P48		917	535	Pphorb *a* steryl ester ($C_{28:1}$) [c]
P49		931	535	Pphorb *a* steryl ester ($C_{29:1}$) [c]

[a]Detected in MS as the corresponding demetallated derivative owing to post column addition of formic acid. [b]Obtained following resonance enhanced collision induced dissociation. The underlined *m/z* value denotes the base peak ion in MS^2. [c]Tentative assignment. Esterifying sterols shown in parentheses in the form $C_{n:m}$. n = carbon number, m = number of double bonds.

The dominant carotenoids P2 and P10 were tentatively assigned as fucoxanthin (**24**, λ_{max} 449 nm, $[M+H]^+$ *m/z* 659) and diatoxanthin (**25**, λ_{max} 427, 450, 479, $[M+H]^+$ *m/z* 567), respectively, each accompanied by their *cis*-isomers, as indicated by the presence of an additional absorption band at ca. 345 nm. The full MS of **24** displayed fragment ions at *m/z* 641 (-18 Da) and *m/z* 581 (-78 Da) corresponding to loss of water and combined loss of water and HCO_2Me, consistent with the structure of fucoxanthin. Similarly, the full MS of **25** displayed a fragment ion at *m/z* 549 corresponding to loss of water, consistent with the structure of diatoxanthin.

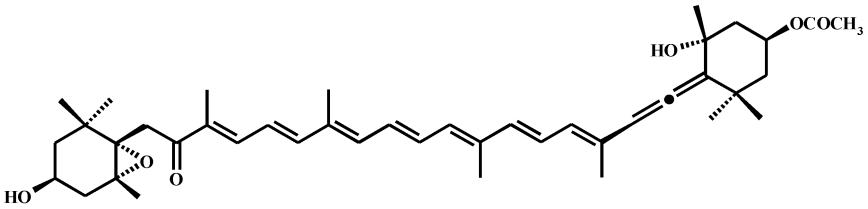

24

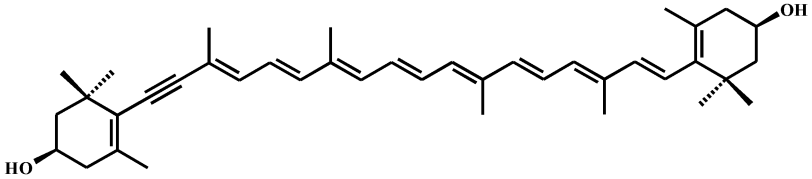

25

Owing to the similarities in the UV/vis spectra of many carotenoids and their poor ionisation under APCI conditions and ambiguous fragmentations, these assignments must be treated with caution (Airs et al., 2001). The presence of fucoxanthin and diatoxanthin suggests that diatoms comprised a significant proportion of the phytoplankton community at the time of deposition (Sigleo et al., 2000; Gibb et al., 2001). As the structure of fucoxanthin contains a labile epoxide moiety, its occurrence suggests that good conditions for preservation prevailed during and following deposition.

By contrast, the chlorophyll component of the extract was present in much lower abundance. Chl *a* (**4**) was not detected in the extract, though its common transformation products, phe *a* (P41, **14**, λ_{max} 409, 665 nm; $[M+H]^+$ *m/z* 871) and pphe *a* (P44, **16**, λ_{max} 409, 666 nm; $[M+H]^+$ *m/z* 813), were identified from their online UV/vis (e.g. Fig. 2.4) and MS^n spectra (Table 2.1) (cf. Airs et al., 2001). Phe *a*

was preceded by a number of smaller peaks P38-40 identified as oxidation products of phe *a*. The first of the three components to elute, P38, exhibited a UV/vis spectrum similar to that of phe *a* (λ_{max} 409, 665 nm). The protonated molecule of this component, *m/z* 887, and product ions in MS^n are consistent with C-13^2 HO-phe *a* (**26**) (Airs et al., 2001), formed via reaction with singlet oxygen-containing species. By virtue of their stability towards further oxidation (Woolley et al., 1998), C-13^2-HO-chl derivatives have been proposed as proxies for the redox status of the depositional environment (Walker et al., 2002).

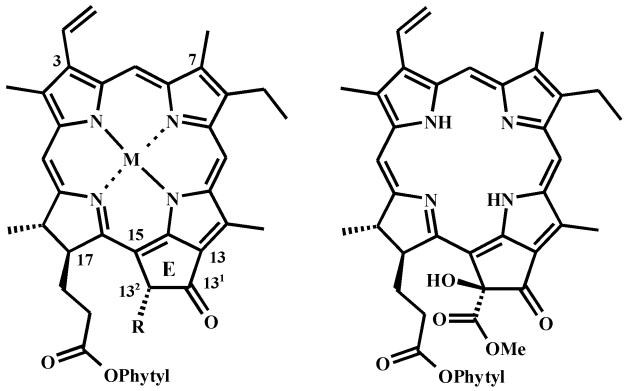

4: R = CO_2Me, M = Mg **26**

14: R = CO_2Me, M = 2H

16: R = H, M = 2H

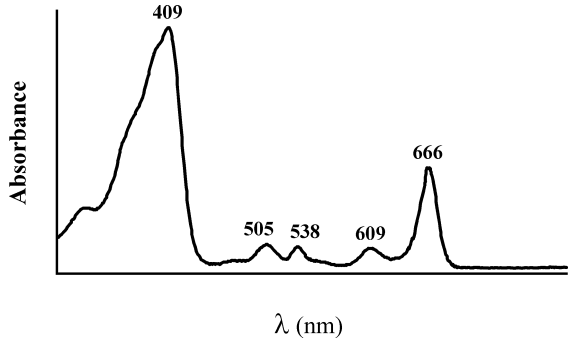

Figure 2.4. Online UV/vis spectrum (300-800 nm) of phe *a* (**14**, P41).

The online UV/vis spectra of components P39 (Fig. 2.5a) and P40 (Fig. 2.5b) revealed an absence of satellite bands on the blue side of the Soret band, which have a more symmetrical appearance with respect to that of phe *a* (Fig. 2.4). Such features in the UV/vis spectra are characteristic of chlorins that lack the strained cyclopentanone ring (ring E) and result from the increase in planarity of the aromatic macrocycle that accompanies expansion or cleavage of ring E (Woolley et al., 1998; Airs et al., 2000). The later eluting component of the pair, P40, displayed a protonated molecule at *m/z* 917 and product ions in MS^n consistent with the ring opened chlorophyll derivative purpurin-7 dimethyl phytyl ester (**27**) (Airs et al., 2000). Notably, the ring opening reaction responsible for the formation of purpurin-7 in the natural environment typically yields the monomethyl ester derivative which possesses a carboxylic acid at the C-13 position (Hynninen, 1991; Walker, 2004). The occurrence of purpurin-7 as the dimethyl phytyl ester is most likely due to routine treatment of sediment samples with diazomethane in order to methylate free acids to improve their chromatographic peak shape and extend sample storage life.

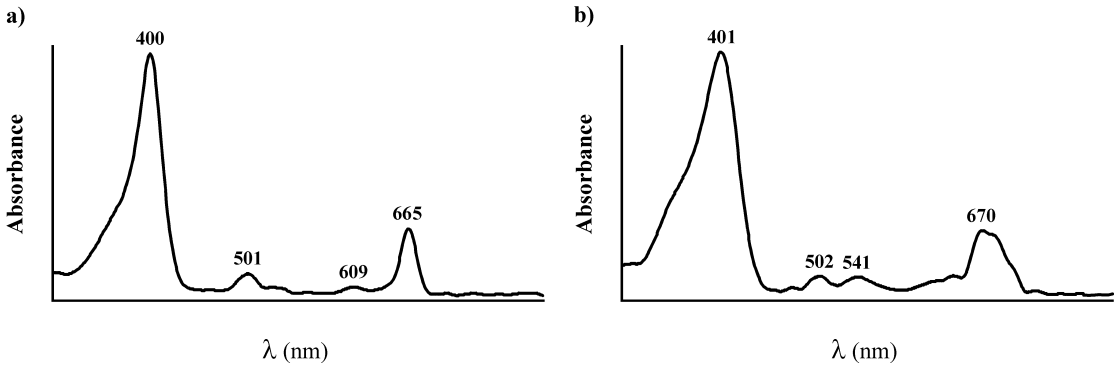

Figure 2.5. Online UV/vis spectra (300-800 nm) of ring E-disrupted chlorins a) chlorin e_6 trimethyl ester (**29**, P39) and b) purpurin-7 phytyl ester (**27**, P40).

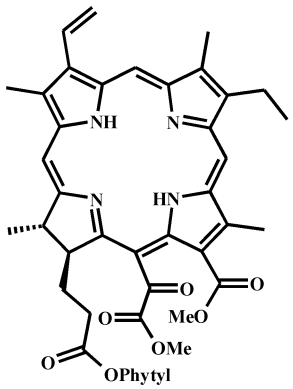

27

The UV/vis spectrum and protonated molecule exhibited by the earlier eluting component P39 (*m/z* 903) are consistent with two possible structures, C-15[1] HO-lact-phe *a* (**28**) or chlorin e_6 dimethyl phytyl ester (**29**), both of which possess a disrupted ring E.

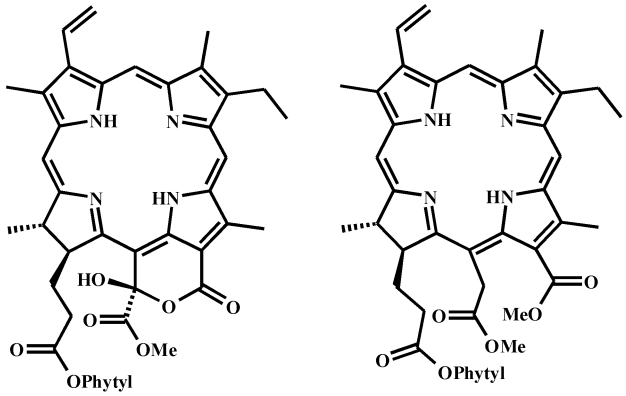

28 **29**

While the difference in retention time of P39 with respect to phe *a* is consistent with that observed between C-15[1] HO-lact-chl *a* and chl *a* (Walker, 2004), which argues in favour of this component being C-15[1] HO-lact-phe *a* (**28**), the losses observed in the MS^n spectra of P39 (Fig. 2.6) are at variance with this assignment. Loss of H_2O in the MS^n spectra, expected for C-15[1] HO-lact-phe *a* (**28**) by comparison with loss of MeOH observed in the MS^n spectra of C-15[1] MeO-lact-chl *a* (Walker et al., 2003), could not be detected. The losses observed in the MS^2 and MS^3 of P39 can, however, still be rationalised for both proposed structures. Resonance enhanced collision induced dissociation (CID) of *m/z* 903 yields a base peak ion in MS^2 (Fig. 2.6b) at *m/z* 625 reflecting loss of the C-17[3] phytyl esterifying alcohol as phytadiene (-278 Da). The MS^3 spectrum (Fig. 2.6c) contains a base peak ion at *m/z* 565 (-60 Da) that can potentially arise via loss of a carbomethoxyl group, with hydrogen abstraction, (HCO_2Me) from the C-15[1] position of **28** or from positions C-13[1] or C-15[1] of chlorin e_6 (**29**). The ion of lesser intensity at *m/z* 552 (-73 Da) can result from radical loss of the propionic acid residue ($^{\cdot}CH_2CH_2CO_2H$) from the C-17 position of **28**. Alternatively, *m/z* 552 could originate from loss of $^{\cdot}CH_2CH_2CO_2H$ from C-17 or $^{\cdot}CH_2CO_2Me$ from C-15 of **29**. Notably, CID of *m/z* 565 generates an MS^4 spectrum (Fig. 2.6d) dominated by a product ion at *m/z* 533 (-32 Da) reflecting loss of methanol. This loss cannot easily be explained for structure of **28** given the losses

proposed to occur in the previous stages of MS^n. In the case of **29**, however, loss of MeOH can be envisaged from the remaining carbomethoxy group. Accordingly component P39 was assigned as chlorin e_6 dimethyl phytyl ester (**29**) and is believed to be the first validated report of chlorin e_6 in sediments to be supported by good structural proof by MS^n. Synthetic chlorin e_6 has been prepared by base hydrolysis of the chlorophyll exocyclic ring involving attack of hydroxide at the C-13^1 position (Hynninen, 1991). Thus, the occurrence of chlorin e_6 in sediment may reflect alkaline conditions.

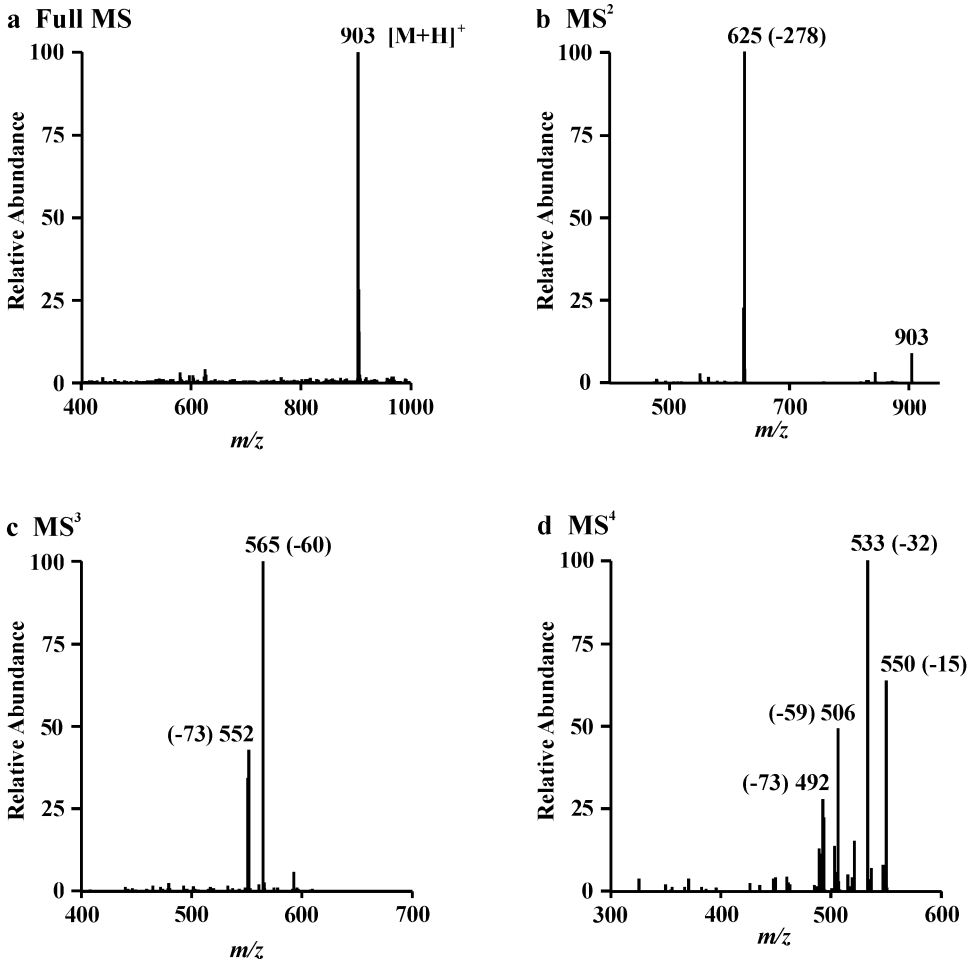

Figure 2.6. APCI multistage tandem mass spectra of chlorin e_6 dimethyl phytyl ester (**29**, P39); a) Full MS, b) MS^2, c) MS^3, d) MS^4. In each case the most abundant ion was selected as the precursor for the next spectrum.

Close inspection of the region of the HPLC chromatogram between phe *a* and pphe *a* established the presence of a minor component, P43, eluting immediately prior to pphe *a*, exhibiting a distinctive online UV/vis spectrum characteristic of purpurin-18 (Fig. 2.7) (Naylor and Keely, 1998; Squier et al., 2002). The protonated molecule of this component ($[M+H]^+$ *m/z* 843) confirms it to be the phytyl ester of purpurin-18 (**30**) (Naylor and Keely, 1998; Squier et al., 2002).

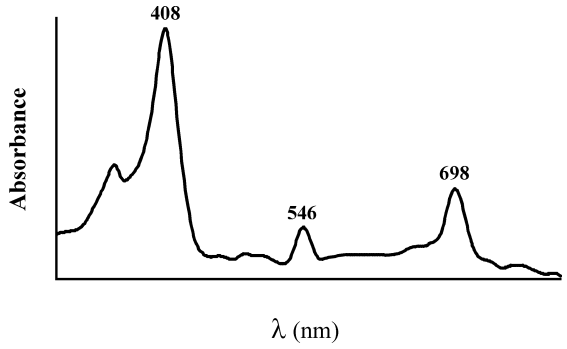

Figure 2.7. Online UV/vis spectrum (300-800 nm) of purpurin-18 phytyl ester *a* (**30**, P43).

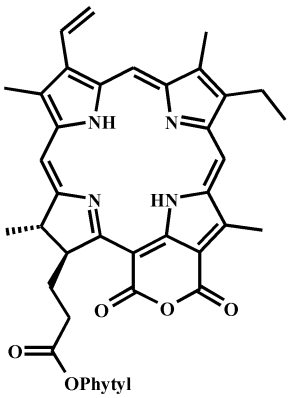

30

An early eluting chlorin, P7 (t_R = 19 min), exhibiting a phe *a* type UV/vis spectrum (λ_{max} 409, 665 nm), could be recognised among the carotenoid peaks. The retention time, online UV/vis spectrum, protonated molecule ($[M+H]^+$ *m/z* 533) and MS^n product ions of this component are consistent with chlorophyllone (chlone, **31**) (Airs et al., 2001). Chlone has been reported in a range of sediments (Harris et al., 1995; Airs et al., 2001), water column particulates (Walker and Keely, 2004) and marine organisms, including the viscera of scallops (Sakata et al., 1990; Watanabe et al., 1993) and mixed cultures of the diatoms attached to them (Watanabe et al., 1993).

Synthetic chlone has been prepared from phorb *a* via a Claisen-type condensation reaction between the C-17 propionic substituent and the C-13^2 position of the cyclopentanone ring with the use of a strong base (Ma and Dolphin, 1996). Such a condensation reaction can be invoked to justify the formation of chlone in the natural environment and may suggest that alkaline conditions are associated with its formation, although its precise origins remain unclear.

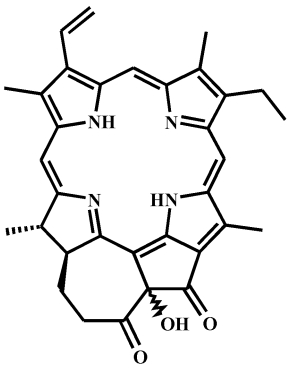

31

Notably, despite the abundance of diatom remains throughout the whole core and the prevalence of diatom-derived carotenoids in the sediment extract, no evidence of the chl *c* could be detected. Chl *c* is the collective term for an increasing number of pigment structures, including chl c_1 (**6**) chl c_2 (**7**), that occur as accessory pigments in marine diatoms with chl *a*:*c* ratios reported to range between 1.65-7.25 (Stauber and Jeffrey, 1988). Other studies have reported a similar failure to detect chl *c*-derived pigments in sediments containing diatom remains (Vincent et al., 1993; Squier et al., 2002) and ascribed the absence to a high chl *a*:*c* ratios in the diatoms.

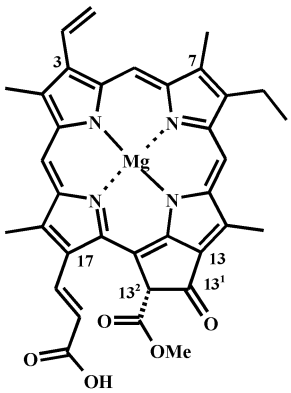

6

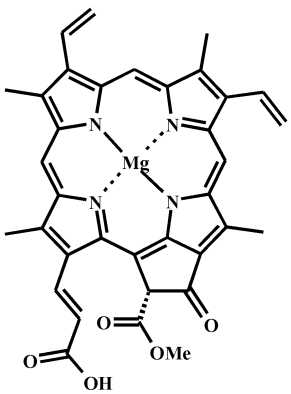

7

The unusually low abundance of chlorophyll-derived pigments relative to carotenoids could indicate a greater environmental stability of the latter. Indeed, the destruction of chlorophylls is observed to proceed at a visibly faster rate than that of carotenoids in the leaves of deciduous trees prior to leaf fall, resulting in loss of green colouration to reveal the autumnal hues of subsisting carotenoids (Hendry et al., 1987). Furthermore, an increased stability of fucoxanthin (**24**) compared with chl *a* has been noted in water column studies (Sigleo et al., 2000). Alternatively, the low relative abundance of chlorophylls in the sediment extracts may be the result of selective removal of chlorophylls from the acetone extractable fraction via sequestration processes (discussed above, Section 2.1). In addition to sequestration as macromolecularly bound moieties, sorption onto mineral surfaces is also regarded to be a key mechanism for the preservation of organic matter in marine sediments (Keil et al., 1994; Hedges and Keil, 1995). Aside from clay minerals, the abundance of diatoms in the sediment provides a ready source of biogenic silica. Thus, chlorophylls may be associated with diatom frustules through sorptive processes or conceivably through formation of ester linkages with available silanol sites.

2.2.3. Methanolytic extraction

The acetone-extracted sediment was subjected to treatment with a 5% solution of H_2SO_4 in methanol for 24 h in the dark, affording a coloured extract. Under these conditions metallated pigments are converted into their free base equivalents and pigments bound via ester bonds are released as methyl esters. Consequently, any biomarker information regarding the presence of a chelated metal or C-17[3] esterifying alcohol is lost. Acid methanolyis is routinely used in the laboratory preparation of phaeophorbide methyl esters from chlorophyll and has been employed to simplify the complex chromatographic properties of distributions of bacteriochlorophyll homologues esterified with different alcohols (Wilson et al., 2004a). No further pigment was extracted when the procedure was performed a second time, or with higher concentrations of H_2SO_4 (up to 25%), suggesting that all acid extractable pigments were removed in the first extraction. The acid-extracted pigments were transferred to diethyl ether, washed with water to remove residual acidity and dried under a gentle stream of N_2. Samples were reconstituted in acetone prior to analysis.

The acid extracted components were analysed by RP-HPLC and LC-MS^n and components assigned on the basis of their online UV/vis and MS^n spectra (analytical data collected in Table 2.1). The RP-HPLC-PDA chromatogram of the acid extract (Fig. 2.3b) reveals a complex mixture of components eluting between t_R 19-40 min. These components can be divided, on the basis of their online UV/vis spectra, into three main groups; i) those that exhibit typical chlorin spectra, ii) chlorins possessing a disrupted ring E and iii) porphyrins.

2.2.3.1. Chlorins

Components P8, P17, P20, P28, P30, P31 and P35 exhibit UV/vis spectra typical of free base chlorins (e.g. Fig. 2.4). Chlorin P17, which represents the major component of the extract, and chlorin P35 correspond to phorb *a* methyl ester (**32**; λ_{max} 408, 665 nm; $[M+H]^+$ *m/z* 607) and pphorb *a* methyl ester (**33**; λ_{max} 409, 666 nm; $[M+H]^+$ *m/z* 549), respectively (cf. Airs et al., 2001). Chlorin P20, eluting approximately 1.5 min later than phorb *a*, present in approximately 15% relative abundance and exhibiting identical UV/vis and MS^n spectra, corresponds to the C-13^2 epimer of phorb *a*. The release of P17, P20 and P35 as methyl esters, without any additional side chain modifications, suggests that they originate from dephytylated chlorophyll precursors, bound to components of the sediment via esterification at their C-17 propionic acid substituents (King and Repeta, 1994; Huseby and Ocampo, 1997). As any information regarding the presence of a chelated metal is lost during methanolysis, phorb *a* methyl ester (**32**) and pphorb *a* methyl ester (**33**) could originate from phorb *a* (**15**) and pphorb *a* (**17**), respectively, or their Mg-containing analogues, chlorophyllide *a* (**13**) and pyrochlorophyllide *a* (**34**). In view of the lack of metallated pigments in the acetone extract the free base precursors appear more likely.

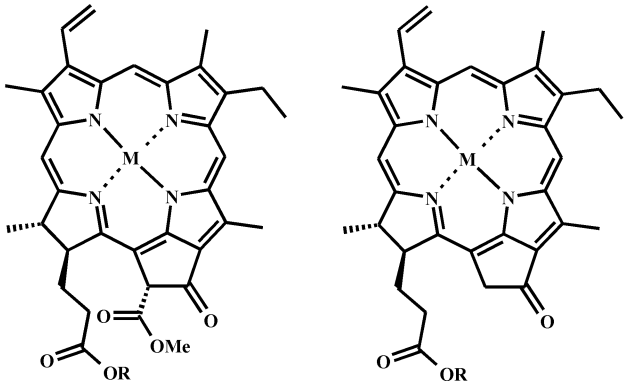

32: M = 2H, R = Me **33**: M = 2H, R =Me

15: M = 2H, R = H **17**: M = 2H, R = H

13: M = Mg, R = H **34**: M = Mg, R = H

An early eluting chlorin P8 (t_R = 20 min) is the second most abundant component in the extract. The retention time, online UV/vis spectrum (λ_{max} 407, 665 nm) and protonated molecule ($[M+H]^+$ *m/z* 623) match those of the oxidation product, C-13^2 HO-phorb *a* methyl ester (**35**) (Squier et al., 2002).

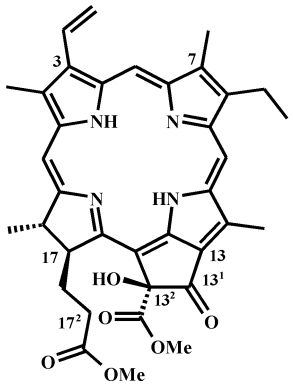

35

Although the MS^n spectra of C-13^2 HO-phorb *a* have not been reported previously, the product ions in the MS^n spectra of P8 (Fig. 2.8) are consistent with this structure. CID of *m/z* 623 yields a number of product ions in MS^2 (Fig. 2.8b). The base peak ion at *m/z* 605 arises through loss of H_2O (-18 Da) from the C-13^2 position. The ion present in slightly lower intensity at *m/z* 564 is attributable to radical loss of the C-13^2 carbomethoxy group ($^{\cdot}CO_2Me$, -59 Da). The MS^3 (Fig. 2.8c) and MS^4 (Fig. 2.8d) spectra display base peak ions at *m/z* 545 and *m/z* 485, respectively, arising from two

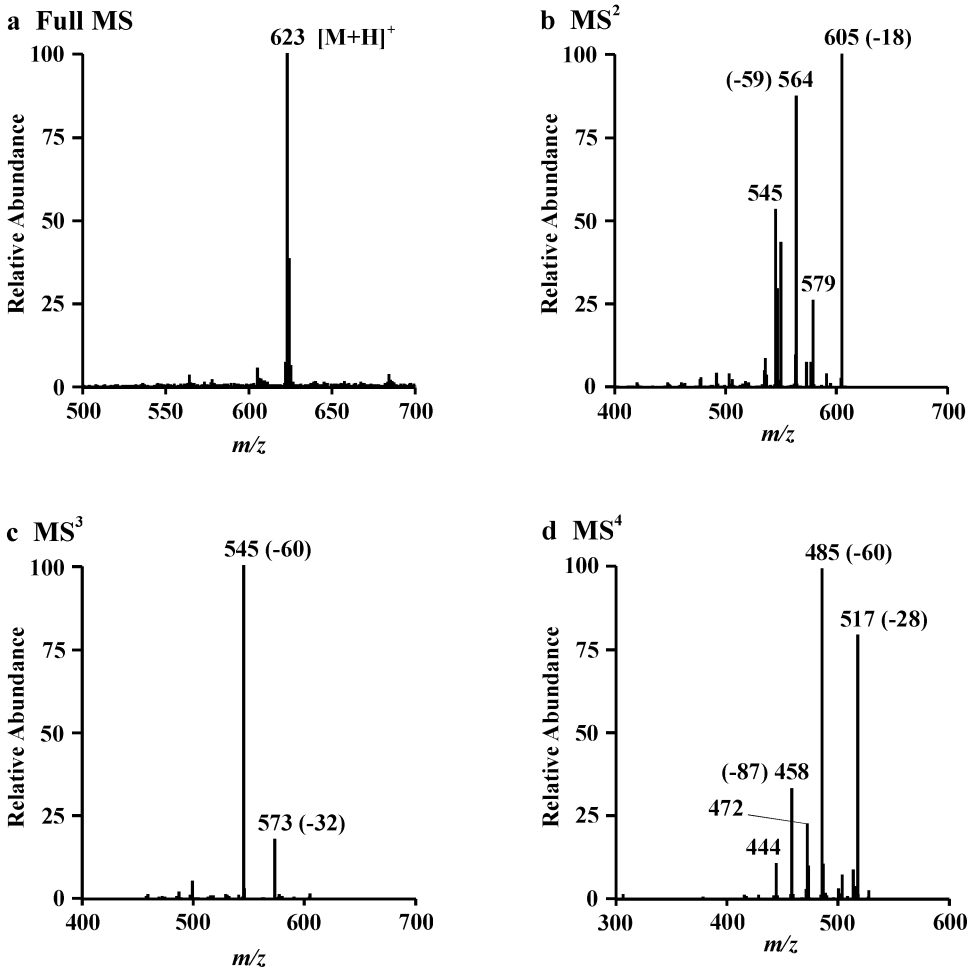

Figure 2.8. APCI multistage tandem mass spectra of C-13^2 HO-phorb *a* (**35**, P8); a) Full MS, b) MS^2, c) MS^3, d) MS^4. In each case the most abundant ion was selected as the precursor for the next spectrum.

sequential losses of 60 Da. These ions can be attributed to losses of HCO_2Me from the C-13^2 position and cleavage at C-17^2 of methyl propionate ester substituent, accompanied in both cases by abstraction of a hydrogen atom. The latter dissociation is unusual in the MS^n of chlorins, which typically favour loss of the entire C-17 substituent via α-cleavage. Notably, loss of the entire C-17 substituent, following prior loss of phytadiene, was absent from the MS^n spectra of C-13^2 HO-chl *a* (Jie et al., 2002; Walker, 2004). In that case, absence of the loss was rationalised by invoking the formation of a double bond between C-17^1 and C-17^2 as a result of hydrogen abstraction(s) by groups lost during earlier stages of MS^n (namely, losses of the C-13^2 hydroxyl and carbomethoxy groups as H_2O and HCO_2Me, respectively) (Walker, 2004). Dissociation of the resulting acrylic acid substituent via α-cleavage would be unfavourable. Interestingly, a loss of 46 Da was observed in the MS^4

spectra of C-13^2 HO-chl *a* (Jie et al., 2002; Walker, 2004), there ascribed to combined losses of CO and H_2O but without any indication provided as to their origin. Given the losses observed in the preceding stages of MS^n (-H_2O from C-13^2, -phytadiene from C-17^3 and -HCO_2Me from C-13^2), loss of 46 Da can only be explained by loss of HCO_2H from C-17^2. This loss is analogous to the additional loss of HCO_2Me (-60 Da), suggested to arise via the same cleavage at C-17^2, observed in MS^n of C-13^2 HO-phorb *a* methyl ester (**35**; Fig. 2.8). The proposed losses from this position clearly disagree with the formation of an acrylic acid substituent during MS^n, as cleavage at C-17^2 of this substituent would be just as unfavourable as α-cleavage. Based on these observations, an alternative mechanism is suggested (Scheme 2.1) in which loss of the C-13^2 hydroxyl group as H_2O involves hydrogen abstraction from C-17^2, accompanied by cyclisation of the charge retaining species to form a 6 membered ring. This rearrangement can provide a rationale for the losses of HCO_2Me (-60 Da) and HCO_2H (-46 Da) from C-17^2, observed in the MS^n spectra of C-13^2 HO-phorb *a* methyl ester (**35**; Fig. 2.8) and C-13^2 HO-chl *a*, respectively, and explain why α-cleavage to lose the entire C-17 residue is not the dominant process.

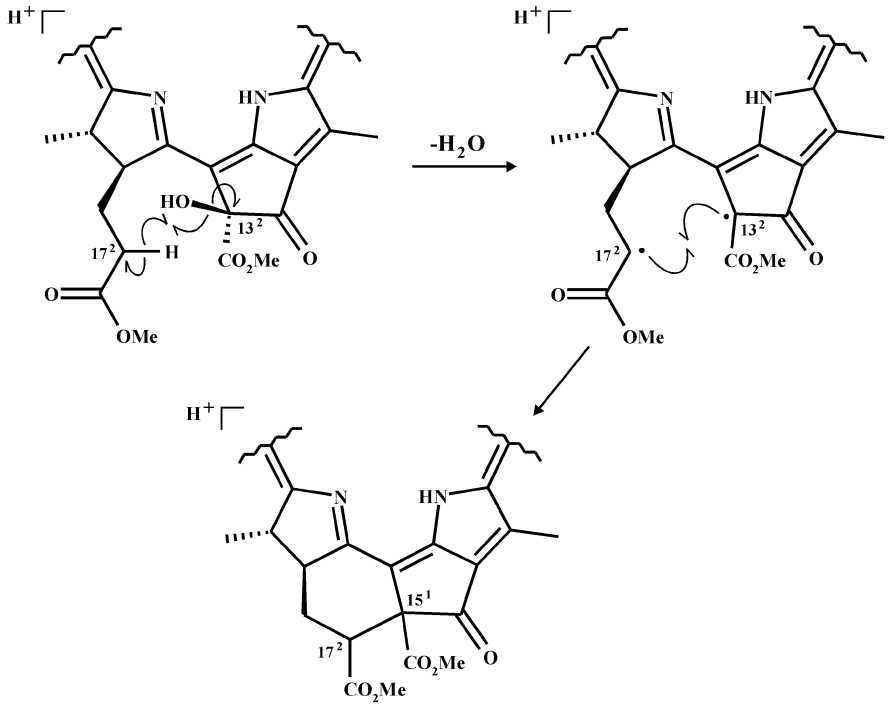

Scheme 2.1. Proposed rearrangement accompanying loss of H_2O during MS^n of C-13^2 HO-phorb *a* methyl ester (**35**, P8).

Additional product ions are present in the MS^4 spectrum of **35** at *m/z* 517 and *m/z* 485 (Fig. 2.8d). The first product ion corresponds to loss of CO (-28 Da) from C-13^1. The second product ion reflects a loss of 87 Da, which notably corresponds to loss of the C-17 methyl propionate ester and, thus, appears to disprove the proposed rearrangement (Scheme 2.1). This loss can, however, be rationalised by the combined loss of CO from C-13^1 and $^{\cdot}CO_2Me$ from the remaining carbomethoxy group.

Chlorins P30 (λ_{max} 408, 664 nm; $[M+H]^+$ *m/z* 647) and P31 (λ_{max} 409, 665 nm; $[M+H]^+$ *m/z* 579) partially coelute. Judging from the relative intensities of their protonated molecules in LC-MS, chlorin P30 is present in approximately half the abundance of P31. The MS^n spectra of P31 (Fig. 2.9) contain prominent ions consistent with loss of methanol (-32 Da, *m/z* 547), loss of the C-17 methyl propionate ester (-86 Da, *m/z* 461) and loss of CO (-28 Da, *m/z* 433). The loss of methanol provides evidence for the existence of a methoxyl group in the structure of P31. Notably, the protonated molecule of P31 is 30 *m/z* units greater than that of pphorb *a* methyl ester (P35, **33**, $[M+H]^+$ *m/z* 549). With reference to the structure of pphorb *a*, replacement of a hydrogen with a methoxyl group would account for the difference of 30 *m/z* units between the protonated molecules of the two compounds. The *meso* bridge positions of the chlorin macrocycle are susceptible to attack by electrophiles or radical species (Hynninen, 1991) and methoxyls incorporated at these positions have been identified as products from the autoxidation of chlorophyll and bacterioviridin in methanol (Walker, 2004). Notably, however, direct attachment of a methoxyl to the aromatic chlorin macrocycle would be evident from the UV/vis spectrum. Furthermore, alkoxyl groups situated at the *meso* positions of porphyrins and chlorins habitually fragment via β–cleavage to lose the alkyl group as a radical (Budzikiewicz, 1978; Quirke, 2000; Walker, 2004) as opposed to loss as methanol, observed in the MS^n spectra of P31. The most likely site for incorporation of a methoxyl in P31 is, therefore, the C-13^2 carbon of ring E (**36**). The lack of conjugation of a C-13^2 methoxyl with the macrocycle means that the structural modification has negligible effect on the UV/vis spectrum and loss of this group as methanol during MS^n can be inferred by analogy with the losses of water and methanol observed in the MS^n spectra of C-13^2 HO-chl *a* and C-15^1 MeO-lact-chl *a*, respectively (Jie et al., 2002; Walker et al., 2003). Still, it is difficult to reconcile the structure of **36** with those of

any known chlorophyll transformation products and consequently the direct precursor of this compound and its authenticity remain unclear.

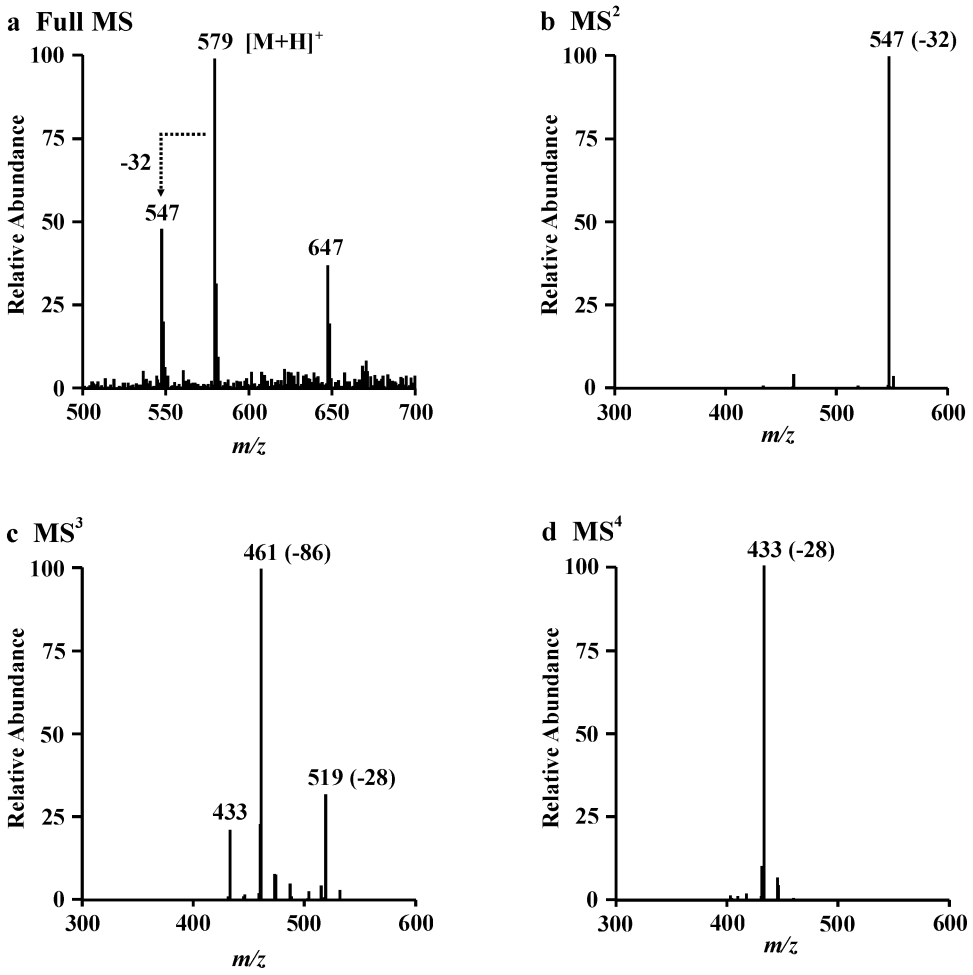

Figure 2.9. APCI multistage tandem mass spectra of C-13[2] MeO-pphorb *a* (**36**, P31); a) Full MS, b) MS^2, c) MS^3, d) MS^4. In each case the most abundant ion was selected as the precursor for the next spectrum.

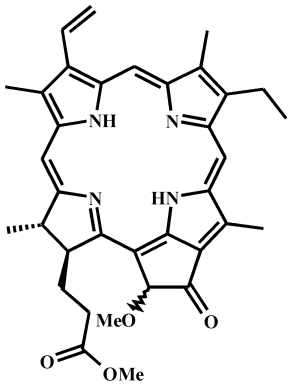

36

Despite being partially concealed beneath P31, it was possible to obtain MS^n spectra for chlorin P30 (Fig. 2.10). These contain notable ions consistent with losses of H_2O (-18 Da), CO (-28 Da), methanol (-32 Da), HCO_2Me (-60 Da), and $^{\cdot}CH_2CH_2CO_2Me$ (-87 Da). On the basis of these losses it appears that the compound possesses the core functionality of phorb *a*. Furthermore, the loss of H_2O suggests the presence of a hydroxyl group in the structure. Unfortunately, however, a structure could not be ventured for P30 that would explain its apparent chlorin-type UV/vis spectrum and mass spectral characteristics.

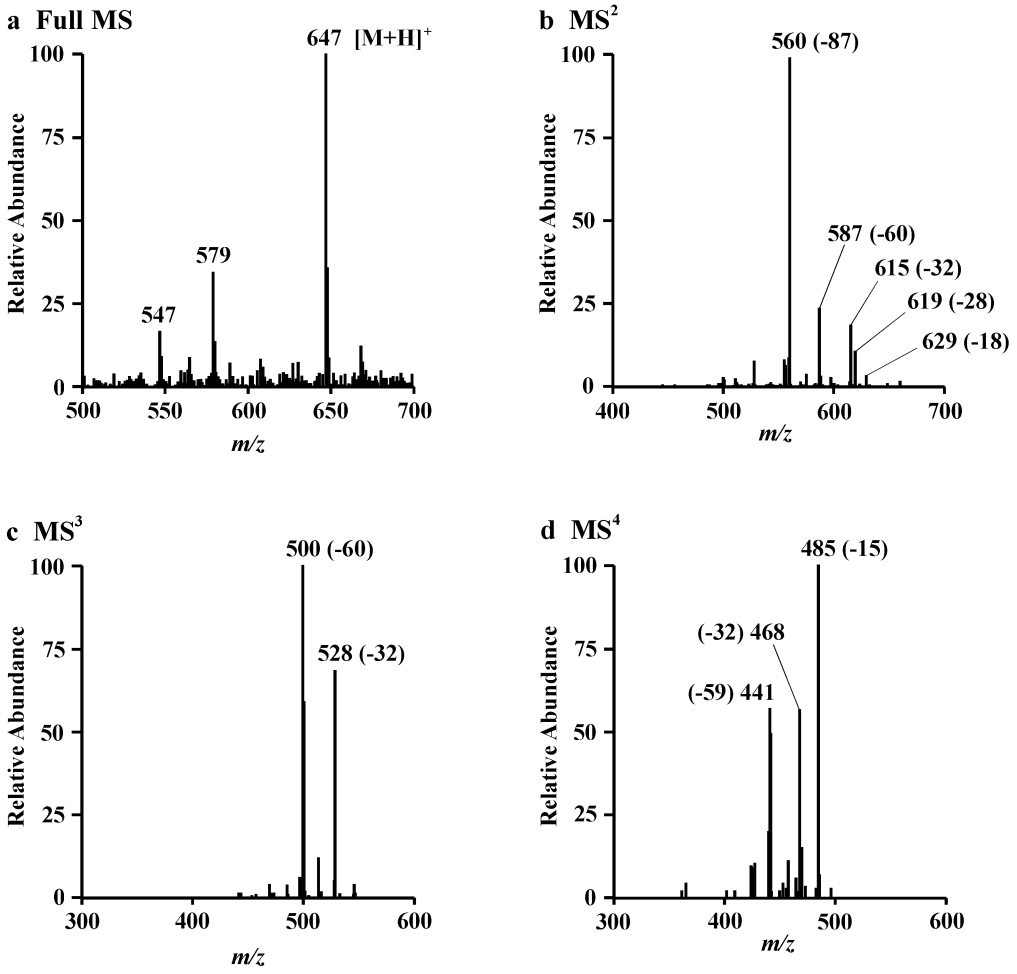

Figure 2.10. APCI multistage tandem mass spectra of chlorin P30; a) Full MS, b) MS^2, c) MS^3, d) MS^4. In each case the most abundant ion was selected as the precursor for the next spectrum.

Chlorin P28 (t_R = 30.5 min; λ_{max} 411, 665 nm; $[M+H]^+$ *m/z* 547) exhibits a slight red shift in the absorption maximum of its Soret band, possibly indicating an increase in conjugation. The protonated molecule is consistent with divinyl pphorb *a* in which the ethyl substituent at C-8 in pphorb *a* has been replaced by a vinyl group. The presence of ions in the MS^n spectra of P28 (not shown) arising from loss of an ethyl radical (-29 Da), however, contradicts such an assignment. Supported by a lack of ions pertaining to the loss of a methylpropionate ester group from C-17 this component was tentatively assigned as a methyl ether of chlone (**37**).

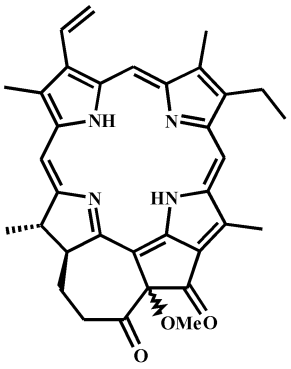

37

Notably the structure of chlone (**31**), which is the most likely precursor for **37**, lacks a free acid residue and consequently the manner by which this component was bound to the sediment matrix is less clear than for the components discussed previously. It does, however, possess oxygen-containing functional groups that could potentially participate in bonding, for example being esterified through its alcohol to a carboxylic acid.

2.2.3.2. Chlorins possessing a disrupted ring E

Several components P9, P11, P22 and P29 exhibit chlorin type UV/vis spectra with smoothed Soret bands (e.g. Fig. 2.5), indicative of a disrupted exocyclic ring E (Woolley et al., 1998; Airs et al., 2000). Chlorins P11 (t_R 23 min; λ_{max} 401, 668 nm) and P22 (t_R 28 min; λ_{max} 399, 670 nm) are isobaric and give rise to protonated molecules at *m/z* 653. The former displays sequential losses in MS^n (Fig. 2.11) consistent with purpurin-7 trimethyl ester (**38**).

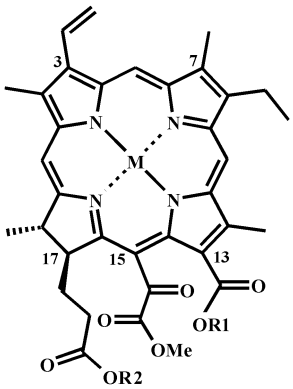

38: M = 2H, R1 = Me, R2 = Me

39: M = 2H, R1 = H, R2 = Phytyl

40: M = 2H, R1 = H, R2 = H

41: M = Mg, R1 = H, R2 = Phytyl

42: M = Mg, R1 = H, R2 = H

CID of the protonated molecule of P11 yields several product ions in MS^2 (Fig. 2.11b). The base peak ion at *m/z* 566 reflects a loss of 87 Da and can be attributed to α-cleavage of either the C-15 or C-17 substituents. The ion at *m/z* 593 represents a loss of 60 Da and can potentially arise via loss of a carbomethoxy group from the C-13, C-15[1] and C-17[2] positions, with hydrogen abstraction. Similarly, the ion at *m/z* 621 can arise via loss from any of the aforementioned substituents and corresponds to loss of methanol (-32 Da). CID of *m/z* 566 yields product ions in MS^3 (Fig. 2.11c) resulting from loss of the remaining C-15 or C-17 substituent (*m/z* 479, -87 Da), loss of $^{\cdot}CO_2Me$ from C-13 (*m/z* 507, -59 Da), loss of an ethyl radical from C-8 (*m/z* 537, -29 Da) and loss of a methyl radical through either α-cleavage of a methyl substituent or β-cleavage of the ethyl substituent (*m/z* 551, -15 Da).

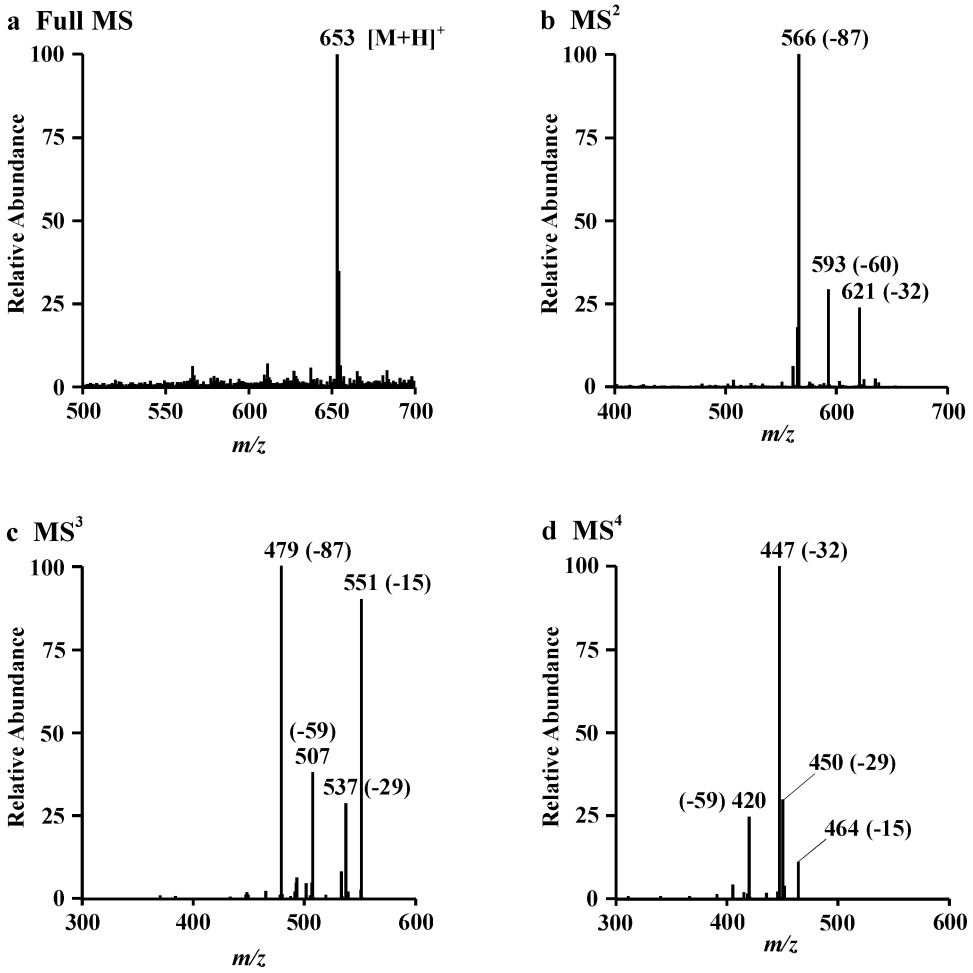

Figure 2.11. APCI multistage tandem mass spectra of purpurin-7 trimethyl ester (**38**, P11); a) Full MS, b) MS^2, c) MS^3, d) MS^4. In each case the most abundant ion was selected as the precursor for the next spectrum.

The oxidative cleavage of ring E that forms purpurin-7 in the natural environment affords a carboxylic acid at C-13 (Hynninen, 1991; Walker, 2004). Consequently purpurin-7 monomethyl phytyl ester (**39**) can become bound to the sediment through this substituent. Additional dephytylation at C-17[3] would yield a second carboxylic acid residue through which the compound may bind. Possible precursors for purpurin-7 trimethyl ester (**38**) in the methanolysis extract are, therefore, purpurin-7 monomethyl phytyl ester (**39**), purpurin-7 monomethyl ester (**40**) and their Mg-containing counterparts (**41** and **42**, respectively).

.

Chlorin P22 experiences losses in MS^n analogous to those observed for C-15[1] MeO-lact-chl *a* (Jie et al., 2002; Walker et al., 2003) and is consistent with C-15[1] MeO-lact-phorb *a* (**43**). Differences between the MS^n spectra of the two molecules arise primarily from the presence of a phytyl esterifying alcohol in C-15[1] MeO-lact-chl *a*, where loss of this group as phytadiene forms the base peak in MS^2 (Jie et al., 2002). CID of the protonated molecule of C-15[1] MeO-lact-phorb *a* (**43**, $[M+H]^+$ *m/z* 653) yields ions in MS^2 (Fig. 2.12b) arising via loss of methanol from C-15[1] (*m/z* 621), loss of $^{\cdot}CO_2Me$ from C-15[1] (*m/z* 594), and concomitant loss of $^{\cdot}CO_2Me$ and a methyl radical (*m/z* 579). The ion at *m/z* 535 represents a loss of 118 Da from the protonated molecule of C-15[1] MeO-lact-phorb *a* ($[M+H]^+$ *m/z* 653) and corresponds a further loss of 86 Da from the base peak ion in MS^2 ($[M+H\text{-}MeOH]^+$ *m/z* 621). Thus, this ion could potentially arise from loss of methanol (-32 Da) in combination with loss of the C-17 methyl propionate ester substituent with back transfer of hydrogen to the charge-retaining fragment (-86 Da). Absence of this ion from the MS^3 spectrum generated from CID of *m/z* 621 suggests otherwise. Loss of 118 (Da) is observed in the MS^n spectra of C-15[1] MeO-lact-chl *a* (Jie et al., 2002; Walker et al., 2003), which carries a phytyl ester instead of a methyl ester at C-17[3], and was attributed to loss of $MeOCOCO_2Me$ originating from the scission of two bonds involved in the lactone ring. Accordingly, the ion at *m/z* 535 can be attributed to the same dissociation. The MS^3 and MS^4 spectra (Fig. 2.12c and d) contain ions resulting from losses of HCO_2Me (-60 Da) from C-15[1] and C-17[2] and CO (-28 Da) from C-13[1].

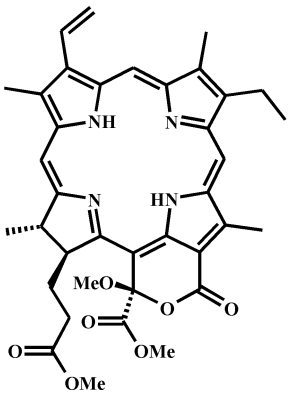

43

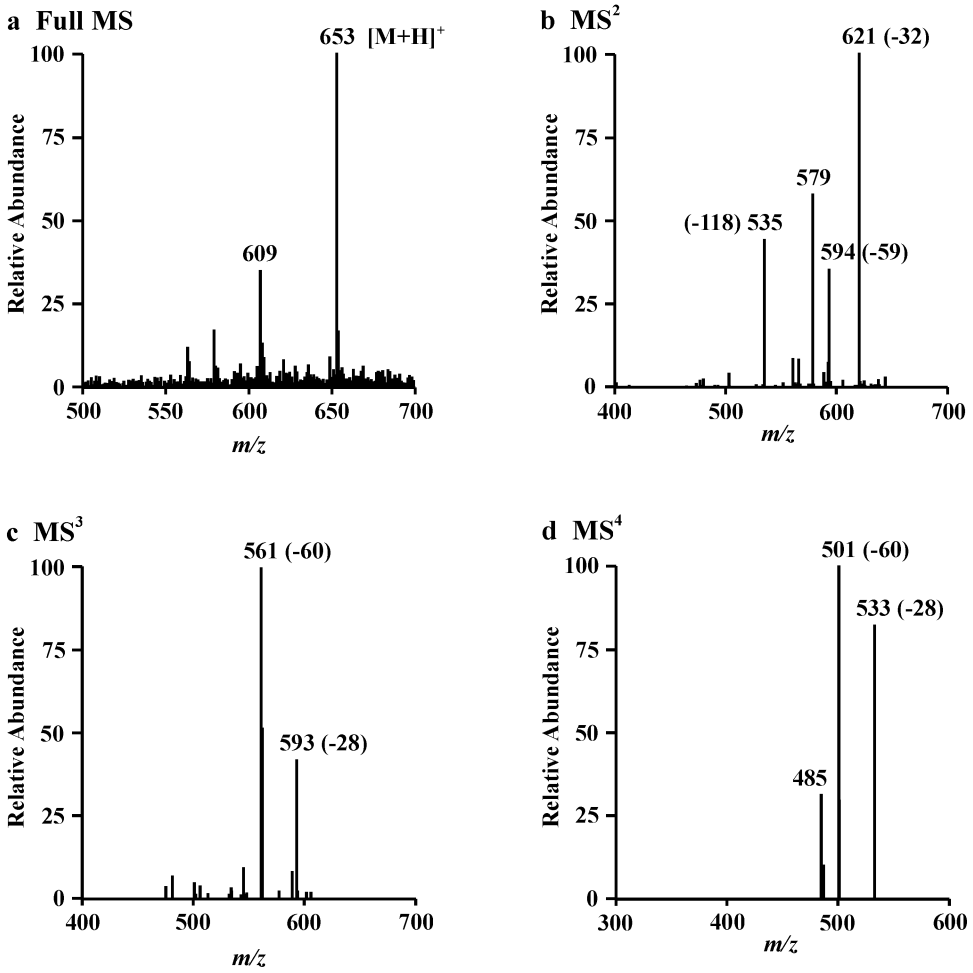

Figure 2.12. APCI multistage tandem mass spectra of C-15[1] MeO-lact-phorb *a* (**43**, P22); a) Full MS, b) MS^2, c) MS^3, d) MS^4. In each case the most abundant ion was selected as the precursor for the next spectrum.

Chlorin P9 gives rise to a protonated molecule at *m/z* 581 (Fig. 2.13a). The MS^n spectra of this component display similar losses to the compounds described previously. CID of *m/z* 581 yields several product ions in MS^2 (Fig. 2.13b). The base peak ion at *m/z* 508 represents a loss of 73 Da corresponding to loss of $^{\cdot}CH_2CO_2Me$ which could potentially originate from β-cleavage of the methyl propionate ester substituent or loss of a group such as that at the C-15 position of chlorin e_6 (**29**). The latter scenario appears more likely given the presence, in MS^2 and MS^3 (Fig.2.13b and c), of an ion at *m/z* 421, representing a further loss of 87 Da from the base peak ion *m/z* 508 that may be attributed to α–cleavage of the C-17 methyl propionate ester. Additional ions in MS^2 arise via loss of an ethyl radical (*m/z* 552) and loss of $^{\cdot}CH_2CO_2Me$ in combination with loss of methanol (*m/z* 476). Further ions in MS^3 and MS^4 (Fig. 2.13c and d) result from losses of methyl and ethyl radicals. On the basis of

UV/vis and mass spectral data this component was tentatively assigned as the ring opened chlorin, **44**. Such a structure could arise from decarboxylation at the C-13 position of chlorin e_6 (**29**).

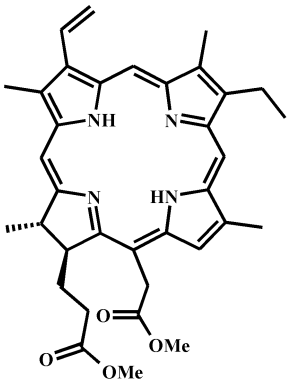

44

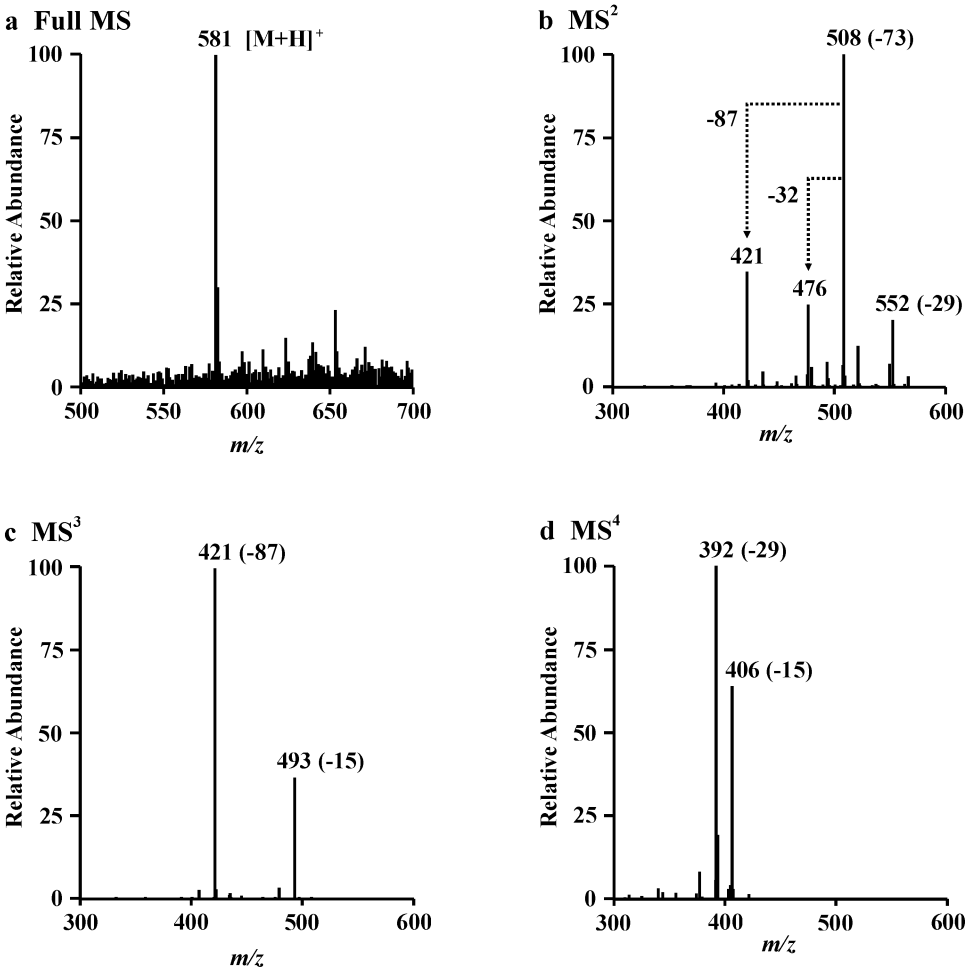

Figure 2.13. APCI multistage tandem mass spectra of the ring opened chlorophyll derivative (**44**, P9); a) Full MS, b) MS^2, c) MS^3, d) MS^4. In each case the most abundant ion was selected as the precursor for the next spectrum.

Chlorin P29 (λ_{max} 398, 667 nm; $[M+H]^+$ *m/z* 563) was tentatively assigned, on the basis of its UV/vis spectrum and fragment ions in MS^n (Table 2.1), as the ring E-opened derivative of chlone, chlorophyllonic acid methyl ester (**45**) which has been reported to occur alongside chlone in clams (Watanabe et al., 1993). Notable features of the MS^n spectra of this compound include ions arising from prominent losses of 60 Da and 59 Da, pertaining to loss of a carbomethoxyl group with and without hydrogen abstraction, loss of 28 Da indicating the existence of a carbonyl and, interestingly, no losses to suggest the presence of a methyl propionate ester at C-17. These observations are all consistent with the putative structure, chlorophyllonic acid methyl ester (**45**).

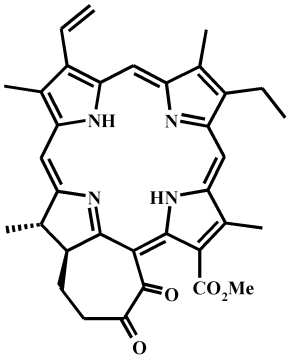

45

Chlorin P37, eluting shortly after pphorb *a*, exhibits a distinctive UV/vis spectrum characteristic of purpurin–18 (Fig. 2.7). The protonated molecule of this component ($[M+H]^+$ *m/z* 579) and its MS^n spectra confirm it to be the methyl ester of purpurin-18 (**46**) (Naylor and Keely, 1998; Walker and Keely, 2004).

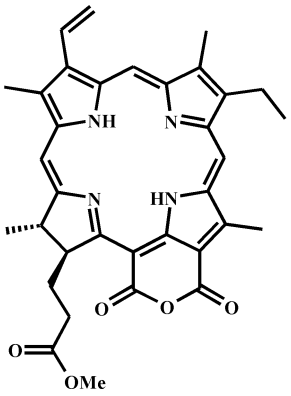

46

2.2.3.3. Porphyrins

The UV/vis spectra of components P14, P25, P27, P33, P34 and P36 feature a prominent Soret band but lack a strong absorption band in the red region of the spectrum (e.g. Fig. 2.14), identifying these components as porphyrins. Unfortunately, owing to their low abundance, protonated molecules for porphyrins P14, and P36 could not be assigned, precluding their structural identification. Porphyrin P34, eluting prior to pphorb *a* methyl ester, exhibits an online UV/vis spectrum (Fig. 2.14a) with maximal absorbance at 400 nm, a protonated molecule ($[M+H]^+$ *m/z* 591) and MS^n spectra (Fig. 2.15) consistent with protoporphyrin-IX dimethyl ester (**47**).

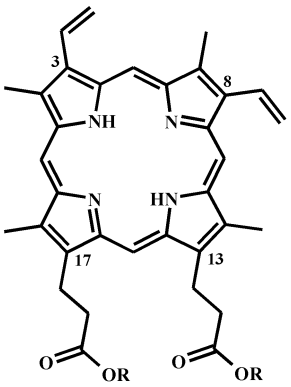

47: R = Me

48: R = H

Prominent ions in MS^n reflecting loss of 87 Da and 73 Da arise from α and β-cleavage of the methyl propionate ester substituents at C-13 and C-17. Additional product ions arise from α-cleavage of a methyl substituent to lose a methyl radical (-15 Da) and loss of methanol (-32 Da) from one of the methyl esters. Protoporphyrin-IX (**48**) is a biosynthetic precursor of both chlorophyll and heme (Leeper, 1985). Heme is the Fe complex of **48** and is present in almost all living organisms (cytochromes etc.; Killops and Killops, 2004). Heme and protoporphyrin-IX each possess two propionic acid substituents at C-13 and C-17, making them more likely to become bound, and form stronger associations, than deesterified chlorophylls, which possess one propionic acid substituent. Previously, the closest functionalised derivative of heme recognised in the sedimentary record was mesoporphyrin-IX (the C-3, C-8 diethyl analogue of protoporphyrin-IX), identified as the nickel complex and

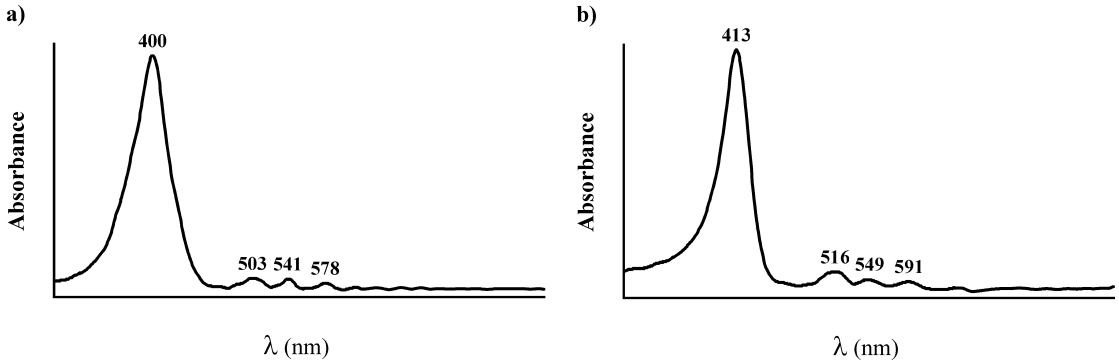

Figure 2.14. Online UV/vis spectra (300-800 nm) of porphyrins a) protoporphyrin-IX dimethyl ester (**47**, P34) and b) the rearranged phaeoporphyrin c_2 derivative (**49**, P33).

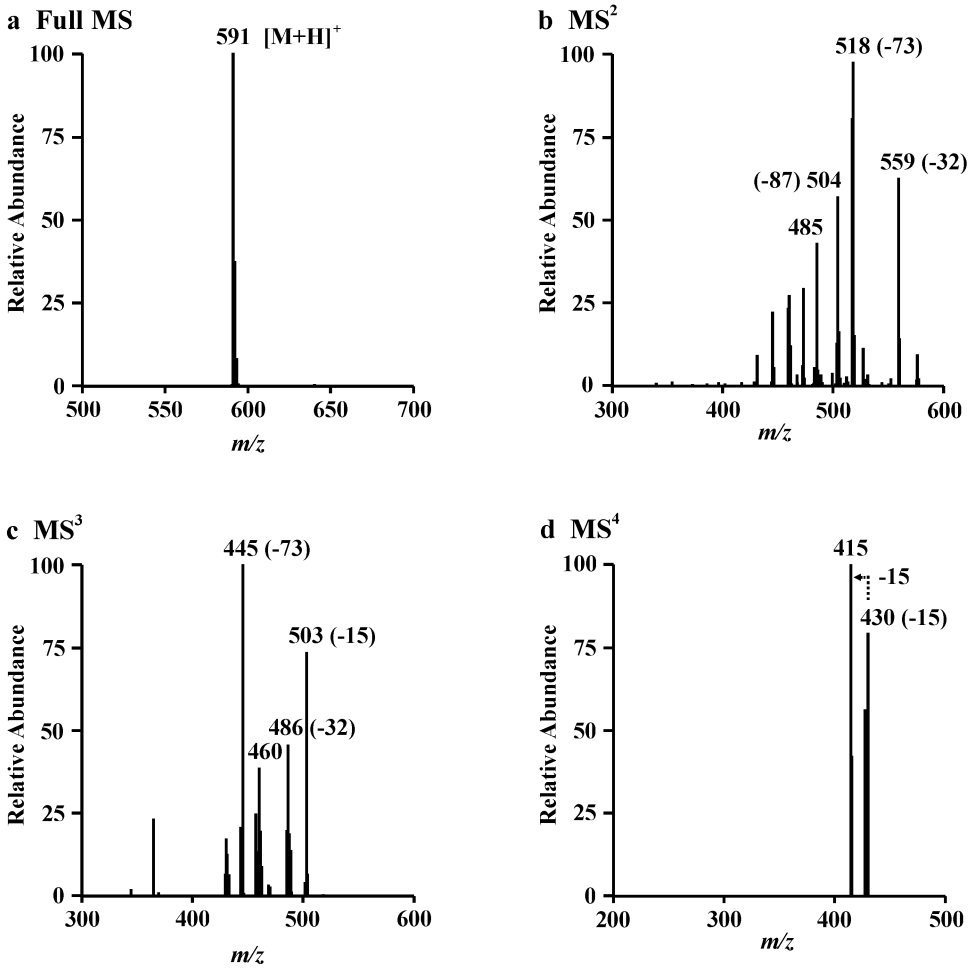

Figure 2.15. APCI multistage tandem mass spectra of protoporphyrin-IX dimethyl ester (**47**, P34); a) Full MS, b) MS^2, c) MS^3, d) MS^4. In each case the most abundant ion was selected as the precursor for the next spectrum.

released in appreciable amounts by hydrolysis of previously extracted Messel oil shale (Huseby and Ocampo, 1997). Hence, the occurrence of protoporphyrin-IX described here, in the methanolysis extract from an Antarctic marine core, represents the closest structural relative to heme identified in sediments to date.

Porphyrins P14, P25, P33, and P36 are proposed to be derivatives of chl *c* which, unlike other chlorophylls, possesses a fully unsaturated porphyrin macrocycle. Porphyrin P33 displays an online UV/vis spectrum with a Soret band at 413 nm (Fig. 2.14b) and protonated molecule at *m/z* 633 (Fig. 2.16a). CID of *m/z* 633 generates prominent ions in MS^2 (Fig. 2.16b) arising from loss of methanol (-32 Da) to form the base peak (*m/z* 601), loss of HCO_2Me (-60 Da,) to form the ion at *m/z* 573, combined loss of methanol and HCO_2Me to form the ion at *m/z* 541, loss of two molecules of methanol to form the ion at *m/z* 569 and loss of $^{\cdot}CH_2CO_2Me$ (-73 Da) to form the ion at *m/z* 560. These losses are also observed in MS^3 and MS^4 (Fig. 2.16c and d) accompanied by loss of CO (-28 Da). Notably, loss of CO only becomes apparent after prior loss of methanol suggesting perhaps that both originate from the stepwise dissociation of a carbomethoxyl group. Losses of HCO_2Me provide evidence for at least two carbomethoxyl groups in the structure of P33 with the possibility of a third, taking into account the losses of methanol and CO. Furthermore, the loss of $^{\cdot}CH_2CO_2Me$ indicates that at least one carbomethoxy group is attached to a CH_2 unit. On the basis of the UV/vis and mass spectral data the structure of P33 was tentatively assigned as **49**, a rearranged derivative chlorophyll c_2. Notably, no other feasible structure could be proposed that could provide a satisfactory explanation for the analytical characteristics of P33.

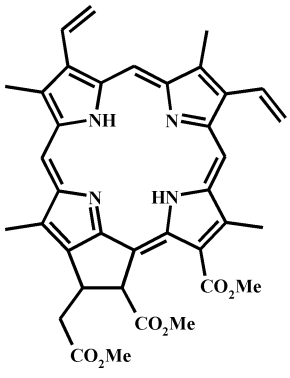

49

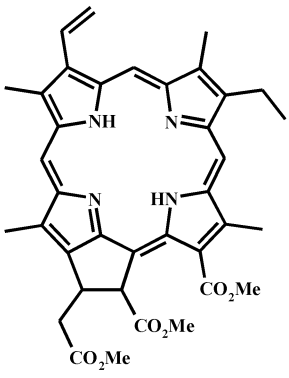

50

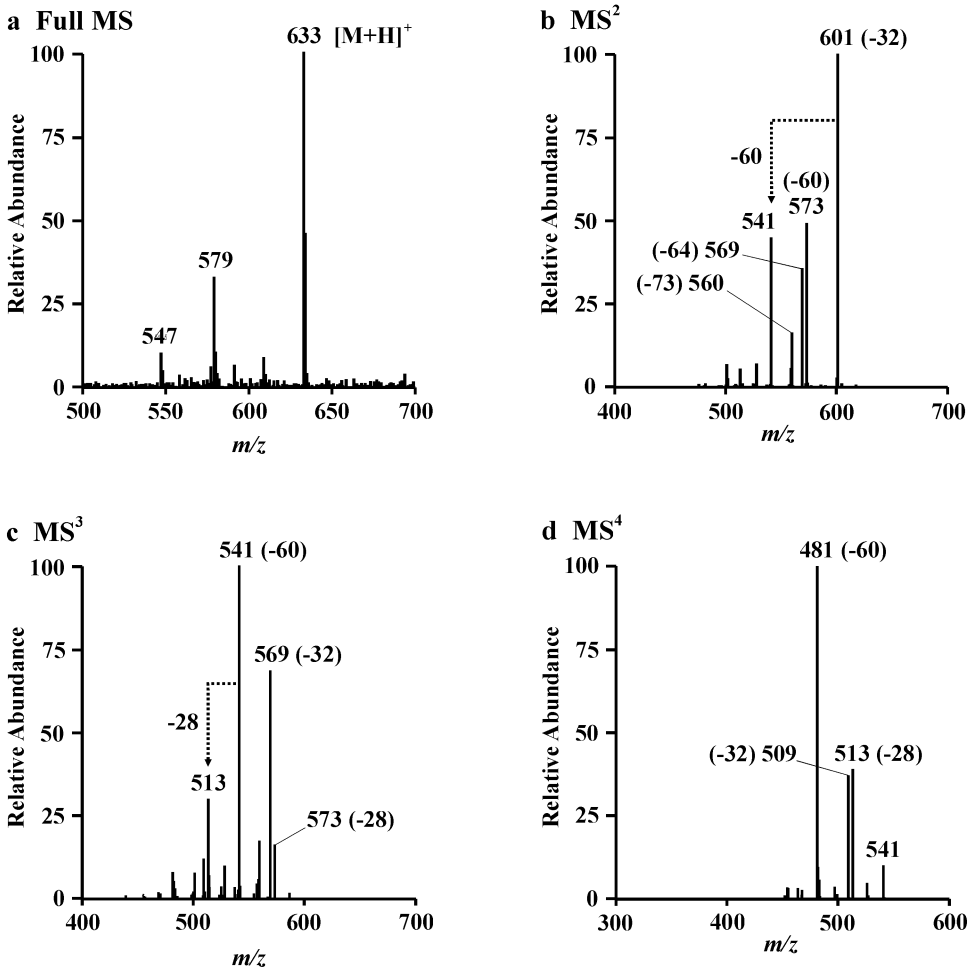

Figure 2.16. APCI multistage tandem mass spectra of the rearranged phaeoporphyrin c_2 derivative (**49**, P33); a) Full MS, b) MS^2, c) MS^3, d) MS^4. In each case the most abundant ion was selected as the precursor for the next spectrum.

The formation of a 5 membered exocyclic ring encompassing positions C-15 and C-17, such as that proposed for **49**, can arise via a rearrangement involving the acrylic acid group of chl c_2 and the neighbouring ketoester and is known to be facilitated by methanolic HCl (Dougherty et al., 1970). Such a rearrangement is known to occur in nature and permits sedimentary alkyl porphyrins containing this motif to be unequivocally ascribed an origin from chl *c* precursors (Callot and Ocampo, 2000). In the case of porphyrin P33, the formation of the C-15, C-17 exocyclic ring is most likely to be an artefact of the extraction. Nevertheless, the presence of this component provides evidence for an input of chl c_2 that is lacking from the acetone extracts. A minor component of the extract, porphyrin P25, exhibits a protonated molecule at *m/z* 635 and similar losses to those of **49** during MS^n (Table 2.1), suggesting it to be the phaeoporphyrin c_1 analogue (**50**).

Chls $c_{1\text{-}3}$ (**6-8**) possess an acrylic acid side chain at C-17. While phytyl-esterified chl *c* derivatives have been identified (Bidigare et al., 1990), chls *c* for the most part lack an esterifying alcohol (Sheer, 1991). The presence of an unesterified acrylic acid moiety may render chls $c_{1\text{-}3}$ more susceptible to sequestration to form solvent inextractable structures than chl *a*, which requires a prior dephytylation step, and can explain the absence of the former in the acetone extract.

2.2.3.4. Authentication of the extracted components

With the exception of the aforementioned transformations (demetallation, transesterification and methylation of free acids) expected to occur during extraction, the question remains as to whether the oxidation products observed in the acid extract are genuine sedimentary transformation products or artefacts of the extraction process. Autoxidation of chl *a* and its derivatives possessing a carbomethoxy group at C-13^2 is known to occur on standing in methanolic solution (Hynninen, 1991; Jie et al., 2002; Walker, 2004). Notably, however, the reaction, which involves the initial formation of an enolate anion following loss of the labile C-13^2 proton, is inhibited by acid (Hynninen, 1991). Nevertheless, in order to ascertain the authenticity of the acid extracted compounds, chl *a*, present in concentrations comparable to those of the components in the sediment extracts, was submitted to the methanolysis procedure. Furthermore, given the possibility that components of the sediment matrix may catalyse oxidative transformations of chl *a*, the procedure was repeated in the presence of either silica gel or previously acid-extracted sediment. In all cases, trace amounts of C-13^2 HO-phorb *a* (**35**) and C-15^1 MeO-lact-phorb *a* (**43**) were observed, although at considerably lower levels than those observed in the methanolysis extracts. Thus, the chlorophyll-derived oxidation products may be considered genuine.

2.2.4. Analysis of the sediment core

2.2.4.1. Pigment distributions

All samples from marine core PC461 were subjected to extraction with acetone followed by a further methanolytic extraction (Fig. 2.17). Extracts were analysed by HPLC and LC-MS^n.

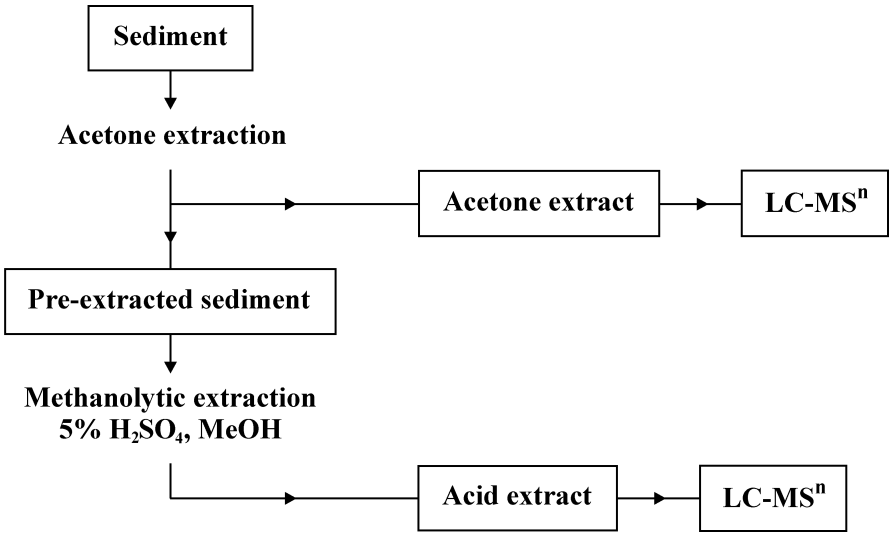

Figure 2.17. Flow diagram showing the extraction procedure for the marine sediment samples.

With the exception of the horizon at 541 cm, the extracts from all depths sampled contained photosynthetic pigments. Chl *a* derived components comprised the major portion of the tetrapyrroles present, indicating the occurrence of oxygenic photoautotrophy at the time of deposition.

The RP-HPLC chromatograms of the acetone and methanolysis extracts from samples taken from the first 7 m of the core resembled those of the preliminary sample (Fig. 2.3). The acetone extracts were consistently dominated by the carotenoids fucoxanthin and diatoxanthin and chl *c*-derived pigments could be identified in some of the corresponding methanolysis extracts with a minimum chl *a*:*c* ratio of 4.9, which falls within the range reported for marine diatoms 1.65-7.25 (Stauber and Jeffrey, 1988), suggesting that diatoms were the major class of photoautotroph during this

period. This is consistent with the wealth of diatom cysts evident throughout the core and similar to the situation in the contemporary environment (Sigleo et al., 2000). As observed for the preliminary sample, phe *a* and pphe *a* were typically the major acetone extractable tetrapyrrole components and were accompanied by various oxidation products, including C-13^2 HO-phe *a*, chlorin e_6, purpurin-7 phytyl ester and purpurin-18 phytyl ester. In addition, several dephytylated derivatives of chl *a* were present in varying abundance including chlone, phorb *a* and pphorb *a*, the latter two of which have been linked with both grazing and senescence. Chl *a* itself (λ_{max} 432, 665 nm; $[M+H]^+$ *m/z* 871) was only present in acetone extracts from horizons taken from the first centimetre and at 50 cm depth and was not detected in the deeper samples. Acid methanolysis consistently liberated appreciable quantities of bound tetrapyrroles with distributions similar to that of the preliminary sample (Fig. 2.3b) and enriched in phaeophorbides and oxidative transformation products of chlorophyll.

The chromatograms of acetone and methanolysis extracts from the two deepest horizons sampled (741 cm and 842 cm) revealed distinctly different pigment distributions. Acetone extracts from these depths (e.g. Fig. 2.18a) contain predominantly phe *a* (P41), pphe *a* (P44), C-13^2 HO-phorb *a* (P8), chlone (P7) and a series of late eluting components identified as pphorb *a* steryl esters (P45-P49). Steryl chlorin esters have been associated with zooplankton herbivory and are indicative of an active population of grazers at the time of deposition (Harradine et al., 1996; Talbot et al., 1999). By comparison with the acetone extracts from the upper portion of the core, the contribution from carotenoids in the extracts from the two deepest horizons was small and consisted of two main components, P4 (λ_{max} 482 nm) and P23 (λ_{max} 447, 475 nm) with no evidence for the presence of fucoxanthin or diatoxanthin. Unfortunately the protonated molecules of P4 and P23 could not be identified, preventing their structural assignment.

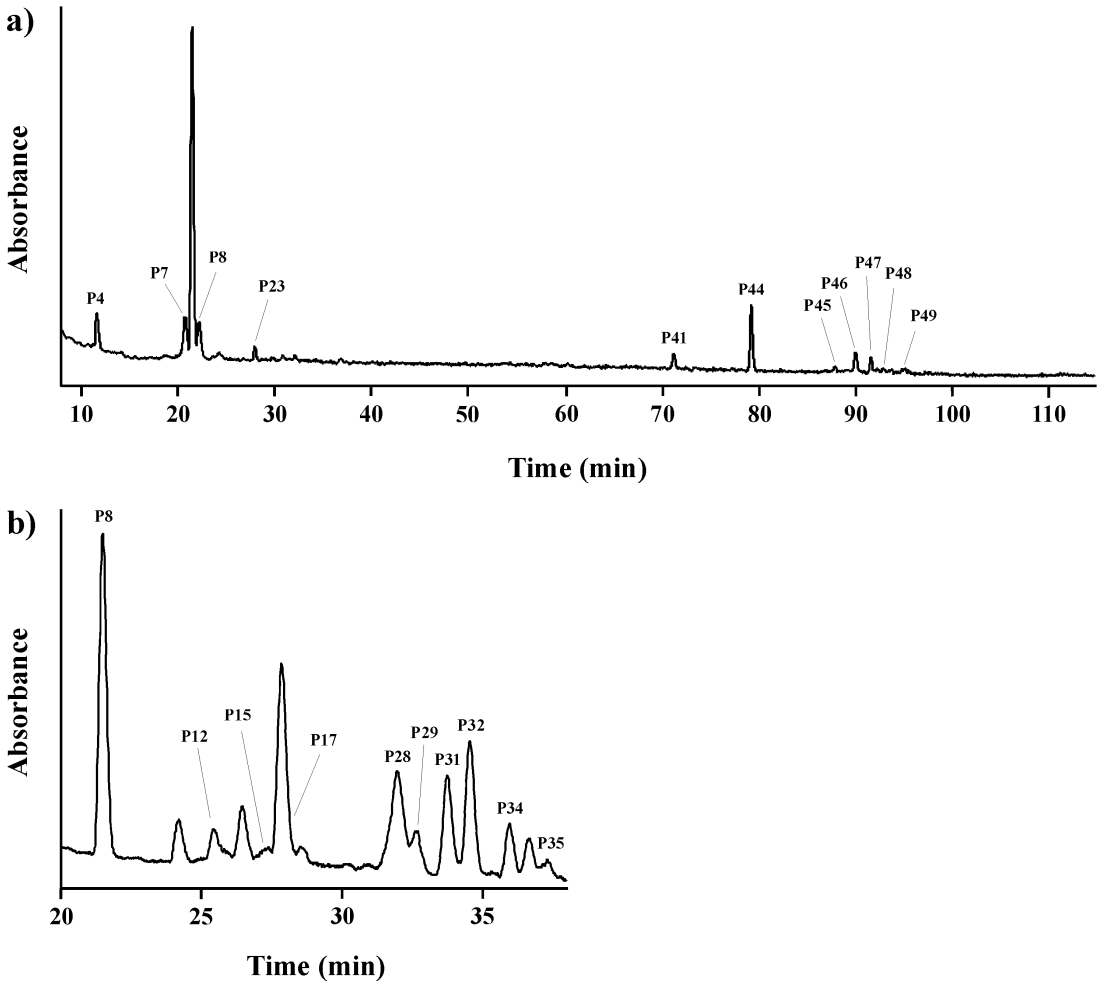

Figure 2.18. Partial RP-HPLC-PDA maxplot chromatograms (300-800 nm) of extracts from 741-742 cm depth extracted by a) acetone and b) methanolysis. Components of the extracts were eluted using the gradient programmes Method A and B (Airs et al., 2001), respectively. For peak assignments see Table 2.1.

The methanolysis extracts from 741 cm and 842 cm depth (e.g. Fig. 2.18b) contained several components observed previously, including HO-phorb *a* (P8), phorb *a* (P17) and pphorb *a* (P35), although no derivatives of chl *c* could be identified. Components P12 and P15, however, exhibited UV/vis spectra reminiscent of free base chl *b* derivatives (Fig. 2.19). On the basis of their retention time and protonated molecules ($[M+H]^+$ *m/z* 621), P12 and P15 could be assigned as phorb *b* (**51**) and its epimer, respectively (Squier et al., 2002). The occurrence of derivatives of chl *b* can be attributed to an input from green algae (Chlorophyta), since a contribution from higher plants is unlikely given the location of the core site. The lack of diatom-derived pigments detected below 640 cm depth, coupled with the prescence of chl *b*

transformation products may indicate an earlier photoautotrophic community in which green algae comprise a significant portion. Thus, there appears to have been a major change in the photoautotrophic community ca. 38 ka (raw radiocarbon age, Fig. 2.2).

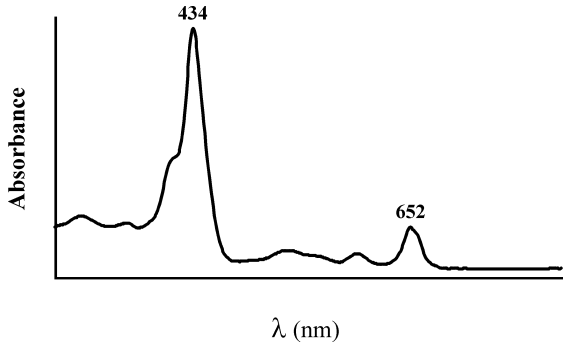

Figure 2.19. Online UV/vis spectrum (300-800 nm) of phorb *b* (**51**, P12)

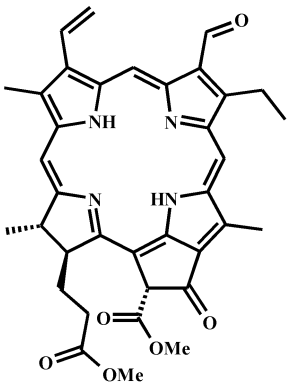

51

2.2.4.2. Stratigraphic profiles

Chlorophyll concentrations can be used to estimate the intensity of primary productivity in times past (Harris et al., 1996). The depth profiles for the amount of total chlorophyll extracted by acetone (Fig. 2.20a) and methanolysis (Fig. 2.20b) reveal significant vertical variations as well as differences between the two fractions. For the majority of horizons, substantial amounts of bound chlorophylls were liberated by methanolysis. The highest concentrations of bound pigment were found at 25 cm and 327 cm depth, in each case representing over twice the amount of acetone-extracted chlorophyll. While generally high levels of chlorophyll oxidation products were observed in both acetone (Fig. 2.20a) and acid extracts (Fig. 2.20b), the

latter were disproportionately so, most likely reflecting the increased propensity of oxidised pigments to take part in sequestration processes.

Given the significant variations in the pigment distributions apparent between acetone and acid extracts, both pools should be considered together in order to provide a faithful reproduction of past conditions. Fig. 2.20c shows the depth profile for the total chlorophyll and chlorophyll oxidation products for the combined extracts. Down core variations in total chlorophyll indicate changes in productivity and/or preservation (Harris et al., 1996) and variations in the amount of oxidation products indicate fluctuations in the oxicity of the water column.

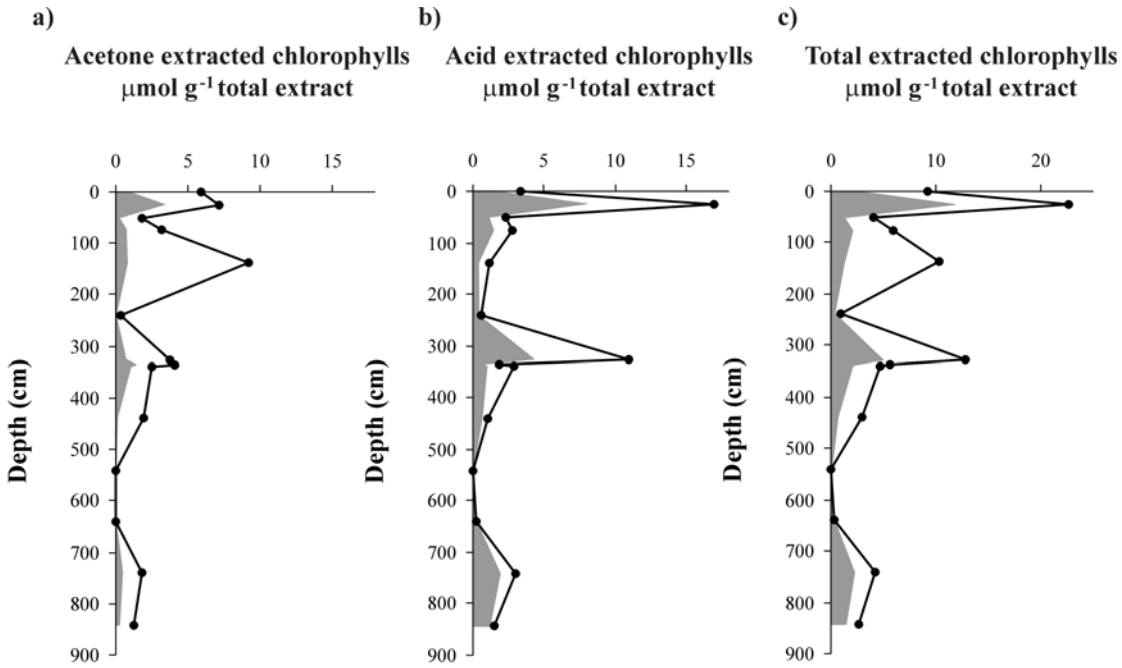

Figure 2.20. Depth profiles for a) acetone extract b) acid extract c) combined acetone and acid extracts. Black line shows the abundance of total chlorophyll derived pigments. Shaded area shows the portion represented by oxidised chlorophyll derivatives. Abundances were normalised per g of total material extracted by both acetone and acid techniques. Tie lines represent values interpolated between sampling intervals.

Interestingly, the molar ratios of bound:free pigments (Fig. 2.21a) and oxidised:unoxidised chlorophylls from the combined extracts (Fig. 2.21b) display similar profiles. A scatter plot of the two ratios shows a linear correlation (broken line Fig. 2.22), with an R^2 value of 0.7795. Notably, two samples (open points Fig. 2.22) appear to have undue influence on the correlation and the potential to create the false impression of a trend. Accordingly, the data from these horizons were excluded. This resulted in a reasonable, albeit weaker, linear correlation (unbroken line, R^2 = 0.6847, Fig. 2.22), suggesting that a relationship exists between the two parameters. The correlation shows an increasing proportion of bound pigment with an increasing proportion of oxidation products. This is perhaps not surprising considering the greater potential of pigments that have suffered oxidative transformations, such as ring-opened chlorophylls, to participate in sequestration reactions. The non-zero intercept with the y-axis indicates the possibility of a bound pigment component in the absence of oxidation products and may reflect the ability of non-oxidised chlorophyll transformation products, such as those deesterified at C-17[3], to become bound through their C-17 propionic acid group.

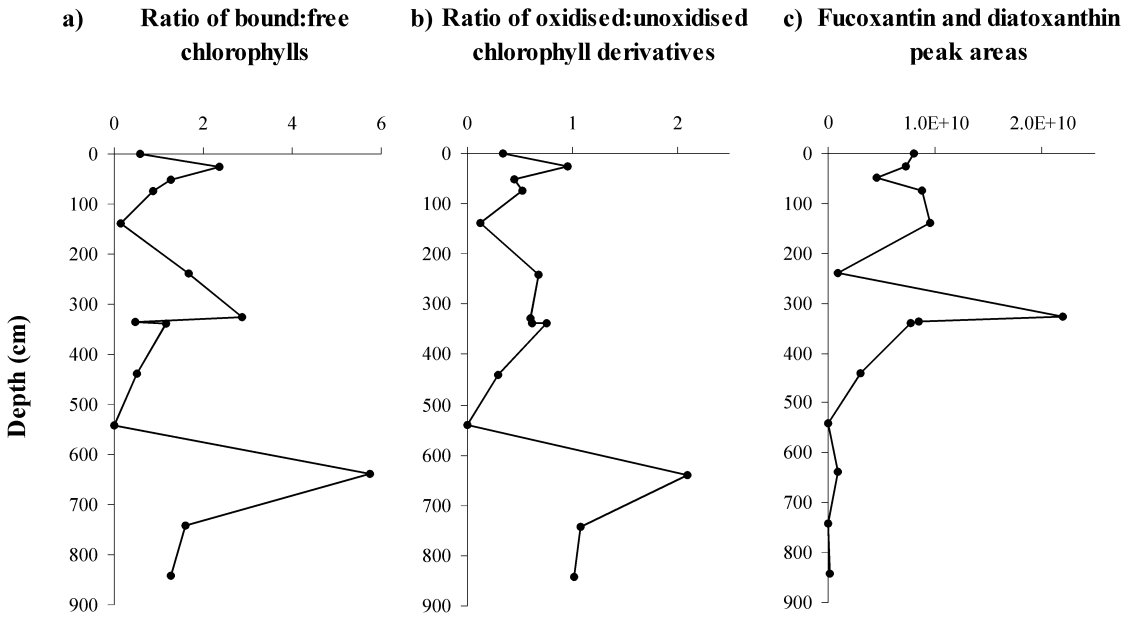

Figure 2.21. Depth profiles of a) the molar ratio of bound:free (acid extractable:acetone extractable) chlorophylls, b) the molar ratio of oxidised:unoxidised chlorophyll derivatives and c) the summed fucoxanthin and diatoxanthin peak areas normalised per gram of extract.

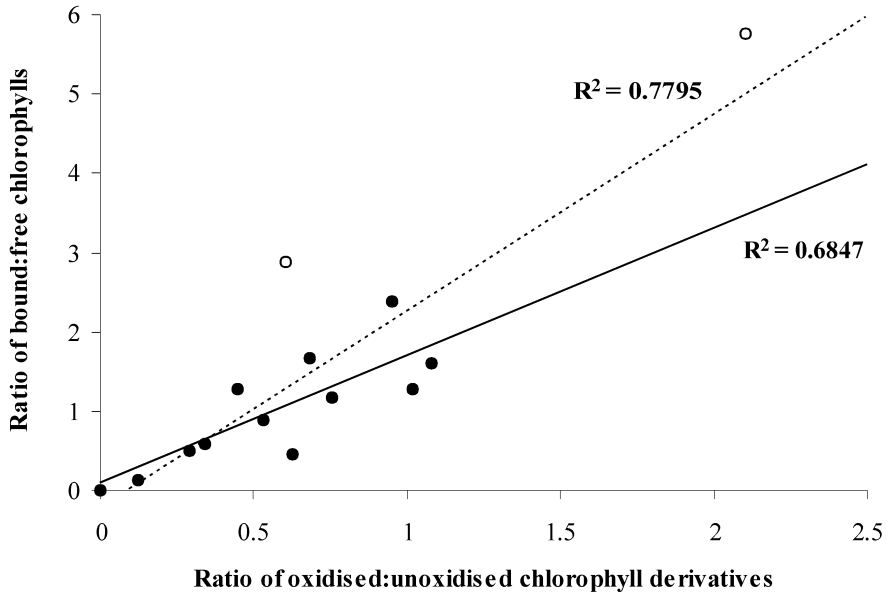

Figure 2.22. Scatter plot showing the molar ratio of bound:free (acid extractable:acetone extractable) chlorophylls versus the molar ratio of oxidised:unoxidised transformation products of chl *a*. Open points were excluded from the unbroken line of best fit.

As diatom cysts represent an abundant component of the sediment that can potentially bind chlorophylls, the ratio of bound:free pigments (Fig. 2.21a) was compared to summed peak areas of fucoxanthin and diatoxanthin (Fig. 2.21c), used to indicate the magnitude of the diatom input to the sediment. The depth profiles for the two parameters are markedly different and a scatter plot of the two confirmed the absence of a correlation. Thus, it appears that the available binding surfaces (e.g. diatom frustules) are not limiting and that the major control on the sequestration of chlorophyll pigments is the degree of oxidation.

The high carotenoid to chlorophyll ratios observed in many of the extracts deserve comment. In addition to aiding light capture, carotenoids fulfil a variety of photoprotective roles within photosynthetic organisms including roles as radical scavenging antioxidants, quenching singlet oxygen species and protecting photosystem II from photo-oxidation (Jialal et al., 1991; Telfer et al., 1991). Given that oxygen may become supersaturated in cold water and the evidence from chlorophyll oxidation products to support a highly oxygenated water column, the

biosynthesis of carotenoids by the organism may have been especially important to protect against oxidative damage.

2.3. Conclusions

Photosynthetic pigments indicating oxygenic primary production were detected throughout the core. The distributions indicate an early phase in which green algae formed a significant portion of the photoautotrophic population followed by the establishment of a community dominated by diatoms. The unprecedented levels of oxidative transformation products of chlorophyll support a highly oxygenated water column and indicate fluctuations in the extent of oxidation.

The analysis of this core presented a unique challenge. Conventional acetone extraction yielded an extract dominated by carotenoids with surprisingly little chlorophyll-derived pigment. This is thought to be due to selective retention of chlorophylls through binding e.g. to mineral grains or diatom cysts. Acid methanolysis liberated appreciable quantities of sequestered pigments whose distributions comprised abundant components believed to originate from deesterified chlorophyll derivatives and disproportionate amounts of oxidised and ring E-opened structures. Such components contain free acid groups and oxygen-containing structural elements that render them more likely to form associations (e.g. via ester linkages) with components of the sediment matrix. Apart from the transformations inherent during the extraction process, e.g. demetallation and transesterification, the acid liberated sedimentary species are thought to represent genuine natural components. In addition, some acid extracts revealed the presence of pigments derived from chls *b* and *c*, which were lacking from the distributions of acetone-extractable components. The major chl *c* derivatives have undergone a rearrangement in which a 5 membered ring, encompassing C-15 and C-17, has been created and ring E lost, forming structures analogous to those of some chl *c*-derived sedimentary alkyl porphyrins. Provided these are authentic natural transformation products and not artefacts formed in the extraction process, this is the first identification of functionalised sedimentary tetrapyrroles containing this structural motif. Furthermore, protoporphyrin-IX, observed among the compounds liberated by acid

methanolysis, represents the closest functionalised derivative of heme identified in sediments to date. In the case of protoporphyrin-IX, chl c_1 and chl c_2, the presence of free propionic acid substituents may predispose these compounds towards sequestration.

These findings illustrate that certain sedimentary pigments may be under represented, if at all, in the distributions of acetone-extractable components. Clearly methanolytic extraction has value in revealing compounds that would have been overlooked by simple acetone extraction alone and may be required in order to provide a faithful reconstruction of past productivity, community composition and environmental conditions.

Chapter 3:

Preparation and liquid chromatography-multistage tandem mass spectrometric characterisation of C-3[1] alkylthioether chlorophyll derivatives

Publication arising from the work detailed in this chapter:

Pickering M.D. and Keely B.J., 2008. Alkyl sulfur chlorophyll derivatives: Preparation and liquid chromatography-multistage tandem mass spectrometric characterisation of analogues of naturally occurring sedimentary species. Organic Geochemistry, 39, 1046-1050.

3.1. Introduction

3.1.1. Sedimentary alkylthioether chlorophyll derivatives

A suite of novel sulfur-containing transformation products of chlorophyll has been identified in an immature lake sediment from Pup Lagoon, Antarctica, providing the best evidence to date for the sulfurisation of chlorophylls (Squier et al., 2003; 2004). The suite comprised derivatives of chl *a*, phe *a* and pphe *a*, each present as a series of homologues bearing alkylthioether groups containing between 1-5 carbon atoms attached to the C-3^1 position (alkylS-chl *a*, **21a-e**; alkylS-phe *a*, **22a-e**; and alkylS-pphe *a*, **23a-e**).

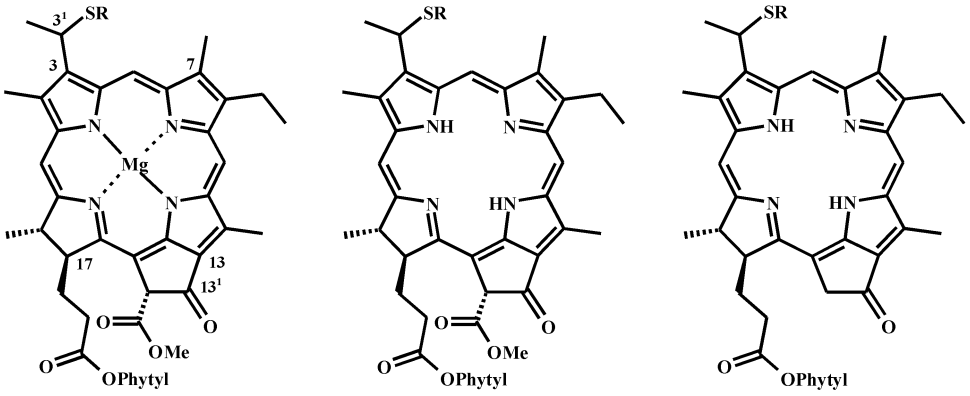

21 **22** **23**

R = Me (**a**), Et (**b**), *n*-Pr (**c**), *n*-Bu (**d**), *n*-Pent (**e**)

The precise mechanism of formation of these derivatives still remains to be established, as does their environmental significance and what they might reveal with regard to the potential of chlorophylls to become sequestered, via sulfur crosslinking reactions, into macromolecular structures. It is clear, from the presence of the alkylthioether derivatives in an immature sediment, that their formation takes place during early diagenesis and is likely to involve the reaction of an alkylthiol, alkylsulfide or alkylthiyl radical with the C-3 vinyl group of the precursor chlorophyll. Of the three principal mechanisms of sulfur incorporation outlined in Chapter 1 (Sections 1.6.1-1.6.3), radical addition and nucleophilic addition can be excluded since these would be expected to yield an alkylthioether moiety at the C-3^2 position (anti-Markovnikov). The attachment of the alkylthioether to the C-3^1

position observed for the derivatives is consistent with the electrophilic addition of an alkylthiol to the C-3 vinyl group, involving an initial protonation step, to yield the Markovnikov product (e.g. Equation 3.1). Laboratory reactions, conducted in acetone, have demonstrated the formation of small amounts of C-3[1] alkylthioether chlorophyll derivatives, via Markovnikov addition of decanethiol or butanethiol to the C-3 vinyl group of pphorb *a*, providing a rationale for the involvement of alkylthiols in the formation of the sedimentary alkylthioether chlorophyll derivatives (Pickering, 2005).

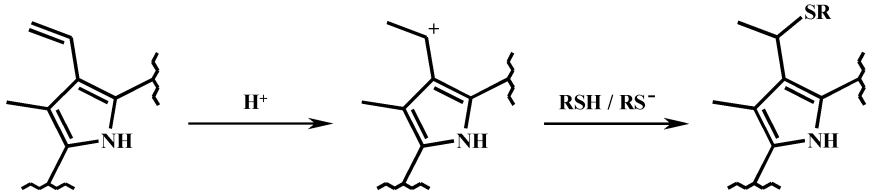

(3.1)

3.1.2. Alkylthiol sources in natural aquatic environments

Methanethiol is produced by numerous sources in the natural environment (Bentley and Chasteen, 2004). It has a short residence time, owing to its chemical and biological reactivity, and occurs at low steady state concentrations sustained by rapid production (Kiene, 1996). In marine ecosystems, methanethiol is derived primarily from the degradation of dimethylsulfoniopropionate (DMSP) (Lomans et al., 2002), which fulfils osmoprotectant and antioxidant roles within marine algae and bacteria (Groene, 1995; Bentley and Chasteen, 2004). In addition, DMSP is suggested to perform a cryoprotective function and occurs in high concentrations in green macroalgae collected from Arctic and Antarctic regions (Kirst et al., 1991; Karsten et al., 1992). Degradation of DMSP is, for the most part, divided between the formation of dimethyl sulfide (DMS) via the operation of lyase enzymes (Cantoni and Anderson, 1956; de Souza and Yoch, 1995) and the production of methanethiol via a suspected demethylation-demethiolation pathway (Kiene, 1996). DMS, originating from the former process, is the dominant sulfur volatile in marine surface waters (Kiene, 1996). It makes a substantial contribution to the flux of sulfur to the atmosphere and DMS-derived particles lead to rain acidification and act as cloud condensation nuclei modifying planetary albedo (Charlson et al., 1987). Formation of the reactive species, methanethiol, has been suggested to represent a significant redirection of DMSP-

sulfur away from climatically active DMS and towards its sequestration in the lithosphere, following reaction with particulates and dissolved organic matter (Kiene, 1996). Other sources of methanethiol include the enzymatic degradation of sulfur-containing amino acids and the methylation of sulfide by thiol methyltransferases or methyl transfer from methoxylated aromatic compounds (Bentley and Chasteen, 2004 and references therein). Any of these processes could potentially supply methanethiol for reaction with chl *a* and its derivatives.

Whereas the sources detailed above can explain the occurrence of the methylsulfur chlorophyll derivatives, the presence of more heavily alkylated homologues implies an additional/alterative input. Furthermore, the restricted range in alkyl chain length exhibited by the alkylthioether chlorophyll derivatives suggests a similarly constrained source of alkylthiols. The presence of short-chain alkylthiols containing between 1-4 carbon atoms has been reported in hypersaline microbial mats (Visscher et al., 2003). In addition to the thiols, DMS was observed (Visscher et al., 2003) and, together with methanethiol, was ascribed to the methylation of sulfide by an unspecified methyl group donor. No indication was given to explain the formation of the thiols other than methanethiol. It is possible that short-chain alkylthiols may be derived from the reaction of alkylhalides with sulfide (Equation 3.2).

$$\text{Alkyl-Hal} + HS^- \rightarrow \text{Alkyl-SH} + \text{Hal}^- \qquad (3.2)$$

Marine algae are considered to be the main producers of halocarbons in marine waters and the volatile components play important roles in the chemistry of the atmosphere (Carpenter, 2003; Gribble, 2003). Macroalgae (seaweeds) represent a significant source of halogenated C_1-C_4 hydrocarbons in coastal marine environments (Laturnus, 2001; Carpenter, 2003). In marine surface waters microalgae (phytoplankton) are the dominant photoautotrophs and are likely to be a major source of halocarbons, culture studies having clearly demonstrated their capacity to produce halogenated methanes (Itoh et al., 1997; Manley and de la Cuesta, 1997; Scarratt and Moore, 1998). Recently, it was observed that monoiodinated compounds with 1-3 carbon atoms are emitted from phytoplankton concentrates and detrital particles formed from the overturn of phytoplankton blooms (Hughes et al., 2008). Any of these short-chain

alkylhalogens could be converted into the corresponding alkylthiols via reaction with dissolved hydrogen sulfide (Equation 3.2).

It is perhaps noteworthy that the natural alkylthioether chlorophyll derivatives were only identified in the section of the Pup Lagoon sediment core deposited under marine conditions, throughout which markers for photic zone anoxia indicate that appreciable concentrations of dissolved sulfide were produced by an active sulfate-reducing bacterial community (Squier et al., 2004). Furthermore, the core sections containing high abundances of alkylthioether chlorophyll derivatives coincided with periods where diatom assemblages indicate long seasons free of ice cover (Squier, 2003), suitable for the development of phytoplankton blooms. It is, therefore, entirely plausible that alkylthioether chlorophyll derivatives are formed in sulfide rich environments by reaction with alkylhalogen-derived alkylthiols, possibly within senescing algal cells that encounter anoxic conditions.

3.1.3. Aims

The work described in this chapter represents an investigation into the reaction of the chlorophyll vinyl group with short chain alkylhalogens and H_2S, in simple laboratory systems, as a potential route to the formation of alkylthioether chlorophyll derivatives. The aims of this work were: to provide a basis for understanding the formation of alkylthioether derivatives in the sediment of Pup Lagoon; to validate the structures assigned by Squier et al. (2003; 2004); to develop suitable methods for the preparation of synthetic standards of alkylthioether chlorophyll derivatives in order to aid their detection, identification and quantification in environmental samples.

The reaction products described in this chapter are discussed primarily from the perspective of their identification, APCI LC-MS^n characterisation and the possible synthetic utility of their preparation. No attempt is made here to elucidate the mechanisms by which the products form. That work forms part of Chapter 4, where the reactions are discussed in greater detail and conducted in systems that provide a more accurate representation of natural conditions, enabling clear conclusions to be drawn as to the origins and environmental significance of some of the reaction products.

3.2. Results and Discussion

An earlier study demonstrated the addition of decanethiol and butanethiol to the C-3 vinyl group of the chl *a* derivative, pphorb *a*, to produce the corresponding alkylthioethers in modest yields (up to 9 %; Pickering 2005). The formation of the alkylthioether derivatives was promoted by the presence of the naturally occurring sulfur species, H_2S, which is believed to act as a proton source in an electrophilic addition of the alkylthiol to the pphorb *a* vinyl group (see Equation 3.1; Pickering, 2005). Those reactions, conducted in acetone, were extended here to involve the in situ generation of alkylthiols from the reaction of H_2S/HS^- with short-chain alkyliodides (Equation 3.2). Alkyliodides were suggested as a likely source of alkylthiols in the natural environment and their reaction with the C-3 vinyl group was investigated under a variety of conditions.

3.2.1. Reactions of pyrophaeophorbide *a* with methyliodide and H_2S in acetone

Reaction of a mixture of pphorb *a* methyl ester (**33**) and phorb *a* methyl ester (**32**) with methyliodide and H_2S in acetone led to partial conversion of the starting compounds, generating a complex mixture of products (Fig 3.1). The reaction products were identified based on their UV/vis and APCI-MS^n spectra (data collected in Table 3.1).

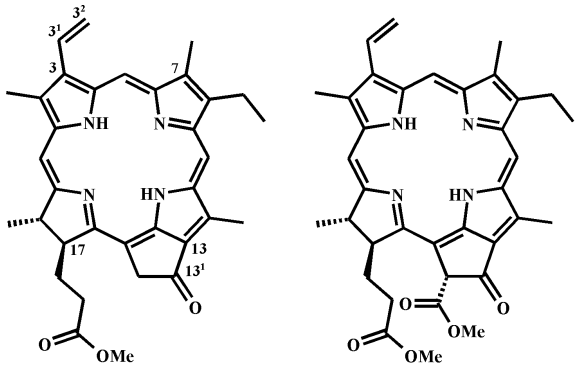

33 **32**

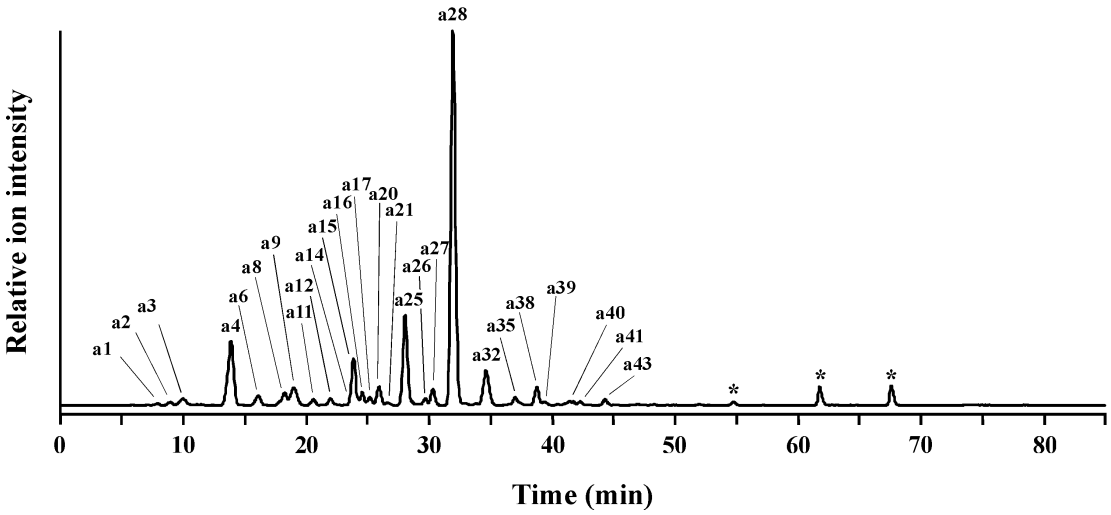

Figure 3.1. Representative mass chromatogram (*m/z* 400-1200) of the total extract from the reaction of a mixture of pphorb *a* (**33**) and phorb *a* (**32**) with methyliodide and H_2S in acetone. Peak assignments in Table 3.1. *Not pigments.

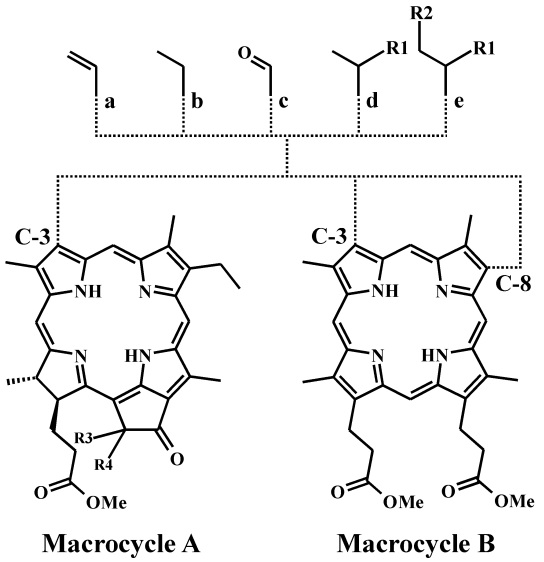

Table 3.1. Analytical data and structural assignments for the components identified in the reaction extracts.

Peak	$[M+H]^+$ (*m/z*)	Prominent ions in MS^n (*m/z*)‡	Macrocycle	C-3	C-8	R1	R2	R3	R4	Structure number
a1	641	623, 581, 521, 495, 435	A	e	n/a	OH	OH	COOMe	H	§
a2	583	565, 555, 523, 495, 409	A	e	n/a	OH	OH	H	H	**59**§
a3	625	607, 581, 565, 479, 435	A	d	n/a	OH	n/a	COOMe	H	**72**
a4	567	549, 539, 523, 495, 409	A	d	n/a	OH	n/a	H	H	**57**
a5	671	653, 624, 606, 593, 546	A	d	n/a	SMe	n/a	COOMe	OH	
a6	645	617, 566, 523, 495, 409								
a7	687	639, 599, 565, 523, 495	A	e	n/a	$SC(CH_3)_2SMe$	OH	H	H	§
a8†	623	605, 545, 517, 485	A	a	n/a	n/a	n/a	COOMe	OH	**35**
a9	719	631, 565, 523, 495, 409	A	e	n/a	$SSC(CH_3)_2SMe$	OH	H	H	§
a10	673	631, 565, 523, 495, 409								
a11	655	608, 593, 548, 462, 434	A	d	n/a	SMe	n/a	COOMe	H	**53**
a12	565	537, 523, 495, 409	A	d	n/a	=O	n/a	H	H	**58**
a13	655	608, 593, 548, 462, 434	A	d	n/a	SMe	n/a	COOMe	H	**53'**
a14	551	523, 495, 437, 409	A	c	n/a	n/a	n/a	H	H	**65**
a15†	607	547, 519, 461, 433	A	a	n/a	n/a	n/a	COOMe	H	**32**
a16	641	594, 579, 551, 546, 533								
a17†	607	547, 519, 461, 433	A	a	n/a	n/a	n/a	COOMe	H	**32'**
a18	683	608, 593, 548, 462, 434	A	d	n/a	S-*i*-Pr	n/a	COOMe	H	
a19	687	640, 593, 578, 561, 506	B	d	d	SMe	n/a	n/a	n/a	**62**
a20	629	582, 567, 539, 533, 453	A	e	n/a	SMe	SH	H	H	**55**§
a21	729	641, 607, 547, 519, 461	A	d	n/a	$SC(CH_3)_2SMe$	n/a	COOMe	H	
a22	719	640, 592, 577, 545, 503	B	d	d	SMe/SSMe	n/a	n/a	n/a	
a23	639	592, 577, 503, 430, 415	B	a (d)	d (a)	SMe	n/a	n/a	n/a	**63**
a24	639	592, 577, 503, 430, 415	B	a (d)	d (a)	SMe	n/a	n/a	n/a	**63**
a25	597	550, 535, 521, 507, 421	A	d	n/a	SMe	n/a	H	H	**52**
a26	629	550, 535, 521, 507, 421	A	d	n/a	SSMe	n/a	H	H	**54**
a27	551	523, 437, 422, 408	A	b	n/a	n/a	n/a	H	H	**67**
a28†	549	521, 435, 420, 406	A	a	n/a	n/a	n/a	H	H	**33**
a29	591	559, 518, 445, 430, 415	B	a	a	n/a	n/a	n/a	n/a	**47**
a30	625	550, 535, 521, 507, 421	A	d	n/a	S-*i*-Pr	n/a	H	H	**60**
a31	657	550, 535, 521, 507, 421	A	d	n/a	SS-*i*-Pr	n/a	H	H	**61**
a32	671	583, 549, 521, 435	A	d	n/a	$SC(CH_3)_2SMe$	n/a	H	H	**56**
a33	661	550, 535, 521, 507, 421	A	d	n/a	SSSMe	n/a	H	H	
a34	687	549, 521, 435, 420								
a35	703	550, 535, 521, 507, 421	A	d	n/a	$SSC(CH_3)_2SMe$	n/a	H	H	
a36	653	625, 539, 505, 465, 433								

Table 3.1. Continued.

Peak	$[M+H]^+$ (*m/z*)	Prominent ions in MS^n (*m/z*)‡	Macrocycle	C-3	C-8	R1	R2	R3	R4	Structure number
a37	731	623, <u>550</u>, 535, 521, 507								
a38	777	729, 689, 623, <u>550</u>, 535	A	d	n/a	$SC(CH_3)_2S_2C(CH_3)_2SMe$	n/a	H	H	
a39	735	647, 623, <u>550</u>, 535, 521	A	d	n/a	$S_3C(CH_3)_2SMe$	n/a	H	H	
a40	809	721, <u>550</u>, 535, 521, 507	A	d	n/a	$SC(CH_3)_2S_3C(CH_3)_2SMe$	n/a	H	H	
a41	567	<u>539</u>, 453, 438, 424								
a42	763	623, <u>550</u>, 535, 521, 507								
a43	809	Does not fragment								

† Compound present in the starting mixture. ‡ Obtained following resonance enhanced collision induced dissociation of the protonated molecule. The underlined *m/z* value denotes the base peak ion in MS^2. The C-3 and C-8 assignments in brackets represent an alternative structural configuration. Apostrophe (e.g. 32') denotes the epimer. § Tentative assignment.

3.2.1.1. Sulfur-containing products of the reaction

The major product of the reaction was a component (a25, t_R = 28 min, Fig 3.1) eluting approximately 4 min prior to pphorb *a* (a28, t_R = 32 min), the earlier elution indicating a greater polarity. The online UV/vis spectrum of a25 (λ_{max} 406, 662 nm) displays a blue shift of ~3 nm in the Soret and Q_y bands relative to those of pphorb *a* (λ_{max} 409, 665 nm). The spectral characteristics of chlorins are extremely sensitive to structural modifications, in particular those at positions directly conjugated to the extended tetrapyrrole π-system that comprises the chlorin chromophore. Similar shifts in absorption maxima are observed for chlorins that possess a reduced C-3 vinyl substituent e.g. mpphorb *a* (Keely et al., 1990; Spooner et al., 1995) and C-3^1 alkylthioether chlorophyll derivatives (Squier et al., 2003; 2004). The component a25 was detected in APCI-IT MS as the protonated molecule at *m/z* 597 (Fig. 3.2a), 48 *m/z* units greater than that of pphorb *a* ($[M+H]^+$ = 549), corresponding formally to the empirical formula CH_4S and suggesting the addition of methanethiol. This was confirmed by high resolution APCI time of flight mass spectrometry (APCI TOF MS) which provided an accurate $[M+H]^+$ of *m/z* 597.2897, corresponding to $C_{35}H_{41}N_4O_3S$ (calculated *m/z* = 597.2894) and consistent with the empirical formula of the methylthioether derivative of pphorb *a* (MeS-pphorb *a*, **52a**) formed from addition of methanethiol to the C-3 vinyl group.

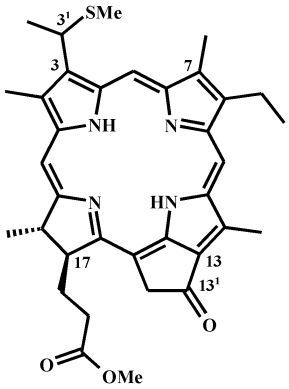

52a

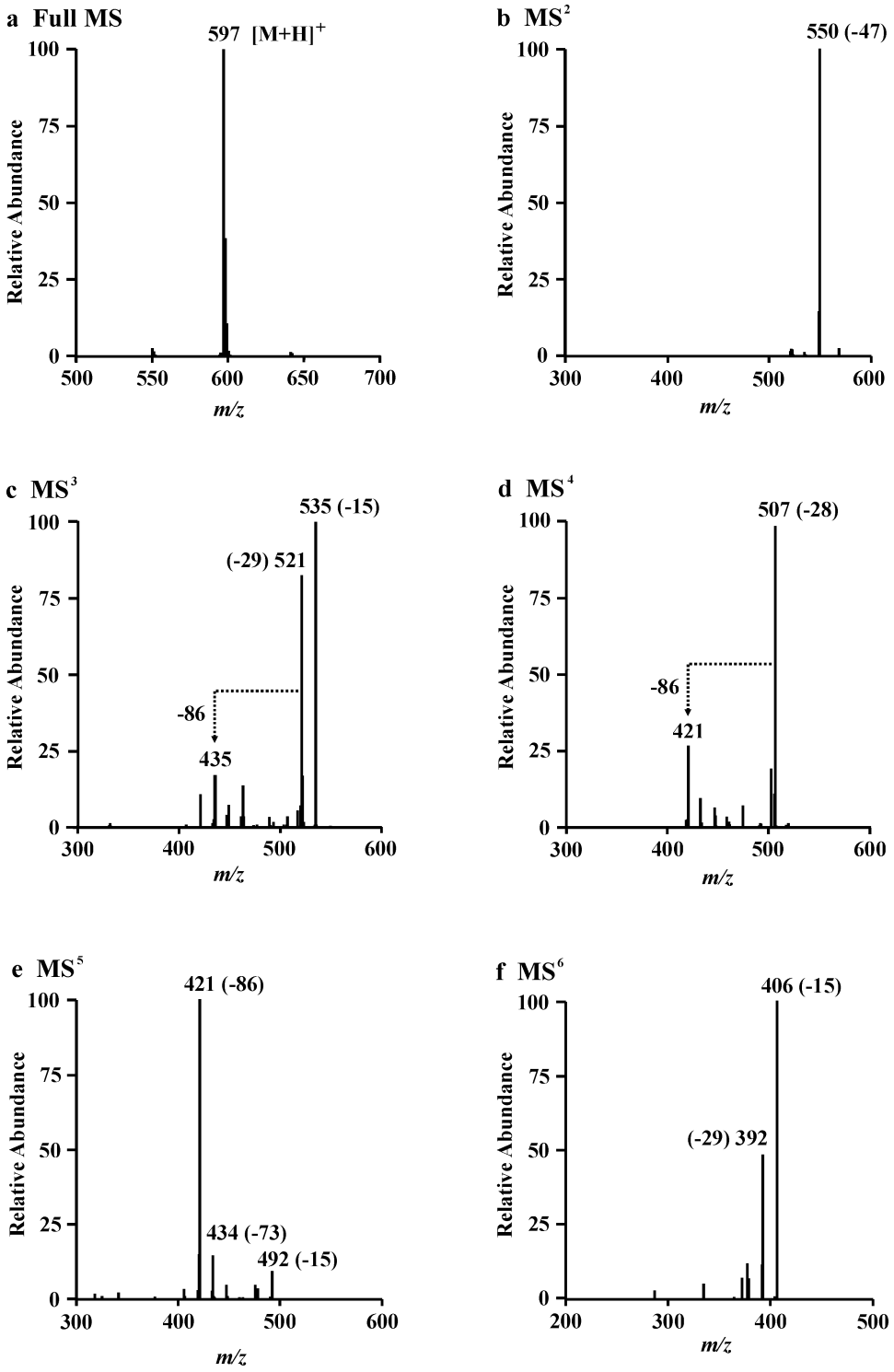

Figure 3.2. APCI multistage tandem mass spectra of MeS-pphorb *a* (**52a**); a) Full MS, b) MS^2, c) MS^3, d) MS^4, e) MS^5, f) MS^6. In each case the most abundant ion was selected as the precursor for the next spectrum.

Selection and resonance enhanced collision induced dissociation (CID) of *m/z* 597 by IT-MS generated a product ion in MS^2 at *m/z* 550 (Fig. 3.2b), reflecting loss of -47 Da, attributed to loss of the methylthioether moiety as a radical. Previous work has shown that decyl and butyl thioethers attached to the C-3^1 and C-3^2 positions can be distinguished by their MS^n spectra (Pickering, 2005). In that study, CID of the C-3^1 regioisomer resulted in the prominent loss of the thioether moiety as a radical species. By contrast, fragmentation of the C-3^2 thioether led to either a mixture of product ions formed via expulsion of the thioether group as a neutral thiol, or cleavage of the C-3^1-C-3^2 bond to lose a decyl-S-methyl or a butyl-S-methyl radical (Pickering, 2005). The fragmentation behaviour observed for the two regioisomers is driven by the formation of a radical situated at the C-3^1 position, which is stabilised by resonance with the aromatic macrocycle (Scheme 3.1). Thus, loss of a methanethiyl radical (-47 Da) from *m/z* 597 is indicative of the methylthioether being attached to the C-3^1 position (**52a**).

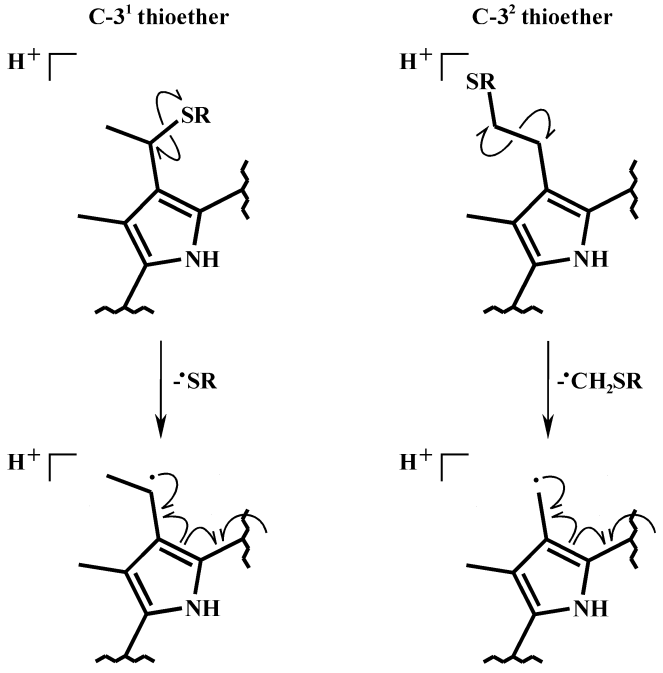

Scheme 3.1. The mechanisms for radical loss from C-3^1 and C-3^2 alkylthioether pphorb *a* derivatives.

Similarly, loss of 47 Da was observed for the natural methylthioether chlorophyll derivatives from Pup Lagoon (Squier et al. 2003; 2004). It is worth noting, however,

that the sedimentary derivative reported in detail by those authors was MeS-phe *a* (**22a**), which retains its phytyl ester and carbomethoxy group, and that the prominent losses in MS^2 for this compound, as for phe *a*, are of phytadiene and the carbomethoxy group, loss of the methylsulfur group occurring later, in MS^3. The absence of the phytyl esterifying alcohol and carbomethoxy functionalities in MeS-pphorb *a* mean that loss of the methanethiyl radical is observed one stage earlier in multistage tandem MS, comparable to the MS^3 stage for MeS-phe *a*. Chlorins typically dissociate by neutral loss during the early stages of MS^n. The prominent radical loss observed for MeS-pphorb *a* in MS^2 may be attributed to the relatively weak C-S bond and the resonance stabilisation of the resulting C-3^1 radical from conjugation with the macrocycle. The MS^3 spectrum of a25 (Fig 3.2c) is dominated by even electron product ions at *m/z* 535 (100%) and *m/z* 521 (80%), resulting from expulsion of either a methyl radical (-15 Da) or an ethyl radical (-29 Da), respectively. The MS^4 (Fig. 3.2d) and MS^5 (Fig. 3.2e) spectra reveal ions arising from losses of the C-3^1 carbonyl (-28 Da) and C-17 methylpropionate ester moieties, the latter accompanied by hydrogen transfer to the charge retaining fragment (-86 Da), confirming that these structural features, present in pphorb *a*, have remained unchanged during the reaction. The MS^6 (Fig. 3.2f) spectrum is dominated by product ions arising from losses of methyl and ethyl radicals.

The component a25 was isolated by preparative HPLC for ^{1}H NMR spectroscopy. The ^{1}H NMR spectrum (data collected in Table 3.2) closely resembles that of the natural methylthioether phe *a* derivative (Squier, 2003) with identical resonances corresponding to CH_3S-3^1 (δ = 2.17, s, 3H), H-3^1 (δ = 5.66, q, J = 7 Hz, 1H) and CH_3-3^2 (δ = 2.28, d, J = 7 Hz, 3H), replacing those of the vinyl group of the precursor, here pphorb *a* (Keely et al., 1990; H-3^1, δ = 8.23, dd, J = 12, 18 Hz; H-3^2, δ = 6.40, dd, J = 18, 1 Hz; H-$3^{2'}$, δ = 6.22, dd, J = 12, 1 Hz; Table 3.2). The multiplicity, chemical shifts and integral values confirm the location of the alkylsulfur moiety at the C-3^1 position. Accordingly, the structure of a25 could be unambiguously assigned to MeS-pphorb *a* (**52a**), formed in the reactions in 14% yield.

Table 3.2. ^{1}H NMR data for MeS-pphorb *a*. Literature data for pphorb *a* (Keely et al., 1990) and MeS-phe *a* (Squier, 2003) are included for comparison. All spectra recorded in $(CD_3)_2CO$.

	pphorb *a* (33)		**MeS-phe *a* (22a)**		**MeS-pphorb *a* (52a)**	
Proton	**δ (ppm)**[a]	**multiplicity**[b]	**δ (ppm)**[a]	**multiplicity**[b]	**δ (ppm)**[a]	**multiplicity**[b]
H-10	9.82	s	9.84	s	9.80	s
H-5	9.57	s	9.89	s	9.88	s
H-20	8.92	s	8.87	s	8.86	s
H-3^1	8.23	dd (12, 18)	5.65	q (7)	5.66	q (7)
H-3^2	6.40	dd (18, 1)				
H-3$^{2'}$	6.22	dd (12, 1)				
H-18	4.67	dq (7, 2)	4.36	m	4.66	m
H-17	4.43	m (2)	4.22	m	4.43	m
$CO_2\underline{CH_3}$-13^2			3.87	s		
CH_2-8^1	3.78	q (8)	3.78	q (9)	3.79	q (8)
CH_3-12^1	3.66	s	3.68	s	3.67	s
CH_3O-17^3	3.55	s			3.55	s
CH_3-2^1	3.49	s	3.50	s	3.51	s
CH_3-7^1	3.29	s	3.30	s	3.30	s
CH_2-17^1, 17^2	2.8-2.3	m	2.70-2.51	m	2.70-2.25	m
CH_3-3^2			2.28	d (7)	2.28	d (7)
CH_3S-3^1			2.18	s	2.17	s
CH_3-18^1	1.84	t (7)	1.83	dd (4)	1.83	dd (7, 3)
CH_3-8^2	1.69	t (8)	1.70	t (8)	1.71	t (8)

[a] referenced to the chemical shift of the solvent. [b] (*J*, Hz); s = singlet, d = doublet, t = triplet, q = quartet, m = multiplet.

Peak a11 gave a protonated molecule at *m/z* 655 (Fig 3.3a) and corresponds to the C-3^1 methylthioether derivative of phorb *a* (MeS-phorb *a*, **53**). The compound displays an identical UV/vis spectrum to MeS-pphorb *a* and similar reduction in retention time relative to its precursor. The MS^n spectra of MeS-phorb *a* contain many of the same losses as those observed in the MS^n spectra of MeS-pphorb *a*, differences arising from the presence of the carbomethoxy group at C-13^2. As observed for MeS-pphorb *a*, the MS^2 spectrum of MeS-phorb *a* (Fig 3.3b) is dominated by loss of the C-3^1 methylthioether moiety as a methanethiyl radical (-47 Da) to form an odd electron radical cation at *m/z* 608. The minor product ion at *m/z* 595, corresponding to a loss of 60 Da, originates from loss of the C-13^2 carbomethoxy group. Loss of this group from *m/z* 608 forms the base peak ion in MS^3 (*m/z* 548, Fig 3.3c) with the losses of methyl and ethyl radicals, which dominate the MS^3 spectrum of MeS-pphorb *a*, contributing ions of lower relative intensity (*m/z* 593 and *m/z* 579). The MS^4 spectrum contains several product ions (Fig. 3.3d). The base peak ion at *m/z* 462 corresponds to loss of the C-17 methylpropionate ester and the ions at *m/z* 447 and *m/z* 434 to loss of that group in combination with a methyl radical and CO (from C-13^1), respectively. The MS^5 spectrum (Fig. 3.3e) contains ions arising from losses of methyl and ethyl radicals to form more stable, closed shell ions. The MS^6 spectrum (Fig. 3.3f) is dominated by a product ion at *m/z* 419, formed via loss of CO from the C-13^1 position.

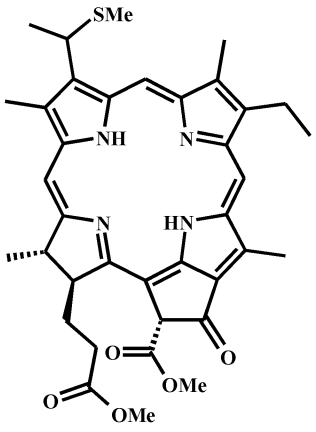

53

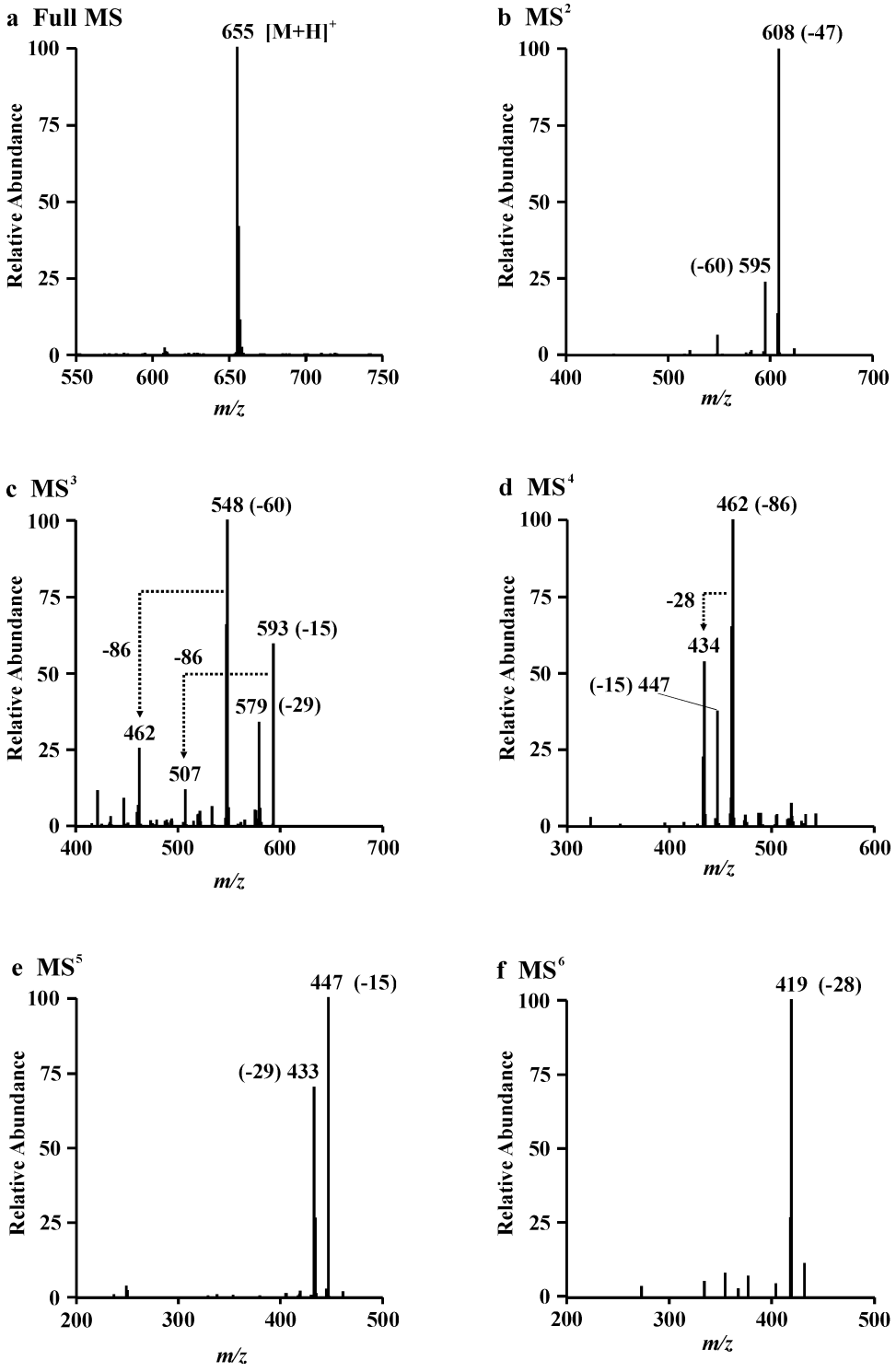

Figure 3.3. APCI multistage tandem mass spectra of MeS-phorb *a* (**53**); a) Full MS, b) MS^2, c) MS^3, d) MS^4, e) MS^5, f) MS^6. In each case the most abundant ion was selected as the precursor for the next spectrum.

In addition to the C-3^1 methylthioethers, a number of minor sulfur-containing products were identified in the reaction mixture. Two isobaric components, a26 and a20, eluting at t_R = 29.5 and 26 min, exhibit protonated molecules at *m/z* 629 (Figs. 3.4a and 3.5a, respectively), 80 *m/z* units greater than pphorb *a*. Notably, the $[M+H+2]^+$ peaks for both components are significantly enhanced, relative to non-sulfurised components, indicating the inclusion of an element with an abundant +2 isotope, such as sulfur. The ion at *m/z* 550 in the mass spectrum of a26 (Fig 3.4a) corresponds to a fragment ion arising from loss of 79 Da from *m/z* 629, and forms the base peak ion in MS^2 (Fig 3.4b). The appearance of fragment ions in the APCI mass spectra of chlorins is unusual, owing to the 'soft' nature of the ionisation technique producing a protonated molecule with relatively little internal energy. Thus, the occurrence of the fragment ion indicates that the loss is facile. Notably, the loss of 79 Da is 32 Da greater than that observed for loss of a methanethiyl radical, a difference corresponding to the mass of a sulfur atom. Accordingly, the structure of a26 is suggested to contain a methyldisulfide moiety at C-3^1 (**54**). Facile loss of this group compared with the methylthioether may reflect either a weaker C-S bond or greater stability of the resulting $^{\cdot}$SSMe radical. The MS^3-MS^6 spectra for the component a26 (not shown) display identical fragment ions to those observed in the MS^n spectra of MeS-pphorb *a*, present in virtually identical relative abundances, supporting the interpretation that these two compounds share a strong structural similarity. The tendency of sulfur to form bonds with itself is well known (Senning, 1972) and can be invoked to explain the formation of MeSS-pphorb *a*. The reaction of polysulfides with organic molecules is considered to be responsible for the formation of di- and polysulfide crosslinked sedimentary organic matter (Kohnen et al., 1989; Sinninghe Damsté and de Leeuw, 1990; Kohnen et al., 1991b; Aizenshtat et al., 1995). By contrast, H_2S is suggested to yield only monosulfide crosslinks. These views have been supported by laboratory sulfurisation experiments (cf. Adam et al., 1998). The formation of MeSS-pphorb *a* in the reactions described here indicate that reactions involving H_2S are capable of forming disulfide linkages. The involvement of polysulfides in the formation of MeSS-pphorb *a* is unlikely, given that the reactions were conducted under acidic conditions, as a result of the dissolved H_2S, that discourage the formation of polysulfides.

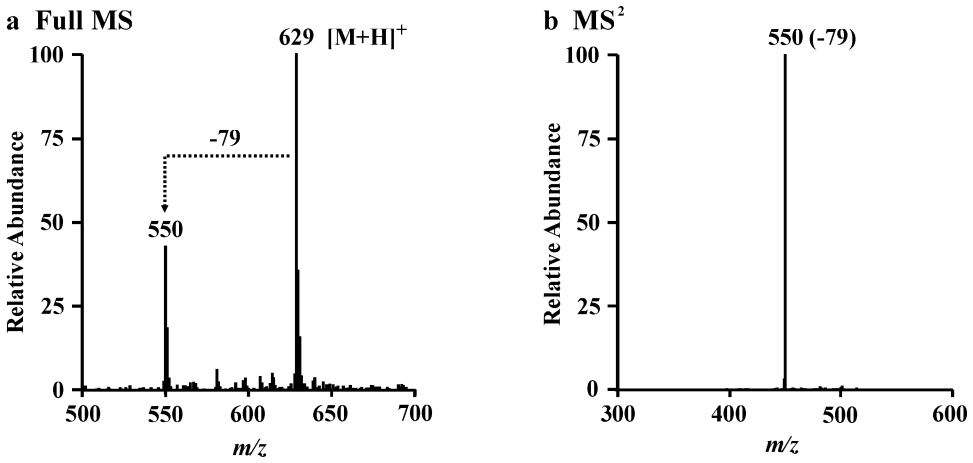

Figure 3.4. APCI tandem mass spectra of MeSS-pphorb *a* (**54**); a) Full MS, b) MS^2.

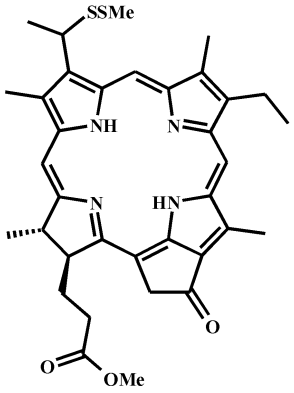

54

The early eluting isobar a20 displays distinctly different MS^n characteristics. The MS^2 spectrum (Fig. 3.5b) contains a base peak ion at *m/z* 582 arising from loss of a methanethiyl radical (-47 Da) indicating the likely presence of a methylthioether moiety at C-3^1. The ion at *m/z* 567 (45%), reflecting a loss of 62 Da, was ascribed to the further loss of a methyl radical from *m/z* 582 and forms the base peak ion in MS^3 (Fig. 3.5c). The MS^4-MS^6 spectra of a20 (Fig. 3.5d-f) display a similar series of losses, producing product ions in comparable relative abundances to those observed in the MS^2-MS^4 spectra of pphorb *a*. Losses of 28 Da and 86 Da indicate that the C-13^1 carbonyl (-28 Da) and C-17 methylpropionate ester moiety of the starting material have not been modified. The MS^4 spectrum (Fig. 3.5d) contains an ion at *m/z* 533 arising from a loss of 34 Da, ascribed to loss of a neutral molecule of H_2S. By analogy with the MS^n spectra of chlorophyll derivatives containing alcohol substituents, which experience loss of H_2O during MS^n (e.g. Wilson et al., 2005), loss of H_2S is likely to be indicative of a thiol group in the structure of a20. Incorporation of thiol and methylthioether moieties into the structure of pphorb *a* accounts for the mass difference of 80 Da between a20 and its precursor, pphorb *a*. Given the evidence that the other functional groups of pphorb *a* remain unaltered during the reaction, the most likely site for the thiol is at the C-3^2 carbon. Thus, a20 was tentatively assigned as **55**. The addition of sulfur to both ends of a double bond has not been reported in laboratory sulfurisation reactions and no sedimentary organosulfur compounds in which sulfur is bonded to adjacent carbon atoms have be ascribed to alkene precursors. Thus the formation of **55** may indicate an, as yet, unrecognised mode of sulfur incorporation.

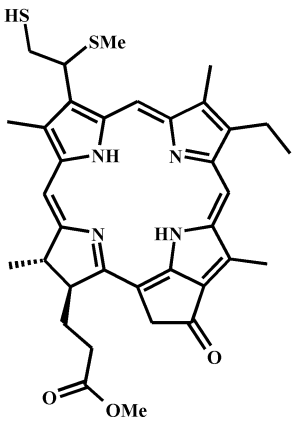

55

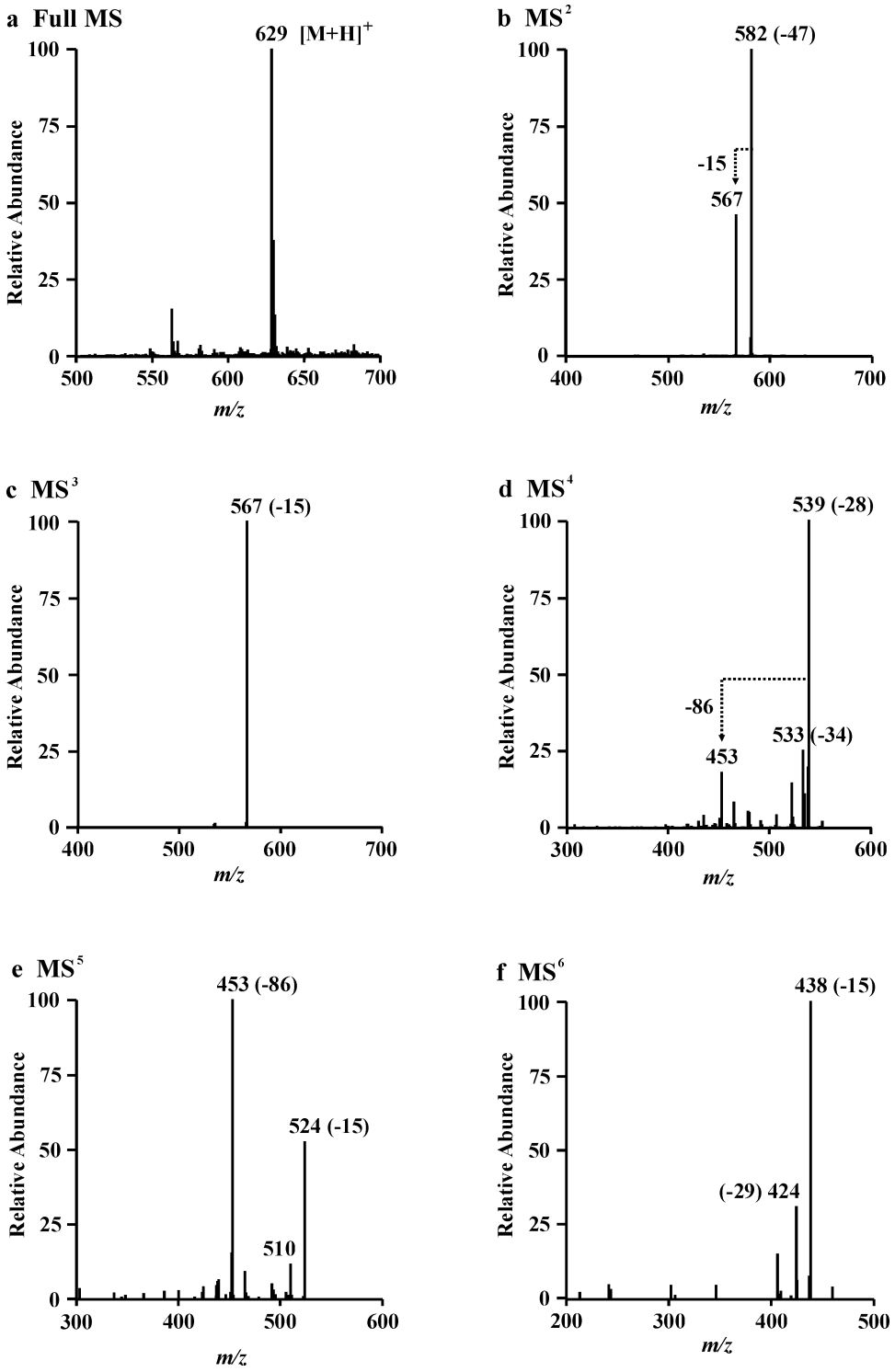

Figure 3.5. APCI multistage tandem mass spectra of HS,MeS-pphorb *a* (**55**); a) Full MS, b) MS^2, c) MS^3, d) MS^4, e) MS^5, f) MS^6. In each case the most abundant ion was selected as the precursor for the next spectrum.

A cluster of late eluting sulfurised chlorins (a32, a35, and a38-a40) present in the LC-MS chromatogram result from side reactions involving acetone. The mass spectrum of the most abundant of these components, a32, exhibits a protonated molecule at *m/z* 671 (Fig. 3.6a), 122 *m/z* units greater than the protonated molecule of pphorb *a*, and exhibits an enhanced [M+H+2] isotope peak symptomatic of the inclusion of sulfur. Judging by the magnitude of the enhancement, and by comparison with the full MS of MeSS-pphorb *a* (**54**) and HS,MeS pphorb *a* (**55**), it is likely that this component contains at least two sulfur atoms. CID of *m/z* 671 yields a number of ions in MS^2 with an ion at *m/z* 549 being dominant (Fig. 3.6b). Further CID of this ion produced MS^3-MS^6 spectra (not shown) identical to the MS^2-MS^5 spectra of the starting material, pphorb *a* Thus, the product ion at *m/z* 549 corresponds to the protonated molecule of pphorb *a*, formed from loss of the modified portion of the molecule as a neutral molecule (-122 Da). Similarly, the ion at *m/z* 550, reflecting a loss of 121 Da, corresponds to loss of the modified portion of the molecule as a radical species. The prominence of this radical loss suggests that it involves the cleavage of a relatively weak bond such as a C-S bond connecting it to the macrocycle. The ion at *m/z* 583 arises from loss of 88 Da, 34 *m/z* units less than the loss of 122 Da, a difference that corresponds to the mass of H_2S. Unlike the losses observed in the MS^n spectra of the sulfurised components described previously, the losses in the MS^2 spectrum of a32 cannot be accounted for by iterations of methyl groups and sulfur atoms alone, suggestive of the involvement of other reagents in the formation of a32. Based on the available evidence, the most likely structure is **56** involving the incorporation of a C_3 unit derived from acetone. While not as reactive as aldehydes, reactions of ketones with reduced sulfur species are well known (Schouten et al., 1993; 1994; Aizenshtat et al., 1995; Schneckenburger et al., 1998), although those studies did employ higher temperatures than used here (>50°C). The occurrence of such a reaction with acetone would yield a sulfurised intermediate capable of adding to the C-3 vinyl group of pphorb *a*. With regard to the proposed structure of **56**, losses of 122 Da and 121 Da can be explained by losses of the C-3^1 substituent as a neutral molecule and as a radical, respectively. The loss of 88 Da may be attributed to loss of C_3H_5SMe.

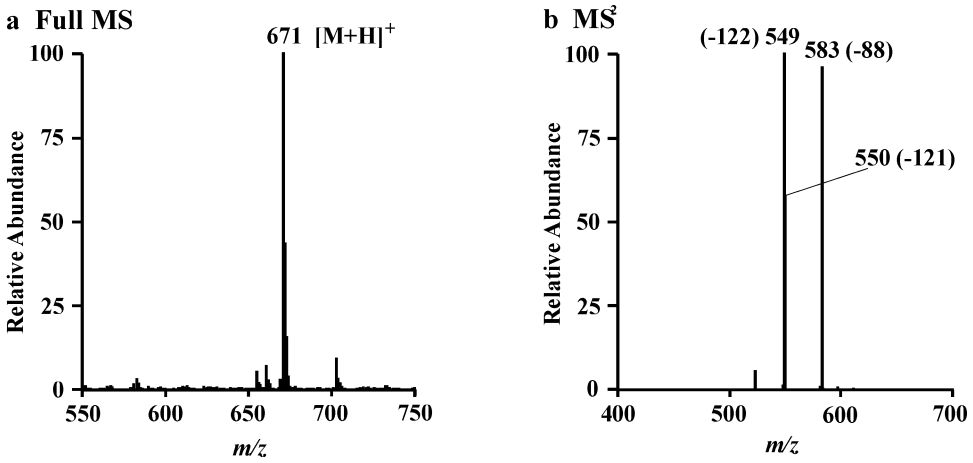

Figure 3.6. APCI tandem mass spectra of MeS-*i*-Pr-S-pphorb *a* (**56**); a) Full MS, b) MS^2.

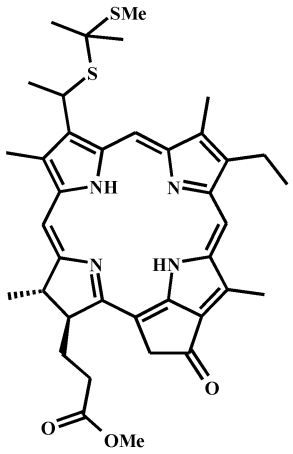

56

The other peaks in the cluster (a35 and a38-a40) correspond to analogues of a32 with structures varying in the number and combinations of sulfur atoms and acetone-derived C_3 units (see Table 3.1). Notably, while the occurrence of these compounds indicates that sulfurisation of the carbonyl functionality of acetone occurs under the reaction conditions, no products could be ascribed to the reaction of sulfide with the C-13^1 carbonyl of pphorb *a* or phorb *a*. It is possible that the greater steric hinderance of the C-13^1 carbonyl, with respect to that of acetone, protects it from reaction with sulfur nucleophiles. Alternatively, donation of electron density by the aromatic macrocycle could reduce the electrophilicity of the carbonyl carbon.

3.2.1.2. Oxidised products of the reaction

Several derivatives of pphorb *a* resulting from the oxidation of the C-3 vinyl group were evident among the reaction products, possibly resulting from side reactions with traces of water or oxygen present in the reaction.

The mass spectrum of component a4 (t_R = 14 min; λ_{max} 406, 661 nm) exhibits a protonated molecule at *m/z* 567 (Fig. 3.7a), 18 *m/z* units greater than that of pphorb *a* ($[M+H]^+$ = 549) suggesting the incorporation of H_2O. CID of *m/z* 567 yielded a number of ions in MS^2 (Fig. 3.7b). The product ion at *m/z* 549 represents a loss of 18 Da from *m/z* 567, ascribed to loss of a neutral molecule of H_2O. Such a loss is indicative of the presence of an alcohol functionality in the parent compound. The ion at *m/z* 539 arises from loss of 28 Da, corresponding to loss of CO, most likely from C-13^1. The base peak ion at *m/z* 523 represents a loss of 44 Da from *m/z* 567, consistent with loss of C_2H_4O. Notably, the losses and relative abundances of the resultant product ions match those in the MS^2 spectra of bacteriophaeophorbide (bphorb) *d* methyl esters, which possess a 1-hydroxyethyl group at C-3 (Wilson, 2004). In the case of bphorb *d*, loss of 18 Da relates to loss of the C-3^1 OH group as water and loss of 44 Da to removal of the entire C-3^1 substituent (most likely as ethylene oxide) with hydrogen transfer to the charge-retaining fragment. Furthermore, the MS^3-MS^6 spectra of a4 (Fig. 3.7c-f) display identical losses, and relative ion abundances, to those contained in the same spectra of bphorb *d* (Wilson, 2004) and the MS^2-MS^5 spectra of pphorb *a*. In the latter case, loss of 86 Da indicates that the C-17^1 methyl propionate ester has remained unaltered during the reaction. Accordingly, the structure was assigned as the C-3 (1-hydroxyethyl) derivative of pphorb *a* (**57**), i.e. bphorb *d* methyl ester with a [C-8, C-12] configuration of [Et, Me]. Formation of bphorb *d* in these reactions suggests that such a transformation of the chlorophyll vinyl group could occur in the natural environment with the potential to create a false signal, indicating green sulfur bacterial input in sediments.

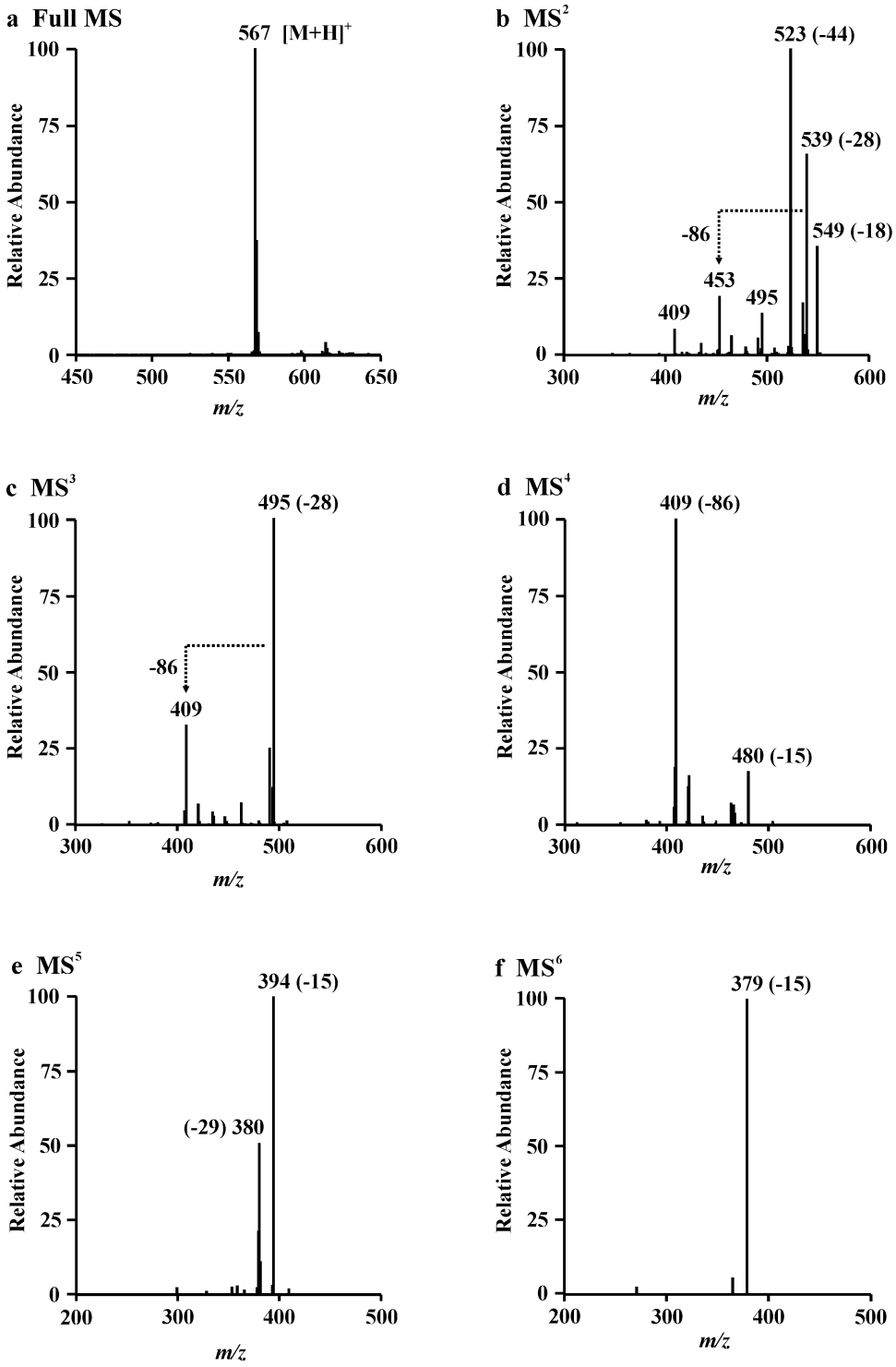

Figure 3.7. APCI multistage tandem mass spectra of C-3 (1-hydroxyethyl) pphorb *a* (bphorb *d* [Et, Me], **57**); a) Full MS, b) MS^2, c) MS^3, d) MS^4, e) MS^5, f) MS^6. In each case the most abundant ion was selected as the precursor for the next spectrum.

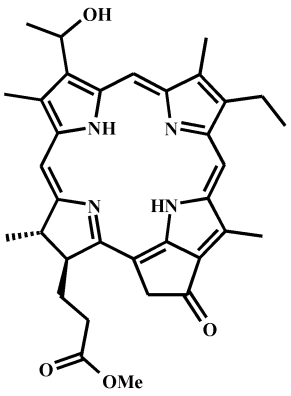

57

Component a12 (t_R = 22 min) exhibits a protonated molecule at *m/z* 565 (Fig. 3.8a), 16 *m/z* units greater than the protonated molecule of pphorb *a*. The online UV/vis spectrum for the component revealed a bifurcated Soret band and shift in the Q_y band relative to pphorb *a* (λ_{max} 385, 410, 692 nm cf. λ_{max} 409, 665 nm). The spectral characteristics are similar to those of bacterioviridin (λ_{max} 383, 412, 680 nm; Wilson et al., 2004b) which contains an acetyl group at C-3. CID of *m/z* 565 yields ions in MS^2 (Fig 3.8b) at *m/z* 523 (100%), reflecting loss of 42 Da, and *m/z* 537 (63%), a loss of 28 Da. Loss of 28 Da is attributed to expulsion of CO from the C-13^1 position. Loss of 42 Da is observed in the MS^n spectra of bphorb *a* methyl ester (Wilson, 2004), which possesses an acetyl group at C-3, and corresponds to loss of the entire C-3 substituent as CH_2CO with hydrogen transfer to the macrocycle. The MS^3-MS^6 spectra are identical to those of the C-3 (1-hydroxyethyl) pphorb *a* derivative (Fig. 3.7c-f). On the basis of the UV/vis and mass spectral characteristics, the component was assigned as the C-3 acetyl analogue of pphorb *a* (**58**), i.e. pyrobacterioviridin methyl ester. Pyrobacterioviridin can been prepared from bchl *a* by the dehydrogenation of ring B using 2,3-dichloro-5,6-dicyanoquinone in acetone (Lindsay-Smith and Calvin, 1966) followed by decarbomethoxylation from C-13^2 by reflux in pyridine (Hynninen, 1991). Given further investigation, the reaction described here could possibly be optimised to enable preparation of bacterioviridins from chl *a* derivatives, which are a more readily available starting material than bchl *a*.

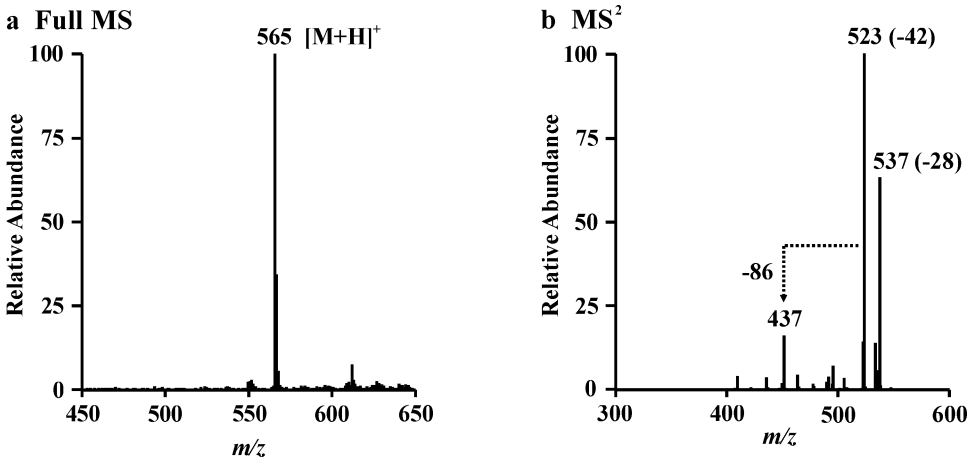

Figure 3.8. APCI tandem mass spectra of C-3 acetyl pphorb *a* (**58**); a) Full MS, b) MS^2.

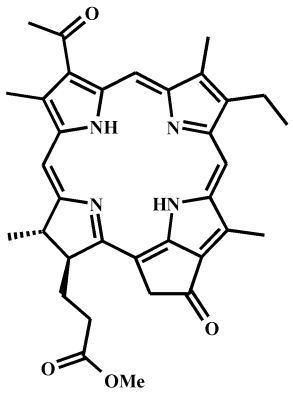

58

An early eluting component, a2 (t_R = 9 min), exhibits a protonated molecule at *m/z* 583 (Fig. 3.9a), 32 *m/z* units greater than pphorb *a*. The incorporation of a sulfur atom into pphorb *a*, which would account for the observed mass difference, can be excluded from the lack of an enhancement of the $[M+H+2]^+$ isotope peak of a2, relative to that of pphorb *a*. CID of *m/z* 583 yields numerous product ions in MS^2 (Fig. 3.9b). The product ion at *m/z* 565 represents loss of H_2O (-18 Da) indicating the presence of an alcohol functionality. The ion at *m/z* 555 arises from loss of the C-13^1 CO group (-28 Da). The base peak ion at *m/z* 523 reflects a loss of 60 Da. This loss is consistent with loss of a C-13^2 carbomethoxy group and may suggest that phorb *a* ($[M+H]^+$ = 607) is the precursor of a2. Notably, the presence of a C-13^2 carbomethoxy group in the structure of a2 cannot be accommodated by *m/z* value of its protonated molecule (*m/z* 583) without loss having occurred from the structure of phorb *a*, the most likely sites for which being from the C-13^1 CO and C-17 methyl propionate ester moieties. CID of *m/z* 523 generates MS^3-MS^6 spectra identical to

those of the C-3 (1-hydroxyethyl) and C-3 acetyl pphorb *a* derivatives, **57** and **58**, losses of 28 and 86 Da attesting to the C-13^1 CO and C-17 methyl propionate ester functionalities having remained unaltered during the reaction. Accordingly, the presence of a C-13^2 carbomethoxy group can be ruled out. The similarity of the MS^3-MS^6 spectra between a2 and compounds **57** and **58** suggests that the loss of 60 Da, forming the base peak in the MS^2 spectrum of a2 (Fig. 3.9b), pertains to loss of the entire C-3 residue. The mass spectral evidence supports the presence of at least one alcohol in the structure, the most likely site being the C-3 vinyl group. Inclusion of a further hydroxyl into the vinyl group would account for the increased mass of this component relative to pphorb *a*. Furthermore, loss of the entire modified C-3 substituent ($C_2H_4O_2$) with hydrogen transfer to the charge retaining macrocycle would account for the observed loss of 60 Da in MS^2. Accordingly, the structure of a2 was tentatively assigned to a C-3^1, 3^2 diol derivative of pphorb *a* (**59**).

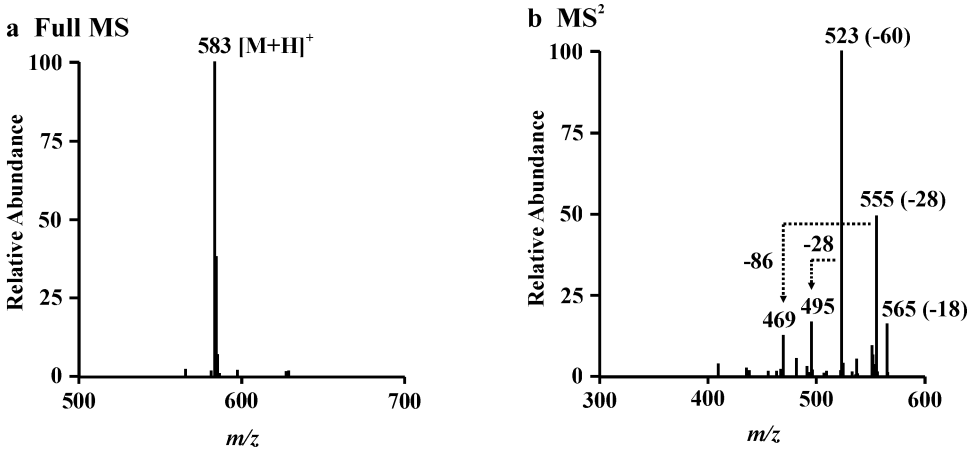

Figure 3.9. APCI tandem mass spectra of C-3^1, 3^2 diol-pphorb *a* (**59**); a) Full MS, b) MS^2.

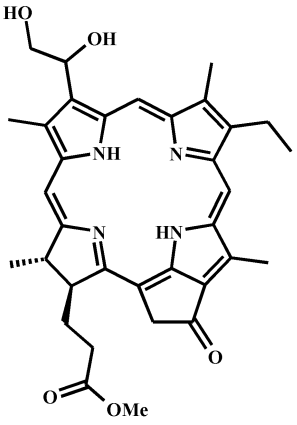

59

Similarly, the MS^n spectra of components a1 and a3, observed in the LC-MS chromatogram (Fig 3.1, Table 3.1), suggest that these compounds correspond to the C-3^1, 3^2 diol, and C-3 (1-hydroxyethyl) derivatives of phorb *a*, respectively.

3.2.2. Reactions of pyrophaeophorbide *a* with short chain alkyliodides and H_2S in acetone buffered to pH 7

While the reactions described in the previous section produced MeS-pphorb *a* in modest yields, it was found that buffering the reaction to pH 7 with aqueous ammonium acetate improved reproducibility and allowed greater yields of MeS-pphorb *a* to be attained. At this pH, H_2S (pK_{a1} = 7.02; Crampton, 1974) exists in the forms of HS^- and H_2S, present in approximately equal proportions. The former species is involved in the nucleophilic substitution of iodide and conversion of methyliodide into methanethiol (Equation 3.2). H_2S, on the other hand, provides a proton source for the suspected acid catalysed addition of the alkylthiol to the pphorb *a* vinyl group (Equation 3.1). Thus, buffering at pH 7 fosters both reactions and consequently enhances the rate of formation of MeS-pphorb *a*. An aqueous content of at least 30% was required for the reaction to be buffered effectively while higher aqueous contents led to a reduction in the solubility of the pigment component and its tendency to form aggregates.

LC-MS analysis of the total extract from the reaction of pphorb *a* with methyl iodide and H_2S in buffered acetone (70:30 acteone:water pH 7; Fig. 3.10) revealed a complex mixture of products dominated by MeS-pphorb *a* (a25, max yield 82%), pphorb *a* having been almost completely consumed in the reaction.

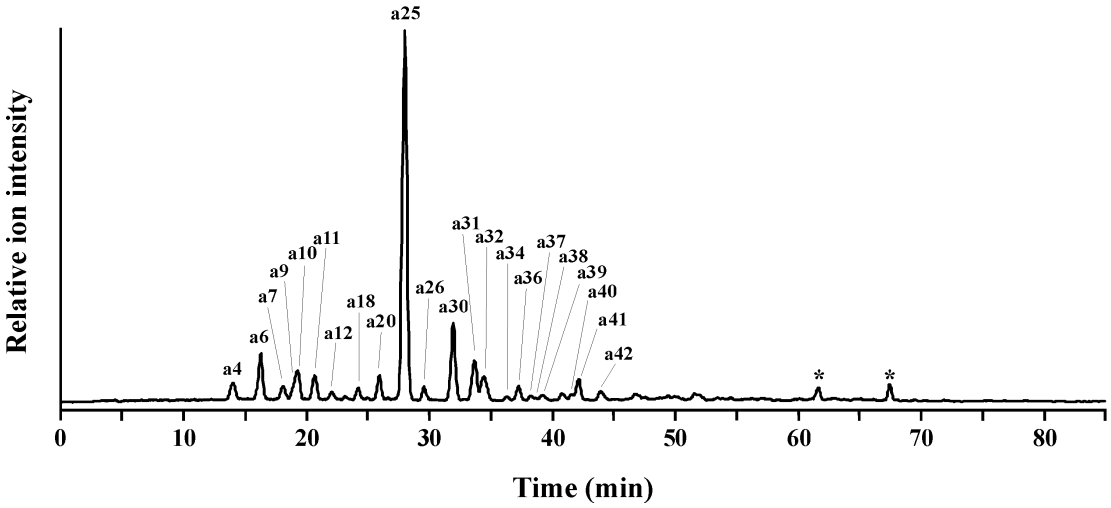

Figure 3.10. Representative mass chromatogram (*m/z* 400-1200) of the total extract from the reaction of a mixture of pphorb *a* (**33**) and phorb *a* (**32**) with methyliodide and H_2S in a 70:30 mixture of acetone and aqueous ammonium acetate pH 7. Peak assignments in Table 3.1. *Not pigments.

As was the case with the reactions conducted in 100% acetone, the LC-MS chromatogram of the reaction in buffered acetone (Fig. 3.10) displays a cluster of peaks (a30-a32, a39-a41) corresponding to acetone-derived components. Notably, the most abundant members of this cluster, peaks a30 and a31 had not been observed in the previous reactions. The mass spectrum of a30 (Fig. 3.11a) reveals a protonated molecule at *m/z* 625. The smaller ion at *m/z* 549 corresponds to unreacted pphorb *a* starting material concealed beneath the a30 peak. CID of *m/z* 625 yields a product ion in MS^2 at *m/z* 550 (Fig. 3.11b) corresponding to a radical loss of 75 Da, the prominence of this radical loss most probably indicating that it involves cleavage of a weak bond such as a C-S bond. Later stages of MS^n (not shown) are identical to those of MeS-pphorb *a*. The mass spectrum of peak a31 (Fig. 3.11c) displays a protonated molecule at *m/z* 657, 32 *m/z* units greater than a30 (*m/z* 625) indicating that the structures of these two compounds differ in the number of sulfur atoms. The ion at *m/z* 550 in the full MS of a31 (Fig 3.11c) corresponds to a fragment ion resulting from loss of 107 Da from *m/z* 657 and forms the base peak in MS^2 (Fig. 3.11d). Later stages of MS^n match those of alkylthioether pphorb *a* derivatives. The mass spectrum of a31 is similar in appearance to that of MeSS-pphorb *a*, which also displays a fragment ion at *m/z* 550, and may indicate that a31 contains a disulfide bond at the C-3^1 position. From the available data the components a30 and a31 were assigned as **60**

and **61**, which represent variations on previously identified members of the acetone derived cluster. Losses of 75 Da and 107 Da observed in MS^n of the two compounds are explained by the entire loss of their respective C-3^1 substituents.

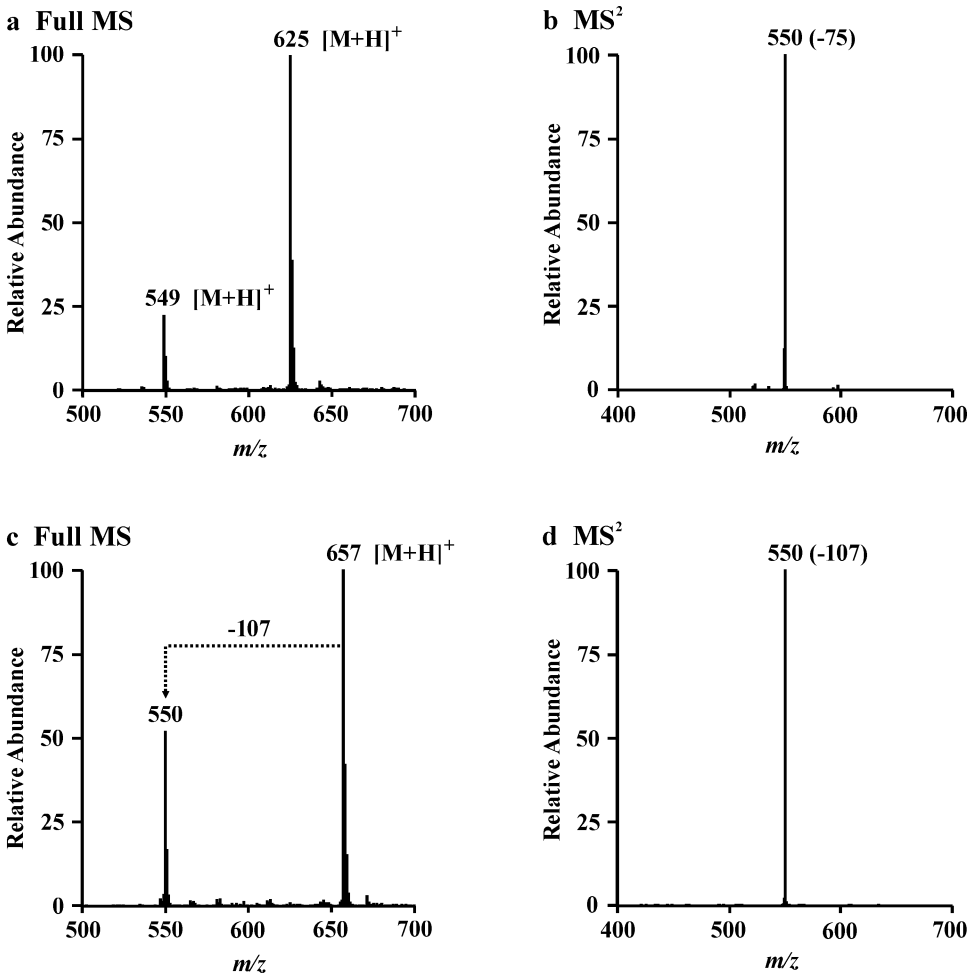

Figure 3.11. APCI tandem mass spectra. a) Full MS of a30, b) MS^2 of a30. c) Full MS of a31, d) MS^2 of a31.

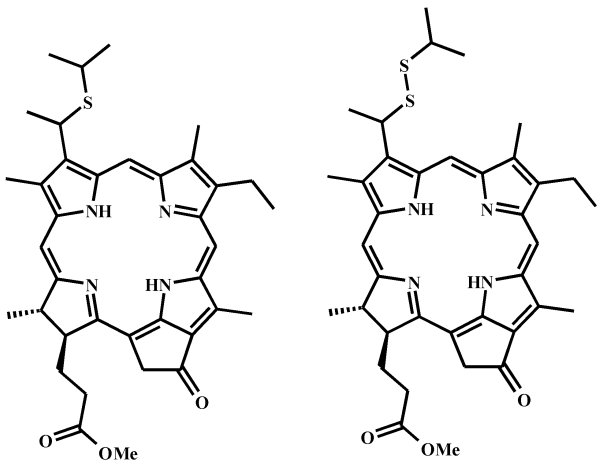

60 **61**

The reaction of pphorb *a* with each of the other four alkyliodides (ethyl, *n*-propyl, *n*-butyl, and *n*-pentyliodide) led to the generation of the corresponding alkylthioether derivatives (EtS-pphorb *a*, **52b**, 71%; *n*-PrS-pphorb *a*, **52c**, 76%; *n*-BuS-pphorb *a*, **52d**, 60%; *n*-PentS-pphorb *a*, **52e**, 65%). As illustrated by the partial mass chromatograms (Fig. 3.12), the compounds elute as a regularly spaced series in order of increasing alkylsulfur chain length, with intervals of approximately 2 min consistent with those observed between the retention times of the natural homologues (Squier et al., 2004). Each component displays a blue shift in its online UV/vis absorption maxima similar to that observed in MeS-pphorb *a*, and for the natural derivatives.

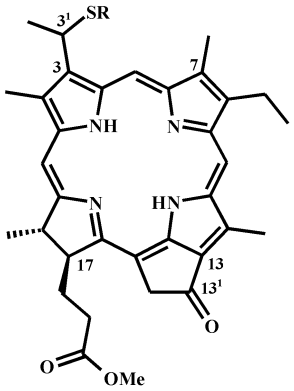

52: R = Me (**a**), Et (**b**), *n*-Pr (**c**), *n*-Bu (**d**), *n*-Pent (**e**)

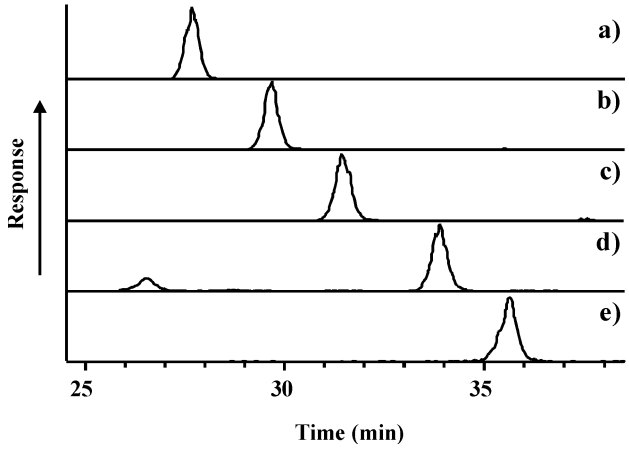

Figure 3.12. Partial LC-MS chromatograms of the products from reaction of pphorb *a* with the five alkyliodides. a) MeS-pphorb *a*, **52a**, *m/z* 597; b) EtS-pphorb *a*, **52b**, *m/z* 611; c) *n*-Pr-pphorb *a*, **52c**, *m/z* 625; d) *n*-BuS-pphorb *a*, **52d**, *m/z* 639; e) *n*-PentS-pphorb *a*, **52e**, *m/z* 653.

The MS^n spectra for these components (exemplified by EtS-pphorb *a*, **52b**, Fig. 3.13) all display the characteristic loss of the C-3^1 alkylthioether residue as a radical in MS^2, as observed for the MeS-pphorb *a* derivatives, followed by a series of consistent and highly reproducible ions in MS^3-MS^6. Formation of the alkylthioether derivatives creates a chiral centre at C-3^1. Whereas the C-13^2 diastereomers of chl *a*, phe *a* and phorb *a*, which possess a carbomethoxy moiety at C-13^2, give rise to chromatographically distinct peaks, separate peaks corresponding to the C-3^1 alkylthioether diastereomers are not readily apparent in the LC-MS chromatogram. It is improbable that the formation of the alkylthioethers would be stereoselective for one diastereomer as there is little present in the structure of either pphorb *a* or alkyliodide to enforce such control, thus, it is likely that each peak consists of two unresolved C-3^1 diastereomers. Provided that the alkylthioether chain does not restrict its movement, the C-3–C-3^1 bond is free to rotate about its axis. Thus, for any given orientation of the alkylthioether chain the only difference between the two diastereomeric forms is a transposition of the methyl and hydrogen substituents attached to the C-3^1 carbon atom. Such a difference would be unlikely to have a significant influence on the chromatographic properties of the two molecules. Notably, a slight increase in peak width of the derivatives can be observed with increasing alkyl chain length which could possibly indicate an incremental increase in separation between the diastereomers. Peak broadening as a result of increased longitudinal diffusion, associated with an increasing t_R of the heavier homologues, can be excluded by comparison of the peak widths with those of other late eluting components. Presence of small shoulders on each of the chromatographic peaks of the natural alkylthioether derivatives were noted and believed to represent an unresolved C-3^1 diastereomer (Squier, 2003). Notably those derivatives possess a phytyl side chain, and elute much later in the HPLC gradient programme (cf. t_R = 63 min for MeS-phe *a* Squier, 2003). Thus, the partial separation of their C-3^1 diastereomers could be the result of a longer time on column.

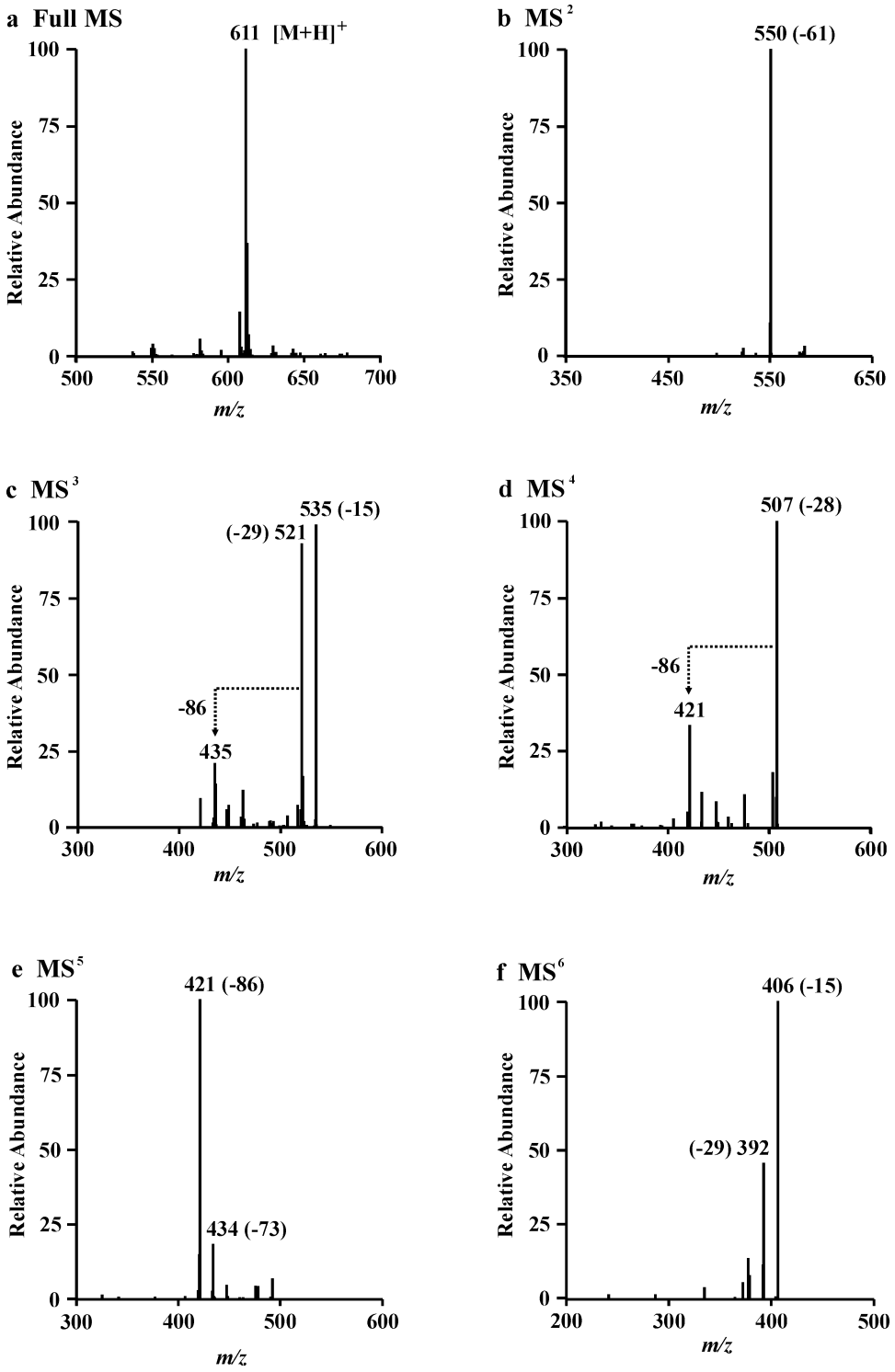

Figure 3.13. APCI multistage tandem mass spectra of EtS-pphorb *a* (**52b**); a) Full MS, b) MS^2, c) MS^3, d) MS^4, e) MS^5, f) MS^6. In each case the most abundant ion was selected as the precursor for the next spectrum.

Given the formation of acetone-derived side products in the reaction, the use of methanol, which is miscible with water, has similar polarity to acetone, and is widely used in solution phase manipulations of chlorophyll pigments, was investigated as a possible alternative solvent. Replacement of acetone with methanol as the reaction solvent did not affect the reaction mechanism and enabled the formation of acetone-derived byproducts to be avoided. There were some compromises, however, in terms of solubility. Specifically, difficulty in solubilising the dry pigment starting material and a greater tendency for the pigment component to aggregate to the walls of the flask during the course of the reaction (even in solvent systems comprising 100% methanol), which detracted from the overall yield of product. Furthermore, it is widely known that, in methanolic solutions, chlorins that possess C-13^2 carbomethoxy groups are susceptible to oxidation (allomerisation) reactions centred on the exocyclic ring (Walker et al., 2002; 2003). On balance, the benefits of using acetone in terms of greater pigment solubility outweigh the drawbacks with regard to side reactions.

3.2.3. Reaction of pyrophaeophorbide *a* and protoporphyrin-IX with dimethyl disulfide and H_2S

Thiols readily form disulfides following oxidation, which are often used as protecting groups and a convenient method of storing reactive thiols owing to their relatively low reactivity (Wolman, 1974). They can be converted back into their corresponding thiols via reduction with reagents such as lithium aluminium hydride and sodium borohydride, or through cleavage with nucleophiles including, HO-, CN-, or sulfides such as HS^- (Equation 3.3) (Wardell, 1974; Wolman, 1974). Indeed, EtS- has been used in the mild chemical degradation of sedimentary organic matter to cleave polysulfide bonds, and the resulting thiols subsequently methylated with methyliodide (Adam et al., 2000).

$$MeSSMe + HS^- \rightarrow MeS^- + HSSMe \qquad (3.3)$$

In natural aquatic environments, oxidation of sulfide to di- and polysulfides is suggested to be important at the oxic/anoxic interface (Aplin and Macquaker, 1993). While dialkyldisulfides are not reputed to be widespread in nature and, therefore, are unlikely to represent a significant natural source for the formation of alkylthioether

chlorophyll derivatives, the reaction of pphorb *a* with dimethyl disulfide in combination with H_2S was investigated as an alternative route to the preparation of standards of alkylthioether chlorophyll derivatives.

The reaction of pphorb *a* with dimethyl disulfide and H_2S was found to deliver high yields (up to 90%) of MeS-pphorb *a* (a25) with fewer by-products (Fig. 3.14) compared with the reactions involving methyliodide. The most abundant byproduct was MeSS-pphorb *a* (a26). Furthermore, an aqueous buffer component of the reaction mixture was found to be unnecessary in this case, having no significant effect on the yields of MeS-pphorb *a* obtained. The greater yields of MeS-pphorb *a* obtained using H_2S with dimethyl disulfide, than with methyliodide, suggests a more efficient generation of methanethiol in the case of the former. Alternatively, the lower yield in the case of MeI could be attributed to the generation of DMS from the reaction of methanethiol with unreacted MeI. By contrast, reaction of methanethiol with unreacted dimethyl disulfide would regenerate both methanethiol and dimethyl disulfide. Notably, MeS-pphorb *a* was not formed in reactions conducted with dimethyl disulfide in the absence of H_2S, demonstrating its involvement in the generation of methanethiol as per Equation 3.3. The possibility that the effect of H_2S is simple acid catalysis can be discounted on the basis that no MeS-pphorb *a* was formed upon reaction of pphorb *a* with MeSSMe in the presence of HCl.

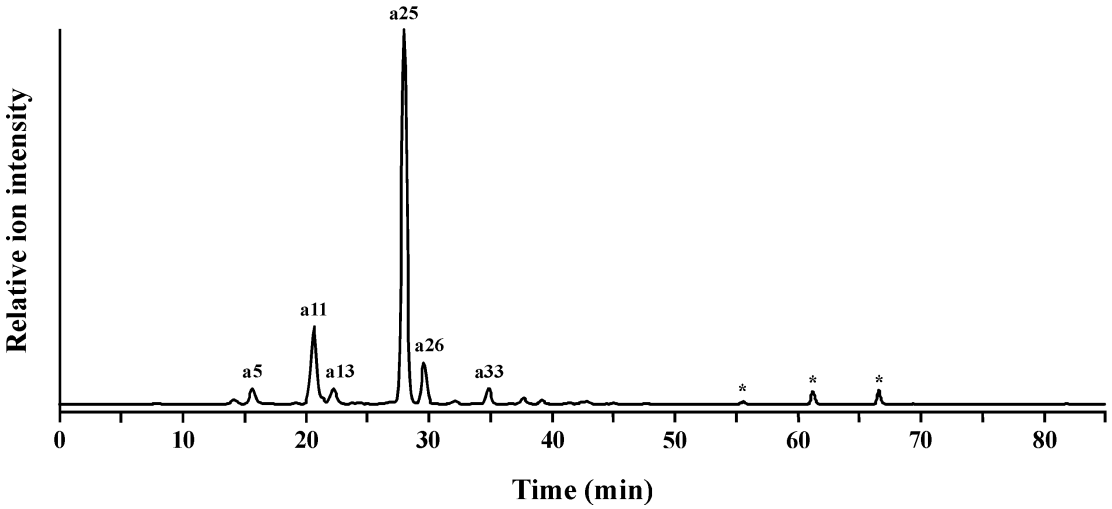

Figure 3.14. Representative mass chromatogram (*m/z* 400-1200) of the total extract from the reaction of pphorb *a* and phorb *a* with dimethyl disulfide and H_2S in acetone. Peak assignments in Table 3.1. *Not pigments.

Biologically occurring porphyrins and chlorins, which can often be isolated from their natural sources in large amounts, offer certain economic and environmental advantages over the synthetic compounds. The ability to manipulate the periphery of natural and synthetic chlorin and porphyrin structures is of considerable interest for a number of applications, enabling characteristics such as solubility and UV/vis absorption to be tuned, as well as providing a means to incorporate the tetrapyrrole skeleton into more complex molecular architectures. Photodynamic therapy (PDT) is an example of one such application. It involves the delivery of a photosensitising drug, which accumulates in tumour cells, followed by irradiation with light of an appropriate wavelength (Nyman and Hynninen, 2004; Calzavara-Pinton et al., 2007). Upon activation, the photosensitiser transfers energy to oxygen molecules forming reactive oxygen species, such as singlet oxygen ($^1O_2$), that have a cytotoxic effect. The photophysical and electrochemical properties of porphyrins and chlorins make them attractive for use as photosensitisers in PDT. The transmission of light through mammalian tissues increases as a function of increasing wavelength. Thus, chlorins, which posses a strong absorption band (Q_y) in the far red region of the visible electromagnetic spectrum (cf. Q_y band of chl *a* at λ_{max} 660 nm), are of particular interest for PDT, enabling a deeper therapeutic effect to be achieved with smaller doses than is possible with porphyrins, which possess much weaker Q bands in that waveband (Nyman and Hynninen, 2004; Calzavara-Pinton et al., 2007). One of the challenges affecting the use of chlorins and porphyrins in PDT is their solubility in physiological fluids. This is important and can affect the mechanism of uptake and localisation of the drug the tumour cells (Calzavara-Pinton et al., 2007).

The reactions detailed above permit the coupling of the vinyl substituents, common to many porphyrin and chlorin structures, with the sulfhydryl group of organic thiols and could be used to extend vinyl-bearing tetrapyrroles, without the need for employing harsh conditions or reagents, and in doing so change their properties (e.g. hydrophobicity) or even to tether them to globular structures such as proteins, via sulfhydryl-containing amino acid residues (e.g. cysteine).

In order to demonstrate the reaction with a porphyrin substrate, protoporphyrin-IX was introduced as its dimethyl ester (**47**), for reasons of solubility, and subjected to

reaction with dimethyl disulfide and H_2S under the conditions employed above. The reaction led primarily to formation of a component a19 (Fig. 3.15, Table 3.1) exhibiting a protonated molecule at *m/z* 687, corresponding to the C-3[1], C-8[1] dimethylthioether derivative (**62**). The MS^n spectra of this component (Fig. 3.16a-f) display the prominent losses of two methanethiyl radicals (-47 Da) in succession to form the base peak ions in MS^2 and MS^3. Later stages of MS^n contain losses typically observed for protoporphyrin-IX (Fig. 2.15; Chapter 2). The loss of 15 Da corresponds to elimination of a methyl radical and that of 32 Da to loss of methanol from one of the methyl propionate ester substituents. Losses of 87 and 73 Da arise via α– or β–cleavage of the methyl propionate ester substituents, respectively.

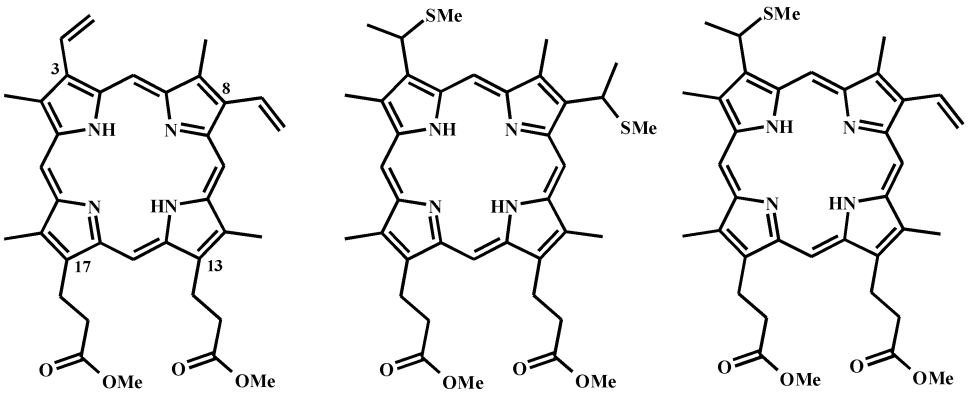

47 **62** **63**

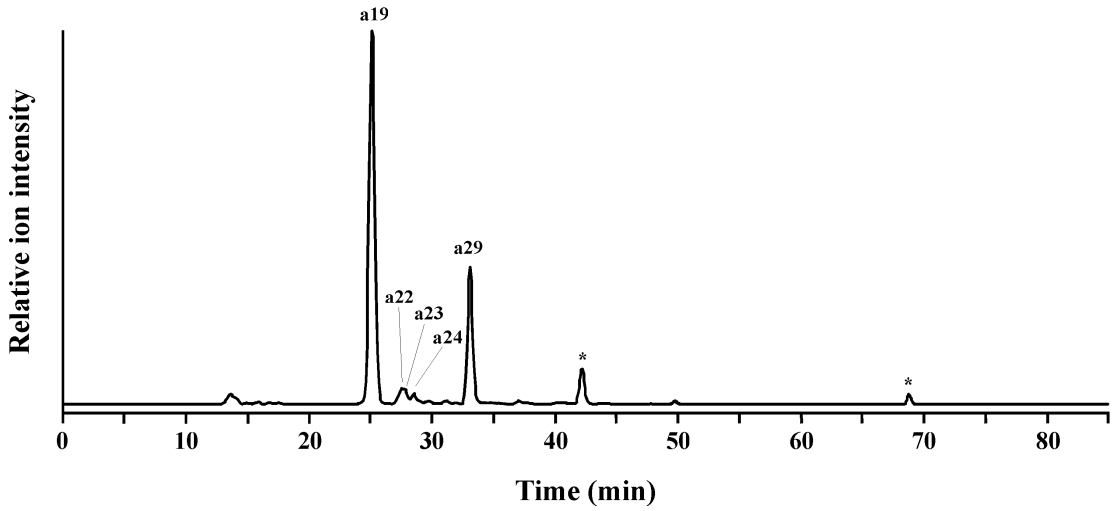

Figure 3.15. Representative mass chromatogram (*m/z* 400-1200) of the total extract from the reaction of protoporphyrin-IX (**47**, a29) with dimethyl disulfide and H_2S in acetone. Peak assignments in Table 3.1. *Not pigments.

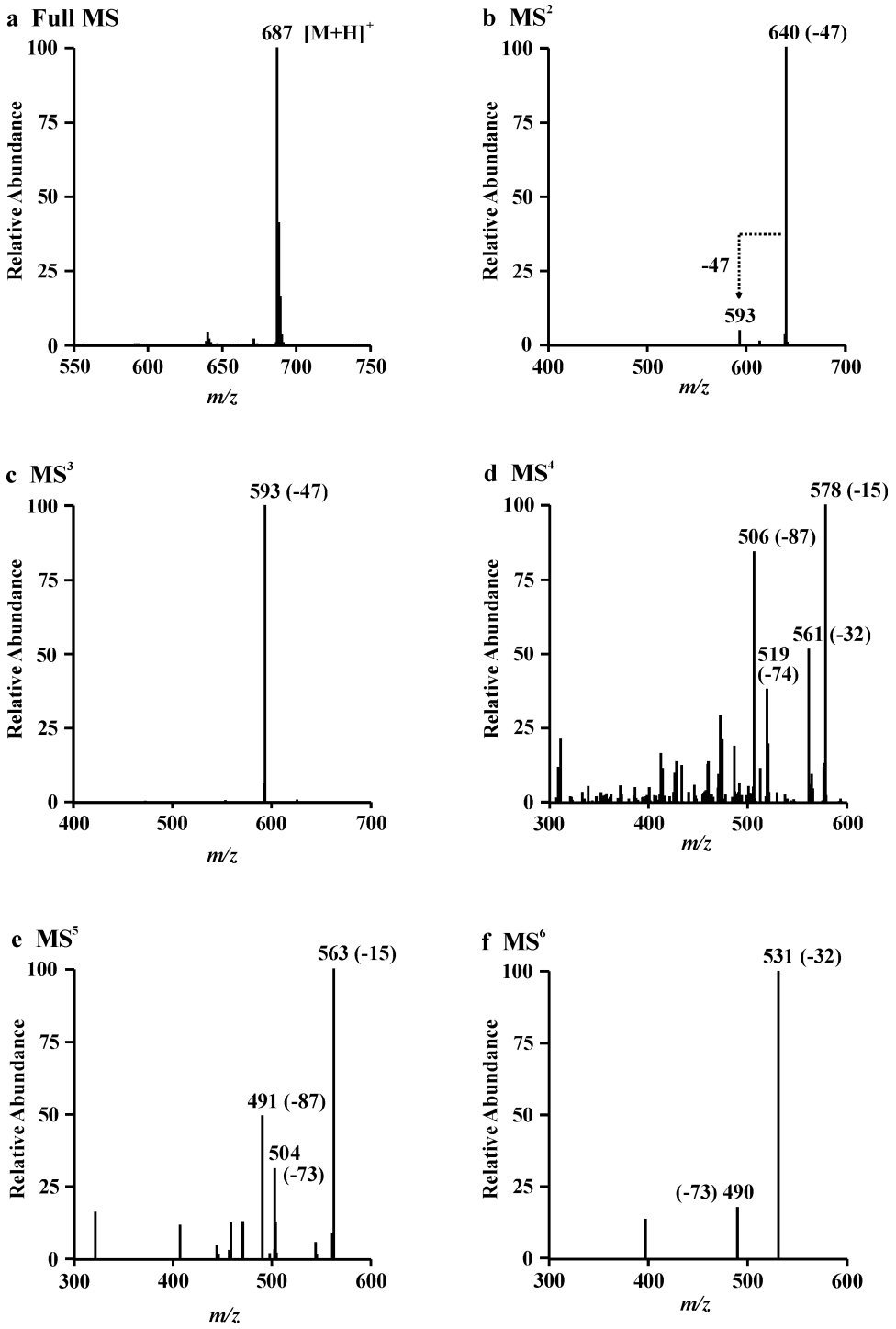

Figure 3.16. APCI multistage tandem mass spectra of $(MeS)_2$-protoporphyrin-IX (**62**); a) Full MS, b) MS^2, c) MS^3, d) MS^4, e) MS^5, f) MS^6. In each case the most abundant ion was selected as the precursor for the next spectrum.

Two isobaric components a23 (t_R = 28 min) and a24 (t_R= 28.5 min), exhibiting protonated molecules at *m/z* 639 (Figs. 3.17a and 3.18a, respectively), correspond to mono methylthioether derivatives of protoporphyrin-IX (e.g. **63**). These components represent structural isomers differing in the location of the alkylthioether moiety. The structure of protoporphyrin-IX contains two available vinyl groups at C-3 and C-8 and, owing to the asymmetry of the vinyl substituents, reaction of either produces two chromatographically distinct species. The compounds display the same main sequence of losses during MS^n, although slight differences were evident in the relative ion intensities, most noticeably in the MS^3-MS^5 spectra (Figs. 3.17c-e and 3.18c-e). Unfortunately, it was not possible, on the basis of their MS^n spectra, to assign the location of the methylthioether to either C-3^1 or C-8^1 in either derivative and the small amounts of these components precluded their isolation by preparative HPLC for more rigorous structural characterisation by ^{1}H NMR.

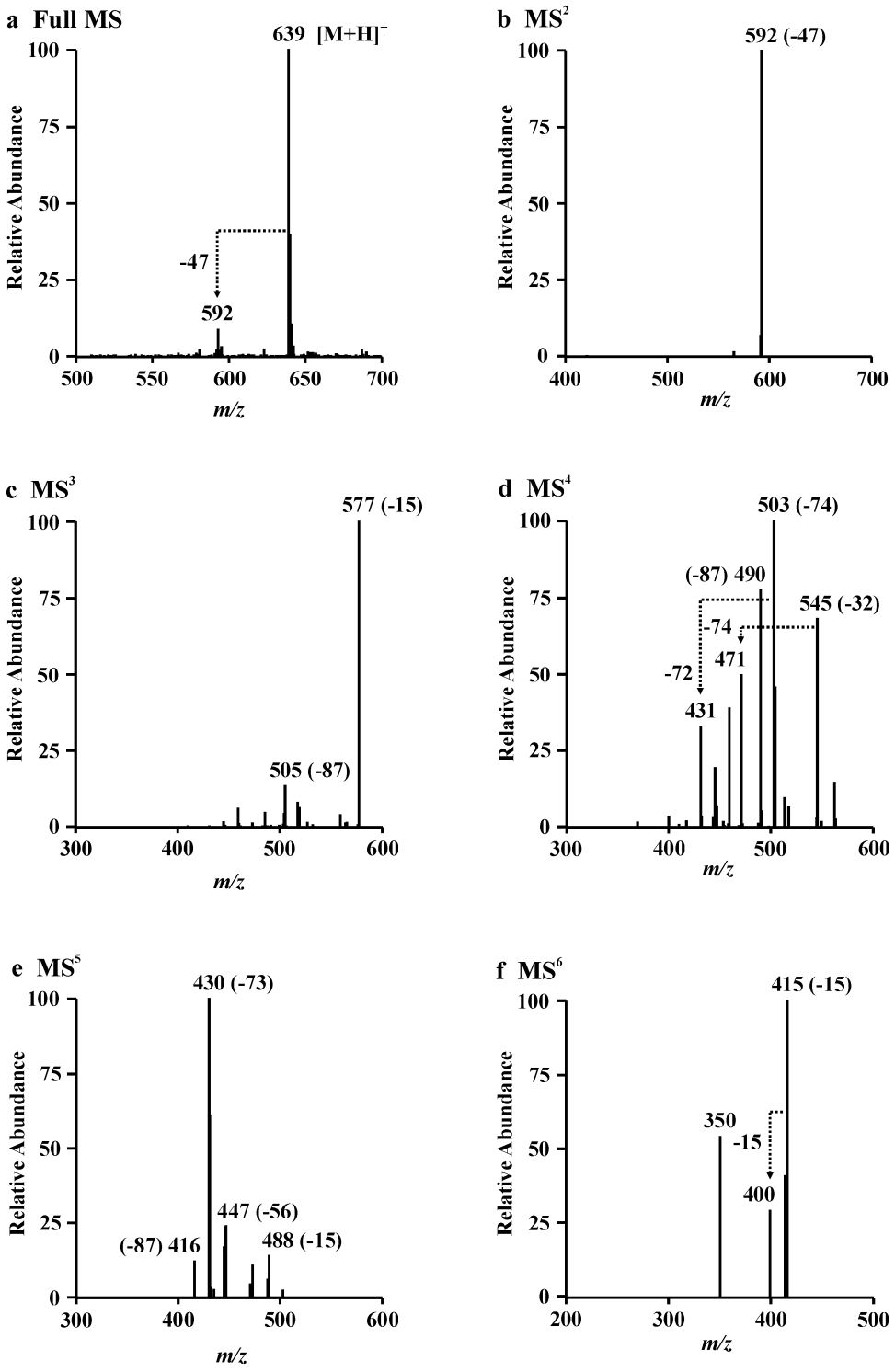

Figure 3.17. APCI multistage tandem mass spectra of a23; a) Full MS, b) MS^2, c) MS^3, d) MS^4, e) MS^5, f) MS^6. In each case the most abundant ion was selected as the precursor for the next spectrum.

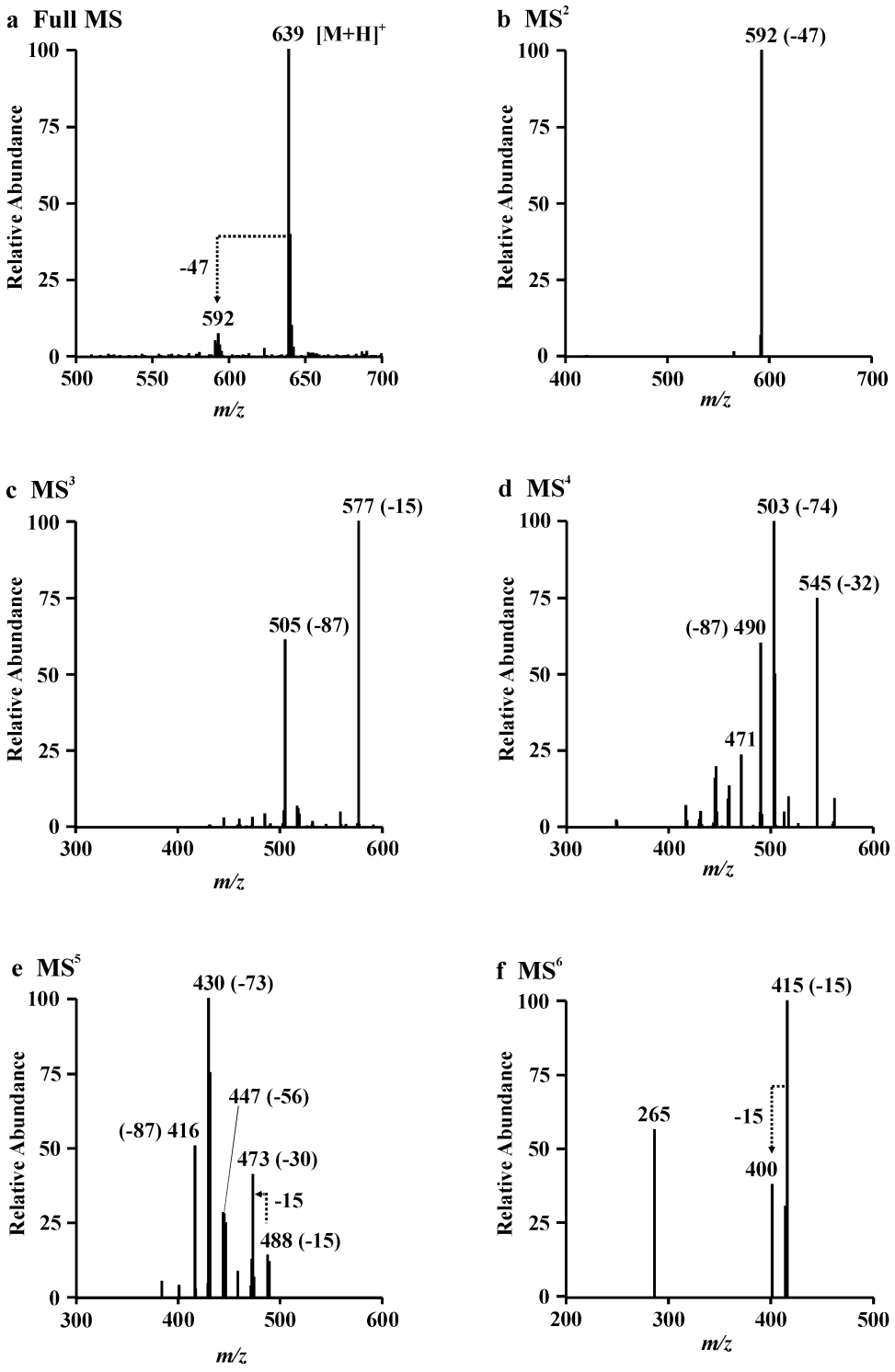

Figure 3.18. APCI multistage tandem mass spectra of a24; a) Full MS, b) MS^2, c) MS^3, d) MS^4, e) MS^5, f) MS^6. In each case the most abundant ion was selected as the precursor for the next spectrum.

Notably, in the case of protoporphyrin-IX, the reaction was incomplete (Fig. 3.15) with a product distribution containing predominantly the $(MeS)_2$-proto (a19) and unreacted starting material (a29), with little contribution from the mono methylthioether species (a23 and a24). This unusual feature of the distribution may be due to the fact that the solubility of protoporphyrin-IX in acetone was noticeably lower than that of pphorb *a*, leading to a greater tendency for aggregation during the reaction. This would result in the aggregated pigment being less available for reaction with dimethyl disulfide and H_2S, thus, remaining predominantly unreacted, while reaction of the dissolved pigment was able to proceed to completion forming the $(MeS)_2$-proto (yield 68%).

3.3. Conclusions

Five C-3[1] alkylthioether chlorophyll derivatives (**52a-e**), analogous to those found to occur naturally in the sediment from Pup lagoon, have been prepared in high yields by reaction of pphorb *a* with alkyliodides in the presence of H_2S. The formation of alkylthioether chlorophyll derivatives in the relatively simple laboratory systems detailed above provides a rationale for the formation of the natural derivatives from reaction of the chlorophyll vinyl group with alkyhalogen-derived alkylthiols. Detailed investigation of the formation of these and other products of the sulfurisation reactions, under reaction conditions that provide a much closer approximation to natural conditions, forms the basis of the work presented in Chapter 4.

Detailed study of the synthetic alkylthioether compounds using RP-HPLC, LC-MS^n and ^{1}H NMR provides valuable insight into their analytical characteristics, validating the assignments of the natural derivatives in the sediment of Pup Lagoon (Squier et al., 2003; 2004). The prominent loss of the alkylthioether moiety as a radical during MS^n analysis, observed for all five derivatives, has been confirmed as a diagnostic feature of the spectra.

Reactions of vinyl-bearing chlorophyll derivatives with H_2S and i) alkyliodides in acetone buffered to pH 7 or ii) dialkyl disulfides in acetone, produce high yields of C-3[1] alkylthioether chlorophyll derivatives with relatively few by-products and are suitable for the preparation of standards. The availability of standards and an understanding of their analytical characteristics will facilitate routine identification of alkylthioether chlorophyll derivatives in environmental samples on the basis of online UV/vis and mass spectral data obtained during APCI-LC-MS^n analysis. It is likely that future examination of sediments, in order to learn more from their stratigraphic profiles, will play an important role in developing an understanding of the causes for the formation of these derivatives and their palaeoenvironmental significance. In addition, the reactions described above may have other useful synthetic applications for the modification of chlorin and porphyrin vinyl substituents.

Chapter 4:

Micellar reactions of chlorophylls: simulation of reaction conditions in natural aquatic environments

4.1. Introduction

4.1.1. Sulfurisation of organic matter

Natural sulfurisation is intrinsically linked to the cycling of carbon and sulfur in the geosphere and is recognised to play a key role in the formation and preservation of sedimentary organic matter in anoxic aquatic environments (Sinninghe Damsté and de Leeuw, 1990). Such environments typically contain high concentrations of reduced sulfur species, such as H_2S and polysulfides, which are liable to react with functionalised biomolecules leading to the generation of both low molecular weight organosulfur compounds and sulfur-crosslinked macromolecular structures (Sinninghe Damsté and de Leeuw, 1990; Kohnen et al., 1991b; Wakeham et al., 1995; Hartgers et al., 1997; Adam et al., 2000).

The incorporation of sulfur into organic matter has been examined by a number of different approaches; i) the analysis of the low molecular weight organosulfur compounds contained within Recent sediments (Wakeham et al., 1995; Hartgers et al., 1997; Kok et al., 2000; Squier et al., 2004), ii) the characterisation of sulfur-bound organic matter via selective chemical degradation of the high molecular weight substances contained within older sediments (Kohnen et al., 1991b; Schaeffer et al., 1995; Adam et al., 2000) and iii) the experimental simulation of the natural sulfurisation of organic matter within controlled laboratory systems (see below).

4.1.2 Laboratory simulation reactions

The sulfurisation potential of numerous geochemically relevant substrates possessing functionalities such as aldehydes, including α, β-unsaturated aldehydes, (Rowland et al., 1993; Schouten et al., 1993; 1994; Krein and Aizenshtat, 1994; Schneckenburger et al., 1998; van Dongen et al., 2003; Amrani and Aizenshtat, 2004a; 2004b; Amrani et al., 2007); ketones (Schouten et al., 1993; 1994; Schneckenburger et al., 1998); alkenes (de Graaf et al., 1992; Rowland et al., 1993; Schouten et al., 1994; de Graaf et al., 1995; Adam et al., 1998; Hebting et al., 2006); alcohols (de Graaf et al., 1992; Fukushima et al., 1992; Schouten et al., 1994); carboxylic acids (Vairavamurthy and

Mopper, 1987; Schouten et al., 1994) and esters (Schouten et al., 1994) have been investigated in laboratory simulation reactions. These studies employed a wide variety of reagents and reaction conditions and led to the formation of organosulfur compounds, some of which are identical to those found to occur naturally. Of the various functionalities investigated, aldehydes, ketones and double bonds were found to be the most susceptible, especially those in conjugated arrangements, while isolated alcohols, carboxylic acids and esters were largely inert. Typically reactions employ H_2S, polysulfides or elemental sulfur as an inorganic sulfur source. Of these, polysulfides have been demonstrated, both theoretically and experimentally, to be the most reactive sulfur species (Amrani and Aizenshtat, 2004a; 2004b and references therein). Consequently, they have been suggested to be the most important sulfur species involved in the sulfurisation of organic matter. Reagent incompatibility presents a major challenge for the experimental simulation of natural sulfurisation; reduced inorganic sulfur species are highly water soluble, whereas the substrates for the reactions are typically water insoluble lipidic compounds. To alleviate this problem some studies have employed homogeneous organic media such as DMF (de Graaf et al., 1992; 1995) or hexane (Adam et al., 1998), in which the reduced sulfur species are sufficiently soluble. Such systems differ considerably from the aqueous systems that dominate natural marine/lacustrine environments. Other studies have used water/organic biphasic systems, e.g. water and ethyl acetate or water and toluene, often in conjunction with phase transfer catalysts (PTCs) such as tetrabutyl ammonium bromide (Schouten et al., 1993; 1994) or dimethyldidecylammonium bromide (Krein and Aizenshtat, 1994). These PTCs are cationic species in solution which form ion-pairs with the (poly)sulfide anions enabling them to pass from the aqueous layer into the organic layer containing the substrate. While this offers some improvements over the homogeneous organic systems, potential PTCs, which have a strong influence on reaction kinetics, are not abundant in natural aquatic environments (Krein and Aizenshtat, 1994). Reactions conducted in deionised water, lacustrine freshwater or (artificial) seawater provide a closer approximation of the natural environment and have been used in the simulation of the sulfurisation of water soluble substrates, such as glucose (van Dongen et al., 2003), or hydrophobic substrates, such as phytol and its derivatives present as an emulsion (Fukushima et al., 1992; Schneckenburger et al., 1998; Amrani and Aizenshtat, 2004a; 2004b). In addition to differences in the media, some studies also employ catalysts including the

aforementioned phase transfer agents, acids (Schneckenburger et al., 1998), bases (Rowland et al., 1993), and even photoinitiation (Adam et al., 1998). Further differences between sulfurisation studies are associated with the reaction temperatures used. These typically range from 50°C to as high as 100°C, although examples of low (ambient) temperature simulation reactions also exist (Krein and Aizenshtat, 1994; Adam et al., 1998; Amrani and Aizenshtat, 2004a). While elevated temperatures can accelerate reactions, allowing them to be observed on a reasonable timescale, they may also enable high energy reactions that would be unfeasible in the majority of depositional environments.

In addition to providing a greater understanding of the processes by which sulfur can become incorporated into organic matter, laboratory simulation studies serve to illustrate that even small variations in the conditions used can lead to changes in reaction mechanisms and the formation of different products from the same substrates. The sulfurisation of phytenal, a diagenetic product of phytol, serves as a good example having been the subject of numerous studies. Sulfurisation of phytenal resulted in the formation of i) isoprenoid thiophenes (ca. 30% yield), following reaction with elemental sulfur in DCM:MeOH:H_2O (48:48:4) with trimethylamine for 60 h at 45°C (Rowland et al., 1993); ii) phytenethiol and diphytenenylsulfide dimers (ca. 10-30% yield), when reacted with polysulfides in aqueous DMF for 20 h at 70°C or in water in the presence of sulfuric acid for several months at 100°C (Schneckenburger et al., 1998); iii) isoprenoid dithiolanes and trithianes (100% yield), when reacted with polysulfides in water and ethyl acetate (1:1) under PTC conditions for 1 week at 50°C (Schouten et al., 1993); and iv) polysulfide crosslinked oligo-polymeric isoprenoid skeletons (close to 100% yield), following reaction with polysulfides in either toluene:water (1:1) under PTC conditions for 4 h at room temperature (Krein and Aizenshtat, 1994) or artificial seawater for 1 week at 25°C (Amrani and Aizenshtat, 2004a). Clearly, reaction conditions can have a considerable influence on the mechanism of sulfurisation and the resulting product distributions. Thus, in order for laboratory simulation reactions to serve as a representative model, it is crucial that the conditions employed be as close as possible to those of the natural situation under study.

4.1.3. Sulfur-bound chlorophylls

The reactions detailed in Chapter 3 implicate short chain organohalogens, such as those produced during the overturn of phytoplankton blooms, and H_2S in the formation of natural alkylthioether chlorophyll derivatives; alkylS-chl *a* **21a-e**, alkylS-phe *a* **22a-e** and alkylS-pphe *a* **23a-e**. While those reactions provide a basis for understanding the formation of these derivatives, the conditions used (i.e. acetone based media) do not provide a close representation of the conditions in the natural environment.

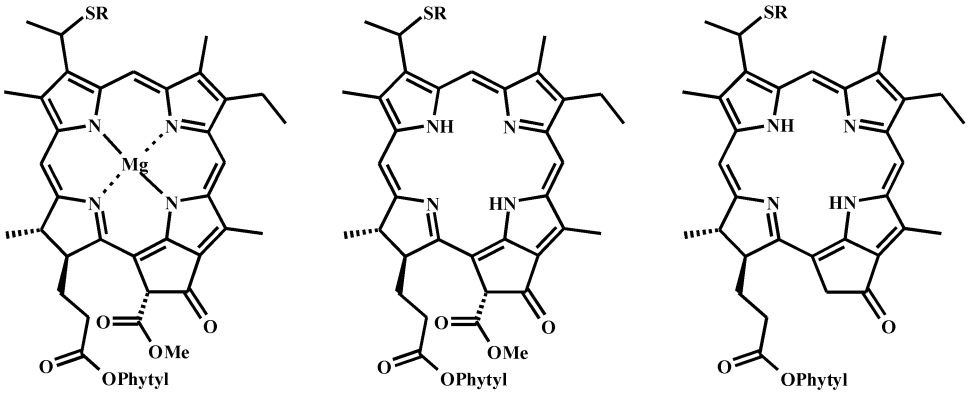

21 **22** **23**

R = Me (**a**), Et (**b**), *n*-Pr (**c**), *n*-Bu (**d**), *n*-Pent (**e**)

4.1.4. Aims

In this chapter, the reaction of chlorophyll and its derivatives with alkyliodides and H_2S is examined in greater detail in laboratory model systems that provide a close approximation of natural anoxic aquatic environments. The aims were to provide a firm rationale for the formation of the natural alkylthioether chlorophyll derivatives, to clarify the mechanism of their formation and to understand the significance of their occurrence and the distinguishing features of their sedimentary distributions.

4.2. Results and Discussion

4.2.1. Features of the model system

In order to provide a close mimic of natural anoxic aquatic environments it was necessary that the model reactions be conducted in aqueous media rather than systems comprising large proportions of organic solvent. This gave rise to problems regarding the solubility of the pigment substrate. With the exception of low pH, at which protonation of the ring nitrogen can render tetrapyrroles soluble in water, chlorophylls are water insoluble and have a propensity to form aggregates. This was overcome by introducing the anionic surfactant sodium dodecyl sulfate (SDS) to ensure dispersion of the lipophilic substrates and reagents in aqueous SDS micelles (illustrated in Fig. 4.1).

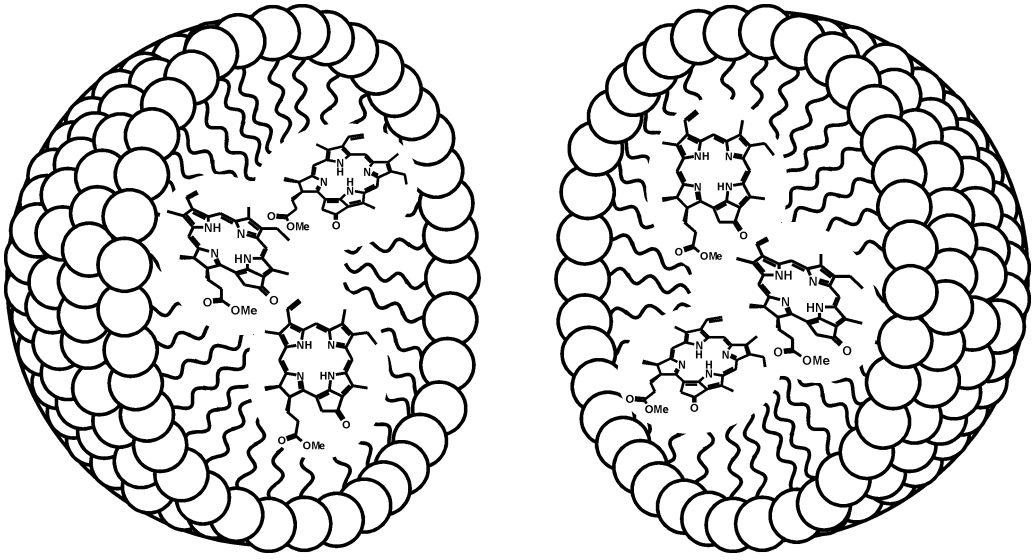

Figure 4.1. Illustration showing a representational cross section of a sodium dodecyl sulfate micelle containing encapsulated pigments.

The environment of the encapsulated pigment would not be unlike that of algal chlorophylls during senescence where they would presumably remain closely associated with lipidic cell constituents such as membrane lipids. This colloidal environment would greatly influence the nature of the species able to take part in, and mechanisms of, reaction with the chlorophyll molecule. Importantly, the simulation

reactions were performed at low temperature (room temperature). In addition, the reaction solution was buffered at a range of different pH values (pH 8.5, 7 or 5) to represent a wide variety of natural aquatic environments (typically pH 7.3-8.5; Killops and Killops, 2004), and to permit some control over the speciation of reduced sulfur compounds present in order to observe their effect on the reaction. In aqueous solution, H_2S exists in three different forms (H_2S, HS^-, and S^{2-}). The proportion of each individual species is dependant on pH and can be calculated using the Henderson-Hasselbalch equation (Equation 4.1).

$$pH = pK_a + \log_{10}([A^-]/[HA]) \quad (4.1)$$

Where: [HA] = the concentration of the acid (in this case H_2S).
[A-] = the concentration of its conjugate base (HS^-).

H_2S has a pk_{a1} of 7.02 and pk_{a2} of 14 (Crampton, 1974), thus the proportion of S^{2-} is negligible for the pH range used in these experiments (pH 5-8.5). At pH 7, close to the pk_{a1} of H_2S, H_2S and HS^- are present in approximately equal measure. At pH 5, H_2S accounts for over 99% of the total with a H_2S:HS^- ratio of approximately 100:1. At pH 8.5, HS^- predominates over H_2S in a ratio of approximately 30:1.

In a typical reaction, the pigment substrate was introduced into the reaction vessel in a small amount of acetone followed by the addition of an aqueous solution of SDS (buffered to pH 8.5, 7 or 5). The reaction vessel was sealed and evacuated to remove air and acetone before the introduction of H_2S to the flask headspace. Finally, the alkyliodide was admitted via a septum and the reaction stirred at room temperature in the dark for up to 12 d (for more detail see Chapter 6: Experimental).

4.2.2. Reaction of pyrophaeophorbide *a* with alkyliodides and H_2S

4.2.2.1. Alkylthioether derivatives

Reaction of pphorb *a* methyl ester (**33**) with methyliodide and H_2S at pH 8.5 led to its partial conversion into a number of products (Fig. 4.2a). Components of the reaction mixture were identified on the basis of their UV/vis and MS^n spectra (analytical data collected in Table 4.1). The major product of the reaction was MeS-pphorb *a* (s19, **52a**, formed in 12% yield) eluting prior to pphorb *a* (s23). The peaks s12 and s15 correspond to unreacted phorb *a* (**32**) and pphorb *b* (**64**), respectively, and were present as impurities in the starting mixture. The former species was preceded by a component s10 identified as its methylthioether derivative (MeS-phorb *a*, **53**). The only significant byproduct of the reaction was the acetone-derived compound s25 (**56**).

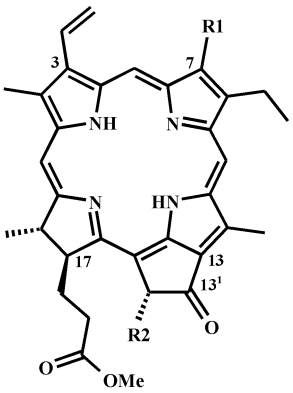

33: R1 = Me, R2 = H

32: R1 Me, R2 = CO_2Me

64: R1 = CHO, R2 = H

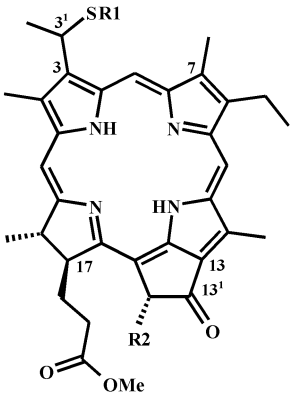

52: R1 = Me (**5a**), Et (**5b**), *n*-Pr (**5c**), *n*-Bu (**5d**), *n*-Pent (**5e**); R2 = H

53: R1 = Me, R2 = CO_2Me

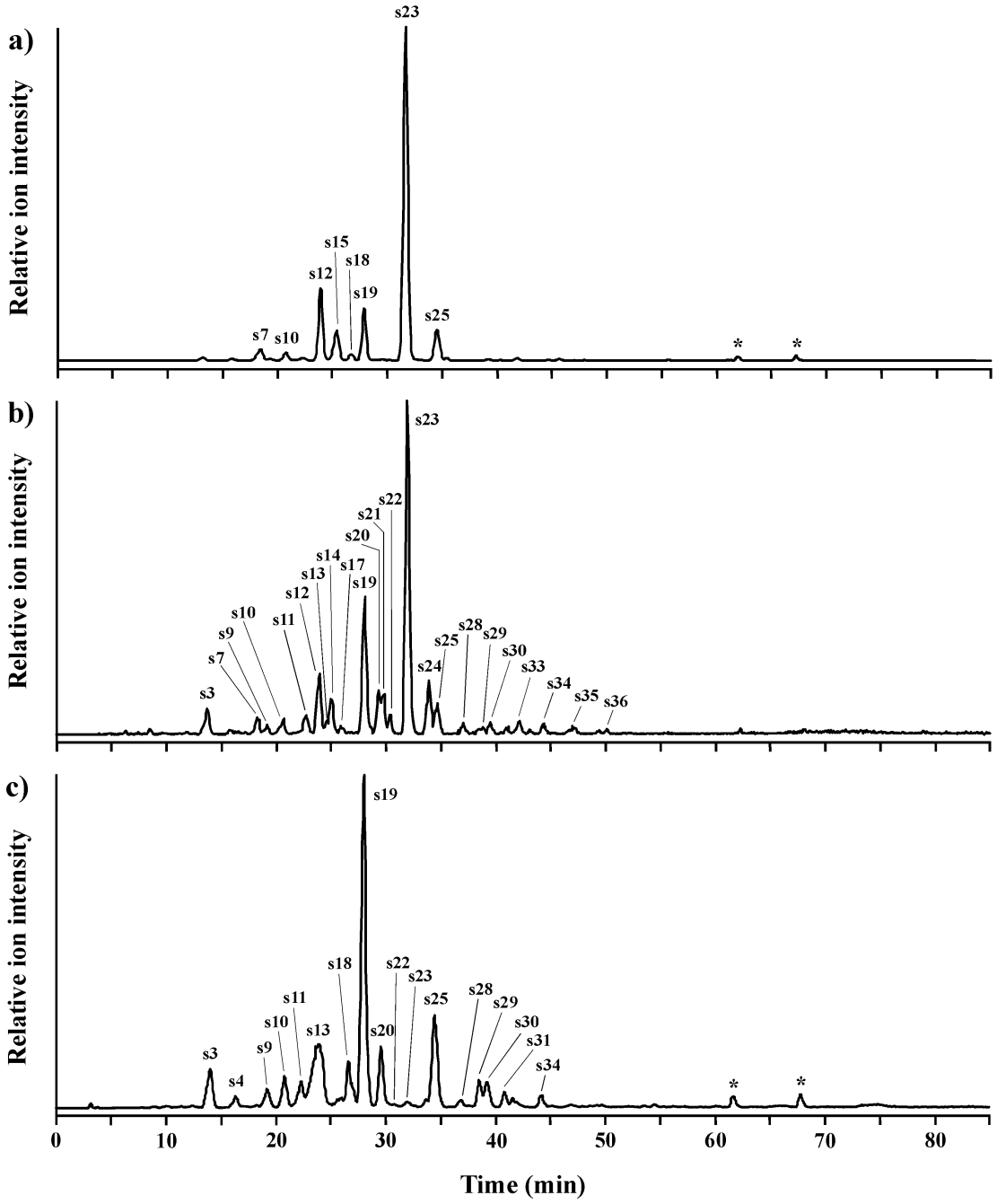

Figure 4.2. Representative mass chromatogram (*m/z* 400-1200) of the total extract from the reaction of a mixture of pphorb *a* (**33**) and phorb *a* (**32**) with methyliodide and H_2S in aqueous micellar solution for 12 d at; a) pH 8.5 b) pH 7 and c) pH 5. Peak assignments in Table 4.1. * Not chlorins.

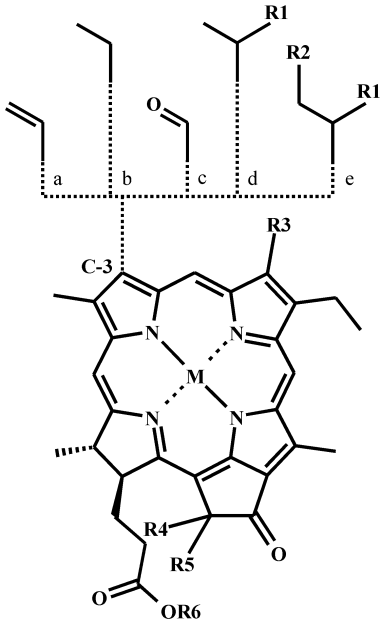

Table 4.1. Analytical data and structural assignments for the components identified in the reaction extracts.

Peak	$[M+H]^+$ (*m/z*)	Prominent ions in MS^n (*m/z*)‡	M	C-3	R1	R2	R3	R4	R5	R6	Structure number
s1	583	565, 555, 523, 495, 409	2H	e	OH	OH	Me	H	H	Me	**59**§
s2	625	607, 581, 565, 479, 435	2H	d	OH	n/a	Me	H	COOMe	Me	**72**
s3	567	549, 539, 523, 495, 409	2H	d	OH	n/a	Me	H	H	Me	**57**
s4	645	617, 566, 523, 495, 409									
s5	609	549, 521, 463, 435, 493	2H	c	n/a	n/a	Me	H	COOMe	Me	**71**
s6	639	607, 579, 493, 461, 435									
s7†	623	605, 545, 517, 485	2H	a	n/a	n/a	Me	OH	COOMe	Me	**35**
s8	721	641, 568, 523, 495, 409									
s9	719	631, 565, 523, 495, 409	2H	e	$SSC(CH_3)_2SMe$	OH	Me	H	H	Me	§
s10	655	608, 593, 548, 462, 434	2H	d	SMe	n/a	Me	H	COOMe	Me	**53**
s11	565	537, 523, 495, 409	2H	d	=O	n/a	Me	H	H	Me	**58**
s12†	607	547, 519, 461, 433	2H	a	n/a	n/a	Me	H	COOMe	Me	**32**
s13	551	523, 495, 437, 409	2H	c	n/a	n/a	Me	H	H	Me	**65**
s14	581	553, 549, 523, 521, 435									
s15†	563	535, 507, 492, 421	2H	a	n/a	n/a	-C=O	H	H	Me	**64**
s16	549	521, 493, 461, 434, 419									
s17	629	582, 567, 539, 533, 453	2H	e	SMe	SH	Me	H	H	Me	**55**§
s18	729	641, 607, 547, 519, 461	2H	d	$SC(CH_3)_2SMe$	n/a	Me	H	COOMe	Me	
s19	597	550, 535, 521, 507, 421	2H	d	SMe	n/a	Me	H	H	Me	**52a**
s20	629	550, 535, 521, 507, 421	2H	d	SSMe	n/a	Me	H	H	Me	**54**
s21	639	581, 553, 548, 467									
s22	551	523, 437, 422, 408	2H	b	n/a	n/a	Me	H	H	Me	**67**
s23†	549	521, 435, 420, 406	2H	a	n/a	n/a	Me	H	H	Me	**33**
s24	657	550, 535, 521, 507, 421	2H	d	SS-*i*-Pr	n/a	Me	H	H	Me	**61**
s25	671	583, 549, 521, 435	2H	d	$SC(CH_3)_2SMe$	n/a	Me	H	H	Me	**56**
s26	687	549, 521, 435, 420									
s27	653	625, 539, 505, 465, 433									
s28	703	550, 535, 521, 507, 421	2H	d	$SSC(CH_3)_2SMe$	n/a	Me	H	H	Me	
s29	777	729, 689, 623, 550, 535	2H	d	$SC(CH_3)_2S_2C(CH_3)_2SMe$	n/a	Me	H	H	Me	
s30	735	647, 623, 550, 535, 521	2H	d	$S_3C(CH_3)_2SMe$	n/a	Me	H	H	Me	
s31	735										
s32	719	613 , 549, 521, 435,									
s33	767	550, 535, 521, 507, 421									
s34	809	721, 550, 535, 521, 507	2H	d	$SC(CH_3)_2S_3C(CH_3)_2SMe$	n/a	Me	H	H	Me	
s35	841	Does not fragment									
s36	873	Does not fragment									

Table 4.1. Continued.

Peak	$[M+H]^+$ (*m/z*)	Prominent ions in MS^n (*m/z*)‡	M	C-3	R1	R2	R3	R4	R5	R6	Structure number
s37	935	657, 639, 579, 532	Mg	d	SMe	n/a	Me	OH	COOMe	Phytyl	
s38	887	609, 591, 531, 487, 475	Mg	a	n/a	n/a	Me	OH	COOMe	Phytyl	
s39	917	639, 579, 532	Mg	d	SMe	n/a	Me		COOMe	Phytyl	§
s40	869	591, 531, 487, 475, 472	Mg	a	n/a	n/a	Me		COOMe	Phytyl	§
s41	949	671, 639, 579, 532	Mg	d	SMe	n/a	Me	OMe	COOMe	Phytyl	§
s42	901	623, 591, 531, 487	Mg	a	n/a	n/a	Me	OMe	COOMe	Phytyl	§
s43	919	641, 594, 581, 534, 461	Mg	d	SMe	n/a	Me	H	COOMe	Phytyl	**21a**
s44	871	593, 533, 461, 433	Mg	a	n/a	n/a	Me	H	COOMe	Phytyl	**4**
s45	919	641, 594, 581, 534, 461	Mg	d	SMe	n/a	Me	H	COOMe	Phytyl	**21a'**
s46	871	593, 533, 461, 433	Mg	a	n/a	n/a	Me	H	COOMe	Phytyl	**4'**
s47	983	872, 593, 533, 506									
s48	919	641, 594, 581, 534, 461	2H	d	SMe	n/a	Me	H	COOMe	Phytyl	**22a**
s49	871	593, 533, 461, 433	2H	a	n/a	n/a	Me	H	COOMe	Phytyl	**14**
s50	871	593, 533, 461, 433	2H	a	n/a	n/a	Me	H	COOMe	Phytyl	**14'**
s51	861	550, 535, 521, 493, 435	2H	d	SPhytyl	n/a	Me	H	H	Me	**78**
s52	861	550, 535, 521, 493, 435	2H	d	SPhytyl	n/a	Me	H	H	Me	**78**
s53	1183	905, 845, 594, 593	2H	d	SPhytyl	n/a	Me	H	COOMe	Phytyl	**73**
s54	1183	905, 845, 594, 593	2H	d	SPhytyl	n/a	Me	H	COOMe	Phytyl	**73**
s55	1183	905, 845, 594, 593	2H	d	SPhytyl	n/a	Me	H	COOMe	Phytyl	**73**
s56	1183	905, 845, 594, 593	2H	d	SPhytyl	n/a	Me	H	COOMe	Phytyl	**73**

† Compound present in the pphorb *a* starting mixture. ‡ Obtained following resonance enhanced collision induced dissociation of the protonated molecule. The underlined *m/z* value denotes the base peak ion in MS^2. Apostrophe (e.g. **4'**) denotes the epimer. § Tentative assignment.

Reaction of the pphorb *a* (**33**) with each of the other four alkyliodides (ethyl-, *n*-propyl-, *n*-butyl- and *n*-pentyliodide) and H_2S at pH 8.5 led to formation of the corresponding alkylthioether derivatives (EtS-pphorb *a*, **52b**, 16% yield; PrS-pphorb *a*, **52c**, 43%; BuS-pphorb *a*, **52d**, 60%; and PentS-pphorb *a*, **52e**, 91%) analogous to the natural sedimentary species identified in Pup Lagoon (Squier et al., 2003; 2004). Whereas the yields obtained for the different alkylthioethers formed in the reactions conducted in Chapter 3 did not show great differences, here a definite increase in yield is observed with increasing alkyl chain length. This may be attributed to a greater hydrophobicity of the higher order alkyliodides and their corresponding thiols resulting in greater access to/preference for the hydrophobic micelle interior, increasing the potential for reaction.

The formation of alkylthioether chlorophyll derivatives under conditions that provide a good model of natural anoxic aquatic environments (aqueous media, low temperature, moderate pH, presence of H_2S and limitation of oxygen) provides clear evidence to support a route to their formation in nature from reaction between the chlorophyll vinyl group and alkylthiols formed from the reaction of H_2S with organohalogens.

In order to probe the mechanism of formation of the alkylthioether derivatives of pphorb *a*, the reaction was conducted at pH 7 and pH 5. Low pH was found to increase the rate of formation of MeS-pphorb *a* (Fig. 4.3). This, together with the alkylthioether formation at the C-3^1 position (Markovnikov product), supports an electrophilic addition mechanism involving initial protonation of the C-3 vinyl group (illustrated in Scheme 4.1) to form a C-3^1 carbocation, stabilised by resonance with the aromatic macrocycle. Subsequent attack of this cation by either an alkylthiol/alkylsulfide derived from reaction of H_2S and alkyliodide, or H_2S/HS^- with alkylation by the alkyliodide, can yield the alkythioether at C-3^1.

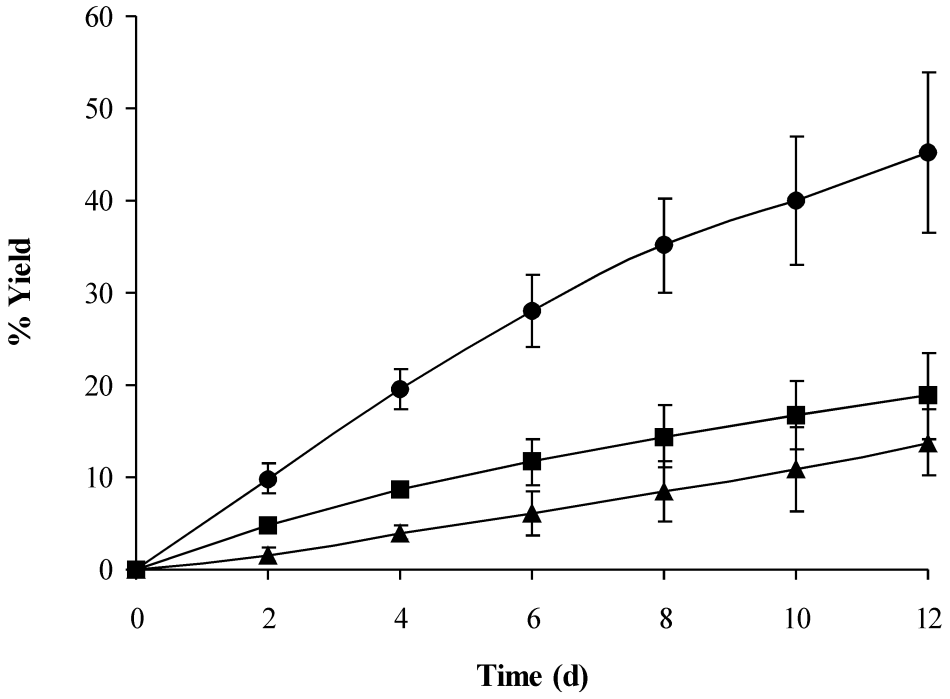

Figure 4.3. Plot showing the % yield of MeS-pphorb *a* obtained during reaction of pphorb *a* with methyliodide and H_2S at pH 8.5 (▲), 7 (■) and 5 (●). Error bars represent ±1 s.d. (n = 3).

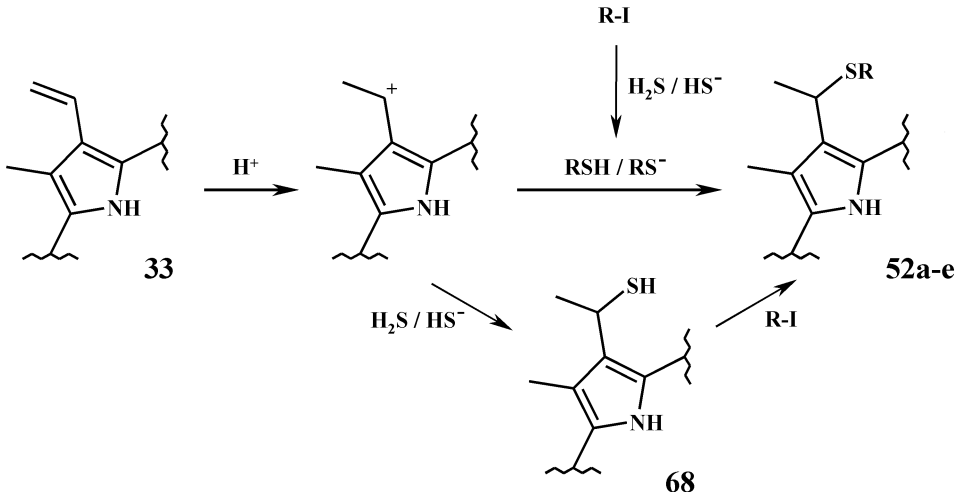

Scheme 4.1. Proposed mechanism for the formation of the C-3[1] alkylthioether chlorophyll derivatives (**52a-e**) from the reaction of pphorb *a* (**33**) with alkyliodide and H_2S. R = Me (**52a**), Et (**52b**), *n*-Pr (**52c**), *n*-Bu (**52d**), *n*-Pent (**52e**).

4.2.2.2. Other products of the reaction

Notably, the LC-MS chromatograms of extracts from the reactions conducted at pH 7 and pH 5 reveal the formation of higher proportions of byproducts with decreasing pH (Fig. 4.2b and c). These include many of the same components as those identified in the products from reactions conducted in acetone-based media (Chapter 3). Peaks a24-a31, and a34 represent byproducts derived from residual acetone, used as a solubilising agent to introduce the pigment into the aqueous micelles. Peaks s3 and s11 correspond to the oxidation products, C-3 (1-hydroxyethyl) pphorb *a* (**57**) and C-3 acetyl pphorb *a* (**58**), respectively, and are suspected to arise from reactions involving traces of oxygen still present in the reaction system.

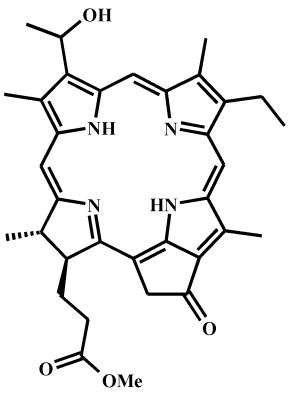

57

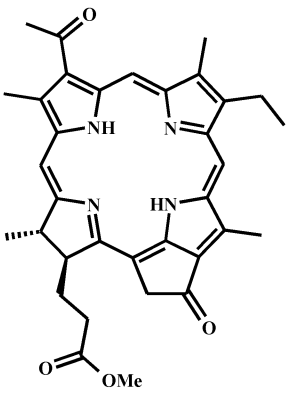

58

Component s13 represents a significant product of the reactions conducted at pH 5 (Fig. 4.2c), eluting as a broad peak at t_R = 23.5 min, approximately 8 min earlier than pphorb *a*. The earlier elution indicates an increase in polarity. The online UV/vis spectrum of s13 (Fig. 4.4) exhibits a bifurcated Soret band with maxima at 385 and 423 nm, and a red shift in the Q_y band to 692 nm (cf. pphorb *a*, λ_{max} 409, 665 nm). The appearance of the chlorin UV/vis absorption spectrum is extremely sensitive to structural modification of substituents directly conjugated to the macrocycle, such as the C-3 vinyl group. The spectral characteristics of the unidentified reaction product suggest a strong structural similarity with pphorb *d* (**65**) and bacterioviridin (**66**), both of which possess carbonyls conjugated to the chlorin macrocycle at position C-3 and exhibit similar bifurcation of the Soret band (Tamiaki et al., 1996; Wilson et al., 2004b).

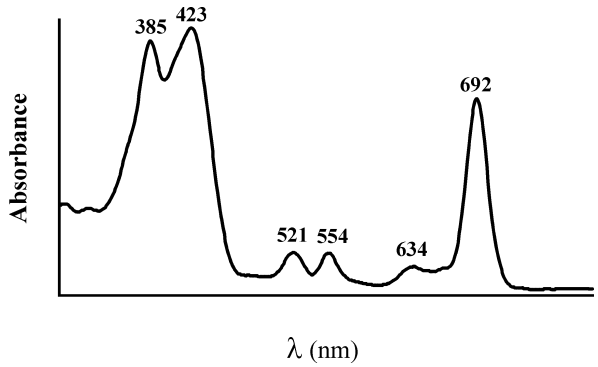

Figure 4.4. Online UV/vis spectrum (300-800 nm) of component s13.

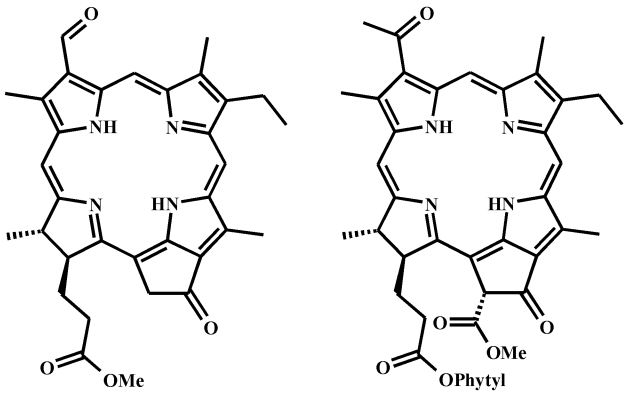

65 **66**

The mass spectra (unit resolution) across the broad peak of s13 (Fig. 4.5a) revealed it to comprise a single component with a protonated molecule ($[M+H]^+$) at *m/z* 551, 2 *m/z* units greater than pphorb *a* ($[M+H]^+$ = *m/z* 549). High resolution APCI TOF MS provided an accurate $[M+H]^+$ at *m/z* of 551.2653 corresponding to $C_{33}H_{35}N_4O_4$, consistent with the empirical formula of pphorb *d* and the replacement of a methylene in pphorb *a* with an oxygen atom. CID of *m/z* 551 generated product ions in MS^2 (Fig. 4.5b) at *m/z* 523 (-28 Da, 100%) and *m/z* 437 (-114 Da, 15%) consistent with losses of CO from the C-13^1 position and its loss in combination with the entire C-17^1 methyl propionate ester with back-transfer of hydrogen to the charge retaining macrocycle, respectively. These losses are both observed in the MS^2 spectrum of pphorb *a* (s23, Table 4.1). Notably, the relative abundance of *m/z* 437 is significantly lower than that of the analogous fragment ion in the MS^2 spectrum of pphorb *a* indicating an increased probability of losing 28 Da to form the base peak at *m/z* 523.

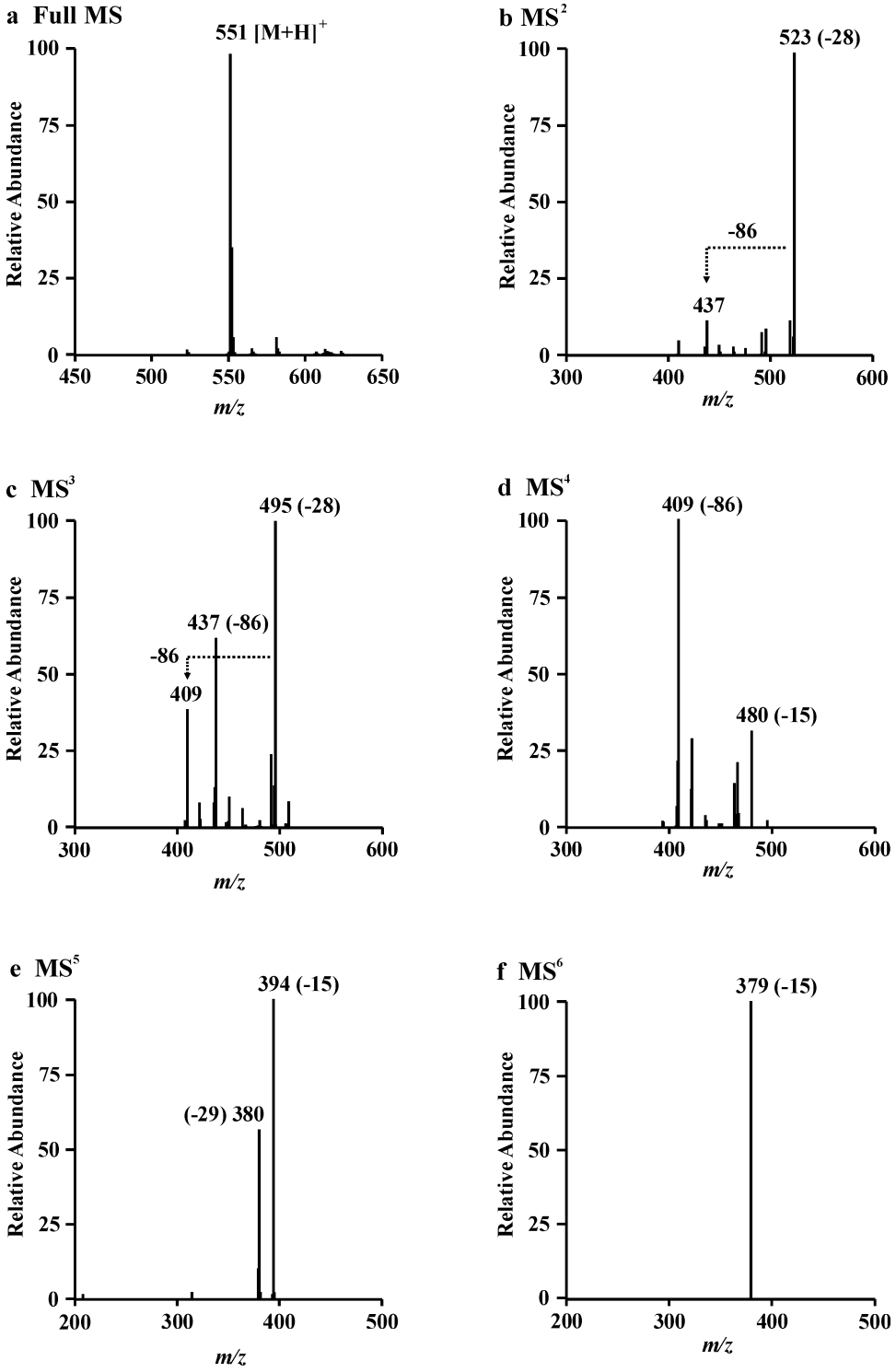

Figure 4.5. APCI multistage tandem mass spectra of pphorb *d* methyl ester (**65**); a) Full MS, b) MS^2, c) MS^3, d) MS^4, e) MS^5, f) MS^6. In each case the most abundant ion was selected as the precursor for the next spectrum.

CID of *m/z* 523 gave rise to a base peak ion in MS^3 at *m/z* 495 (Fig. 4.5c) representing a further loss of 28 Da. This was attributed to loss of a second CO, indicating an additional ketone or aldehyde group in the structure. Support for this interpretation comes from the analogous MS^n spectra of pphorb *b* (**64**; s15, Table 4.1). Pphorb *b* contains an aldehyde group at position C-7 in addition to the carbonyl at C-13^1 and also shows two successive losses of CO (-28 Da) in MS^2 and MS^3. Notably, an additional loss of 28 Da is not observed in the MS^n spectra of pphorb *a* for which the only cleavage that could account for such a loss, expulsion of the C-3 vinyl as C_2H_4, is extremely unfavourable. Additional product ions in the MS^3 spectrum of the reaction product occur at *m/z* 437 (-86 Da, 62%), corresponding to loss of the C-17^1 methyl propionate ester with hydrogen transfer to the macrocycle, and *m/z* 409 (-114 Da, 44%), reflecting the concerted loss of the CO and C-17^1 substituents. On the basis of UV/vis and mass spectral evidence the reaction product can be assigned as pphorb *d* (**65**), apparently formed via oxidative cleavage of the C-3 vinyl group of pphorb *a*.

The LC-MS chromatogram of the products from the reaction of pphorb *a* with methyliodide and H_2S at pH 7 (Fig. 4.2b) shows the presence of a product s22 eluting immediately prior to pphorb *a* (t_R = 27.5 min cf. t_R = 29.5 min) and exhibiting a similar online UV/vis spectrum (λ_{max} 405, 652 nm), suggesting that the two compounds share strong structural similarities. Notably, both the Soret and Q_y bands for s22 are blue-shifted relative to pphorb *a* (λ_{max} 409, 665 nm). Similar shifts in absorption maxima are observed for pphorb *a* derivatives that contain a reduced C-3 vinyl substituent, such as mpphorb *a* (**67**) (Keely et al., 1990; Spooner et al., 1995) and C-3^1 thioether pphorb *a* derivatives (Chapter 3).

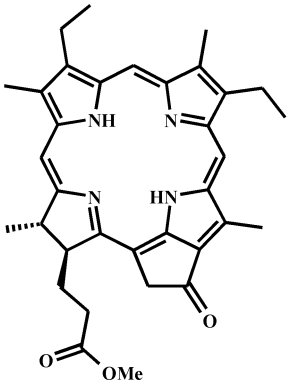

67

APCI LC-MS^n analysis (Fig. 4.6a) revealed s22 to exhibit a protonated molecule ($[M+H]^+$) at *m/z* 551, 2 *m/z* units greater than that of pphorb *a* ($[M+H]^+$ = 549). The data are consistent with addition of two hydrogen atoms suggesting reduction of the C-3 vinyl group to form mpphorb *a*. Aside from the difference of 2 *m/z* units, which is maintained throughout each stage of MS^n analysis, the MS^2 and MS^3 spectra of *m/z* 551 (Fig. 4.6b and c) and those of pphorb *a* (s23, Table 4.1) display strong similarities. Both compounds exhibit analogous product ions which occur in approximately equal relative abundance. The most prominent product ions correspond to $[M+H-28]^+$ in MS^2 and $[M+H-28-86]^+$ in MS^2 and MS^3. Losses of -28 and -86 Da reflect losses of the C-13^1 ketone as CO and the C-17 methyl propionate ester moiety with hydrogen transfer to the charge-retaining fragment. Notably, the MS^4 spectra for the unknown component and pphorb *a* show a distinct difference. In the case of pphorb *a*, loss of a methyl radical via α-cleavage of a methyl substituent or β-cleavage of an ethyl substituent gives a base peak ion at *m/z* 420. A second loss, of an ethyl radical via α-cleavage of the C-8 ethyl substituent, forms a subordinate peak at *m/z* 406 (60%). By contrast, the MS^4 spectrum of the reaction product (Fig. 4.6d) reveals that loss of an ethyl radical to form *m/z* 408 (100%) is favoured over loss of a methyl radical to form *m/z* 422 (75%). The greater tendency in the reaction product for loss of an ethyl radical indicates that the structure contains a greater number of ethyl substituents. On the basis of the UV/vis and mass spectral evidence, the reaction product was assigned as mpphorb *a* methyl ester (**67**), in which the C-3 vinyl group of pphorb *a* has been reduced to an ethyl substituent. Comparison of the LC retention time, online UV/vis spectrum and multistage tandem mass spectra of the reaction product with those of an authentic standard of mpphorb *a* methyl ester, confirmed the assignment. Mpphorb *a* is a key intermediate in the series of diagenetic transformations linking chl *a* to sedimentary alkyl porphyrins (**18**, Fig. 1.2, Chapter 1). Its formation in the simulation reactions is investigated in greater detail below (Section 4.2.5).

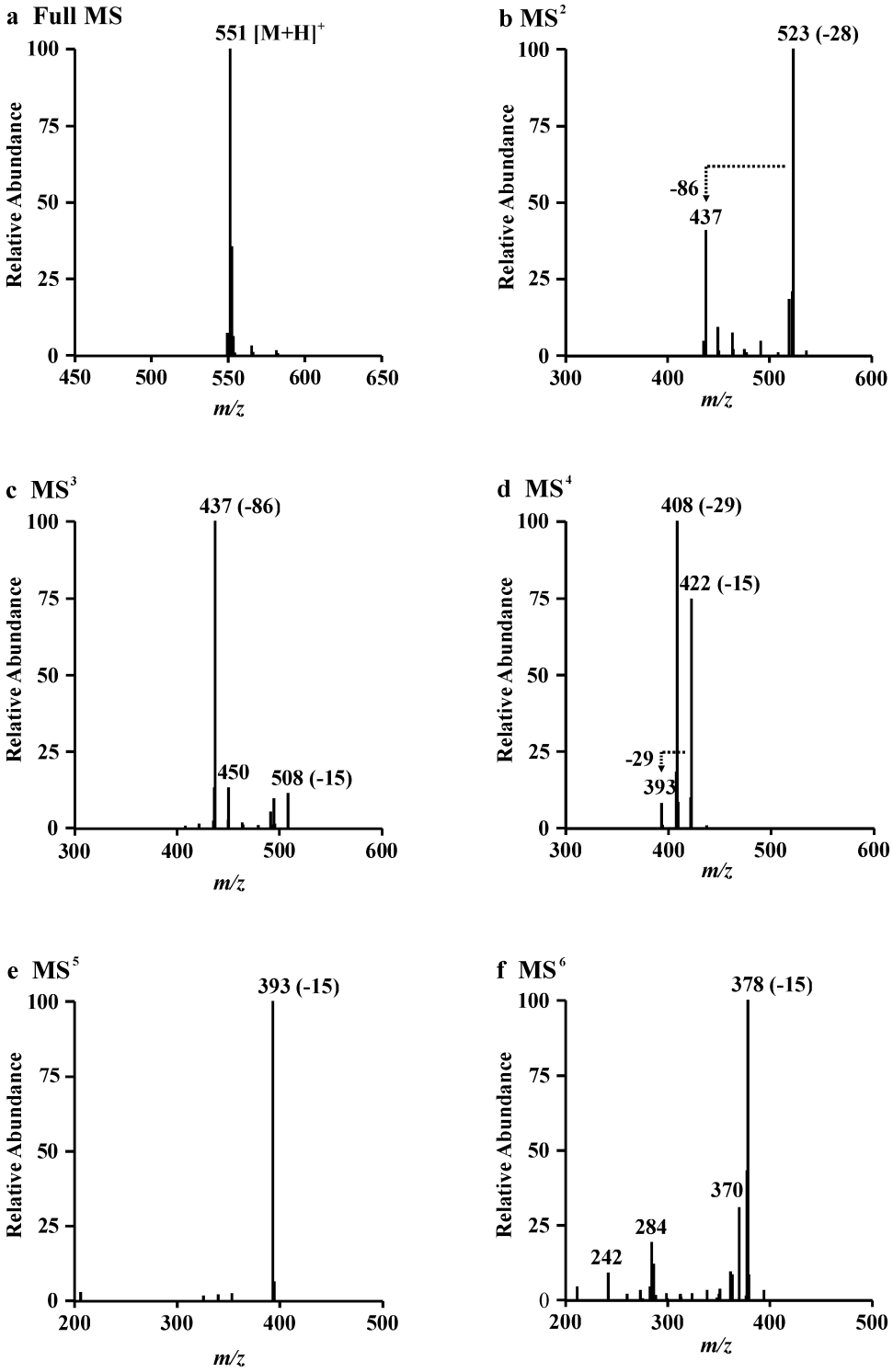

Figure 4.6. APCI multistage tandem mass spectra of mpphorb *a* methyl ester (**67**); a) Full MS, b) MS^2, c) MS^3, d) MS^4, e) MS^5, f) MS^6. In each case the most abundant ion was selected as the precursor for the next spectrum.

4.2.3. Reaction of chlorophyll *a* with alkyliodides and H_2S

LC-MS analysis of the product mixture from reaction of chl *a* (s44) with methyliodide and H_2S at pH 8.5 (Fig. 4.7) did not reveal any detectable MeS-chl *a* (**21a**) after 12 d and partial demetallation to phe *a* (s49) was observed. Chl *a* is readily demetallated under acidic conditions, however, alkaline pH was maintained throughout the reaction. Control reactions performed in the absence of H_2S did not show any demetallation, thus, it appears that H_2S is involved in the displacement of the central Mg ion; possibly, given the affinity of sulfur for metals, through direct binding to the metal itself and proton transfer to the tetrapyrrole nitrogens.

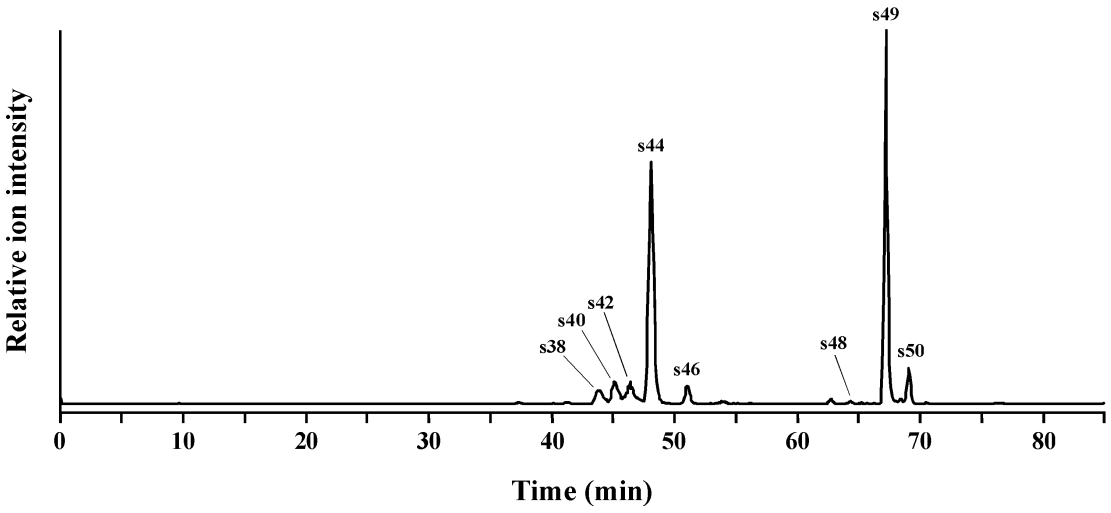

Figure 4.7. Representative mass chromatogram (*m/z* 400-1200) of the total extract from the reaction of chl *a* (**4**), in aqueous micelles buffered to pH 8.5, with methyliodide and H_2S for 12 d.

A trace amount of MeS-phe *a* (s48, **22a**) was formed in the reaction, confirmed by comparison of its UV/vis and MS^n spectral characteristics (Fig. 4.8) with those of the natural species (Squier et al., 2003; 2004). CID of the protonated molecule of MeS-phe *a* (*m/z* 919) yields a base peak ion in MS^2 (Fig. 4.8b) at 641 (-278 Da), reflecting loss of the C-17[3] phytol esterifying alcohol as phytadiene with hydrogen transfer to the charge retaining fragment. Ions of lesser intensity at *m/z* 593 and *m/z* 581 arise via further loss of the C-3[1] alkylthioether as methanethiol (-48 Da) and the C-13[2] carbomethoxy group (-60 Da), respectively. CID of *m/z* 641 generates a base peak ion in MS^3 (Fig. 4.8c) at *m/z* 594 corresponding to loss of a methanethiyl radical (-47 Da) from C-3[1].

The formation of MeS-phe *a* in the reaction, and lack of formation of MeS-chl *a*, may indicate a greater susceptibility of the phe *a* vinyl group to reaction with alkylthiols. It is possible that the presence of a chelated metal could moderate the nucleophilicity of the vinyl group, thereby discouraging the initial protonation step by withdrawing electron density from the chlorin π-system. Interestingly, differences were evident between the sulfurised and non-sulfurised fractions in the sedimentary pigment distributions from Pup Lagoon (Squier et al., 2004). Whereas chl *a* was consistently a major component of the non-sulfurised chlorin fraction, the sulfurised fraction was dominated by demetallated alkylthioether derivatives with alkylS-chl *a* present intermittently and in relatively low abundance. These distributional differences raise several possibilities: i) that demetallated pigments are more susceptible to the sulfurisation reaction and are, therefore, selectively sequestered into the sulfurised fraction; ii) that there are two parallel processes in operation and that the conditions that favour formation of the alkylthioether chlorophyll derivatives also promote demetallation and iii) that the observed distribution is the result of mixed inputs from different sources/palaeoenvironmental conditions, indistinguishable at the temporal resolution sampled.

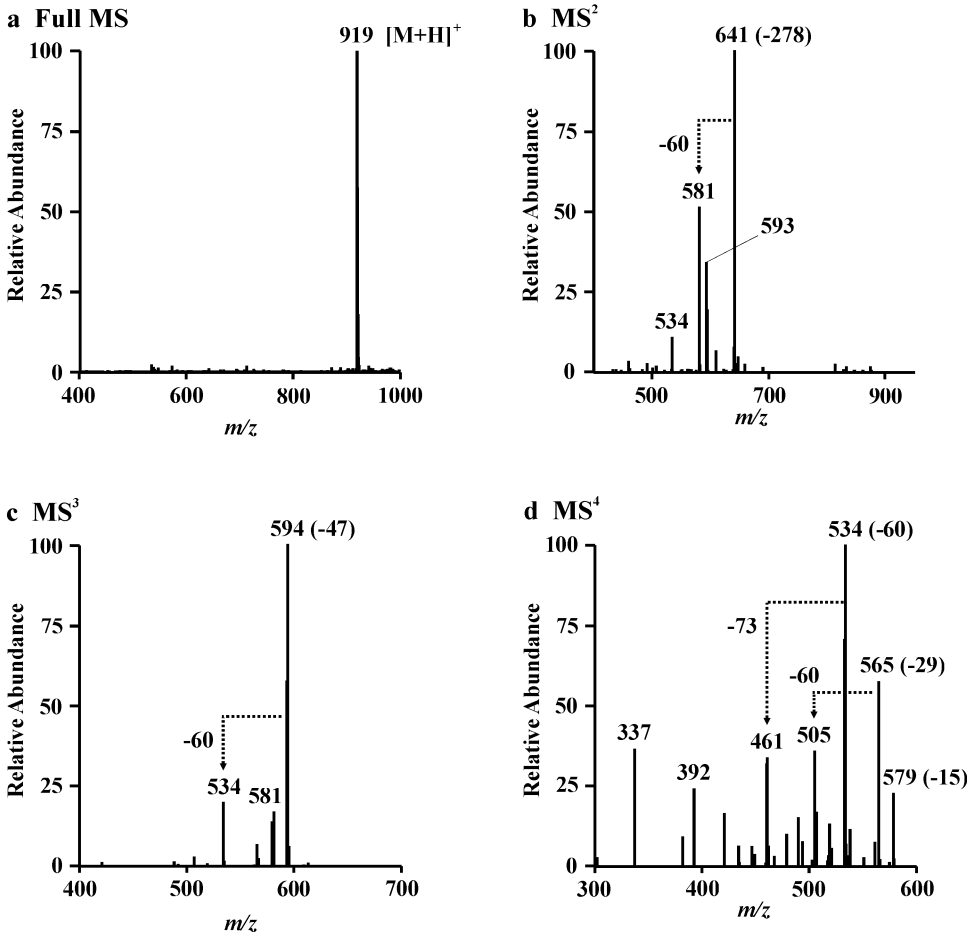

Figure 4.8. APCI multistage tandem mass spectra of MeS-phe *a* (**22a**); a) Full MS, b) MS^2, c) MS^3, d) MS^4. In each case the most abundant ion was selected as the precursor for the next spectrum.

4.2.4. Reaction of pyrophaeophorbide *a* and chlorophyll *a* with dimethyl disulfide and H_2S

The use of dimethyl disulfide in the reactions conducted in acetone-based media (Chapter 3) was found to deliver high yields of methylthioether pphorb *a* derivatives. Reaction of chl *a* with dimethyl disulfide and H_2S led to a marked increase in the rate of formation of the methylthioether derivative, allowing the formation of MeS-chl *a* (s43) to be observed on a faster timescale than the competing demetallation process (Fig. 4.9 shows the LC-MS chromatogram of an extract from the reaction after 8h). The online UV/vis spectrum for the component (λ_{max} 430, 660 nm) matches that of the natural derivative (Squier et al., 2003; 2004). Owing to demetallation post column, MeS-chl *a* is detected in the mass spectrometer as MeS-phe *a* ($[M+H]^+$ = 919) and therefore displays identical MS^n spectra (Fig. 4.8).

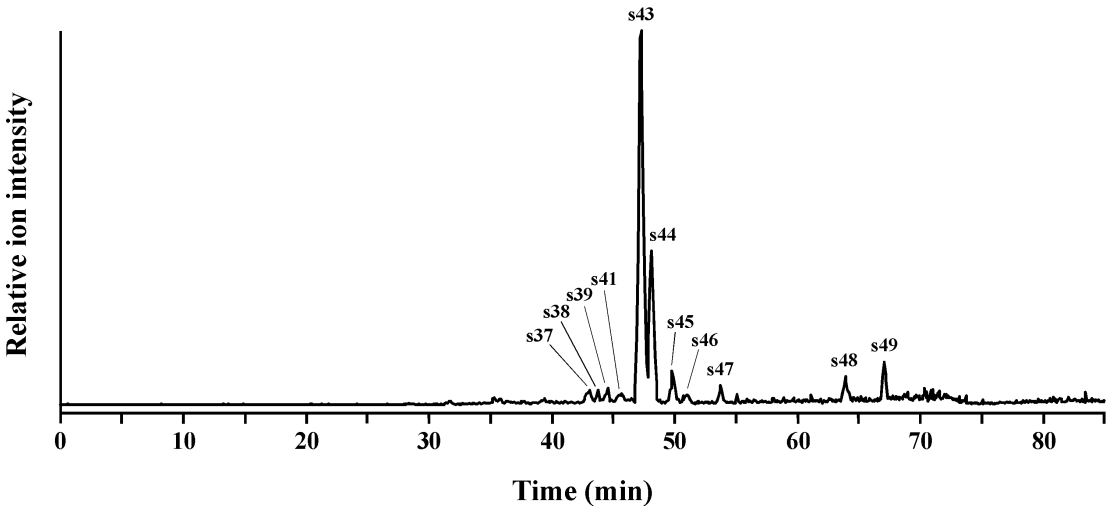

Figure 4.9. Representative mass chromatogram (*m/z* 400-1200) of the total extract from the reaction of chl *a*, in aqueous micelles buffered to pH 8.5, with dimethyl disulfide and H_2S, extracted after 8h.

By conducting the reaction on an equimolar mixture of chl *a* and pphorb *a* it was possible to compare directly the rate of formation of MeS-chl *a* with that of MeS-pphorb *a* (Fig. 4.10). A steady escalation in the proportion of MeS-pphorb *a* was observed during the reaction accompanied by a corresponding decline in the proportion of pphorb *a*. The proportion of MeS-chl *a* can be seen to maximise after a reaction time of around 16 h, after which it begins to convert to MeS-phe *a*. Notably, the initial rate of formation of MeS-chl *a* is more than twice that of MeS-pphorb *a*, clearly demonstrating that chl *a* is more reactive than its demetallated counterparts.

In light of these findings, it is unlikely that the distributional differences observed between the sulfurised and non-sulfurised chlorins in sediment extracts from Pup Lagoon are the result of preferential sulfurisation of the demetallated chlorophylls, rather the operation of two parallel sulfurisation and demetallation processes associated with the same environmental conditions.

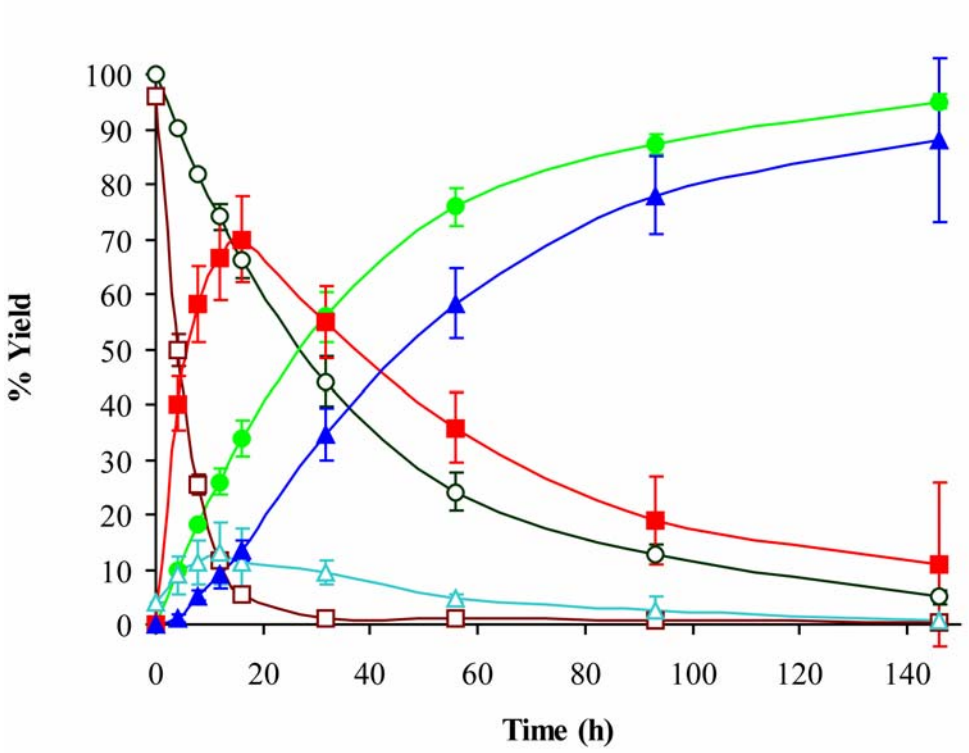

Figure 4.10. (Original in colour). Plot showing the % yields for the conversion of pphorb *a* (○) into MeS-pphorb *a* (●) and chl *a* (□) into MeS-chl *a* (■), phe *a* (△) and MeS-phe *a* (▲) during reaction with dimethyl disulfide in the presence of H_2S at pH 8.5. Error bars represent ±1 s.d. (n = 3).

4.2.5. Reaction of pyrophaeophorbide *a* with H_2S in aqueous micelles

The formation of several of the products from the reaction of pphorb *a* with methyliodide and H_2S (Section 4.2.2.) does not appear to involve methanethiol or methyliodide directly. This prompted an investigation into the reaction of pphorb *a* with H_2S in the absence of methyliodide. LC-MS analysis of the extract from reaction of an aqueous micellar solution of pphorb *a* with H_2S at pH 8.5 after 4 d revealed its limited conversion into a number of minor components (Fig. 4.11).

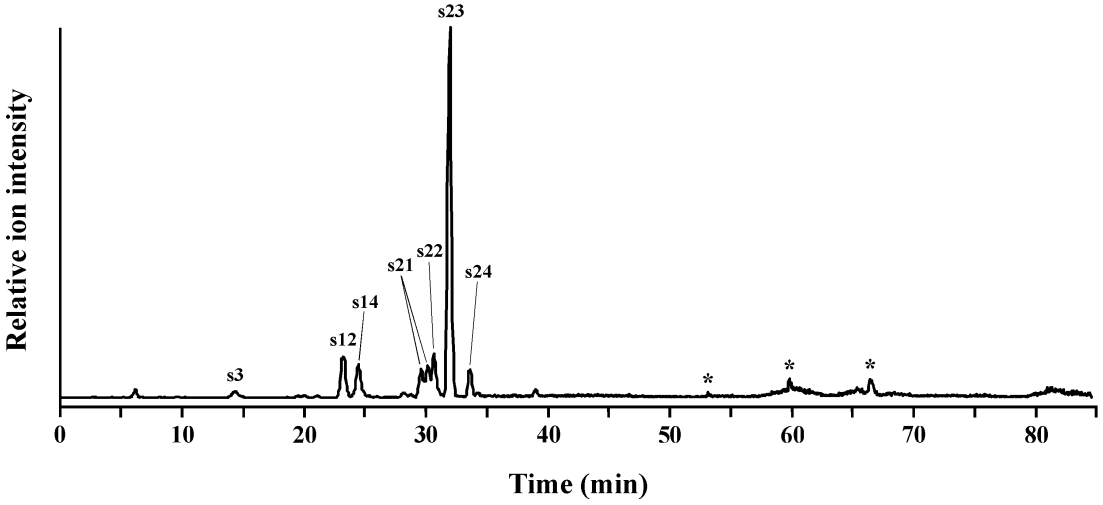

Figure 4.11. Representative mass chromatogram (*m/z* 400-1200) of the total extract from the reaction of a mixture of pphorb *a* and phorb *a* with H_2S in aqueous micellar solution for 4 d at pH 8.5. *Not chlorins.

4.2.5.1. Reduction of the C-3 vinyl substituent

Component s22, formed in the reaction, corresponds to mpphorb *a* in which the C-3 vinyl substituent of pphorb *a* has been reduced to an ethyl substituent. Mpphorb *a* (**67**) is a recurring product of the reactions involving methyliodide and H_2S in both aqueous (e.g. Fig. 4.2b) and acetone based systems (component a27, Fig. 3.1, Chapter 3). When formed it is present in variable abundances, representing yields of up to 6%. The involvement of H_2S in the reduction of the C-3 vinyl group is demonstrated by a lack of mpphorb *a* formation in reactions performed in the absence of H_2S, the LC-MS chromatogram of the recovered material being indistinguishable from that of the starting material.

4.2.5.2. Mechanism

The reaction of β-carotene with H_2S, under conditions similar to those employed above (aqueous media) but at considerably higher temperatures (50-90 ^oC) and over periods of up to 180 d, has been shown to generate β-carotene derivatives in which 1-2 double bonds have been reduced in, at best, 1% yield (Hebting et al., 2006). In addition, derivatives of β-carotene having incorporated between 1-3 molecules of H_2S were detected in low abundance. Previous work by those authors, employing the same reaction conditions, showed the reductive desulfurisation of phytene thiols by H_2S, in which the sulfhydryl group is replaced by hydrogen, affording phytenes in yields of up to 3.8% from the thiol (Hebting et al., 2003). Thus, the authors proposed a two-step reaction sequence to explain the partial reduction of β-carotene: initial formation of a thiol intermediate followed by reductive desulfurisation (Hebting et al., 2003; 2006). Although no indication was given as to the yield of the thiol intermediates, a yield of 26% can be estimated from that of the reduced products, assuming the same conversion efficiency for reductive desulfurisation as that observed for phytenethiol (3.8%). The reduction of the C-3 vinyl group of pphorb *a* in the reactions described above is consistent with the same pathway (illustrated for pphorb *a*, **33,** in Scheme 4.2).

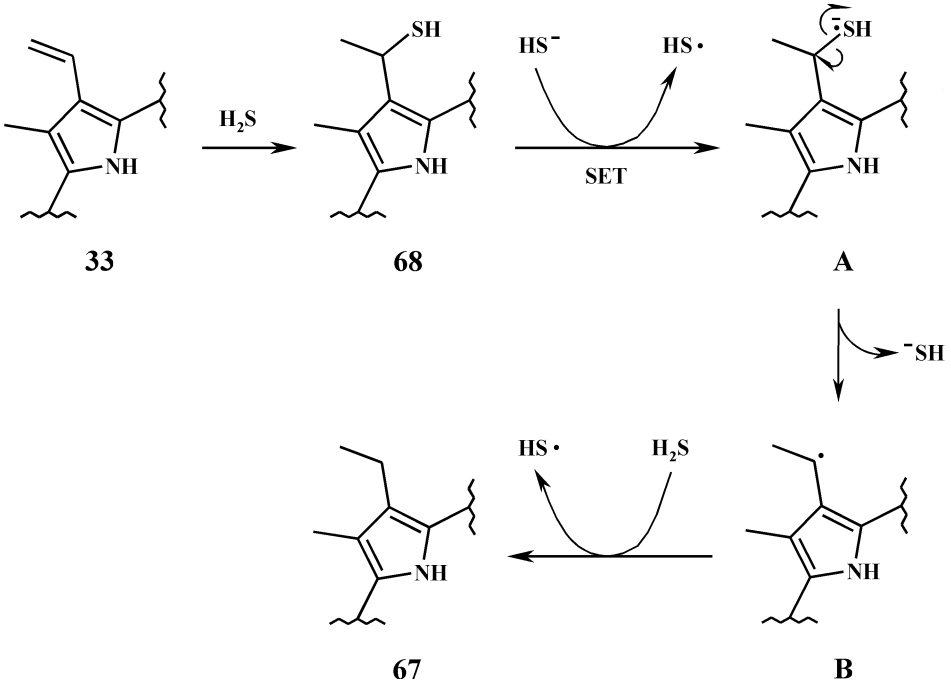

Scheme 4.2. Proposed mechanism for the formation of mpphorb *a* (**67**) from reduction of the C-3 vinyl substituent of pphorb *a* (**33**).

The formation of an intermediate thiol derivative of pphorb *a* (HS-pphorb *a*, **68**; Scheme 4.2) could not be observed directly in the products from the reaction, most likely as a result of its high reactivity and short lifetime. The mass spectrum generated from direct injection of an extract of the reaction mixture (Fig. 4.12a) revealed the presence of dimeric products, that could not be observed in the LC-MS chromatograms, formed from the crosslinking of either two molecules of HS-pphorb *a* ($[M+H]^+$ = 1163, **69**) or of HS-pphorb *a* with pphorb *a* ($[M+H]^+$ = 1131, **70**). In addition, the mass spectrum features prominent ions at *m/z* 615, 583 and 550, which do not correspond to any components present in the LC-MS chromatograms, attributed to fragment ions derived from **69** and **70**.

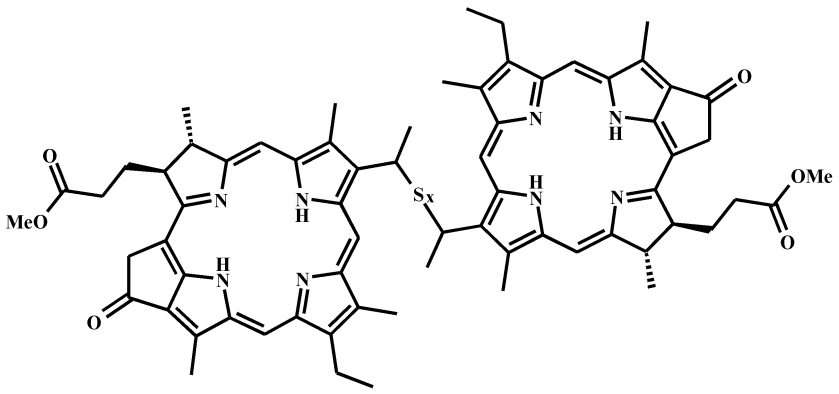

69: x = 2

70: x = 1

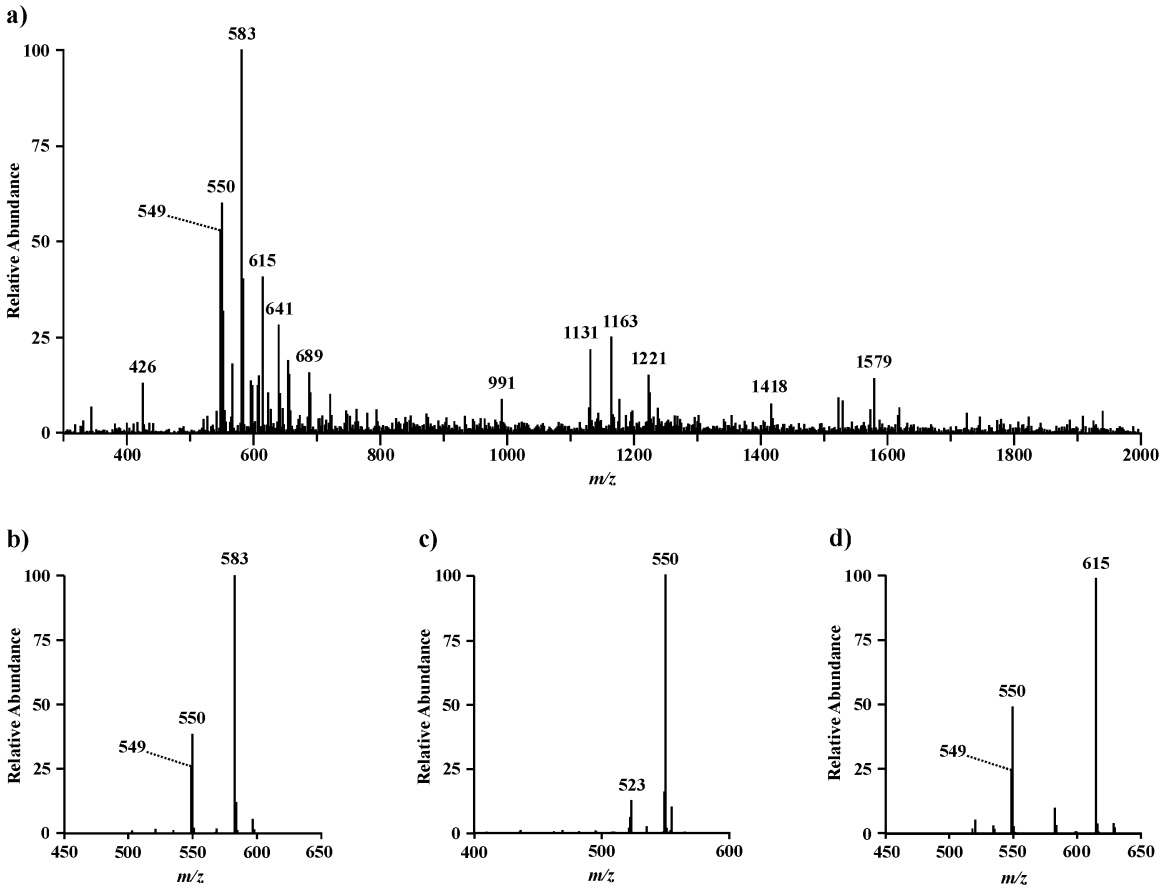

Figure 4.12. a) Representative full APCI mass spectrum (*m/z* 300-2000) of the total extract from the reaction of pphorb *a* (**33**) with H_2S, b) MS^2 of *m/z* 1131 (**70**), c) MS^2 of *m/z* 583 (HS-pphorb *a*, **68**), d) MS^2 of *m/z* 1163 (**69**).

CID of *m/z* 1131 (**70**) yields product ions in MS^2 at *m/z* 583, 550 and 549 (Fig. 4.12b). The dominant product ion at *m/z* 583 (100%) corresponds to the protonated molecule of HS-pphorb *a* arising from scission of the thioether linkage to lose a neutral molecule of pphorb *a* with hydrogen transfer to the charge-retaining fragment. Conversely, the product ion at *m/z* 549 (26%) corresponds to the protonated molecule of pphorb *a* resulting from loss of HS-pphorb *a* as a neutral molecule. The relative abundances of *m/z* 583 and 549 reflect the favourability of the two fragmentations and can be rationalised as being influenced by the sulfur atom and its effect on the stability of the protonated molecule. The product ion at *m/z* 550 (39%) corresponds to a C-3[1] radical species arising from cleavage of the C-S bond and loss of the sulfur-containing portion of the dimer as a radical. Loss of a radical species is unusual during the early stages of MS^n of chlorins, which typically favour neutral losses (Airs

et al., 2001). Notably, however, prominent loss of an alkylthiyl radical during MS^n is characteristic of C-3^1 alkylthioether chlorophyll derivatives (Chapter 3; Squier et al., 2003; 2004) in which the ready generation of radicals is attributed to the relatively weak carbon-sulfur bond and resonance stabilisation of the resulting C-3^1 radical by the aromatic macrocycle. Early generation of radical product ions in MS^2 of **70** suggests attachment of the thioether linkage at the C-3^1 position. Absence of a product ion at *m/z* 582, corresponding to a S-pphorb *a* radical, shows that cleavage of the C-S bond occurs exclusively at the C-3^1 position of the charge-carrying moiety of the dimer. The protonated molecule of HS-pphorb *a* (*m/z* 583), which represents the most abundant product ion in MS^2 of **70** (Fig. 4.12b), forms the base peak in the full mass spectrum of the reaction extract (Fig. 4.12a) and is attributed to a fragment ion formed by rearrangement. CID of *m/z* 583 yields a prominent ion in MS^2 at *m/z* 550 (Fig. 4.12c) reflecting a loss of 33 Da attributed to loss of the sulfhydryl group as a radical, analogous to loss of alkylthiyl radicals from C-3^1 alkylthioether pphorb *a* derivatives discussed above. Furthermore, the MS^3 and MS^4 spectra formed from CID of the product ion at *m/z* 550 (not shown) are identical to those of alkylthioether pphorb *a* derivatives (Chapter 3). The similarity of the mass spectral characteristics indicates attachment of the sulfhydryl group in HS-pphorb *a* at the C-3^1 position and provides further evidence for the presence of the thioether moiety in its progenitor (**70**), linking the C-3^1 carbons of two pphorb *a* molecules. CID of the protonated molecule of **69** ($[M+H]^+$ = 1163) yields a base peak ion in MS^2 (Fig. 4.12d) at *m/z* 615, attributed to HSS-pphorb *a*, accompanied by ions at *m/z* 550 (49%) and 549 (25%) corresponding to the C-3^1 radical species and pphorb *a*, as observed in MS^2 of **70**.

The presence of the dimeric species **69** and **70** attests to the formation of HS-pphorb *a* (**68**) during the reaction and could also represent potential intermediates in the reduction of the C-3 vinyl group. Unfortunately, owing to the extensive fragmentation of the dimeric species evident in the full mass spectrum, the precise yields of each of these compounds could not be determined, although it is clear that they represent a significant portion of the products formed. The combined yield of **69** and **70** was estimated as being ca. 63% on the basis of their relative ion abundances, taking into account their fragment ions.

Cleavage of carbon-sulfur bonds is known to occur under $S_{RN}1$ conditions (Rossi and Bunnett, 1973; 1974; Cheng and Stock, 1991). Hebting et al. (2003) proposed an $S_{RN}1$ mechanism for the replacement of the sulfhydryl group with hydrogen (Scheme 4.2), analogous to the replacement of nitro and thioether groups with hydrogen following reaction with thiolate anions (Kornblum et al., 1978; 1979). The first step is suggested to involve single electron transfer (SET) from a hydrogen sulfide anion to the sulfhydryl group of the thiol intermediate. The resulting radical anion (**A**) can undergo homolytic cleavage of the carbon-sulfur bond, losing the sulfhydryl group as a hydrogen sulfide anion and affording a resonance stabilised carbon centred radical (**B**). The radical (**B**) is subsequently quenched by abstraction of a hydrogen radical from H_2S to complete the reduction and yield mpphorb *a* (**67**). The lack of formation of mpphorb *a* when the reaction was repeated in the presence of the radical scavenger, ascorbic acid, is consistent with the involvement of radicals in the reduction, as proposed by Hebting et al. (2003; 2006).

Replacement of thioether groups with hydrogen was found to be slow (Kornblum et al., 1979), a fact that is probably reflected in the low yields obtained for the products of the reduction observed in this and previous studies (Hebting et al., 2003; 2006). Notably, the reduction of the C-3 vinyl substituent of pphorb *a* occurs at lower temperature (room temp) and over shorter timescales (4 d), forming mpphorb *a* in apparently higher yields than were found for the reduction of β-carotene and the reductive desulfurisation of phytenethiol (Hebting et al., 2003; 2006). The apparent susceptibility of the pphorb *a* vinyl substituent towards such a transformation is most likely a consequence of the resonance stabilisation of the intermediate radical species (**B**). It is noteworthy that, had reductive desulfurisation of the dimeric species **69** and **70** proceeded to completion, the yield of mpphorb *a* obtained would have been nearer to 69%.

4.2.5.3. Significance

As with sulfurisation, the reductive transformation of functionalised oxygen-sensitive biomolecules into thermodynamically more stable derivatives plays a crucial role in the preservation of sedimentary organic matter. The formation of mpphorb *a* has been

linked with the anaerobic bacterial degradation of algal matter in the presence of sulfate reducing bacteria (Spooner et al., 1995). Its formation in the simulation reactions described here clearly demonstrates that H_2S can initiate the reduction of the C-3 vinyl substituent, providing firm evidence for an abiotic route to the formation of C-3 ethyl-containing chlorins and porphyrins in the natural environment. Given the evidence to support replacement of thioether groups with hydrogen in the presence of sulfide (Kornblum et al., 1979), C-3[1] thioether derivatives of chlorophyll *a*, identified in Recent Antarctic sediments (Squier et al., 2003; 2004), may also be considered as potential intermediates in the reduction of the C-3 vinyl substituent. Furthermore, the involvement of H_2S in the formation of mpphorb *a* strongly implies that the reduction observed by Spooner et al. (1995), ca. 1 % yield, was not the result of direct bacterial action. Rather, it was the product of an abiological reaction with dissolved sulfide present during the experiments, through the activity of the sulfate-reducing bacteria that were present as the active community.

The formation of the dimeric chlorin species provides evidence for the addition of H_2S to the C-3 vinyl group and formation of a short lived thiol species **68**, supporting the operation of the second pathway to the formation of alkylthioether chlorophyll derivatives outlined in Scheme 4.1. Re-inspection of the extracts from the reactions of pphorb *a* with alkyliodide and H_2S revealed the presence of the dimeric species, but in far lower abundance than was formed in the reactions in the absence of alkyliodide. This suggests that, in the case of the former, any thiol formed is rapidly trapped as the corresponding alkylthioether by reaction with the alkyliodide.

4.2.6. Reactions of pyrophaeophorbide *a* with H_2S and air in aqueous micelles

Despite the limitation of oxygen in the reactions described above, small amounts of oxidation products of the reactions still emerged from the reactions conducted at pH 7 and pH 5, presumed to be formed from reaction with traces of oxygen still present in the system. Formation of these compounds, under the mild reaction conditions employed, suggests that they may represent potential diagenetic transformation products of chl *a* in the natural environment and so warrant further investigation.

An aqueous micellar solution of pphorb *a*, buffered to pH 5, was stirred for periods of up to 12 d in the presence of H_2S and air. LC-MS analysis of the reaction mixture (Fig. 4.13) revealed a distribution dominated by products resulting from oxidation of the C-3 vinyl group (s1, s2, s3, s5, s11, and s13). The major component s13 was identified as pphorb *d* (**65**) on the basis of its online UV/vis and MS^n spectra. Similarly the peak s5 (t_R = 16 min) could be assigned to the corresponding phorb *a* derivative, phorb *d* (**71**). Peak s1 corresponds to the C-3^1, C-3^2 diol pphorb *a* derivative (**59**). Peaks s2 and s3 correspond to the C-3 (1-hydroxyethyl) derivatives of phorb *a* (**72**) and pphorb *a* (**57**), respectively. Peak s11 corresponds to the C-3 acetyl derivative of pphorb *a* (**58**).

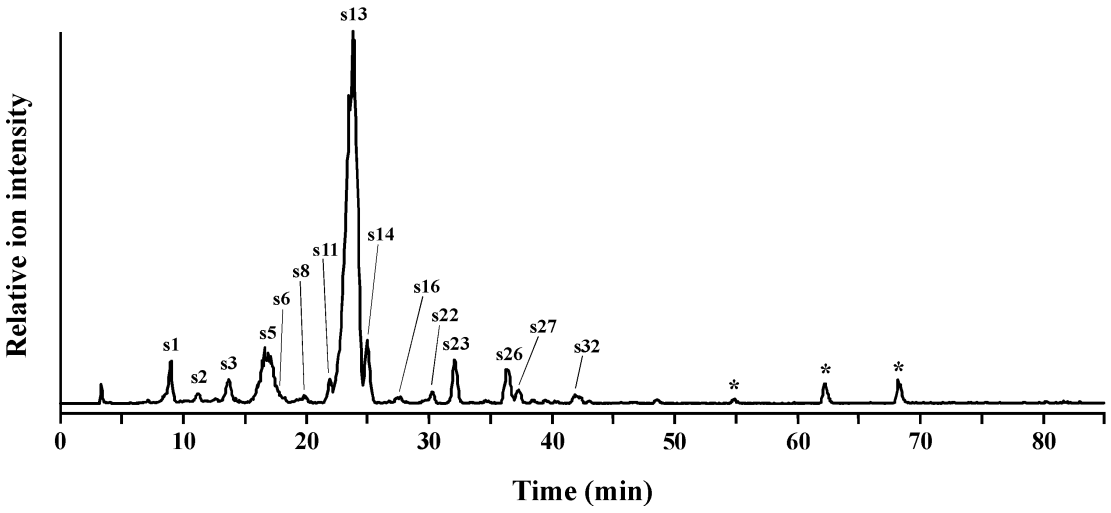

Figure 4.13. Representative mass chromatogram (*m/z* 400-1200) of the total extract from the reaction of pphorb *a* with H_2S and air in aqueous micellar solution for 12 d at pH 5. *Not chlorins.

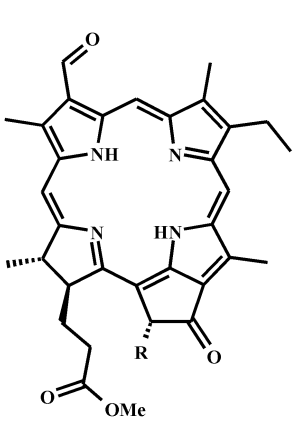

65 R = H

71 R = COOMe

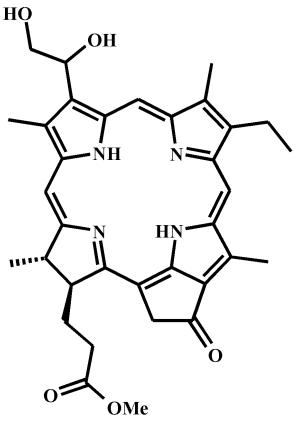

59

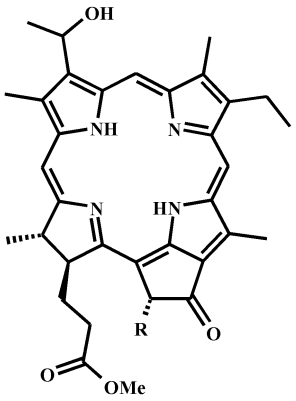

57 R = H

72 R = COOMe

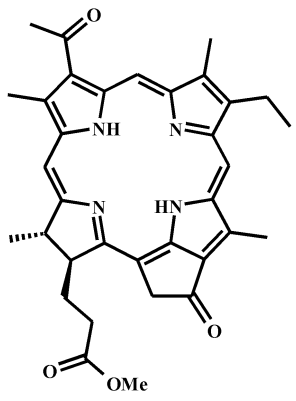

58

In order to investigate the source of the additional oxygen atom(s) incorporated into the C-3 vinyl substituent, the reaction of pphorb *a* with H_2S was performed in the presence of $^{18}O_2$. LC-MS analysis of the reaction products revealed an increase of 4 *m/z* units in the *m/z* value of the protonated molecule of **59** ($[M+H]^+$ 587 cf. 583) indcating incorporation of $^{18}O_2$ into the C-3 vinyl group. This was confirmed by inspection of the MS^2 spectrum of **59**, which showed losses of 20 and 64 Da corresponding to losses of $H_2{}^{18}O$ and the entire C-3 substituent ($C_2H_4{}^{18}O_2$) with back-transfer of hydrogen, respectively. Thus, it appears that the C-3^1, C-3^2 diol (**59**) is formed via addition of oxygen across the double bond.

Surprisingly, no evidence of $^{18}O_2$ incorporation could be detected in any of the other oxidation products, implying a different source for the additional oxygen atom in those compounds. Pphorb *a* was reacted with H_2S and $^{16}O_2$ in which the aqueous

component of the reaction comprised 10 atom % $H_2{}^{18}O$. LC-MS analysis revealed enhancement of the $[M+H+2]^+$ peaks of each of the oxidation products, indicating incorporation of the ^{18}O label. Notably, however, this enhancement was not confined to the oxidation products and was present to a lesser degree in the full MS of all pphorb *a* derivatives. This can be explained by the operation of an acid catalysed exchange process between water and the C-13[1] carbonyl (Morishita and Tamiaki, 2005). A similar exchange process can occur at the C-3 carbonyls in **58**, **65** and **71**, removing any signature of ^{18}O introduced during the $^{18}O_2$ experiment. Accordingly, the involvement of molecular oxygen in the formation of these compounds can neither be confirmed nor disproved on the basis of isotopic evidence, although, in view of the lack of formation of these products in the absence of air (Fig. 4.11) molecular oxygen appears the most likely source. The C-3 (1-hydroxyethyl) pphorb *a* derivative (**57**) is formed in small amounts in the absence of air (s3, Fig. 4.11). Compounds **57** and **72** may, therefore, result from the acid catalysed addition of H_2O to the C-3 vinyl group in a manner analogous to the addition of H_2S or methanethiol.

4.2.6.1. Oxidative cleavage of the C-3 vinyl substituent

Pphorb *d* (**65**), the major product of the reaction of pphorb *a* with H_2S and air (s13, Fig. 4.13), was formed in yields ranging between 65-89%. In order to probe the mechanism of formation of pphorb *d* from pphorb *a*, reactions were conducted with various different reagents and conditions. The presence of both oxygen and sulfide was found to be necessary for the reaction to proceed and no pphorb *d* was produced in the absence of either. Operation of the reaction was not conditional on hydrogen sulfide as the sulfide source: its replacement with decanethiol also led to the formation of pphorb *d*, albeit with an approximate 50% reduction in yield. It is well known that thiols can react with molecular oxygen to generate radicals (Capozzi and Modena, 1974 and references therein). Involvement of radicals in the reaction was supported by inhibition of pphorb *d* formation (22% yield) following introduction of the radical scavenger, ascorbic acid, into the reaction mixture. The inability of ascorbic acid to prevent the formation of pphorb *d* completely is most likely due to its polar character preventing free access to the hydrophobic micelle core, and close competition from H_2S which is also an efficient radical scavenger.

Increasing the pH of the reaction mixture led to a decline in yields at pH 7 (max yield 20%) and virtually no pphorb *d* formation at pH 8.5 (max yield 8%). A radical mechanism should not be affected by pH, thus, it is likely that the pH dependence in the formation of pphorb *d* results from control over the speciation of sulfur present in the reaction mixture. At pH 5 the equilibrium between the intact and deprotonated species is shifted in favour of the former, whereas at pH 8.5 the majority of sulfur species are present in solution as sulfide anions and disulfides. The intact sulfide can be expected to access the hydrophobic micelle interior more freely than its deprotonated counterpart resulting in higher yields of pphorb *d* at low pH. The enhancement in yields may also suggest that retention of the sulfhydryl hydrogen is of importance for the reaction. Furthermore, basic conditions promote the formation of disulfides resulting in a redirection of reagent away from the formation of pphorb *d*. These interpretations are supported further by the lack of formation of pphorb *d* with dimethyl disulfide as a reagent.

4.2.6.2. Mechanism

The cooxidation of olefins and thiols with oxygen is well known and can occur in quantitative yields under non-radical inducing conditions (Kharasch et al., 1951; Capozzi and Modena, 1974; Szmant et al., 1976; D'Souza et al., 1987). The currently accepted mechanism (Scheme 4.3) involves the initial formation of a charge-transfer complex (**C**) between the thiol and olefin followed by abstraction of the exposed sulfhydryl hydrogen by molecular oxygen (Szmant et al., 1976; D'Souza et al., 1987). The resulting carbon-centred radical may be trapped as a β-hydroperoxysulfide (**D**), in which sulfur is selectively attached to the least substituted carbon atom of the olefin (anti-Markovnikov), either by reaction with the hydroperoxy radical formed in the previous step or by reaction with oxygen to form a peroxide radical followed by abstraction of a hydrogen from a thiol molecule. The β-hydroperoxysulfide can then undergo intramolecular rearrangement to a β-hydroxysulfoxide (**E**) (Capozzi and Modena, 1974; Iriuchijima et al., 1974).

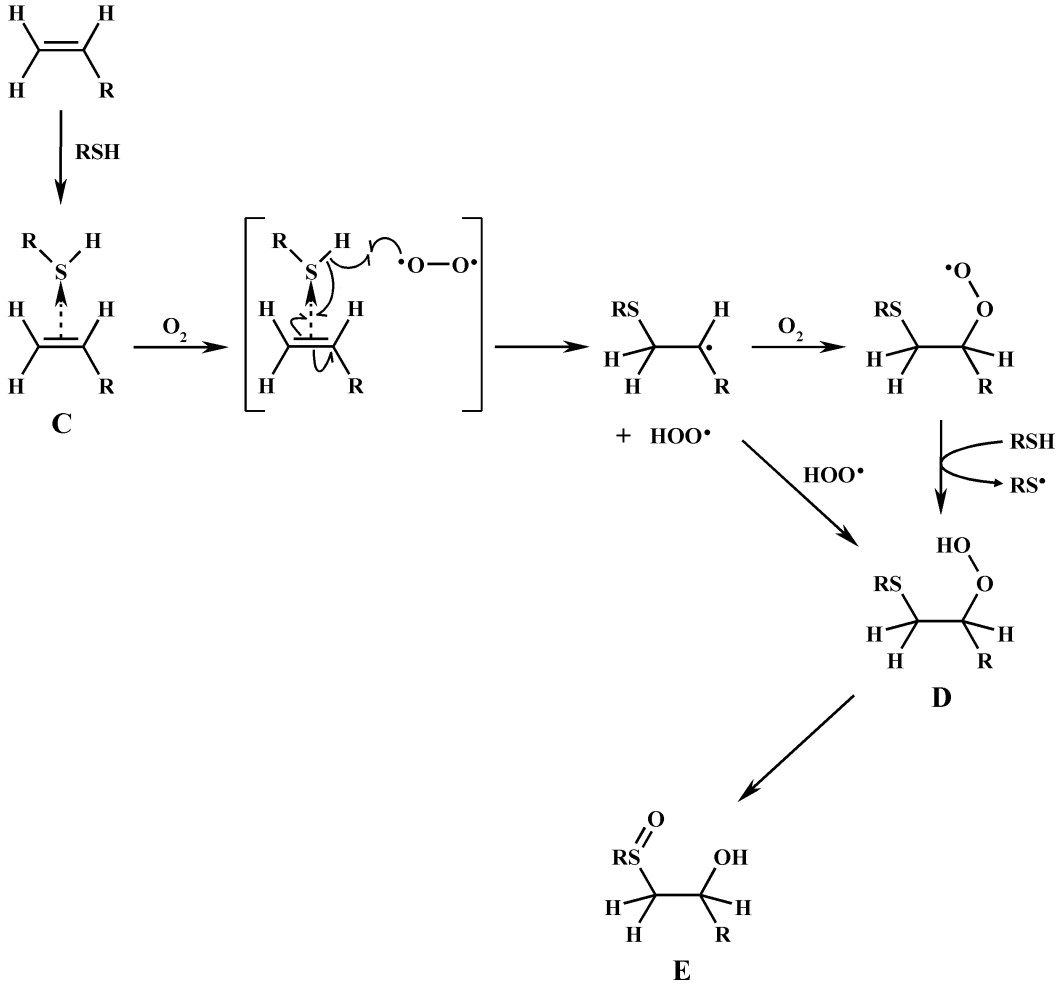

Scheme 4.3. A simplified representation of the currently accepted mechanism for thiol-olefin cooxidation.

The requirements for oxygen and sulfide in the formation of pphorb *d*, exhibited by the reactions described above, and evidence for the involvement of radicals is in agreement with a cooxidation reaction involving the pphorb *a* vinyl group. Hydrogen sulfide is expected to behave in a similar manner to an alkylthiol and conjugated olefins such as the pphorb *a* vinyl group are ideal substrates for the reaction. The observed formation of the aldehyde could result from degradation of the cooxidation products. Interestingly, Baucherel et al. (2001) reported the oxidative cleavage of various olefins to their respective carbonyls following reaction with thiophenol and molecular oxygen in the presence of transition metal complexes. Furthermore, the reaction was found to be accelerated by acid, consistent with observations made for the formation of pphorb *d*. Baucherel et al. (2001) propose that cleavage of the olefin arises via degradation of the β-hydroperoxysulfide intermediate (**D**), formed from

cooxidation of the olefin and thiophenol, catalysed by transition metal complexes. Although there is no obvious source of catalysis, a similar degradation of either the β-hydroperoxysulfide or the β-hydroxysulfoxide (**E**) is proposed to operate in the reactions described above to afford the aldehyde at C-3 (as illustrated for **E** in Scheme 4.4) where the formation of an aldehyde in conjugation with the chlorin macrocycle could provide sufficient driving force for such a transformation in the absence of a catalyst.

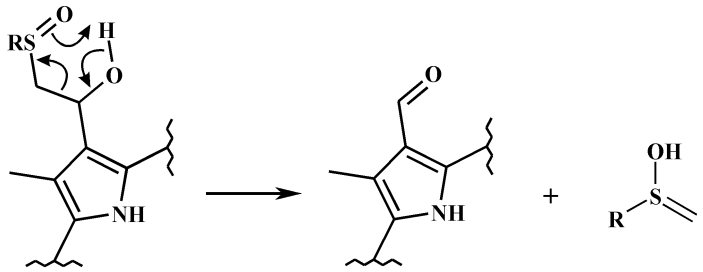

E **65**

Scheme 4.4. Proposed degradation of the β-hydroxysulfoxide of pphorb *a* (**E**) to form pphorb *d* (**65**). R = H or decyl.

4.2.6.3. Significance

Interestingly, (Koizumi et al., 2005) reported the formation of small amounts of chl *d* from chl *a* during incubations with papain (a sulfhydryl protease). The authors were unable explain its formation although they were able to discount an enzymatic process (Fukuyo et al., 2007). In light of our findings it appears that the cysteine group of papain, or the sulfides typically used to activate it (e.g. cysteine), led to the oxidation of the chl *a* vinyl group. Chl *d* occurs as the primary photosynthetic pigment in *Acaryochloris marina* a unique cyanobacterium (Miyashita et al., 1996) and its biosynthesis has yet to be elucidated. Whereas the biosynthetic precursor for the C-7 aldehyde of chl *b* is a methyl substituent (Leeper, 1985; Porra and Scheer, 2000), the likely precursor for that at the C-3 position of chl *d* is a vinyl substituent. Thus, it is tempting to suggest that, on the basis of this work, the biosynthesis of chl *d* involves modification of this substituent by thiols or thiol containing enzymes.

From a geochemical perspective, oxidative cleavage of the C-3 vinyl group could be an important transformation of chlorophylls in natural environments in which the requirements for oxygen and sulfide are satisfied. These conditions are fulfilled at the chemocline, the transition zone between oxic and sulfide-rich regions of the sediment or water column. Oxygen and sulfide-rich microenvironments also occur in close proximity within microbial mats, in which fluctuations between oxic and anoxic conditions can occur within a few hours (Revsbech et al., 1983). In addition, thiols and sulfur-containing amino acids are widespread in the natural environment and could also represent potential reactants.

Pphorb *d* may represent a key intermediate in the formation of C-3 β-CH_3 and β-H fossil porphyrins. Alkyl porphyrins archived within the sedimentary record represent the ancient remains of chlorophylls, bacteriochlorophylls and hemes. Although much of their original functionality has been lost during diagenesis and catagenesis, many alkyl porphyrins possess structural features that permit their assignment to a specific precursor or group of precursors (for a detailed review see Callot and Ocampo, 2000). Of the numerous porphyrin structures identified in sediments and oils, several exhibit structural evidence of dealkylation at positions C-3, 7 and 17. Alkyl porphyrins possessing a C-7 β-H are suggested to arise from chls *b* and/or c_3, both of which possess labile functionalities at this position (Chicarelli and Maxwell, 1984; Verne-Mismer et al., 1990). In the case of chl c_3, loss of the C-7 methyl ester via decarbomethoxylation is proposed to occur under sedimentary conditions (Verne-Mismer et al., 1990). Loss of the C-7 aldehyde in chl *b* has been suggested to occur via preliminary oxidation to a carboxylic acid and subsequent decarboxylation (Chicarelli and Maxwell, 1984). The origins of porphyrins dealkylated at C-3 and C-17 are less clear. Typically chls, bchls and hemes possess substituents containing two carbon atoms (vinyl, acetyl or 1-hydroxyethyl) at the C-3 position, rendering ethyl substituents in the majority of fossil porphyrins structures. Such ethyl-substituted porphyrins are, however, often accompanied by lower mass homologues that bear a β-CH_3 or β-H at position C-3. The former generally occur in carbonate-rich sediments while the latter are more often associated with clay-rich sediments (Callot and Ocampo, 2000 and references therein). Devinylation reactions of porphyrins are not unprecedented; the Schumm reaction, which involves heating to 180°C in resorcinol

(Bonnett et al., 1977; DiNello and Dolphin, 1981), has been used extensively in laboratory porphyrin chemistry and is often invoked to provide a rationale for the formation of the β-H homologue. Interestingly, Sundararaman and Boreham (1991) observed a systematic increase in the ratio of vanadyl C-3 β-H/β-Et porphyrins with depth in lacustrine shales from the Bucomazi Formation, Cabinda, West Africa. They attributed the increase to a decrease in the pH of the depositional environment, as interpreted from an increasing VO/(VO + Ni) porphyrin ratio. Notably, the VO/(VO + Ni) porphyrin ratio also indicated a decrease in oxicity with depth (Sundararaman and Boreham, 1991) which contrasts with suggestions that an oxidative process might activate the C-3 vinyl group towards loss (Callot and Ocampo, 2000). Currently, however, no clear and consistent explanation exists for the occurrence of C-3 β-CH_3 and β-H porphyrins. Similarly, uncertainty exists concerning the formation of C-17 modified porphyrins: structures with β-CH_3 and β-H at this position are believed to originate from sources that contain a unique C-17 substituent. Thus, chls $c_{1\text{-}3,}$ which possess an acrylic acid side-chain in place of the typical propionic acid group, have been suggested as likely precursors (Verne-Mismer et al., 1988). Degradation of the C-17 acrylic acid has been proposed to involve decarboxylation to afford a vinyl group, which is then suggested to follow the same transformation pathways as the C-3 vinyl group mentioned above (Verne-Mismer et al., 1988).

The formation of pphorb *d* from pphorb *a*, observed in the simulation reactions described above, could provide insight into the formation of sedimentary alkyl porphyrins that possess β-CH_3 and β-H substituents at the C-3 position (Scheme 4.5). Following the initial formation of a C-3 aldehyde, from oxidative cleavage of the C-3 vinyl group, loss of the C-3 substituent can occur via oxidation to a carboxylic acid followed by decarboxylation in a manner analogous to that proposed for the loss of the C-7 aldehyde of chl *b* (Chicarelli and Maxwell, 1984; Pathway 1, Scheme 4.5). Alternatively, in a reducing sedimentary environment, reduction of the aldehyde would yield a β-CH_3 at C-3 (Pathway 2, Scheme 4.5).

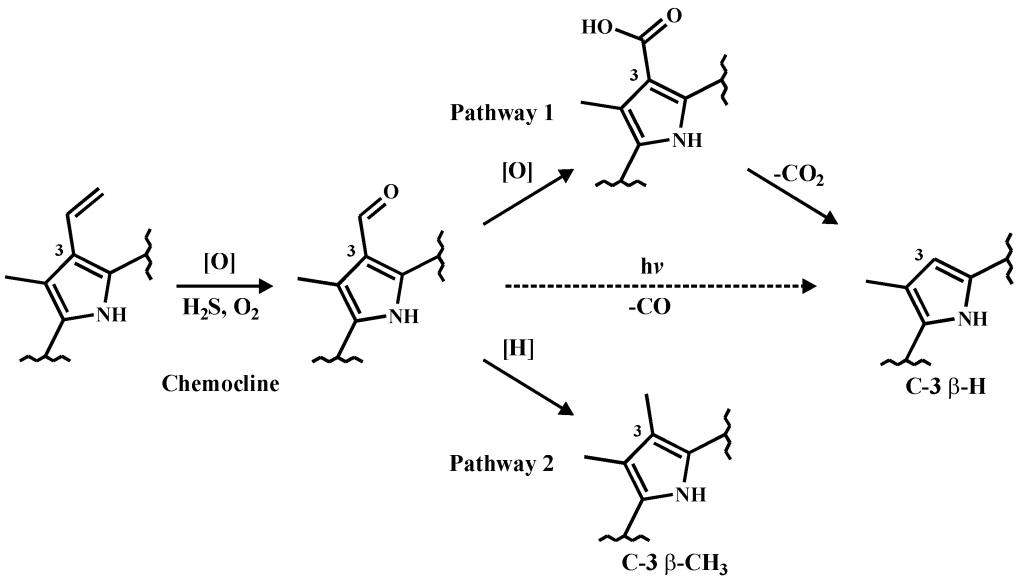

Scheme 4.5. Proposed routes to the formation of C-3 β-H and C-3 β-CH_3 porphyrins.

A similar mechanism could apply for the formation of porphyrins exhibiting dealkylation at C-17 via initial oxidative cleavage of the acrylate side-chain in chls c_1-c_3. In view of the pH dependence exhibited in the oxidative cleavage of the C-3 vinyl group, and the potential importance of the redox status of the depositional environment suggested by the proposed transformation pathways (Scheme 4.5), it is likely that pH and E_h are important factors in the formation of C-3 dealkylated porphyrins. Sundararaman and Boreham (1991) observed a systematic increase in the ratio of vanadyl C-3 β-H/β-Et porphyrins with depth, accompanied by an increase in the VO/(VO + Ni) porphyrin ratio. The VO/(VO + Ni) porphyrin ratio is suggested to be a good indicator of the pH and E_h of the depositional environment with both lower pH and E_h favouring the formation of vanadyl porphyrins (Lewan, 1984). Sundararaman and Boreham (1991) attributed the increase in the ratio of C-3 β-H/β-Et to the decreasing pH of the depositional environment, with E_h suggested to have little influence. The increasing extent of devinylation observed with decreasing pH is in agreement with the greater yields of the C-3 aldehyde intermediate obtained at low pH in the reactions described above. Notably, however, the concomitant decrease in E_h (i.e. a shift to more reducing conditions) of the depositional environment, indicated by the VO/(VO + Ni) porphyrin ratio (Sundararaman and Boreham, 1991), contrasts with the proposed oxidative route to the formation of C-3 β-H porphyrins (Scheme 4.5). Although this may at first appear a contradiction, oxygen depleted and reducing environments are commonly associated with the development of sulfate reducing

bacteria, which produce H_2S, and can raise the level of the chemocline. As the concentration of dissolved oxygen in the water column is greatest nearer the surface and generally decreases with depth, an elevated chemocline would favour formation of the aldehyde and its subsequent oxidation to a carboxylic acid, ultimately leading to formation of the C-3 β-H derivative (Pathway 1). Given that the formation of the aldehyde is proposed to occur at the chemocline, this raises the interesting possibility that the operation of either pathway 1 or 2 is dependent upon its height in the water column. Thus, the lower local concentration of dissolved oxygen at a lower chemocline would favour formation of the C-3 β-CH_3 derivative (Pathway 2) via initial formation of the C-3 aldehyde followed by its transport out of the oxic zone into reducing conditions and subsequent reduction. If the chemocline resides within the photic zone the additional possibility of photochemically induced transformations can be considered. Such environments are indicated by the presence of anaerobic photosynthetic bacteria (Squier et al., 2002) and photochemical reactions have been suggested to play a role in the sulfurisation of organic matter (Adam et al., 1998). Aldehydes absorb light in the region 230-330 nm, resulting from $n \rightarrow \pi^*$ transitions (March, 1992). The excited aldehyde can then decompose via the extrusion of CO (March, 1992) e.g. to yield the C-3 β-H derivative (dashed arrow, Fig. 4.5). While light <290 nm is absorbed strongly by atmospheric ozone, light within the active wavelength range (290-330 nm) is incident at the Earth's surface and has been detected in water bodies at depths of up to 70 m (Williamson, 1995). Thus, the photochemically induced decomposition of the C-3 aldehyde may be a viable route to the formation of C-3 β-H derivative in nature. Notably, the transparency of aquatic environments to the wavelengths of light involved with the decomposition varies considerably between environments and is dependent upon factors such as the concentration of particulates and dissolved organic carbon (Häder et al., 2003).

The occurrence of C-3 β-CH_3 and β-H porphyrins in sediments has been correlated with sediment mineralogy, with the former typical for carbonate environments and the latter for clay-rich sediments (Callot and Ocampo, 2000). Clay minerals have been suggested to catalyse numerous transformations of organic matter during maturation and petroleum generation (Seewald, 2003 and references therein) and have even been shown to be capable of catalysing the air oxidation of *n*-alkanes in experiments

believed to mimic thermal maturation (Faure and Landais, 2000; Faure et al., 2003). Notably, however, the catalytic activity of clays is attenuated by the presence of water (Tannenbaum and Kaplan, 1985; Seewald, 2003), a significant component of surface sediments. Nevertheless, the possibility that mineral-catalysed oxidations play a role in the formation of C-3 β-H porphyrins cannot be discounted, particularly since prevalence of reductive transformations, in the absence of clay minerals, leads to the generation of C-3 β-CH_3 porphyrins. Clearly more work is needed to unravel the precise mechanisms by which C-3 modified sedimentary alkyl porphyrins form, considering different conditions of the depositional environment such as the effect of pH and E_h, fluctuating oxic and anoxic conditions, and the possible role of photochemical or clay-catalysed reactions during early diagenesis.

The reactions described above proceed equally well in acetone or methanol and may find application in tetrapyrrole chemistry for the modification of peripheral vinyl substituents by oxidative cleavage, thus avoiding the need to use undesirable reagents such as osmium tetroxide and sodium periodate (Kenner et al., 1976; Morishita and Tamiaki, 2005).

4.2.7. Phytylthioether derivatives

In addition to the short-chain alkylthioether chlorophyll derivatives, derivatives of phe *a* and pphe *a* believed to contain phytylthioether moieties attached to the C-3 position (phytylS-phe *a*, **73**, and phytylS-pphe *a*, **74**, respectively) were identified in sediment extracts from Pup Lagoon from their UV/vis and MS^n spectra (Squier, 2003).

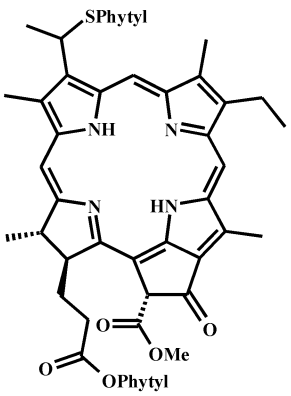

73

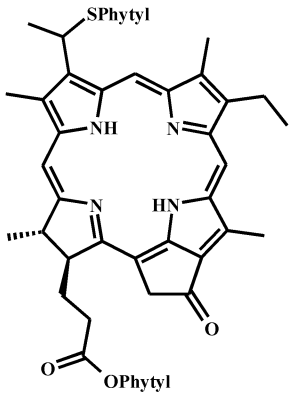

74

Phytol (**75**) occurs primarily in nature as the esterifying alcohol in chl *a*, although other sources exist in the natural environment (Rontani and Volkman, 2003 and references therein). Phytol-derived compounds are widely distributed in sediments and have been detected in high abundance within sulfurised geochemical fractions (Sinninghe Damsté and de Leeuw, 1990). Incorporation of sulfur into phytol and its derivatives has been demonstrated in a number of simulation studies (de Graaf et al., 1992; Fukushima et al., 1992; Rowland et al., 1993; Schouten et al., 1994) and phytenethiol (**76**) has been reported as a product emerging from the photochemically-induced reaction of phytadienes (e.g. **77**) with hydrogen sulfide (Adam et al., 1998) and from the reaction of phytenal with polysulfides (Schneckenburger et al., 1998).

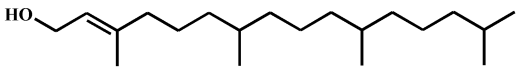

75

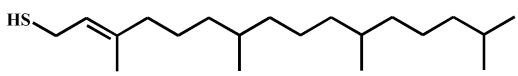

76

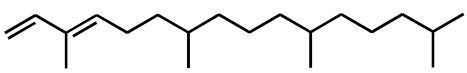

77

In order to validate the assignment of phytylS-phe *a* and phytylS-pphe *a* made by Squier (2003) and understand more about their formation, pphorb *a* and phe *a* were each subjected to reaction with phytol in the presence of H_2S. No reaction was observed over 12 d at pH 8.5. The reaction at pH 5, however, led to the formation of phytylS-pphorb *a* (**78**) and phytylS-phe *a* (**73**).

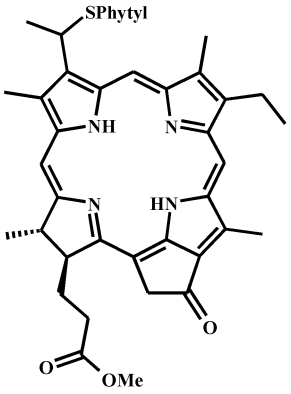

78

LC-MS analysis of the products from the reaction of pphorb *a* with phytol and H_2S at pH 5 revealed the presence of two late eluting components s51 and s52 (Fig. 4.14) exhibiting protonated molecules at *m/z* 861, 312 *m/z* units greater than that of pphorb *a* ($[M+H]^+$ = 549), corresponding formally to the addition of phytylSH. Both components exhibited identical MS^n spectra (Fig. 4.15). CID of *m/z* 861 yielded the base peak ion in MS^2 at *m/z* 550 reflecting a loss of 311 Da (Fig. 4.15b). This loss is consistent with the loss of a phytenethiyl radical, observed in the MS^n spectra of the natural phytylS-phe *a* and phytylS-pphe *a* (Squier, 2003) and the characteristic alkylthiyl radical loss exhibited in the MS^n spectra of the short-chain alkylthioether chlorophyll derivatives (Chapter 3), suggesting attachment of a phytylthioether moiety at the C-3^1 position. The minor ion at *m/z* 583 reflects a loss of 278 Da, attributed to loss of the phytyl chain as phytadiene with hydrogen transfer to the charge-retaining fragment. The MS^3 spectrum (Fig. 4.15c), generated from CID of *m/z* 550 resembles that of the short chain alkylthioether pphorb *a* derivatives (Chapter 3), containing prominent ions arising from losses of ethyl (-29 Da) and methyl radicals (-15 Da). Prominent ions in MS^4 reflects losses of 28 and 86 Da corresponding to losses of the C-13^1 CO and C-17^1 methyl propionate ester groups, respectively. The formation of the thioether creates a chiral centre at C-3^1. Whereas the diastereomers of the short chain C-3^1 alkylthioethers are not resolved under the HPLC conditions employed (Chapter 3), the larger phytylthioether moiety has a greater bearing in this respect producing two chromatographically distinct species (cf. phytylS-pphe *a*, Squier, 2003). Accordingly, the two components can be assigned as phytlyS-pphorb *a* (**78**) diastereomers differing only in their configuration at C-3^1. Together these components represent a 17% yield.

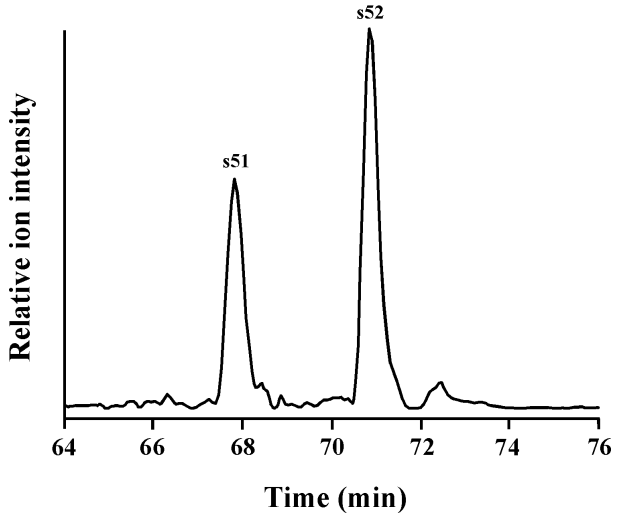

Figure 4.14. Partial LC-MS chromatogram (*m/z* 861) of the products from reaction of pphorb *a* with phytol and H_2S at pH 5.

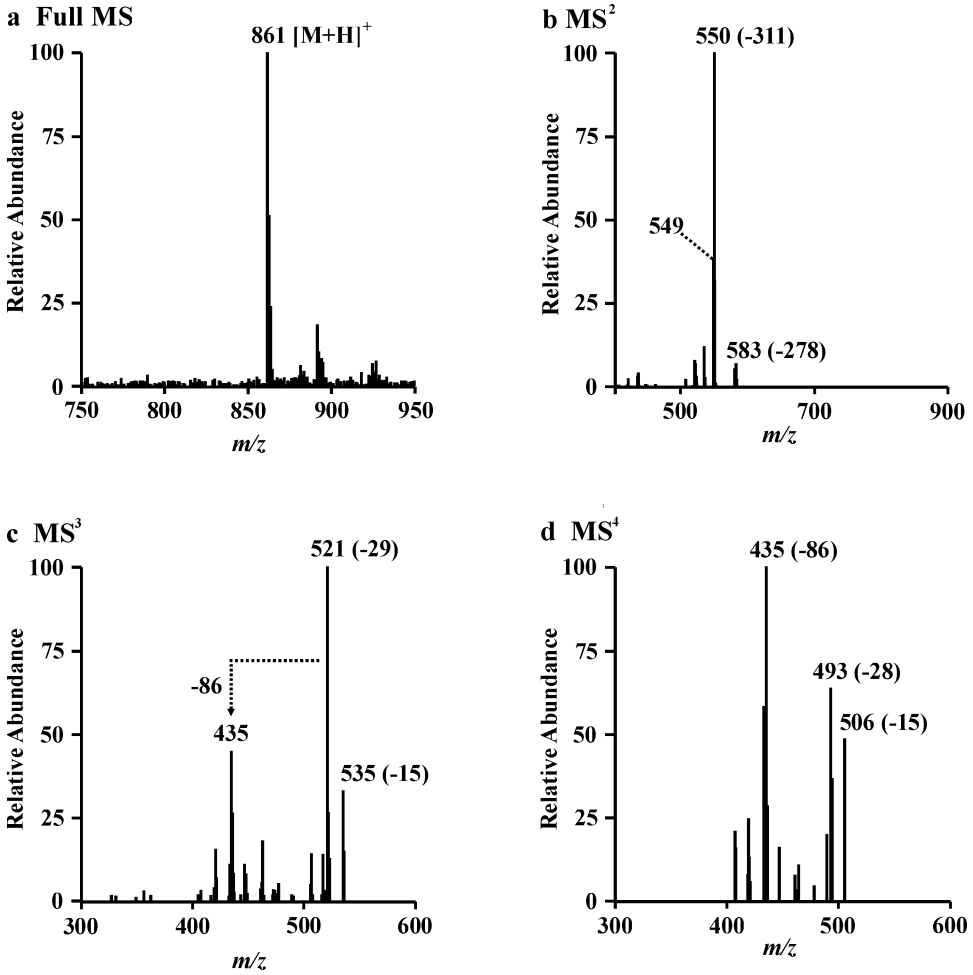

Figure 4.15. APCI multistage tandem mass spectra of phytylS-pphorb *a* (**78**); a) Full MS, b) MS^2, c) MS^3, d) MS^4. In each case the most abundant ion was selected as the precursor for the next spectrum.

Reaction of phe *a* with phytol and H_2S under the above conditions led to the formation of four isobaric peaks s53-s56 exhibiting protonated molecules at *m/z* 1183 clearly shown by a partial mass chromatogram extracted at that *m/z* value (Fig. 4.16). The MS^n spectra for these components (e.g. s53, Fig. 4.17) match those of phytylS-phe *a* (Squier 2003). CID of *m/z* 1183 produced ions in MS^2 at *m/z* 905 (100%) and *m/z* 845 (52%) corresponding to losses, regularly observed in the MS^n spectra of chlorins, of phytadiene (-278 Da) and phytadiene plus the C-13^2 carbomethoxy group (-338 Da), respectively. In addition, an atypical product ion was present at *m/z* 593 (29%), representing a loss of 590 Da, assigned to loss of phytadiene accompanied by further 312 Da. CID of *m/z* 905 yielded a base peak ion at *m/z* 594 arising from loss of 311 Da. The losses of 312 and 311 Da correspond, respectively, to losses of phytenethiol and a phytenethiyl radical. Accordingly, the four components were assigned as diastereomers of phytylS-phe *a* (**73**). Alternate pairs of peaks [s53 and s55] and [s54 and s56], present in approximately equal abundance and separated in retention time by ca. 2.2 min, differ in the configuration at C-3^1. Adjacent pairs of peaks [s53 and s54] and [s55 and s56], separated by ca. 1.2 min, differ in the configuration at C-13^2. Collectively these components represent a yield of 2%. The relative abundances of the peaks s53-s56 match those of the natural phytylS-phe *a* diastereomers (Squier, 2003), implying a similar mechanism of formation and indicating that the simulation reactions accurately mimic the formation of the natural species.

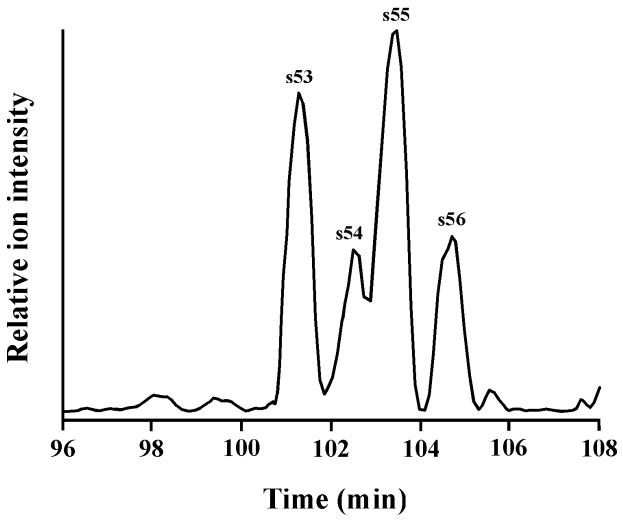

Figure 4.16. Partial LC-MS chromatogram (*m/z* 1183) of the products from reaction of phe *a* with phytol and H_2S at pH 5.

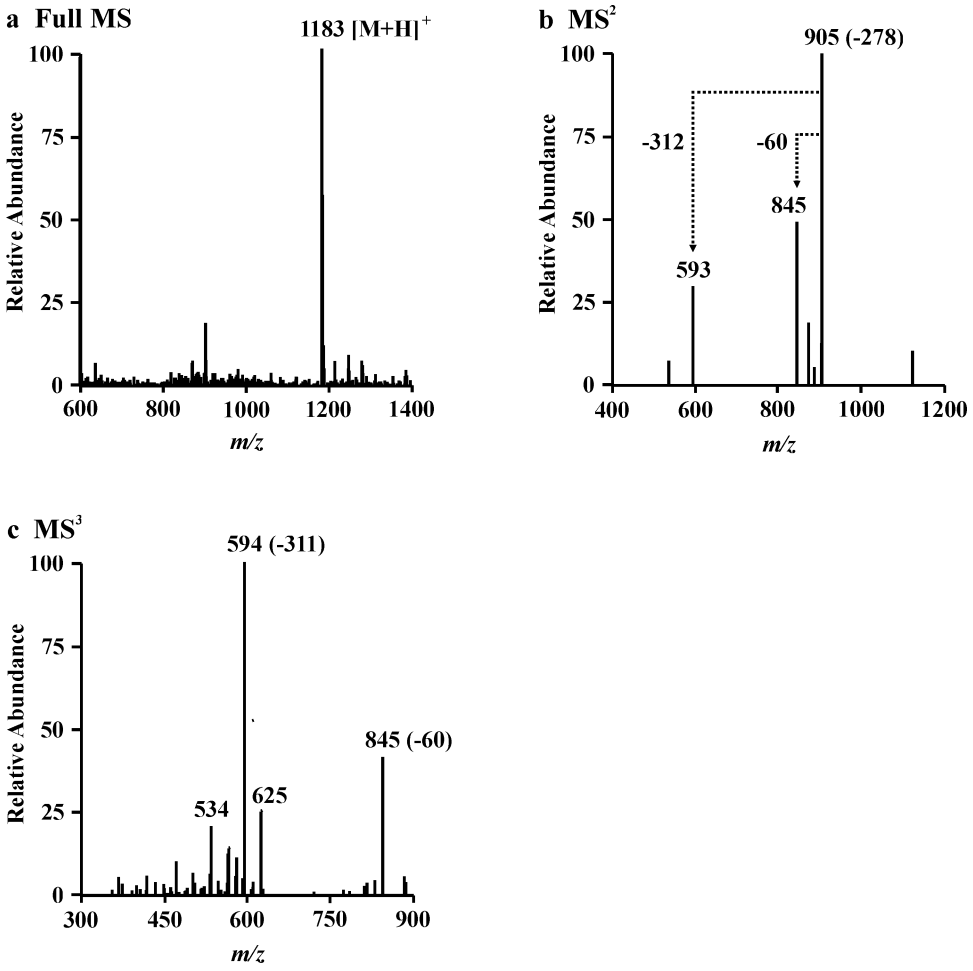

Figure 4.17. APCI multistage tandem mass spectra of phytylS-phe *a* (s53, **73**); a) Full MS, b) MS^2, c) MS^3. In each case the most abundant ion was selected as the precursor for the next spectrum.

The mechanism of formation probably involves the formation of phytenethiol, via acid promoted substitution of the phytol hydroxyl group by H_2S (cf. de Graaf et al., 1992), followed by its addition to the C-3 vinyl group. The formation of the thiol could occur via a photochemically initiated reaction in illuminated anoxic natural environments (Adam et al., 1998). Alternatively, initial acid catalysed dehydration of phytol to a phytadiene could occur followed by incorporation of H_2S. In the case of phytadiene, however, addition of H_2S to one of the two conjugated double bonds would be likely to proceed in an intramolecular fashion forming a mixture of cyclic thiophenes and thiolanes (Fukushima et al., 1992). This interpretation is supported by the lack of formation of phytylS-pphorb *a* in reactions carried out with a mixture of phytadienes (e.g. **77**) and H_2S. Given that the reaction between phytenethiol and the substrate is likely to be confined to the hydrophobic core of the micelle, the lower

yield of phytylS-phe *a* compared to that of phytylS-pphorb *a* could be the result of the hydrophobic phytyl side-chain of phe *a* having an effect on the orientation of the molecule such that the vinyl group is directed towards the micelle exterior. This would make the vinyl group less available for reaction.

4.2.8. Sulfur-containing bacteriochlorophylls

Throughout the marine section of the core from Pup Lagoon, bacteriochlorophylls *c* and *d* made a significant contribution to the total pigment signal, indicating an input from obligate anaerobic Chlorobiaceae (Squier, 2003). When present in the HPLC chromatograms, the dominant farnesyl homologues, bacteriophaeophytins c_2 (bphe c_2, **79**) and d_2 (bphe d_2, **80**), were preceded by a number of components suspected to result from incorporation of H_2S in the C-17[3] farnesyl side chain (Squier, 2003).

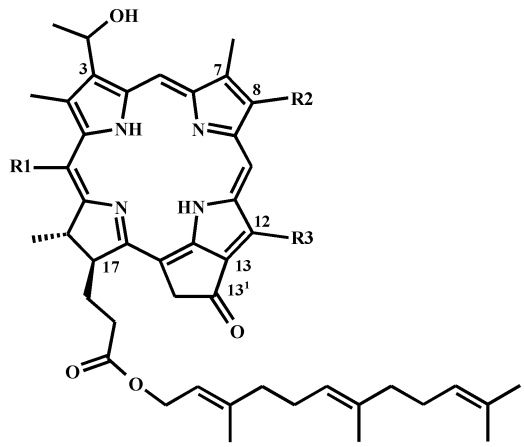

79: R1 = Me, R2/R3 = *n*-Pr/Me or Et/Et

80: R1 = H, R2/R3 = *n*-Pr/Me or Et/Et

The structure of the farnesyl chain contains three non-conjugated carbon-carbon double bonds; sulfur incorporation into isolated double bonds has been demonstrated to occur at relatively low temperatures by the reaction of hydrogen polysulfides (Schouten et al., 1994; de Graaf et al., 1995) and the photochemically-induced reaction of H_2S (Adam et al., 1998) to form a mixture of sulfide-bridged dimers and thiols. By contrast with the sulfur-containing chlorophylls, a strong correlation was observed between the abundances of non-sulfurised bphes and their sulfurised counterparts, with the latter present in approximately 27% relative abundance (Squier,

2003). Such a strong precursor-product relationship would not be expected if sulfide concentrations were limiting suggesting that, in this case, bchl abundance was the controlling factor in their formation. The occurrence of the suspected sulfurised bchls is perhaps not surprising given the requirements of Chlorobiaceae for sulfide. In order to validate these assignments and investigate the sulfurisation of the bchl farnesyl side-chain, a mixture of bphe *c* homologues, comprising mainly bphe c_2 (**79**), was subjected to reaction with dimethyl disulfide in the presence of H_2S. Dimethyl disulfide was selected as the thiol source as it had proven the most efficient out of the other sulfur reagents and its addition to the farnesyl double bond would produce a methyl thioether that was unable to dimerise.

LC-MS analysis of the reaction mixture after 12 d established the presence of two peaks, together representing 3% of the total chlorin signal, eluting immediately prior to the dominant bphe *c* homologue, bphe c_2. Both peaks revealed a protonated molecule at *m/z* 833 (Fig. 4.18) and UV/vis spectra consistent with bphe *c* (λ_{max} 411, 667). CID of the protonated of each component (*m/z* 833) yielded a base peak ion in MS^2 at *m/z* 581 (Fig. 4.18b), corresponding to a loss of 252 Da. This product ion is consistent with that observed in the MS^2 spectrum of bphe c_2 following loss of the C-17^3 farnesyl esterifying alcohol, suggesting that the reaction product possesses a c_2 macrocycle and that loss of 252 Da pertains to loss of the C-17^3 side-chain. Loss of 252 Da is 48 Da greater than that observed for loss of farnesyl (204 Da), indicative of the incorporation of methanethiol into the farnesyl chain. The site of sulfur incorporation could not be determined, although, in view of the lack of evidence in sediments and simulation reactions to support the incorporation of sulfur into phytol-esterified chlorins it appears that the double bond proximal to the ester is inactive, possibly for steric reasons. Thus, the two isobaric components most likely result from sulfur incorporation at either of the other two double bonds. Accordingly, the two products were assigned as methylthioether analogues to the natural sulfurised bchl c_2 derivatives, occurring as regioisomers arising from sulfur incorporation into different double bonds on the farnesyl side-chain. Corresponding methylthioether derivatives were also observed for the other bchl *c* farnesyl homologues present in the starting mixture.

The reaction described above clearly demonstrates incorporation of sulfur into the isolated double bonds of the bchl farnesyl side chain, providing a rationale for the sulfurised bchls in Pup Lagoon. While the conversion (3%) is significantly lower than that implied from analysis of the sedimentary components, it is worth noting that the duration of the laboratory reaction (12 d) is likely to be significantly shorter than the time associated with the formation of the sedimentary species.

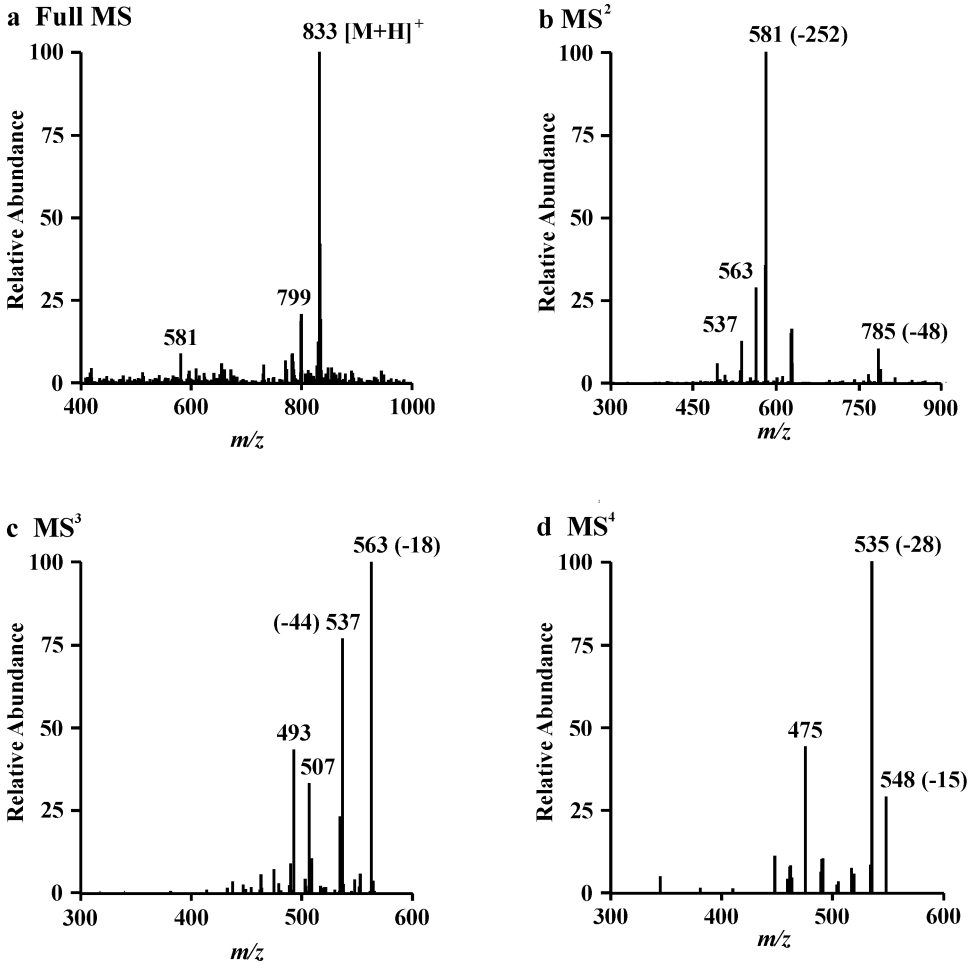

Figure 4.18. APCI multistage tandem mass spectra of the sulfurised bchl c_2 derivative resulting from incorporation of methanethiol into the farnesyl side-chain; a) Full MS, b) MS^2, c) MS^3, d) MS^4. In each case the most abundant ion was selected as the precursor for the next spectrum.

4.3. Conclusions

The reactions described above have demonstrated numerous transformations of chlorophylls under conditions that resemble natural aquatic environments.

The formation of C-3 alkylthioether and phytylthioether chlorophyll derivatives in the simulation reactions, demonstrates the susceptibility of the chlorophyll vinyl group towards reaction with sulfides. Similarly, sulfurisation of bchls *c* and *d*, which possess a secondary alcohol instead of a vinyl group at C-3, may occur at the farnesyl side-chain. The facile nature of these reactions, which have been shown to occur over short timescales under mild conditions (low temperature, moderate pH), clearly demonstrates the potential for photosynthetic pigments to form sulfur cross-links with other biomolecules and, by inference, become sequestered into macromolecular structures.

The reaction of alkylhalogen-derived alkylthiols with the chlorophyll vinyl group has been demonstrated as a viable route to the formation of alkylthioether chlorophylls in the natural environment. Their formation is likely to be associated with the high local concentrations of alkylhalides produced by phytoplankton during the termination of blooms and therefore to be most important in coastal and continental shelf regions. Thus, alkylthioether chlorophylls have potential, not only as markers for high concentrations of dissolved sulfide, but also to record the distributions of alkyhalogens emitted by marine algae and may act as an important sink for volatile halocarbons, which have been implicated in ozone depletion.

Reduction of the C-3 vinyl group to an ethyl substituent is a key, yet poorly understood, event in the diagenetic pathway linking chl *a* to sedimentary alkyl porphyrins. The formation of mpphorb *a* from pphorb *a* in the simulation reactions described above provides strong evidence for the involvement of H_2S in this transformation. Moreover, these reactions indicate that low temperature abiotic reactions involving H_2S are important in the geochemical reduction of sedimenting organic matter.

The reaction of pphorb *a* with hydrogen sulfide and oxygen, under mild conditions (low temperature, moderate pH) that resemble those in certain natural environments, leads to its near quantitative conversion into pphorb *d* (65-89%). The transformation, which involves the oxidative cleavage of the C-3 vinyl substituent of pphorb *a* to afford an aldehyde at the C-3 position, most likely results from degradation of products that are formed from cooxidation of the vinyl group and H_2S by molecular oxygen. Potentially, this is an important transformation affecting vinyl-bearing chlorophylls in the natural environment, representing a key intermediate step in the formation of C-3 β-CH_3 and β-H porphyrins found in mature sediments and providing a plausible, low temperature, alternative to the Schumm reaction to explain devinylation in nature. In addition, the oxidative cleavage of the C-3 vinyl group may both provide insight into the biosynthesis of chl *d* by the unique cyanobacterium, *Acaryochloris marina*, and offer a greener alternative to classical methods for the synthetic manipulation of the vinyl substituents of tetrapyrroles.

Owing to the mild reaction conditions associated with their formation, some of the other transformation products described here, such as the C-3 (1-hydroxyethyl) and C-3 acetyl derivatives, may potentially represent natural transformation products that have yet to be identified in sediments. Given that the structure of the C-3 (1-hydroxyethyl) derivative is the same as that of bphe *d* with a [C-8, C-12] configuration [Et, Me], operation of this transformation pathway in the natural environment has the potential to create a false signal for input from green sulfur bacteria to the sedimentary record.

Chapter 5:

Conclusions and future work

5.1. Conclusions

The primary aim of the work presented in this thesis was to develop a clearer understanding of the factors and environments conducive to the formation of sedimentary C-3[1] alkylthioether chlorophyll derivatives (Pup Lagoon, Antarctica; Squier et al., 2003; 2004) and the environmental significance of their occurrence. This involved two key areas of study; i) examination of the sedimentary pigment distributions contained within an Antarctic marine core to try to find sulfur-containing chlorophylls which could be related to those identified in Pup Lagoon and ii) to recreate and study the formation of C-3[1] alkylthioether chlorophyll derivatives in laboratory reactions that simulate natural aquatic environments.

Although no sulfur-containing chlorophylls were detected, examination of the Antarctic marine core PC461 revealed some interesting features, including a wealth of information present in a form that was inaccessible to conventional acetone extraction alone. Acetone extracts from the core were overwhelmingly dominated by carotenoids with chlorophylls present in much lower abundance. Acid methanolysis of the previously acetone-extracted sediment released large quantities of tetrapyrroles believed to have been bound to components of the sediment matrix (mineral grains, diatom cysts, etc.) via ester linkages or similar bonds susceptible to methanolic cleavage. The yield of acid liberated pigments often exceeded that extractable by acetone, indicating that ester bound tetrapyrroles may constitute a significant repository for photosynthetic pigments in the sedimentary record. Significant differences were apparent between the distributions of acetone and acid extractable tetrapyrroles, the latter being enriched in compounds originating from dephytylated chlorophyll derivatives and those having experienced oxidative transformations centred upon ring E. These components possess structural elements such as free acid groups and other oxygen-containing functionalities liable to form associations (e.g. via ester linkages) with components of the sediment matrix. Whereas, acetone extracts contained exclusively tetrapyrroles derived from chl *a*, which is ubiquitous in oxygenic photoautotrophic organisms, acid methanolysis revealed the presence of pigments derived from chls *b* and *c* that indicate contributions from more specific groups of photoautotrophs and signify a major shift in the photoautotrophic

community ca. 38 ka (raw radiocarbon age). Furthermore, methanolysis revealed the presence of protoporphyrin-IX, as its dimethyl ester, representing the closest functionalised derivative of heme to be identified in sediments to date.

These findings illustrate that certain sedimentary pigments may be under represented, if at all, in the distributions of acetone-extractable components. Furthermore, this study demonstrates the value in performing methanolyitic extraction, in addition to conventional acetone extraction, to reveal compounds that would otherwise have been overlooked and, thus, provide a more accurate reconstruction of past environmental conditions and the primary producer communities in palaeo-water bodies.

Laboratory simulation reactions, employing conditions that closely resemble those that occur in many natural aquatic environments, have demonstrated a wide variety of transformations of several chlorophylls and their derivatives. Some of the compounds formed are identical to those known to occur in nature, while others may represent currently undiscovered natural transformation products. Given the mild reaction conditions used, the transformations demonstrated in the simulation experiments are applicable to the earliest stages of diagenesis, affecting sedimentary/sedimenting organic matter.

Reactions of chl *a*, and some of its common sedimentary transformation products, with short chain alkyliodides/dialkyl disulfides and H_2S, in a variety of different media, led to the formation of synthetic C-3^1 alkylthioether chlorophyll derivatives, analogous to those found occurring naturally. Reactions conducted in acetone-based solutions deliver high yields of the derivatives and are suitable for the preparation of standards. Detailed study of the synthetic compounds by RP-HPLC, LC-MS^n and ^{1}H NMR has provided insight into their analytical characteristics, validating the assignments of the sedimentary species made by Squier et al., (2003; 2004). In addition the prominent loss of the alkylthioether moiety as a radical during MS^n has been confirmed as a diagnostic feature of the spectra. The formation of C-3^1 alkylthioether chlorophyll derivatives in aqueous micellar systems, which offer a more accurate representation of conditions that occur in natural anoxic aquatic environments, provides firm evidence to support a route to their formation in nature from a reaction between the chlorophyll vinyl group and alkylthiols, formed from the

reaction of H_2S with alkylhalogens. The reaction operates over a range of pH, representative of a wide variety of aquatic environments, and low pH was found to favour the reaction, indicating an electrophilic mechanism of thiol addition to the C-3 vinyl group. The C-3 vinyl group of chl *a* proved to be more reactive with regard to sulfurisation than that of its demetallated counterparts, although H_2S was capable of displacing the chelated Mg during the reaction. These observations indicate that the conditions associated with the formation of alkylthioethers also promote demetallation and can explain the predominance of demetallated alkylthioethers, compared with the non-sulfurised components, in the natural pigment distributions from Pup Lagoon (Squier et al., 2004).

Marine algae and phytoplankton are the primary source of short-chain halocarbons in aquatic environments. Thus, the formation of alkylthioether chlorophyll derivatives is likely to be most important in coastal and continental shelf regions. In addition, the requirement for H_2S dictates an anoxic depositional environment and an active sulfate reducing bacterial community. While alkylthioether chlorophylls were formed in simulation reactions conducted at a range of different pH values, higher yields were obtained at low pH indicating that acidic environments are favourable to their formation. The majority of marine environments are slightly alkaline, owing to the buffering effect of dissolved carbonates. By contrast, the buffering capacity of lakes is much lower and, consequently, lakes display more variety in pH, depending on their environment. Thus, the formation of alkylthioether chlorophylls could be particularly favourable in acidic lakes that have an active sulfur cycle. For this, constant replenishment of sulfate would be required in order to sustain the bacterial production of H_2S. The oceans represent the largest reservoir of sulfate. Thus, it appears that the conditions in Pup Lagoon, a coastal lake susceptible to marine incursions, were ideally suited to the formation of alkylthioether chlorophyll derivatives.

The findings of the simulation studies reinforce suggestions that alkylthioether chlorophyll derivatives are potential markers for anoxic conditions and the sulfurisation of organic matter in the natural environment. Furthermore, they raise the possibility that the alkylthioethers may serve as a record of the distributions of alkylhalides emitted by marine algae and that reactions of this kind constitute a

significant sink for volatile halocarbon and sulfur species in anoxic environments. In view of the role these species play in the chemistry of the atmosphere, these findings have potential climatological significance.

In addition to short-chain alkylthioether chlorophyll derivatives, several other sulfur-containing tetrapyrroles were tentatively identified in the sediment of Pup Lagoon. These comprised compounds believed to be phytylthioether derivatives of phe *a* and pphe *a*, as well as sulfurised bchl *c* and *d* homologues having incorporated a molecule of H_2S in their farnesyl side chain (Squier, 2003). Investigation of the origins of these compounds in the simulation reactions demonstrates that phytylthioether chlorophyll derivatives can arise from the reaction of the C-3 vinyl group with phytol and H_2S, most likely via initial formation of phytenethiol, and confirm the feasibility of sulfur incorporation into the farnesyl side-chain of bchl *c* under mild conditions.

The formation of alkyl- and phytylthioether chlorophyll derivatives in the simulation reactions, under mild reaction conditions and over relatively short timescales, clearly demonstrates the susceptibility of the chlorophyll vinyl group to reaction with reduced sulfur species. The facile nature of the reactions implies that the sequestration of chlorophylls, via sulfur crosslinking reactions involving this substituent, may be widespread in anoxic depositional environments and capable of operating in surface sediments and in the water column during particle settling. Consequently, the monomeric natural alkyl and phytylthioethers may represent a relatively minor component of the total sulfurised tetrapyrroles in Pup Lagoon, a significant portion of which may be bound via sulfide bonds to macromolecular structures. Similarly, bchls *c* and *d*, which lack a C-3 vinyl group, may become sequestered through sulfurisation at their farnesyl esterifying alcohol.

In addition to the sulfur-containing products of the reactions, several non-sulfurised products were formed. The reaction of pphorb *a* with H_2S, in the presence and absence of alkyliodide, led to its partial conversion into mpphorb *a* (up to 6% yield) via reduction of the C-3 vinyl substituent to form an ethyl substituent. Reduction of the C-3 vinyl substituent is a key step in the series of transformations linking chlorophylls to many sedimentary alkyl porphyrins and has been associated with the anaerobic bacterial degradation of organic matter (Spooner et al., 1995). Furthermore,

reductive processes are suggested to play a major role in the preservation of organic matter. The reduction of the C-3 vinyl substituent is proposed to occur via the initial formation of a C-3^1 thiol intermediate followed by reductive desulfurisation, similar to that suggested for the reduction of double bonds of carotenoids (Hebting et al., 2006). In reactions performed in the absence of alkyliodide, significant amounts of sulfur crosslinked pphorb *a* dimers were formed that are also believed represent intermediates in the reduction. Had the reductive desulfurisation of all sulfurised pphorb *a* derivatives formed in the reaction proceeded to completion, the yield of mpphorb *a* obtained would have been closer to 69%. Notably, the reduction of the C-3 vinyl substituent of pphorb *a* occurs at lower temperature (room temperature), over shorter timescales (4 d) and forms mpphorb *a* in apparently higher yields than were found for the reduction of β-carotene and reductive desulfurisation of phytenethiol (1% and 3.8%, up to 90ºC, 180 d; Hebting et al., 2003; 2006). Thus, the reactions described here indicate that low temperature abiotic reactions involving H_2S are important in the geochemical reduction of organic matter within surface sediments and possibly even in the water column during particle settling.

The reaction of pphorb *a* with H_2S in the presence of oxygen led to the oxidative cleavage of the C-3 vinyl group to form pphorb *d* (65-89% yield). The reaction is suggested to occur via the cooxidation of H_2S and the pphorb *a* vinyl group by molecular oxygen, followed by cleavage of the resulting β-hydroxysulfoxide to afford the aldehyde at C-3. Oxidative cleavage is a potentially significant transformation for vinyl-bearing chlorins in the natural environment and could activate this substituent towards loss. Consequently, the C-3 aldehyde may represent a key intermediate in the formation of fossil porphyrins that possess β-CH_3 and β-H substituents. Furthermore, this reaction may provide valuable insight into the biosynthesis of chl *d* by the unique cyanobacterium, *Acaryochloris marina*.

The major geochemical chlorophyll transformation pathways that have been proposed or rationalised, on the basis of the laboratory simulation reactions described here, are illustrated in Fig. 5.1.

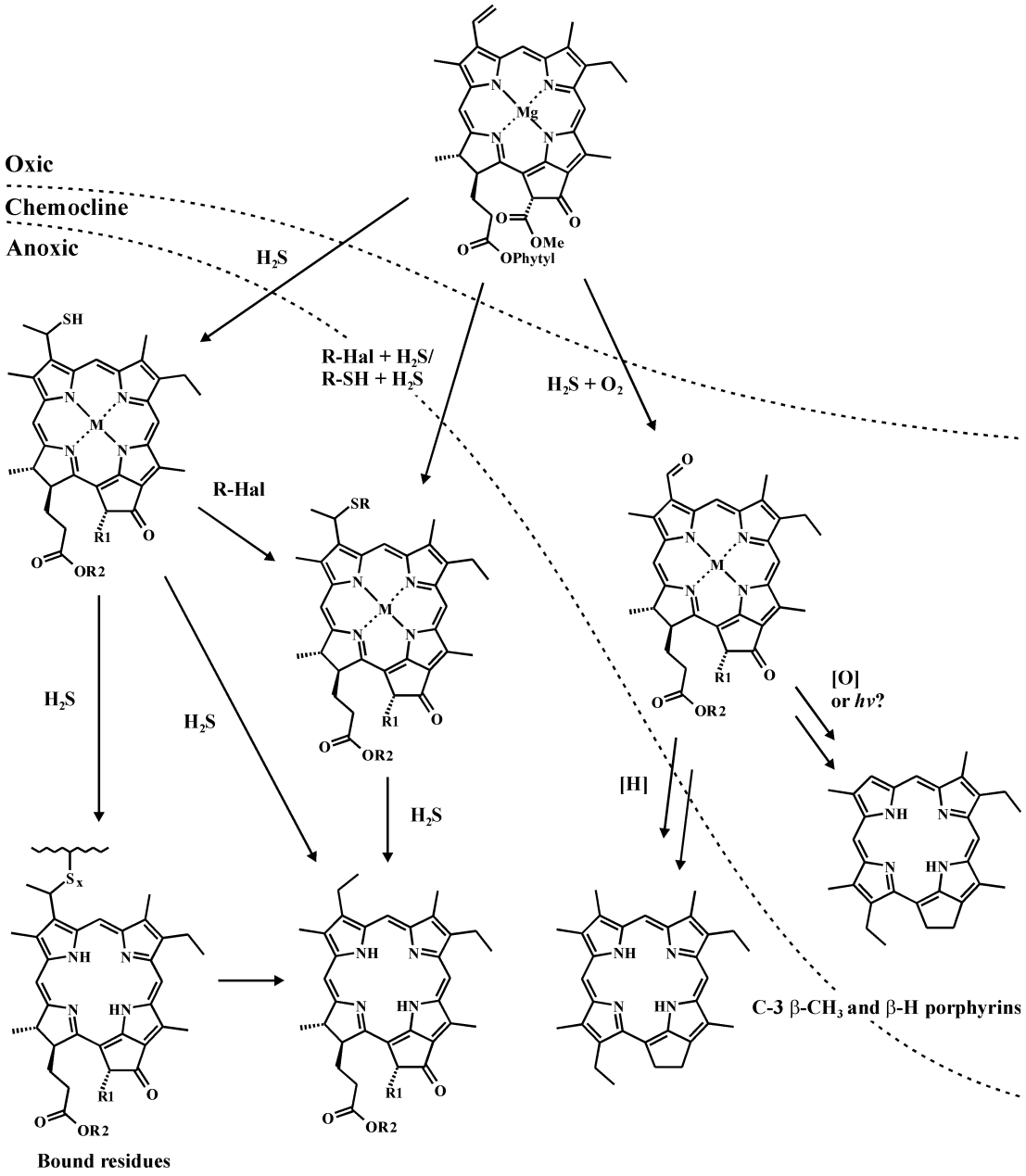

Figure 5.1. Summary of the major geochemical transformation pathways of chlorophylls that have been proposed or rationalised as a result of this work, formulated for chl *a*. The reactions shown form an extension of the Treibs scheme (Fig. 1.2) and may be accompanied by the various other chlorophyll transformation reactions, outlined in Chapter 1. M = Mg or 2H, R = alkyl, R1 = CO_2Me or H, R2 = phytyl or H.

5.2. Future work

5.2.1. Arising from the sediment study

In order for the information provided by methanolytic extraction to be of the greatest value, a full appreciation is needed of the mechanisms by which chlorophylls form associations with the sediment and the effect of methanolysis extraction on the various transformation products. This requires submitting a full spectrum of geochemically relevant chlorophylls and their transformation products to the methanolysis procedure and observing any alteration products that occur. This could establish whether the rearranged chl *c* derivatives, observed in the acid extracts, are in fact genuine sedimentary species or artefacts of the extraction process. In addition, it may be possible to carry out quantitative doping experiments to load sediment with different chlorophyll transformation products before submitting them to extraction with both acetone and methanolysis and determining the recovery. This could reveal compounds particularly susceptible to binding, the percentage recovery following extraction and match precursors to their products in the methanolysis extract.

The methanolysis extraction could be applied to a variety of other sediments in order to assess its value as a routine accompaniment to the established acetone extraction or whether it is only necessary for certain sediment types.

In addition, several of the components of the methanolysis extracts that could not be identified on the basis of their UV/vis and MS^n spectra could be isolated by preparative HPLC for a more rigorous structural characterisation by ^1H NMR.

5.2.2. Arising from the simulation reactions

The search for alkylthioether chlorophyll derivatives in sediments other than Pup Lagoon, in order to learn more their natural distributions, will be an important aspect in developing our understanding of these species. The information gained from formation of alkylthioether chlorophylls in the laboratory simulation reactions will prove useful in identifying suitable environments where alkylthioether chlorophylls

are likely to form. Furthermore, the availability of standards of alkylthioether chlorophyll derivatives, and an appreciation of their analytical characteristics, should aid the identification and quantification of these derivatives in future analyses. Given apparent susceptibility of chlorophylls towards sulfurisation reactions, chemical desulfurisation of Pup Lagoon sediment is warranted to determine whether any tetrapyrroles have been sequestered into macromolecular structures via sulfide bonds.

The mechanisms by which pphorb *d* and mpphorb *a* form in the simulation reactions merit a more detailed investigation, for example using electron spin resonance to confirm unequivocally the involvement of radicals. In addition, chl *c* should be subjected to the reaction with H_2S and air to establish whether oxidative cleavage of the double bond in the acrylic acid side chain can occur under these conditions and whether mechanisms proposed for dealkylation at C-3 can also be applied to those which occur at C-17.

The absence, in the LC-MS chromatograms of the extracts from the simulation reactions, of peaks corresponding to the dimeric pair of sulfur-bridged pphorb *a* molecules, which were readily identifiable in the mass spectrum obtained upon direct injection, may suggest that these components do not elute within the polarity window afforded by the Airs HPLC gradient programme. Further investigation is needed to establish whether this is the case and modification of the HPLC method may be required in order to observe such species in environmental samples.

The sulfurisation reactions could be extended to other geochemically relevant compound classes such as carotenoids and sterols. The chlorophyll derivatives chlone and cyclophaeophorbide enol share the same structural motif as the sulfur-bound porphyrins identified in ancient sediment (Schaeffer et al., 1993; 1994). The possibility of a precursor-product relationship existing between these compounds could be explored further in sulfurisation experiments. Similarly, the micellar model systems could be applied to the study of other transformation reactions of chlorophyll in the natural environment such as oxidative transformations, extending the work of Walker (2004), or to simulate transformations suggested to occur in alkaline conditions such as the formation of chlone or chlorin e_6.

Chapter 6:

Experimental and analytical procedures

6.1. General procedures

6.1.1. Solvents and reagents

All solvents used were analytical grade or higher (Fisher, Loughborough, UK) unless specified otherwise. All reagents used were obtained from Aldrich (Gillingham, UK) unless specified otherwise.

6.1.2. Glassware

To avoid sample contamination, all glassware was rinsed with acetone (laboratory grade) and deionised water before being soaked in a 1% solution of Decon-90 (Decon, Hove, UK) for 12 h. Soaked glassware was washed extensively with deionised water, and acetone (laboratory grade). Immediately prior to use, glassware was washed further with acetone (analytical grade). Glassware used in the sulfurisation reactions was soaked in aqueous bleach (12 h) to destroy traces of thiol, rinsed with large amounts of water and washed with dilute HCl to remove salts before being subjected to the treatment described above.

6.1.3. Sample storage and handling

Prior to extraction, sediment samples were stored in the dark at –20 °C at which pigments have been shown to remain stable over several months (Reuss and Conley, 2005). Pigment standards and extracts were stored dry and in the dark at +4 °C. All manipulations involving pigments were carried out in low light conditions to avoid photodegradation.

6.2. Preparation of standards, substrates and reagents

6.2.1. Preparation of phaeophytin *a*

Phaeophytin *a* was prepared by shaking a solution of chlorophyll *a* (isolated by Deborah Mawson) in diethyl ether (10 ml) with aqueous HCl (4 M, 10 ml) for 10 min. The organic layer was separated and washed with deionised water (4 x 10 ml). On the penultimate wash, a few drops of ammonium hydrogen carbonate (1 M) were added to ensure neutrality. The organic layer was collected and dried under a gentle stream of N_2.

6.2.2. Preparation of pyrophaeophorbide *a* methyl ester

Phaeophorbide *a* methyl ester was prepared from oil soluble chlorophyll tar (British Chlorophyll Company, Lincoln, UK). Chlorophyll tar (3 g) was dissolved in a 5% solution of H_2SO_4 (18 M) in methanol (200 ml) and stirred in for 24 h in the dark. The solution was transferred to a separating funnel and an equal volume of diethyl ether added, followed by the dropwise addition of a solution of 60% H_2SO_4 in methanol (50 ml). The ether layer containing carotenoids (yellow) was discarded and the methanolic phase (green) extracted with portions of diethyl ether (200 ml) until no more carotenoids were transferred. A fresh portion of diethyl ether was added and the methanolic solution progressively diluted with water to initiate transfer of the tetrapyrroles into the ether layer. The ether layer was separated and washed exhaustively with portions of deionised water (10 x 100 ml). On the penultimate washing the pH of the aqueous layer was taken and a couple of drops of ammonium hydrogen carbonate (1 M) added to ensure neutrality. The organic layer was collected and solvent removed in vacuo.

6.2.3. Preparation of protoporphyrin-IX dimethyl ester

Protoporphyrin-IX was prepared from hemin using a method adapted from (Morell et al., 1961). Briefly hemin (ca. 1.5 mg) was dissolved in pyridine (0.5 ml) and glacial acetic acid (10 ml) added. N_2 was bubbled through the solution for 30 min followed

by the addition of a freshly prepared solution of $FeSO_4.7H_2O$ (41 mg in 0.4 ml HCl). The flow of N_2 was maintained over the surface of the solution and the solution stirred for 20 min. Completion of the reaction was indicated by a greenish tinge to the solution under reflected light which can be observed clearly by drawing some of the solution up into a pipette. The solution was poured into a separating funnel containing diethyl ether (50 ml) and aqueous sodium acetate (0.5 M, 50 ml) and shaken. The organic layer was separated, washed with deionised water (3 x 50 ml) and solvent removed under a gentle stream of N_2 to yield dry protoporphyrin-IX. Protoporphyrin-IX was then converted into its dimethyl ester by acid methanolysis. Dry protoporphyrin-IX was dissolved in methanolic H_2SO_4 (5%; 5 ml) and stirred for 12 h in the dark. The solution was placed into a separating funnel with an equal volume of diethyl ether and diluted with deionised water to initiate transfer of the pigment into the ether layer. The ether layer was separated and washed with portions of deionised water (10 x 10 ml). On the penultimate washing the pH of the aqueous layer was taken and a couple of drops of ammonium hydrogen carbonate (1 M) added to ensure neutrality. The organic layer was collected and solvent removed in vacuo.

6.2.4. Preparation of phytadienes

A mixture of phytadienes was prepared by acid deyhydration of phytol using *p*-toluenesulfonic acid (cf. Grossi and Rontani, 1995). Briefly, phytol (1 g) and some 5 Å molecular sieves were added to a solution of *p*-toluenesulfonic acid (64 mg) in acetone (3 ml) and left for 12 h. The solution was extracted into hexane, washed with water and loaded onto a silica/hexane packed pipette column. The column was washed with 3 bed volumes of hexane, which were collected and the solvent removed under a stream of N_2 to afford a clear oil.

6.2.5. Preparation of diazomethane

Diazomethane was generated from the dropwise addition of aqueous potassium hydroxide (6.6 M, 1.5 ml) to a solution of *N*-methyl-*N*-nitroso-*p*-toluenesulfonamide (Diazald, 0.3 g, prepared by Phil Helliwell) in 1:1 ethanol:diethyl ether (2 ml). The diazomethane evolved was collected by distillation into cold diethyl ether (2 ml).

Owing to the hazards associated with the preparation and storage of diazomethane, its generation was performed immediately prior to use in specialised apparatus that was free from scratches or ground glass joints that could potentially initiate an explosion. Excess diazomethane was destroyed with dilute HCl (0.1 M).

6.3. Sediment Extractions (Chapter 2)

6.3.1. Acetone Extraction

Sediment was thawed and approximately 3 g of wet sediment transferred to a plastic centrifuge tube followed by the removal of any excess water with a pipette. The sediment was ultrasonically extracted with acetone (10 ml, analytical reagent grade; 10 min) with subsequent sedimentation of suspended material by centrifugation (10 min; 30,000 rpm; 2000 *g*). The supernatant was collected and filtered through a DCM washed cotton wool plug. Solvent was removed in vacuo and any water present by azeotrope with acetone. The extraction procedure was repeated, up to a maximum of 10 times or until the supernatant was colourless, and all extracts were combined. Prior to storage, the dry extracts were reconstituted in acetone (ca. 2 ml) and treated with 2-3 drops of an ethereal solution of diazomethane to methylate any free acids. This treatment offers improvements in peak shape during chromatography and prolongs sample storage life. The samples were then dried under a gentle stream of N_2.

6.3.2. Methanolytic (acid) extraction

The acetone-extracted sediment from Section 6.3.1. was magnetically stirred in a 5% solution of H_2SO_4 (18 M) in methanol (5 ml) for 24 h in the dark. The suspended material was spun down by centrifugation (10 min; 30,000 rpm; 2000 *g*) and the supernatant transferred, with filtration (DCM washed cotton wool), into a separating funnel followed by the addition of an equal volume of diethyl ether. Pigments were transferred to the ether layer by gradually diluting the acidified methanolic solution with deionised water, accompanied by gentle swirling. The sediment was ultrasonically extracted further with portions of methanol until extracts were

colourless and the pigments transferred into ether, as above. The combined extracts were washed with deionised water (5 x 10 ml). On the penultimate washing, the pH of the aqueous layer was taken and, in some cases, a couple of drops of aqueous ammonium hydrogen carbonate (1 M) were added to ensure neutrality. The organic layer was separated and solvent removed in vacuo. In this case, treatment with diazomethane was not required, as any free acids would have been converted into their respective methyl esters during the extraction with methanolic H_2SO_4.

6.4. Simulation reactions

6.4.1. Reactions in organic media (Chapter 3)

In a typical experiment the pigment substrate, pyrophaeophorbide *a* or protoporphyrin-IX (1 mg), was dissolved in 5 ml of acetone, methanol or a solution of 70:30 acetone:aqueous ammonium acetate pH 7 (0.5 M) and placed into flask A (Fig. 6.1). Flask A was sealed and connected via a plastic cannula to flask B, containing crystals of $Na_2S.9H_2O$ (1.1 g), after which both flasks were evacuated. H_2S gas (~1.7 atm, see Section 6.4.1.1) was generated in flask B, from the addition of HCl (12 M, 1 ml) via the septum, to the $Na_2S.9H_2O$ crystals and allowed to equilibriate between the two flasks before withdrawing the cannula from A. Depending on the reaction, one of the following reagents; methyliodide, ethyliodide, propyliodide, butyliodide, pentyliodide (1 mmol) or dimethyl disulfide (0.5 mmol) was introduced to flask A via the septum. The resulting solution was magnetically stirred at ambient temperature for 4 d in the dark. The solution was then extracted into diethyl ether and washed with portions of deionised water (10 x 20 ml). Extracts from reactions involving methyliodide, ethyliodide or dimethyl disulfide were reduced to dryness under a gentle stream of N_2, venting exhaust gases through a $KMnO_4$ bubbler to destroy thiols and H_2S. Extracts from reactions involving less volatile thiols were first loaded onto silica/hexane packed pipette columns and washed with hexane (3 bed volumes) to remove residual alkylthiols/alkyliodides. The pigments could then be recovered from the top layer of silica into acetone, filtered and dried under N_2.

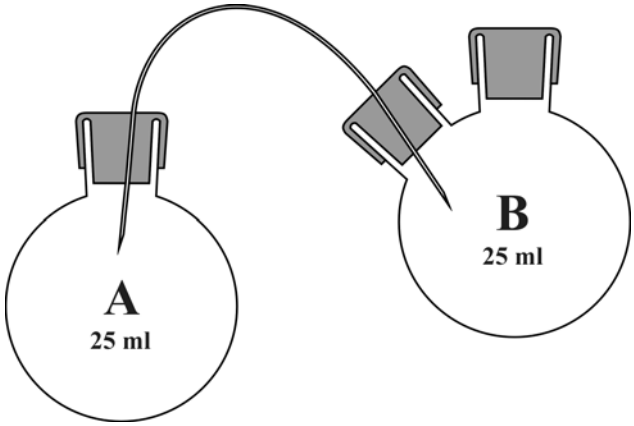

Figure 6.1. Apparatus used for the simulation reactions.

6.4.1.1. Calculation of the quantities of H_2S generated

H_2S gas was generated in the system (Fig. 6.1) from the reaction of $Na_2S.9H_2O$ (1.1 g) with HCl (12 M, 1 ml). The amount of $Na_2S.9H_2O$ used was chosen to produce approximately 1.7 atm of H_2S in the system (volume = ca. 69 ml after the addition of all solutions and reagents), calculated using the ideal gas equation (Equation 6.1). This was estimated to produce a quantity of H_2S in the reaction solution of approximately 1 mmol, calculated using Henry's law (Equation 6.2).

$$PV = nRT \tag{6.1}$$

Where: P = pressure (Pa)
V = volume (m^3)
n = the number of moles of gas (mol)
R = the universal gas constant (8.3145 m^3 Pa K^{-1} mol^{-1})
T = temperature (K)

$$k_H = c_a/p_g \tag{6.2}$$

Where: k_H = Henry's law constant (here, 0.1 mol dm^{-3} atm^{-1} for H_2S in water; Carroll and Mather, 1989)
c_a = the concentration of a species in the aqueous phase (mol dm^{-3})
p_g = the partial pressure of that species in the gas phase (atm)

6.4.2. Reactions in aqueous micelles (Chapter 4)

In a typical experiment, the pigment substrate; pyrophaeophorbide *a*, chlorophyll *a*, phaeophytin *a*, an equimolar mixture of pyrophaeophorbide *a* and chlorophyll *a*, or a mixture of bacteriochlorophyll *c* homologues (1 mg), was dissolved in acetone (100 µl) and added to flask A (Fig. 6.1). This was followed by addition of an aqueous solution of sodium dodecyl sulfate (SDS, 6 mmol, 5 ml) buffered to either pH 5 or 7 with ammonium acetate (0.5 M) or pH 8.5 with ammonium hydrogen carbonate (0.5 M). The flask was sealed, evacuated and the headspace was pressurised with H_2S (~1.7 atm) as for Section 6.4.1. Depending on the reaction, one of the following reagents was introduced via the septum; methyliodide, ethyliodide, propyliodide, butyliodide, pentyliodide, phytol, mixed phytadienes or dimethyl disulfide (all quantities 1 mmol except dimethyl disulfide, 0.5 mmol). The resulting solution was left to stir at ambient temperature, in the dark for up to 12 d. The reaction mixture was extracted into diethyl ether with gentle swirling, so as not to produce an emulsion, and the ether layer washed exhaustively with deionised water. Extracts from reactions involving methyliodide, ethyliodide or dimethyl disulfide were reduced to dryness under a gentle stream of N_2 with exhaust gases vented through a $KMnO_4$ bubbler. Extracts from reactions involving less volatile thiols, phytol or phytedienes were first loaded onto silica/hexane packed pipette columns and washed with hexane (3 bed volumes) to remove residual alkylthiols/alkyliodides/phytol derivatives. The pigments could then be recovered from the top layer of silica into acetone, filtered and dried under N_2.

For the reaction of pyrophaeophorbide *a* with H_2S and air, only flask A was evacuated and the amount of $Na_2S.9H_2O$ crystals used was reduced to 0.65 g.

6.5. Instrumental techniques

6.5.1. Reversed phase-high performance liquid chromatography

Reversed phase-high performance liquid chromatography (RP-HPLC) was performed using a Waters HPLC system (Milford, MA, USA) comprising a 600MS pump and

system controller, a 717 autosampler and a 996 photodiode array (PDA) detector, scanning over the range 300-800 nm. Solvents were passed through a vacuum degasser (Perkin Elmer, Series 200) prior to entering the pump. Instrument control and data processing were performed using Waters Millennium[32] software. Separation was accomplished using two Waters Spherisorb 3 μm ODS2 cartridge columns (150 mm x 4.6 mm i.d.) coupled in series, fitted with a pre-column of the same stationary phase (10 mm x 5 mm i.d.) and a further low cost Phenomenex security guard ODS C_{18} (4 mm x 3 mm i.d.) to prolong the life of the column. A quaternary solvent gradient elution programme was used, the solvent system comprising methanol, acetonitrile, ethyl acetate and 0.01 M ammonium acetate (Table 6.1 showing Methods A and B reproduced from Airs et al., 2001). Samples were prepared in either acetone or methanol for injection.

Table 6.1. HPLC solvent gradient programmes showing variation in percentage compositions of solvent with time (Airs et al., 2001).

Time (min)	Ammonium acetate (0.01 M)	Methanol	Acetonitrile	Ethyl acetate
Method A				
0	5	80	15	0
5	5	80	15	0
100	0	20	15	65
105	0	1	1	98
110	0	1	1	98
115	5	80	15	0
Method B				
0	5	80	15	0
5	5	80	15	0
81	1	32	15	52
85	5	80	15	0

6.5.1.1. Quantification of the tetrapyrroles in sediment extracts

Stock solutions of chlorophyll *a*, and phaeophytin *a* were prepared in acetone and concentrations determined by UV/vis spectroscopy (Hitachi U-3000 dual beam spectrometer; London, UK; scan range 350-800 nm; slit width of 2 nm; scan speed

300 nm min^{-1}; cell path length 1 cm) using the absorbance at λ_{max} of the red band and the molar absorption coefficients of chlorophyll *a*, ε_{662} 81300 M^{-1} cm^{-1} and phaeophytin *a*, ε_{662} 46000 M^{-1} cm^{-1} in acetone (Watanabe et al., 1984). Pigments in the sediment extracts were quantified by reference to calibration curves constructed from dilutions of the stock solution, analysed by HPLC. The chlorophyll *a* calibration curve was used for Mg-containing tetrapyrroles and the phaeophytin *a* calibration curve used for all demetallated tetrapyrroles. See Airs (2001) for the detection limits and reproducibility of the method.

6.5.1.2. Preparative HPLC

Isolation of the C-3[1] methylthioether of pyrophaeophorbide *a* was accomplished using a Jones 5 μ APEX ODS2 semi-preparative column (250 mm x 10 mm i.d) in line with a Phenomenex security guard ODS C_{18} pre-column (4 mm x 3 mm i.d.). Injections of a concentrated sample of the reaction extract were eluted using Method B (Table 6.1) and the fractions from numerous runs manually collected and combined.

6.5.2. Liquid chromatography-multistage tandem mass spectrometry

Liquid chromatography-multistage tandem mass spectrometry ($LC\text{-}MS^n$) was accomplished using a system comprising a Thermo Separations AS3000 autosampler, P4000 gradient pump and UV2000 UV/vis detector coupled to a Finnigan Mat LCQ (San Jose, CA, USA) ion trap mass spectrometer. Instrument control and data processing were performed using Finnigan Navigator software version 1.2. The HPLC conditions were identical to those described in Section 6.5.1. Atmospheric pressure chemical ionisation (APCI) was employed, operated in positive ion mode; vapouriser temperature 450°C, discharge current 5 μA, sheath gas flow 60 (arbitrary units) and capillary temperature of 150°C. Full MS spectra were obtained over the range *m/z* 400-1200. For samples containing chlorins or porphyrins present only as methyl esters, an isolation width of 1.5 *m/z* units was used for precursor ion selection and resonance enhanced collision induced dissociation (CID) performed using a collision energy of 38%. For samples containing chlorins esterified with larger alcohols than methanol, such as the phytol, it was necessary to increase the isolation

width and collision energy to 2 *m/z* units and 60%, respectively. In order to improve the ionisation efficiency of metallated pigments, online demetallation was performed using a flow of formic acid (7 μl min^{-1}), introduced into the HPLC eluant post column (Airs and Keely, 2000). Thus, all metallated pigments were detected in MS as their free base analogues.

6.5.2.1. Calculation of product yields for the simulation reactions

Yields were calculated from the mass chromatographic peak area of a component as a percentage of the total peak areas of its precursor and other compounds derived from that precursor, assuming equal ionisation efficiency.

6.5.3. High resolution MS

Selected reaction extracts were submitted to the departmental mass spectrometry service (Chemistry Department, University of York) for analysis by high resolution mass spectrometry, run on a Bruker MicrOTOF fitted with an APCI ionisation source operated in positive ion mode.

6.5.4. ^{1}H NMR

The C-3[1] methylthioether of pyrophaeophorbide *a*, isolated by preparative HPLC, was submitted to the departmental NMR service (Department of Chemistry, University of York). The ^{1}H NMR data was acquired for 11577 scans in $(CD_3)_2CO$ at a frequency of 500 MHz on a Bruker AV500 instrument running TopSpin software. The spectrum was referenced to the chemical shift of the solvent.

Structure Appendix

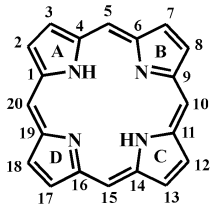

Porphyrin
(**1**)

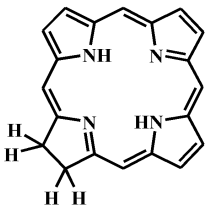

Chlorin
(**2**)

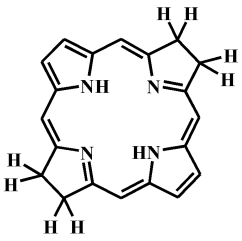

Bacteriochlorin
(**3**)

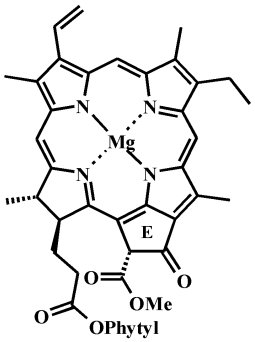

Chlorophyll *a* (**4**)

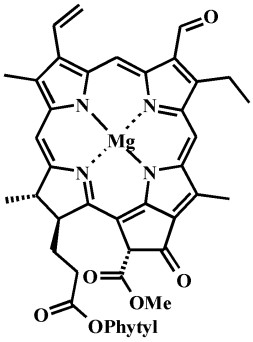

Chlorophyll *b* (**5**)

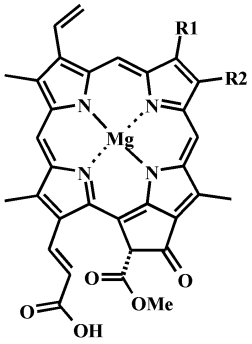

Chlorophyll *c*
(**6**) c_1: R1 = Me, R2 = Et
(**7**) c_2: R1 = Me, R2 = Vinyl
(**8**) c_3: R1 = CO_2Me, R2 = Vinyl

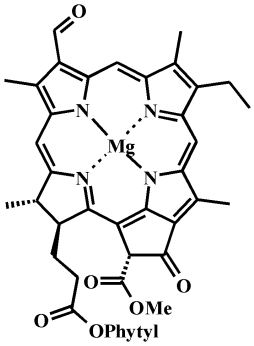

Chlorophyll *d* (**9**)

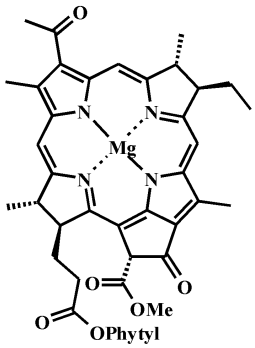

Bacteriochlorophyll *a*
(**10**)

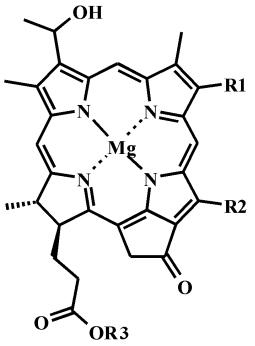

Bacteriochlorophyll *d* (**11**)
R1 = Et, *n*-Pr, *i*-Bu, *neo*-Pent
R2 = Me, Et
R3 = Alkyl (various)

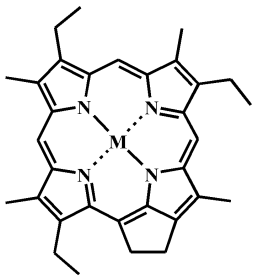

DPEP (**12**)
M = 2H or Metal

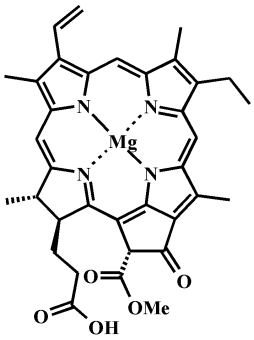

Chlorophyllide *a* (**13**)

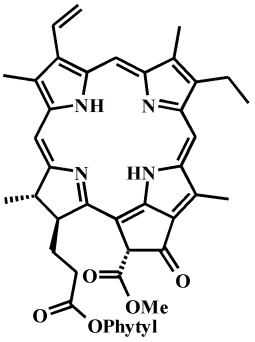

Phaeophytin *a* (**14**)

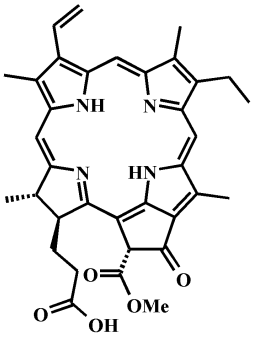

Phaeophorbide *a*
(**15**)

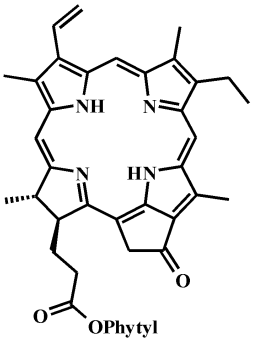

Pyrophaeophytin *a*
(**16**)

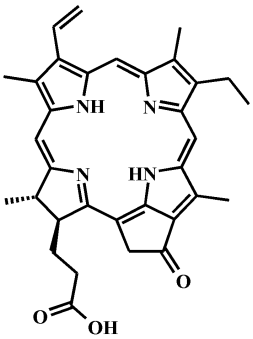

Pyrophaeophorbide *a*
(**17**)

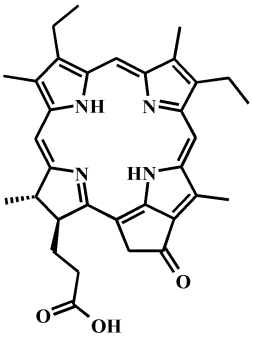

Mesopyrophaeophorbide *a*
(**18**)

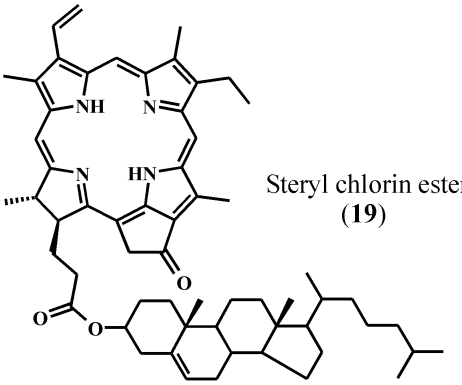

Steryl chlorin ester (**19**)

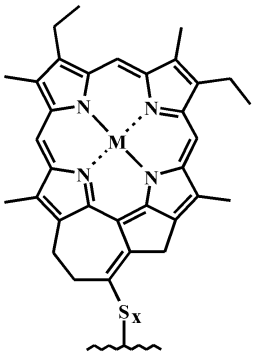

Sulfur-bound porphyrin (**20**)
M = 2H or Metal

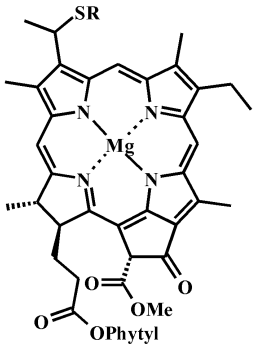

AlkylS-chlorophyll *a* (**21**)
R = Me (**a**), Et (**b**), *n*-Pr (**c**), *n*-Bu (**d**), *n*-Pent (**e**)

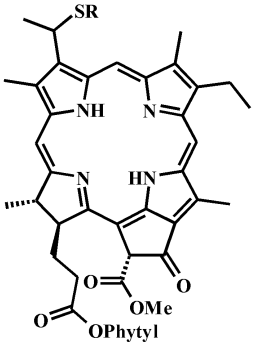

AlkylS-phaeophytin *a* (**22**)
R = Me (**a**), Et (**b**), *n*-Pr (**c**), *n*-Bu (**d**), *n*-Pent (**e**)

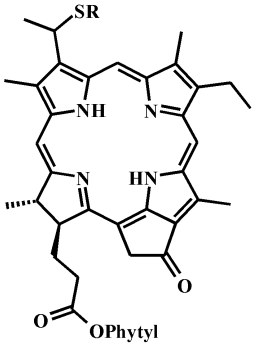

AlkylS-pyrophaeophytin *a* (**23**)
R = Me (**a**), Et (**b**), *n*-Pr (**c**), *n*-Bu (**d**), *n*-Pent (**e**)

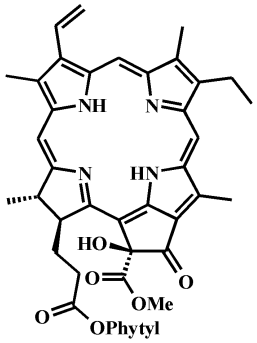

C-13^2 HO-phaeophytin *a* (**26**)

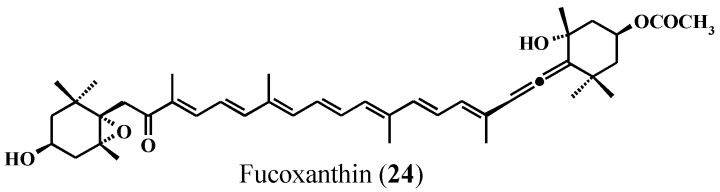

Fucoxanthin (**24**)

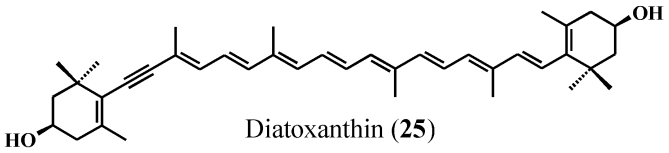

Diatoxanthin (**25**)

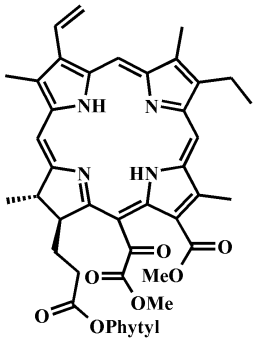

Purpurin-7 dimethyl phytyl ester (**27**)

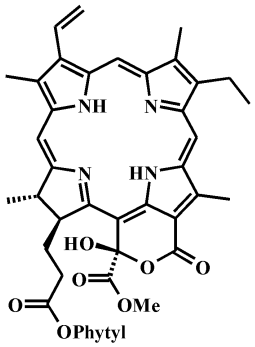

C-15^1 HO-lact-phaeophytin *a* (**28**)

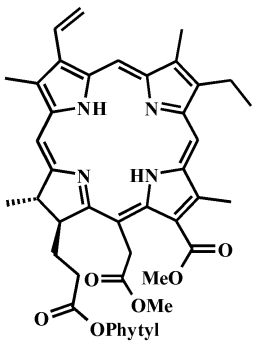

Chlorin e$_6$ dimethyl phytyl ester (**29**)

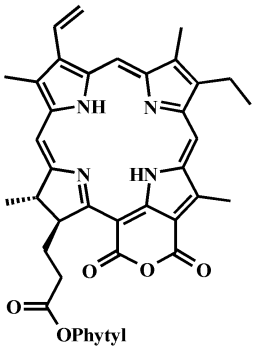

Purpurin-18 phytyl ester (**30**)

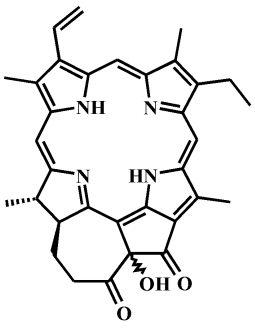

Chlorophyllone (**31**)

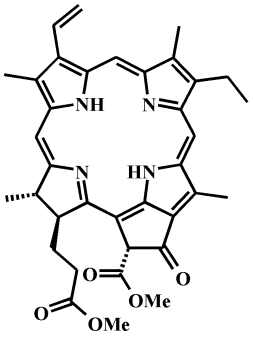

Phaeophorbide *a* methyl ester (**32**)

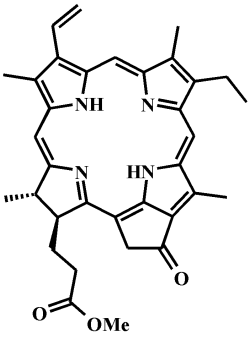

Pyrophaeophorbide *a* methyl ester (**33**)

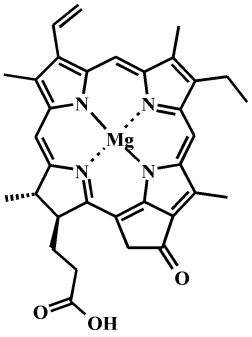

Pyrochlorophyllide *a* (**34**)

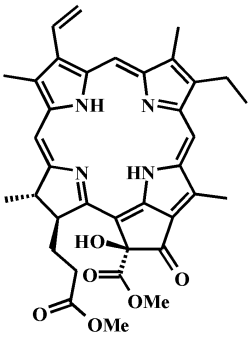

C-13^2 HO-phaeophorbide *a* (**35**)

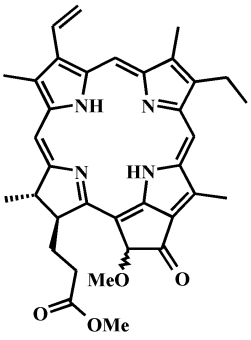

C-13^2 MeO-pyrophaeophorbide *a* (**36**)

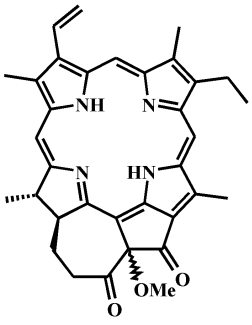

C-15^1 MeO-chlorophyllone (**37**)

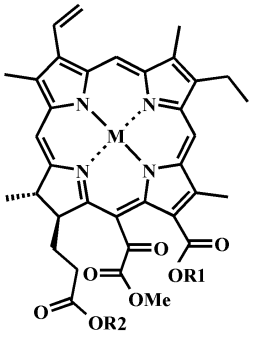

Purpurin-7 (various)
(**38**) M = 2H, R1 = Me, R2 = Me
(**39**) M = 2H, R1 = H, R2 = Phytyl
(**40**) M = 2H, R1 = H, R2 = H
(**41**) M = Mg, R1 = H, R2 = Phytyl
(**42**) M = Mg, R1 = H, R2 = H

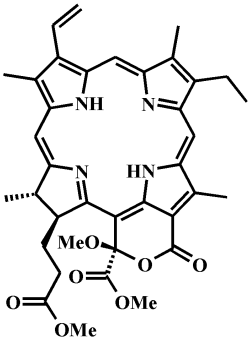

C-15^1 MeO-lact-phaeophorbide *a* (**43**)

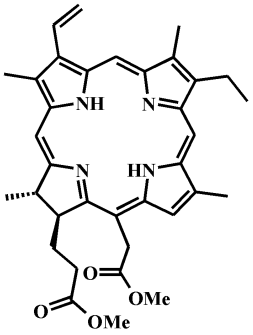

(**44**)

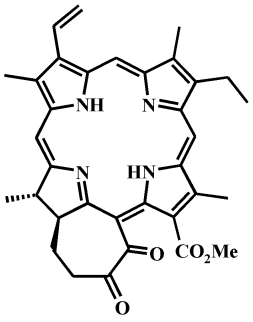

Chlorophyllonic acid (**45**)

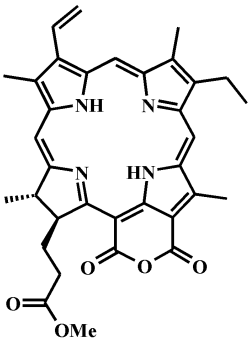

Purpurin-18 methyl ester (**46**)

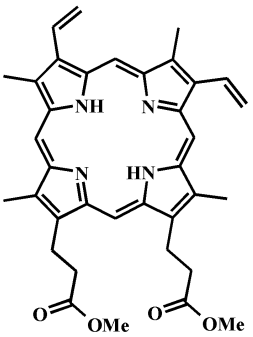

Protoporphyrin-IX dimethyl ester (**47**)

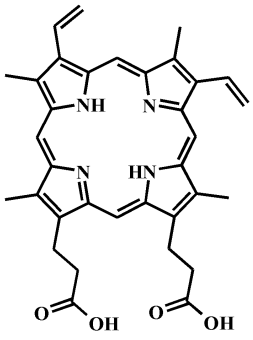

Protoporphyrin-IX (**48**)

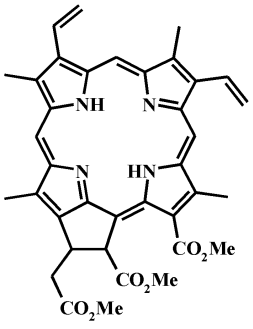

Rearranged phaeoporphyrin c_2 (**49**)

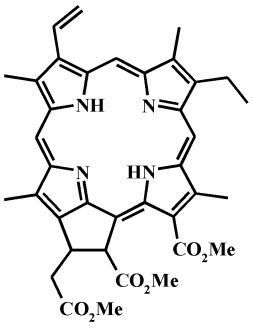

Rearranged phaeoporphyrin c_1 (**50**)

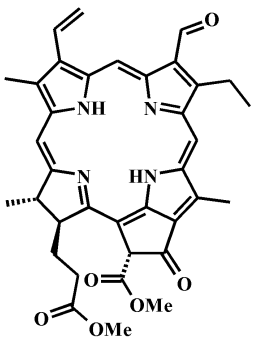

Phaeophorbide *b* methyl ester (**51**)

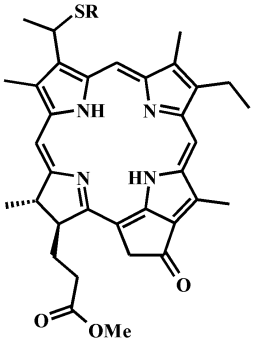

AlkylS-pyrophaeophorbide *a* (**52**) R = Me (**a**), Et (**b**), *n*-Pr (**c**), *n*-Bu (**d**), *n*-Pent (**e**)

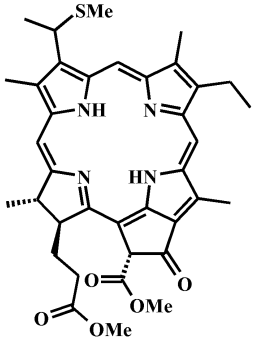

MeS-phaeophorbide *a* (**53**)

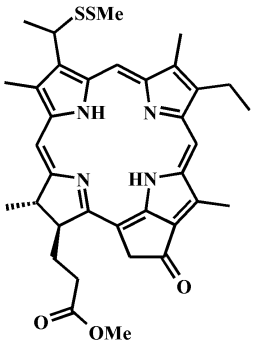

MeSS-pyrophaeophorbide *a* (**54**)

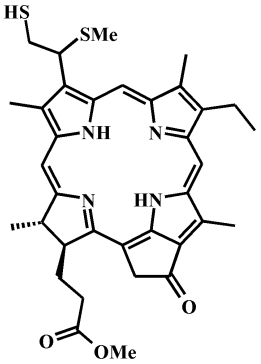

HS, MeS-pyrophaeophorbide *a* (**55**)

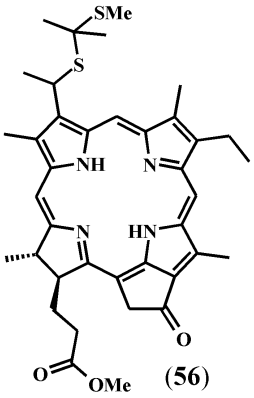

(**56**)

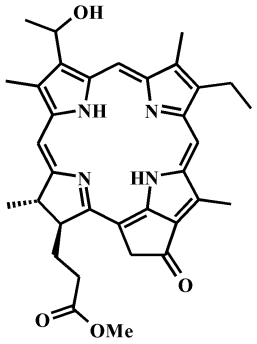

C-3 (1-hydroxyethyl) pyrophaeophorbide *a* (**57**)

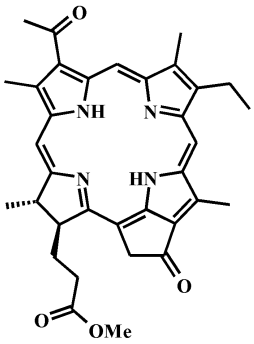

C-3 acetyl pyro-phaeophorbide *a* (**58**)

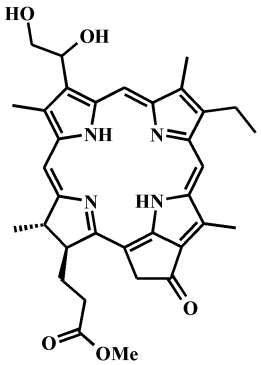

C-3[1], 3[2] diol pyrophaeophorbide *a* (**59**)

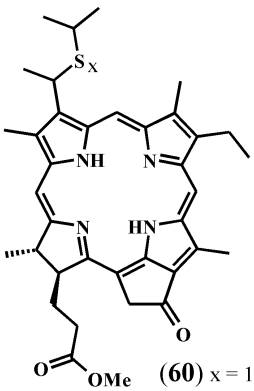

(**60**) x = 1
(**61**) x = 2

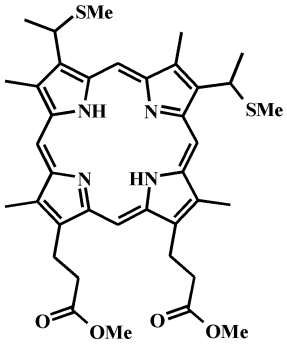

(**62**)

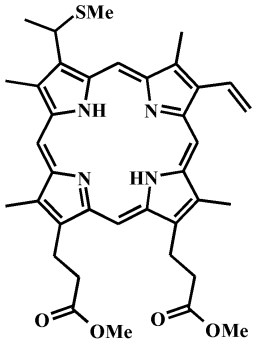

(**63**)

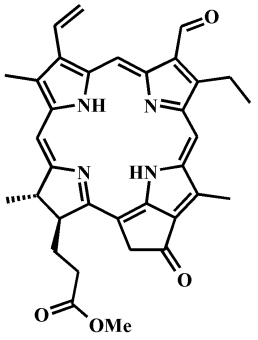

Pyrophaeophorbide *b* methyl ester (**64**)

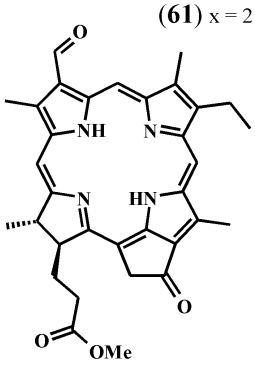

Pyrophaeophorbide *d* methyl ester (**65**)

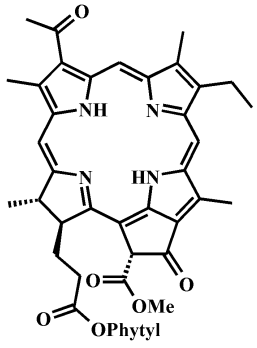

Bacterioviridin (**66**)

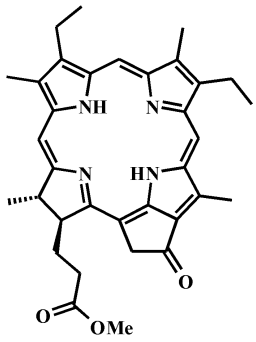

Mesopyrophaeophorbide *a* methyl ester (**67**)

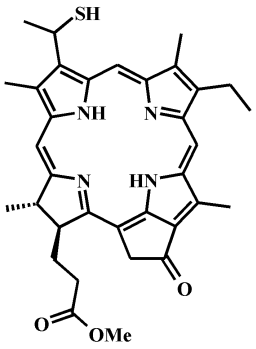

HS-pyrophaeophorbide *a*
(**68**)

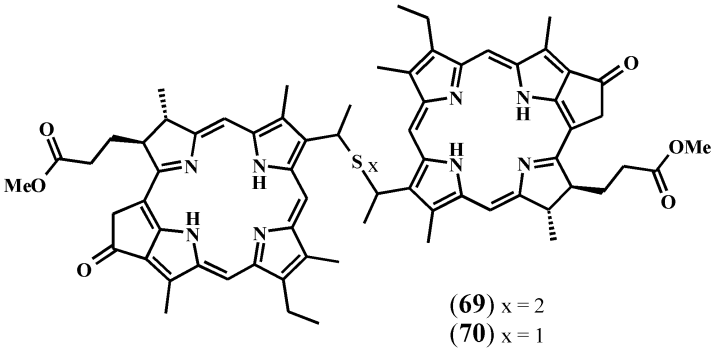

(**69**) x = 2
(**70**) x = 1

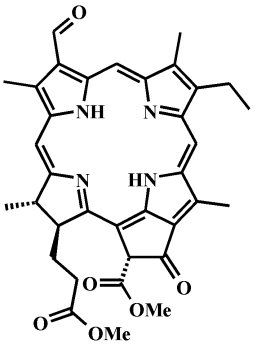

Phaeophorbide *d*
methyl ester (**71**)

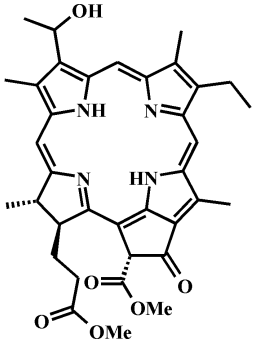

C-3 (1-hydroxyethyl)
phaeophorbide *a* (**72**)

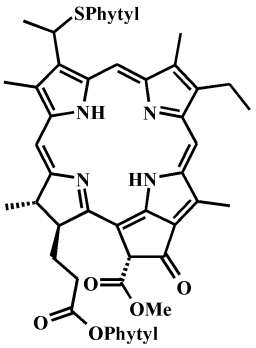

PhytylS-phaeophytin *a*
(**73**)

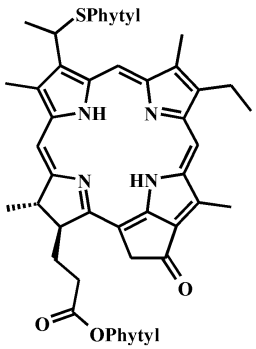

PhytylS-pyro-
phaeophytin *a* (**74**)

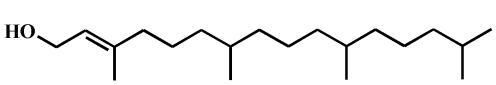

Phytol (**75**)

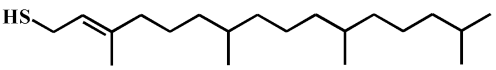

Phytenethiol (**76**)

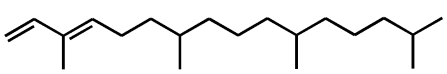

Phytadiene (**77**)

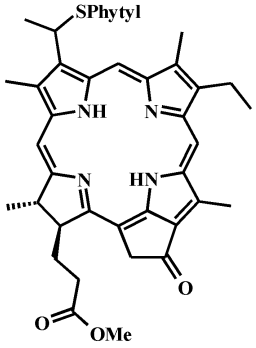

PhytylS-pyro-
phaeophorbide *a* (**78**)

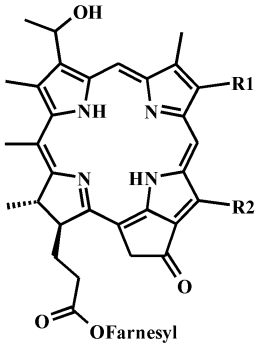

Bacteriophaeophytin c_2 (**79**)
R1/R2 = *n*-Pr/Me or Et/Et

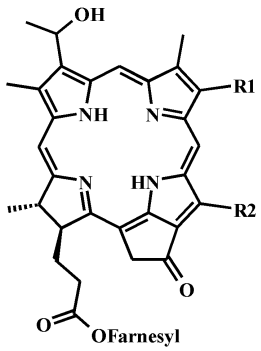

Bacteriophaeophytin d_2 (**80**)
R1/R2 = *n*-Pr/Me or Et/Et

References

Adam, P., Philippe, E., Albrecht, P., 1998. Photochemical sulfurization of sedimentary organic matter: A widespread process occurring at early diagenesis in natural environments? Geochimica et Cosmochimica Acta 62, 265-271.

Adam, P., Schneckenburger, P., Schaeffer, P., Albrecht, P., 2000. Clues to early diagenetic sulfurization processes from mild chemical cleavage of labile sulfur-rich geomacromolecules. Geochimica et Cosmochimica Acta 64, 3485-3503.

Airs, R.L., Jie, C., Keely, B.J., 2000. A novel sedimentary chlorin: structural evidence for a chlorophyll origin for aetioporphyrins. Organic Geochemistry 31, 1253-1256.

Airs, R.L., Keely, B.J., 2000. A novel approach for sensitivity enhancement in atmospheric pressure chemical ionisation liquid chromatography/mass spectrometry of chlorophylls. Rapid Communications in Mass Spectrometry 14, 125-128.

Airs, R.L., Atkinson, J.E., Keely, B.J., 2001. Development and application of a high resolution liquid chromatographic method for the analysis of complex pigment distributions. Journal of Chromatography A 917, 167-177.

Airs, R.L., 2001. Chlorophylls of phototrophic prokaryotes: analytical developments and significance of natural distributions, Ph.D. Thesis. University of York.

Airs, R.L., Keely, B.J., 2003. A high resolution study of the chlorophyll and bacteriochlorophyll pigment distributions in a calcite/gypsum microbial mat. Organic Geochemistry 34, 539-551.

Aizenshtat, Z., Krein, E.B., Vairavamurthy, M.A., Goldstein, T.P., 1995. Role of sulfur in the transformations of sedimentary organic matter: A mechanistic overview. Geochemical Transformations of Sedimentary Sulfur 612, 16-37.

Allen, C.S., Hey, A., Petrie, E., Phipps, R., 2006. British Antarctic Survey R.R.S. James Clark Ross cruise report, J149, 26th February – 17th April 2006. Unpublished data.

Amrani, A., Aizenshtat, Z., 2004a. Reaction of polysulfide anions with α, β unsaturated isoprenoid aldehydes in aquatic media: simulation of oceanic conditions. Organic Geochemistry 35, 909-921.

Amrani, A., Aizenshtat, Z., 2004b. Photosensitized oxidation of naturally occurring isoprenoid allyl alcohols as a possible pathway for their transformation to thiophenes in sulfur rich depositional environments. Organic Geochemistry 35, 693-712.

Amrani, A., Turner, J.W., Qisheng, M., Yongchun, T., Hatcher, P.G., 2007. Formation of sulfur and nitrogen cross-linked macromolecules under aqueous conditions. Geochimica et Cosmochimica Acta 71, 4141-4160.

Aplin, A.C., Macquaker, J.H.S., 1993. C-S-Fe Geochemistry of some modern and ancient anoxic marine muds and mudstones. Philosophical Transactions: Physical Sciences and Engineering 344, 89-100.

Baker, E.W., Palmer, S.E., 1978. Geochemistry of porphyrins. In: Dolphin, D. (Ed.) The Porphyrins. Vol 1. Academic Press, London, UK. pp. 486-552.

Baucherel, X., Uziel, J., Jugé, S., 2001. Unexpected catalyzed C=C bond cleavage by molecular oxygen promoted by a thiyl radical. Journal of Organic Chemistry 66, 4504-4510.

Bentley, R., Chasteen, T.G., 2004. Environmental VOSCs - formation and degradation of dimethyl sulfide, methanethiol and related materials. Chemosphere 55, 291-317.

Bidigare, R.R., Kennicutt, M.C., Ondrusek, M.E., Keller, M.D., Guillard, R.R.L., 1990. Novel chlorophyll-related compounds in marine-phytoplankton: distributions and geochemical implications. Energy & Fuels 4, 653-657.

Bidigare, R.R., Ondrusek, M.E., 1996. Spatial and temporal variability of phytoplankton pigment distributions in the central equatorial Pacific Ocean. Deep-Sea Research II 43, 809-833.

Bonnett, R., Campion-Smith, I.H., Page, A.J., 1977. Protiodevinylation: the Schumm reaction of vinylporphyrins. Journal of the Chemical Society, Perkin Transactions 1, 68-71.

Brown, S.B., Houghton, J.D., Hendry, G.A.F., 1991. Chlorophyll breakdown. In: Sheer, H. (Ed.) Chlorophylls. CRC Press, Boca Raton, Florida. pp. 465-489.

Budzikiewicz, H., 1978. Mass spectra of porphyrins and related compounds. In: Dolphin, D. (Ed.) The Porphyrins Volume 3. Physical Chemistry Part A. Academic Press, London, UK. pp. 395-461.

Callot, H.J., 1991. Geochemistry of chlorophylls. In: Sheer, H. (Ed.) Chlorophylls. CRC Press, Boca Raton, Florida. pp. 339-363.

Callot, H.J., Ocampo, R., 2000. Geochemistry of Porphyrins. In: Kadish, K.M., Smith, K.M., Guilard, R. (Eds.) The Porphyrin Handbook Volume 1. Academic Press, London, UK. pp. 349-398.

Calzavara-Pinton, P.G., Venturini, M., Sala, R., 2007. Photodynamic therapy: update 2006. Part 1: Photochemistry and photobiology. Journal of the European Academy of Dermatology and Venereology 21, 293-302.

Cantoni, G.L., Anderson, D.G., 1956. Enzymatic cleavage of dimethylpropiothetin by *Polysiphonia lanosa*. Journal of Biological Chemistry 222, 171-177.

Capozzi, G., Modena, G., 1974. Oxidation of Thiols. In: Patai, S. (Ed.) The Chemistry of the Thiol Group. Wiley & Sons, London, UK. pp. 827-832.

Carpenter, L.J., 2003. Iodine in the marine boundary layer. Chemical Reviews 103, 4953-4962.

Carroll, J.J., Mather, A.E., 1989. The solubility of hydrogen sulfide in water from 0 to 90ºC and pressures to 1 MPa. Geochimica et Cosmochimica Acta 53, 1163-1170.

Charlson, R.J., Lovelock, J.E., Andreae, M.O., Warren, S.G., 1987. Oceanic phytoplankton, atmospheric sulphur, cloud albedo and climate. Nature 326, 655-661.

Cheng, C., Stock, L.M., 1991. Photochemical anion-promoted carbon-sulfur cleavage reactions of diaryl sulfides, alkyl aryl sulfides, and related sulfoxides and sulfones. Journal of Organic Chemistry 56, 2436-2443.

Chicarelli, M.I., Maxwell, J.R., 1984. A naturally occurring, chlorophyll *b* related porphyrin. Tetrahedron Letters 25, 4701-4704.

Crampton, M.R., 1974. Acidity and hydrogen-bonding. In: Patai, S. (Ed.) The Chemistry of the Thiol Group. Wiley & Sons, London, UK. pp. 379-415.

Currie, R.I., 1962. Pigments in Zooplankton Faeces. Nature 193, 956-957.

D'Souza, V.T., Nanjundiah, R., Baeza, J., Szmant, H.H., 1987. Thiol-olefin cooxidation (TOCO) reaction. 9. A self-consistent mechanism under nonradical-inducing conditions. Journal of Organic Chemistry 52, 1729-1740.

de Graaf, W., Sinninghe Damsté, J.S., de Leeuw, J.W., 1992. Laboratory simulation of natural sulphurization: I. Formation of monomeric and oligomeric isoprenoid polysulphides by low-temperature reactions of inorganic polysulphides with phytol and phytadienes. Geochimica et Cosmochimica Acta 56, 4321-4328.

de Graaf, W., Sinninghe Damsté, J.S., de Leeuw, J.W., 1995. Low-temperature addition of hydrogen polysulfides to olefins: formation of 2,2'-dialkyl polysulfides from alk-1-enes and cyclic (poly)sulfides and polymeric organic sulfur compounds from α,ω-dienes. Journal of the Chemical Society-Perkin Transactions 1, 635-640.

de Hoffmann, E., Stroobant, V., 2002. Mass Spectrometry: Principles and Applications, 2nd edition. Wiley, Chichester.

de Souza, M.P., Yoch, D.C., 1995. Purification and characterization of dimethylsulfoniopropionate lyase from an *Alcaligenes*-like dimethyl sulfide-producing marine isolate. Applied and Environmental Microbiology 61, 21-26.

DiNello, R.K., Dolphin, D.H., 1981. Evidence for a fast (major) and slow (minor) pathway in the Schumm devinylation reaction of vinyl porphyrins. Journal of Organic Chemistry 46, 3498-3502.

Dougherty, R., Strain, H.H., Svec, W.A., Uphaus, R.A., Katz, J.J., 1970. Structure, properties and distribution of chlorophyll *c*. Journal of the American Chemical Society 92, 2826-&.

Falkowski, P.G., Raven, J.A., 1997. Aquatic Photosynthesis. Blackwell Science.

Faure, P., Landais, P., 2000. Evidence for clay minerals catalytic effects during low-temperature air oxidation of *n*-alkanes. Fuel 79, 1751-1756.

Faure, P., Schlepp, L., Burkle-Vitzthum, V., Elie, M., 2003. Low temperature air oxidation of *n*-alkanes in the presence of Na-smectite. Fuel 82, 1751-1762.

Fukushima, K., Yasukawa, M., Muto, N., Uemura, H., Ishiwatari, R., 1992. Formation of C_{20} isoprenoid thiophenes in modern sediments. Organic Geochemistry 18, 83-91.

Fukuyo, S., Ohashi, S., Iwamoto, K., Shiraiwa, Y., Kobayashi, M., 2007. Conversion of chl *a* into chl *d* by heat-treated papain. Photosynthesis Research 91, 270-270.

Gibb, S.W., Cummings, D.G., Irigoien, X., Barlow, R.G., Fauzi, R., Mantoura, C., 2001. Phytoplankton pigment chemotaxonomy of the northeastern Atlantic. Deep-Sea Research II 48, 795-823.

Gribble, G.W., 2003. The diversity of naturally produced organohalogens. Chemosphere 52, 289-297.

Groene, T., 1995. Biogenic production and consumption of dimethylsulfide (DMS) and dimethylsulfoniopropionate (DMSP) in the marine epipelagic zone: a review. Journal of Marine Systems 6, 191-209.

Grossi, V., Rontani, J.F., 1995. Photosensitized oxygenation of phytadienes. Tetrahedron Letters 36, 3141-3144.

Häder, D.P., Kumar, H.D., Smith, R.C., Worrest, R.C., 2003. Aquatic ecosystems: effects of solar ultraviolet radiation and changes and interaction with other climatic change factors. Photochemical & Photobiological Sciences 2, 39-50.

Hall, D.O., Rao, K.K., 1999. Photosynthesis, 6th edition. Cambridge University Press, Cambridge.

Harradine, P.J., Harris, P.G., Head, R.N., Harris, R.P., Maxwell, J.R., 1996. Steryl chlorin esters are formed by zooplankton herbivory. Geochimica et Cosmochimica Acta 60, 2265-2270.

Harris, P.G., Pearce, G.E.S., Peakman, T.M., Maxwell, J.R., 1995. A widespread and abundant chlorophyll transformation product in aquatic environments. Organic Geochemistry 23, 183-187.

Harris, P.G., Zhao, M., Rosell-Melé, A., Tiedemann, R., Sarnthein, M., Maxwell, J.R., 1996. Chlorin accumulation rate as a proxy for Quaternary marine primary productivity. Nature 383, 63-65.

Hartgers, W.A., Lòpez, J.F., de las Heras, F.X.C., Grimalt, J.O., 1996. Sulphur-binding in recent environments. I. Lipid by-products from Ni_2B desulphurization. Organic Geochemistry 25, 353-365.

Hartgers, W.A., Lòpez, J.F., Damsté, J.S.S., Reiss, C., Maxwell, J.R., Grimalt, J.O., 1997. Sulfur-binding in recent environments: II. Speciation of sulfur and iron and implications for the occurrence of organo-sulfur compounds. Geochimica et Cosmochimica Acta 61, 4769-4788.

Hayes, J.M., Takigiku, R., Ocampo, R., Callot, H.J., Albrecht, P., 1987. Isotopic compositions and probable origins of organic molecules in the Eocene Messel shale. Nature 329, 48-51.

Head, E.J.H., Harris, L.R., 1992. Chlorophyll and carotenoid transformation and destruction by *Calanus* spp. grazing on diatoms. Marine Ecology-Progress Series 86, 229-238.

Hebting, Y., Adam, P., Albrecht, P., 2003. Reductive desulfurization of allylic thiols by HS^-/H_2S in water gives clue to chemical reactions widespread in natural environments. Organic Letters 5, 1571-1574.

Hebting, Y., Schaeffer, P., Behrens, A., Adam, P., Schmitt, G., Schneckenburger, P., Bernasconi, S.M., Albrecht, P., 2006. Biomarker evidence for a major preservation pathway of sedimentary organic carbon. Science 312, 1627-1631.

Hedges, J.I., Keil, R.G., 1995. Sedimentary organic matter preservation: an assessment and speculative synthesis. Marine Chemistry 49, 81-115.

Hendry, G.A.F., Houghton, J.D., Brown, S.B., 1987. The degradation of chlorophyll *a* biological enigma (Tansley Review No.11). New Phytologist 107, 255-302.

Hughes, C., Malin, G., Turley, C.M., Keely, B.J., Nightingale, P.D., 2008. The production of volatile iodocarbons by biogenic marine aggregates. Limnology and Oceanography 53, -.

Hurley, J.P., Armstrong, D.E., 1990. Fluxes and transformations of aquatic pigments in Lake Mendota, Wisconsin. Limnology and Oceanography 35, 384-398.

Huseby, B., Ocampo, R., Bauder, C., Callot, H.J., Rist, K., Barth, T., 1996. Study of the porphyrins released from the Messel oil shale kerogen by hydrous pyrolysis experiments. Organic Geochemistry 24, 691-703.

Huseby, B., Ocampo, R., 1997. Evidence for porphyrins bound, via ester bonds, to the Messel oil shale kerogen by selective chemical degradation experiments. Geochimica et Cosmochimica Acta 61, 3951-3955.

Hynninen, P.H., 1991. Chemistry of chlorophylls: Modifications. In: Sheer, H. (Ed.) Chlorophylls. CRC Press, Boca Raton, Florida. pp. 145-209.

Iriuchijima, S., Maniwa, K., Sakakiba.T, Tsuchiha.Gi, 1974. Cooxidation of α olefins and arenethiols with oxygen. Synthesis of β-hydroxy sulfoxides. Journal of Organic Chemistry 39, 1170-1171.

Itoh, N., Tsujita, M., Ando, T., Hisatomi, G., Higashi, T., 1997. Formation and emission of monohalomethanes from marine algae. Phytochemistry 45, 67-73.

Jeffrey, S.W., Hallegraeff, G.M., 1987. Chlorophyllase distribution in 10 classes of phytoplankton: a problem for chlorophyll analysis. Marine Ecology-Progress Series 35, 293-304.

Jialal, I., Norkus, E.P., Cristol, L., Grundy, S.M., 1991. β-carotene inhibits the oxidative modification of low density lipoprotein. Biochimica et Biophysica Acta 1086, 134-138.

Jie, C., Walker, J.S., Keely, B.J., 2002. Atmospheric pressure chemical ionisation normal phase liquid chromatography mass spectrometry and tandem mass spectrometry of chlorophyll *a* allomers. Rapid Communications in Mass Spectrometry 16, 473-479.

Karsten, U., Wiencke, C., Kirst, G.O., 1992. Dimethylsulphoniopropionate (DMSP) accumulation in green macroalgae from polar to temperate regions: interactive effects of light versus salinity and light versus temperature. Polar Biology 12, 603-607.

Keely, B.J., Prowse, W.G., Maxwell, J.R., 1990. The Treibs Hypothesis: an Evaluation Based on Structural Studies. Energy & Fuels 4, 628-634.

Keely, B.J., 2006. Geochemistry of chlorophylls. In: Grimm, B., Porra, R.J., Rüdiger, W., Scheer, H. (Eds.) Advances in Photosynthesis and Respiration, Volume 25. Chlorophylls and Bacteriochlorophylls: Biochemistry, Biophysics, Functions and Applications, Advances in Photosynthesis and Respiration. Springer, Dordrecht, The Netherlands. pp. 535-561.

Keil, R.G., Montluçon, D.B., Prahl, F.G., Hedges, J.I., 1994. Sorptive Preservation of Labile Organic-Matter in Marine-Sediments. Nature 370, 549-552.

Kenner, G.W., Quirke, J.M.E., Smith, K.M., 1976. Pyrroles and related compounds-XXXVI. Transformations of protoporphyrin-IX into harderoporphyrin, pemptoporphyrin, chlorocruoroporphyrin and their isomers. Tetrahedron 32, 2753-2756.

Kharasch, M.S., Nudenberg, W., Mantell, G.J., 1951. Reactions of atoms and free radicals in solution. XXV. The reactions of olefins with mercaptans in the presence of oxygen. Journal of Organic Chemistry 16, 524-532.

Kiene, R.P., 1996. Production of methanethiol from dimethylsulfoniopropionate in marine surface waters. Marine Chemistry 54, 69-83.

Killops, S., Killops, V., 2004. Introduction to organic geochemistry 2nd edition. Blackwell, Oxford.

King, L.L., Repeta, D.J., 1991. Novel pyropheophorbide steryl esters in Black Sea sediments. Geochimica et Cosmochimica Acta 55, 2067-2074.

King, L.L., Repeta, D.J., 1994. High molecular weight and acid extractable chlorophyll degradation products in the Black-Sea: new sinks for chlorophyll. Organic Geochemistry 21, 1243-1255.

Kirst, G.O., Thiel, C., Wolff, H., Nothnagel, J., Wanzek, M., Ulmke, R., 1991. Dimethylsulfoniopropionate (DMSP) in ice-algae and its possible biological role. Marine Chemistry 35, 381-388.

Kohnen, M.E.L., Sinninghe Damsté, J.S., ten Haven, H.L., de Leeuw, J.W., 1989. Early incorporation of polysulfides in sedimentary organic matter. Nature 341, 640-641.

Kohnen, M.E.L., Sinninghe Damsté, J.S., Kock-van Dalen, A.C., ten Haven, H.L., Rullkötter, J., de Leeuw, J.W., 1990. Origin and diagenetic transformations of C_{25} and C_{30} highly branched isoprenoid sulfur-compounds: Further evidence for the formation of organically bound sulfur during early diagenesis. Geochimica et Cosmochimica Acta 54, 3053-3063.

Kohnen, M.E.L., Sinninghe Damsté, J.S., de Leeuw, J.W., 1991a. Biases from natural sulfurization in paleoenvironmental reconstruction based on hydrocarbon biomarker distributions. Nature 349, 775-778.

Kohnen, M.E.L., Sinninghe Damsté, J.S., Kock-van Dalen, A.C., de Leeuw, J.W., 1991b. Di- or polysulfide-bound biomarkers in sulfur-rich geomacromolecules as revealed by selective chemolysis. Geochimica et Cosmochimica Acta 55, 1375-1394.

Koizumi, H., Itoh, Y., Hosoda, S., Akiyama, M., Hoshino, T., Shiraiwa, Y., Kobayashi, M., 2005. Serendipitous discovery of chl *d* formation from chl *a* with papain. Science and Technology of Advanced Materials 6, 551-557.

Kok, M.D., Rijpstra, W.I.C., Robertson, L., Volkman, J.K., Sinninghe Damsté, J.S., 2000. Early steroid sulfurisation in surface sediments of a permanently stratified lake (Ace Lake, Antarctica). Geochimica et Cosmochimica Acta 64, 1425-1436.

Kornblum, N., Carlson, S.C., Smith, R.G., 1978. Substitution-reactions which proceed via radical-anion intermediates.18. Replacement of nitro-group by hydrogen. Journal of the American Chemical Society 100, 289-290.

Kornblum, N., Carlson, S.C., Smith, R.G., 1979. Substitution-reactions which proceed via radical-anion intermediates. 20. Replacement of the nitro-group by hydrogen. Journal of the American Chemical Society 101, 647-657.

Krein, E.B., Aizenshtat, Z., 1994. The formation of isoprenoid sulfur compounds during diagenesis: simulated sulfur incorporation and thermal transformation. Organic Geochemistry 21, 1015-1025.

Laturnus, F., 2001. Marine macroalgae in Polar regions as natural sources for volatile organohalogens. Environmental Science and Pollution Research 8, 103-108.

Lawlor, D.W., 1987. Photosynthesis: Metabolism, control and physiology. Longman Scientific and Technical.

Leeper, F.J., 1985. The Biosynthesis of porphyrins, chlorophylls, and vitamin-B12. Natural Product Reports 2, 19-47.

Lewan, M.D., 1984. Factors controlling the proportionality of vanadium to nickel in crude oils. Geochimica et Cosmochimica Acta 48, 2231-2238.

Lindsay-Smith, J.R., Calvin, M., 1966. Studies on the chemical and photochemical oxidation of bacteriochlorophyll. Journal of the American Chemical Society 88, 4500-4506.

Lomans, B.P., van der Drift, C., Pol, A., Op den Camp, H.J.M., 2002. Microbial cycling of volatile organic sulfur compounds. Cellular and Molecular Life Sciences 59, 575-588.

Louda, J.W., Li, J., Liu, L., Winfree, M.N., Baker, E.W., 1998. Chlorophyll-*a* degradation during cellular senescence and death. Organic Geochemistry 29, 1233-1251.

Louda, J.W., Loitz, J.W., Rudnick, D.T., Baker, E.W., 2000. Early diagenetic alteration of chlorophyll-*a* and bacteriochlorophyll-*a* in a contemporaneous marl ecosystem; Florida Bay. Organic Geochemistry 31, 1561-1580.

Louda, J.W., Liu, L., Baker, E.W., 2002. Senescence- and death-related alteration of chlorophylls and carotenoids in marine phytoplankton. Organic Geochemistry 33, 1635-1653.

Ma, L.F., Dolphin, D., 1996. Stereoselective synthesis of new chlorophyll *a* related antioxidants isolated from marine organisms. Journal of Organic Chemistry 61, 2501-2510.

Manley, S.L., de la Cuesta, J.L., 1997. Methyl iodide production from marine phytoplankton cultures. Limnology and Oceanography 42, 142-147.

March, J., 1992. Advanced Organic Chemistry 4th edition, Wiley, Chichester.

March, R.E., 1998. Quadrupole Ion Trap Mass Spectrometer. In: Meyers, R.E. (Ed.) Encyclopedia of Analytical Chemistry. Wiley, Chichester. pp. 1-25.

March, R.E., 2000. Quadrupole ion trap mass spectrometry: a view at the turn of the century. International Journal of Mass Spectrometry 200, 285-312.

Matile, P., Hörtensteiner, S., Thomas, H., Kräutler, B., 1996. Chlorophyll breakdown in senescent leaves. Plant Physiology 112, 1403-1409.

Mawson, D.H., Keely, B.J., 2008. Novel functionalised chlorins in sediments of the Messinian Vena del Gesso evaporitic sequence: Evidence for a facile route to reduction for biomarkers. Organic Geochemistry 39, 203-209.

McLuckey, S.A., Van Berkel, G.J., Goeringer, D.E., Glish, G.L., 1994. Ion trap mass spectrometry of externally generated ions. Analytical Chemistry 66, A689-696.

Miyashita, H., Ikemoto, H., Kurano, N., Adachi, K., Chihara, M., Miyachi, S., 1996. Chlorophyll *d* as a major pigment. Nature 383, 402-402.

Morell, D.B., Barrett, J., Clezy, P.S., 1961. Prosthetic group of cytochrome oxidase.1. Purification as porphyrin *a* and conversion into haemin *a*. Biochemical Journal 78, 793-796.

Morishita, H., Tamiaki, H., 2005. Synthesis of regioselectively ^{18}O-labelled chlorophyll derivatives at the 3^1- and/or 13^1- positions through one-pot exchange of carbonyl oxygen atoms. Tetrahedron 61, 6097-6107.

Moser, S., Müller, T., Oberhuber, M., Kräutler, B., 2009. Chlorophyll catabolites - chemical and structural footprints of a fascinating biological phenomenom. European Journal of Organic Chemistry, 21-31.

Mühlecker, W., Kräutler, B., Ginsburg, S., Matile, P., 1993. Breakdown of chlorophyll: a terapyrrolic chlorophyll catabolite from senescent rape leaves. Helvetica Chimica Acta 76, 2976-2980.

Naylor, C.C., Keely, B.J., 1998. Sedimentary purpurins: oxidative transformation products of chlorophylls. Organic Geochemistry 28, 417-422.

Naylor, C.C., Keely, B.J., 1999. Sedimentary purpurins: oxidative transformation products of chlorophylls. Organic Geochemistry 30, 471-472.

Nikitas, P., Pappa-Louisi, A., Agrafiotou, P., 2004. New insights on the retention mechanism of non-polar solutes in reversed-phase liquid chromatographic columns. Journal of Chromatography A 1034, 41-54.

Nikitas, P., Pappa-Louisi, A., 2009. Retention models for isocratic and gradient elution in reversed-phase liquid chromatography. Journal of Chromatography A 1216, 1737-1755.

Nyman, E.S., Hynninen, P.H., 2004. Research advances in the use of tetrapyrrolic photosensitizers for photodynamic therapy. Journal of Photochemistry and Photobiology B-Biology 73, 1-28.

Owens, T.G., Falkowski, P.G., 1982. Enzymatic degradation of chlorophyll-*a* by marine phytoplankton in vitro. Phytochemistry 21, 979-984.

Parkin, T.B., Brock, T.D., 1980. Photosynthetic Bacterial production in lakes: The effects of light intensity. Limnology and Oceanography 25, 711-718.

Paul, W., Steinwedel, P., 1960. Apparatus for separating charged particles of different specific charges, German patent 944,900, 1956; US patent 2,939,952, 1960.

Pearce, G.E.S., Harradine, P.J., Talbot, H.M., Maxwell, J.R., 1998. Sedimentary sterols and steryl chlorin esters: distribution differences and significance. Organic Geochemistry 28, 3-10.

Pickering, M.D., 2005. An investigation into the origins of novel sulfur-bound chlorins recently discovered in Antarctic sediments. MChem project. University of York.

Porra, R.J., Scheer, H., 2000. ^{18}O and mass spectrometry in chlorophyll research: Derivation and loss of oxygen atoms at the periphery of the chlorophyll macrocycle during biosynthesis, degradation and adaptation. Photosynthesis Research 66, 159-175.

Prowse, W.G., Keely, B.J., Maxwell, J.R., 1990. A novel sedimentary metallochlorin. Organic Geochemistry 16, 1059-1065.

Prowse, W.G., Maxwell, J.R., 1991. High molecular weight chlorins in a lacustrine shale. Organic Geochemistry 17, 877-886.

Quirke, J.M.E., 2000. Mass spectrometry of porphyrins and metalloporphyrins. In: Kadish, K.M., Smith, K.M., Guilard, R. (Eds.) The Porphyrin Handbook Volume 7: Theoretical and physical characterisation. Academic Press, London, UK. pp. 371-422.

Reuss, N., Conley, D.J., 2005. Effects of sediment storage conditions on pigment analyses. Limnology and Oceanography-Methods 3, 477-487.

Revsbech, N.P., Jørgensen, B.B., Blackburn, T.H., Cohen, Y., 1983. Microelectrode studies of the photosynthesis and O_2, H_2S, and pH profiles of a microbial mat. Limnology and Oceanography 28, 1062-1074.

Riffenburgh, B., 2006. Encyclopedia of the antarctic. Vol 1. Routledge, Oxford.

Rontani, J.F., Volkman, J.K., 2003. Phytol degradation products as biogeochemical tracers in aquatic environments. Organic Geochemistry 34, 1-35.

Rossi, R.A., Bunnett, J.F., 1973. Photostimulated aromatic $S_{RN}1$ reactions. Journal of Organic Chemistry 38, 1407-1410.

Rossi, R.A., Bunnett, J.F., 1974. Sense of cleavage of substituted benzenes on reaction with solvated electrons, as determined by a product criterion. Journal of the American Chemical Society 96, 112-117.

Rowland, S., Rockey, C., Allihaibi, S.S., Wolff, G.A., 1993. Incorporation of sulfur into phytol derivatives during simulated early diagenesis. Organic Geochemistry 20, 1-5.

Sakata, K., Yamamoto, K., Ishikawa, H., Yagi, A., Etoh, H., Ina, K., 1990. Chlorophyllone-*a*, a new pheophorbide-*a* related compound isolated from *Ruditapes philippinarum* as an antioxidative compound. Tetrahedron Letters 31, 1165-1168.

Scarratt, M.G., Moore, R.M., 1998. Production of methyl bromide and methyl chloride in laboratory cultures of marine phytoplankton II. Marine Chemistry 59, 311-320.

Schaeffer, P., Ocampo, R., Callot, H.J., Albrecht, P., 1993. Extraction of bound porphyrins from sulfur-rich sediments and their use for reconstruction of paleoenvironments. Nature 364, 133-136.

Schaeffer, P., Ocampo, R., Callot, H.J., Albrecht, P., 1994. Structure determination by deuterium labelling of a sulfur-bound petroporphyrin. Geochimica et Cosmochimica Acta 58, 4247-4252.

Schaeffer, P., Reiss, C., Albrecht, P., 1995. Geochemical study of macromolecular organic matter from sulfur-rich sediments of evaporitic origin (Messinian of Sicily) by chemical degradations. Organic Geochemistry 23, 567-581.

Schneckenburger, P., Adam, P., Albrecht, P., 1998. Thioketones as key intermediates in the reduction of ketones to thiols by HS^- in natural environments. Tetrahedron Letters 39, 447-450.

Schoch, S., Scheer, H., Schiff, J.A., Rudiger, W., Siegelman, H.W., 1981. Pyropheophytin *a* accompanies pheophytin *a* in darkened light grown cells of Euglena. Zeitschrift Fur Naturforschung 36C, 827-833.

Schouten, S., van Driel, G.B., Sinninghe Damsté, J.S., de Leeuw, J.W., 1993. Natural sulfurization of ketones and aldehydes: A key reaction in the formation of organic sulfur compounds. Geochimica et Cosmochimica Acta 57, 5111-5116.

Schouten, S., de Graaf, W., Sinninghe Damsté, J.S., van Driel, G.B., de Leeuw, J.W., 1994. Laboratory simulation of natural sulfurization: II. Reaction of multi-functionalized lipids with inorganic polysulfides at low temperatures. Organic Geochemistry 22, 825-834.

Seewald, J.S., 2003. Organic-inorganic interactions in petroleum-producing sedimentary basins. Nature 426, 327-333.

Senning, A., 1972. Sulfur in Organic and Inorganic Chemistry Volume 3, Marcel Dekker, New York.

Sheer, H., 1991. Structure and occurrence of chlorophylls. In: Sheer, H. (Ed.) Chlorophylls. CRC Press, Boca Raton, Florida. pp. 3-30.

Shioi, Y., 1991. Analytical chromatography of chlorophylls. In: Sheer, H. (Ed.) Chlorophylls. CRC Press, Boca Raton, Florida. pp. 59-88.

Shuman, F.R., Lorenzen, C.J., 1975. Quantitative degradation of chlorophyll by a marine herbivore. Limnology and Oceanography 20, 580-586.

Sigleo, A.C., Neale, P.J., Spector, A.M., 2000. Phytoplankton pigments at the Weddell-Scotia confluence during the 1993 austral spring. Journal of Plankton Research 22, 1989-2006.

Sinninghe Damsté, J.S., Rijpstra, W.I., Kock-van Dalen, A.C., de Leeuw, J.W., Schenck, P.A., 1989. Quenching of labile functionalized lipids by inorganic sulfur species: Evidence for the formation of sedimentary organic sulfur-compounds at the early stages of diagenesis. Geochimica et Cosmochimica Acta 53, 1343-1355.

Sinninghe Damsté, J.S., de Leeuw, J.W., 1990. Analysis, structure and geochemical significance of organically-bound sulfur in the geosphere: State of the art and future research. Organic Geochemistry 16, 1077-1101.

Sinninghe Damsté, J.S., Rijpstra, W.I.C., Coolen, M.J.L., Schouten, S., Volkman, J.K., 2007. Rapid sulfurisation of highly branched isoprenoid (HBI) alkenes in sulfidic Holocene sediments from Ellis Fjord, Antarctica. Organic Geochemistry 38, 128-139.

Skoog, D.A., Holler, F.J., Neiman, T.A., 1998. Principles of Instrumental Analysis. 5th edition. Saunders College Publishing, London.

Spooner, N., Keely, B.J., Maxwell, J.R., 1994a. Biologically mediated defunctionalization of chlorophyll in the aquatic environment-I. Senescence/decay of the diatom *Phaeodactylum tricornutum*. Organic Geochemistry 21, 509-516.

Spooner, N., Harvey, H.R., Pearce, G.E.S., Eckardt, C.B., Maxwell, J.R., 1994b. Biological defunctionalisation of chlorophyll in the aquatic environment-II. Action of endogenous algal enzymes and aerobic-bacteria. Organic Geochemistry 22, 773-780.

Spooner, N., Getliff, J.M., Teece, M.A., Parkes, R.J., Leftley, J.W., Harris, P.G., Maxwell, J.R., 1995. Formation of mesopyrophaeophorbide *a* during anaerobic bacterial-degradation of the marine prymnesiophyte *Emiliania huxleyi*. Organic Geochemistry 22, 225-229.

Squier, A.H., Hodgson, D.A., Keely, B.J., 2002. Sedimentary pigments as markers for environmental change in an Antarctic lake. Organic Geochemistry 33, 1655-1665.

Squier, A.H., 2003. Pigments of photoautotrophs in lake sediments from the Larsemann Hills, East Antarctica, Ph.D. Thesis. University of York.

Squier, A.H., Hodgson, D.A., Keely, B.J., 2003. Identification of novel sulfur-containing derivatives of chlorophyll *a* in a Recent sediment. Chemical Communications, 624-625.

Squier, A.H., Hodgson, D.A., Keely, B.J., 2004. Structures and profiles of novel sulfur-linked chlorophyll derivatives in an Antarctic lake sediment. Organic Geochemistry 35, 1309-1318.

Stafford, G.C., Kelley, P.E., Syka J.E.P., Reynolds, W.E., Todd, J.F.J., 1984. Recent improvements in and analytical applications of advanced ion trap technology. International Journal of Mass Spectrometry and Ion Processes 60, 85-98.

Stauber, J.L., Jeffrey, S.W., 1988. Photosynthetic pigments in 51 species of marine diatoms. Journal of Phycology 24, 158-172.

Stolp, H., 1988. Microbial Ecology: Organisms, habitats, activities. Cambridge University Press.

Sundararaman, P., Boreham, C.J., 1991. Vanadyl 3-nor C_{30}DPEP: Indicator of depositional environment of a lacustrine sediment. Geochimica et Cosmochimica Acta 55, 389-395.

Szmant, H.H., Mata, A.J., Namis, A.J., Panthananickal, A.M., 1976. The thiol-olefin co-oxidation (TOCO) reaction-IV. Temperature effects on product distribution in the TOCO reaction of indene and aromatic thiols. Tetrahedron 32, 2665-2680.

Talbot, H.M., Head, R.N., Harris, R.P., Maxwell, J.R., 1999. Distribution and stability of steryl chlorin esters in copepod faecal pellets from diatom grazing. Organic Geochemistry 30, 1163-1174.

Talbot, H.M., Head, R.N., Harris, R.P., Maxwell, J.R., 2000. Discrimination against 4-methyl sterol uptake during steryl chlorin ester formation by copepods. Organic Geochemistry 31, 871-880.

Tamiaki, H., Amakawa, M., Shimono, Y., Tanikaga, R., Holzwarth, A.R., Schaffner, K., 1996. Synthetic zinc and magnesium chlorin aggregates as models for supramolecular antenna complexes in chlorosomes of green photosynthetic bacteria. Photochemistry and Photobiology 63, 92-99.

Tannenbaum, E., Kaplan, I.R., 1985. Low-M_r hydrocarbons generated during hydrous and dry pyrolysis of kerogen. Nature 317, 708-709.

Telfer, A., Rivas, J.D., Barber, J., 1991. β-carotene within the isolated photosystem II reaction centre: photo-oxidation and irreversible bleaching of this chromophore by oxidized P680. Biochimica et Biophysica Acta 1060, 106-114.

Thomson, J.J., 1913. Rays of positive electricity and their application to chemical analysis. Longmans Green, London.

Treibs, A., 1936. Chlorophyll and hemin derivatives in organic materials. Angewandte Chemie International Edition 49, 682-686.

Vailaya, A., Horváth, C., 1998. Retention in reversed-phase chromatography: partition or adsorption? Journal of Chromatography A 829, 1-27.

Vairavamurthy, A., Mopper, K., 1987. Geochemical formation of organosulfur compounds (thiols) by addition of H_2S to sedimentary organic matter. Nature 329, 623-625.

van Dongen, B.E., Schouten, S., Baas, M., Geenevasen, J.A.J., Sinninghe Damsté, J.S., 2003. An experimental study of the low-temperature sulfurization of carbohydrates. Organic Geochemistry 34, 1129-1144.

Vandenbroucke, M., Largeau, C., 2007. Kerogen origin, evolution and structure. Organic Geochemistry 38, 719-833.

Verne-Mismer, J., Ocampo, R., Callot, H.J., Albrecht, P., 1988. Molecular fossils of chlorophyll *c* of the 17-nor-DPEP series. Structure determination, synthesis, geochemical significance. Tetrahedron Letters 29, 371-374.

Verne-Mismer, J., Ocampo, R., Callot, H.J., Albrecht, P., 1990. New chlorophyll fossils from Moroccan oil shales. Porphyrins derived from chlorophyll c_3 or a related pigment? Tetrahedron Letters 31, 1751-1754.

Vincent, W.F., Downes, M.T., Castenholz, R.W., Howard-Williams, C., 1993. Community structure and pigment organization of cyanobacteria-dominated microbial mats in Antarctica. European Journal of Phycology 28, 213-221.

Visscher, P.T., Baumgartner, L.K., Buckley, D.H., Rogers, D.R., Hogan, M.E., Raleigh, C.D., Turk, K.A., Des Marais, D.J., 2003. Dimethyl sulphide and methanethiol formation in microbial mats: potential pathways for biogenic signatures. Environmental Microbiology 5, 296-308.

Wakeham, S.G., Sinninghe Damsté, J.S., Kohnen, M.E.L., de Leeuw, J.W., 1995. Organic sulfur compounds formed during early diagenesis in Black-Sea sediments. Geochimica et Cosmochimica Acta 59, 521-533.

Walker, J.S., Squier, A.H., Hodgson, D.A., Keely, B.J., 2002. Origin and significance of 13^2-hydroxychlorophyll derivatives in sediments. Organic Geochemistry 33, 1667-1674.

Walker, J.S., Jie, C., Keely, B.J., 2003. Identification of diastereomeric chlorophyll allomers by atmospheric pressure chemical ionisation liquid chromatography/tandem mass spectrometry. Rapid Communications in Mass Spectrometry 17, 1125-1131.

Walker, J.S., 2004. Autoxidation reactions of chlorophyll, Ph.D. Thesis. University of York.

Walker, J.S., Keely, B.J., 2004. Distribution and significance of chlorophyll derivatives and oxidation products during the spring phytoplankton bloom in the Celtic Sea April 2002. Organic Geochemistry 35, 1289-1298.

Wardell, J.L., 1974. Preparation of Thiols. In: Patai, S. (Ed.) The Chemistry of the Thiol Group. Wiley & Sons, London, UK. pp. 163-269.

Watanabe, T., Hongu, A., Honda, K., Nakazato, M., Konno, M., Saitoh, S., 1984. Preparation of chlorophylls and pheophytins by isocratic liquid chromatography. Analytical Chemistry 56, 251-256.

Watanabe, N., Yamamoto, K., Ihshikawa, H., Yagi, A., Sakata, K., Brinen, L.S., Clardy, J., 1993. New chlorophyll *a* related compounds isolated as antioxidants from marine bivalves. Journal of Natural Products 56, 305-317.

Werne, J.P., Hollander, D.J., Behrens, A., Schaeffer, P., Albrecht, P., Sinninghe Damsté, J.S., 2000. Timing of early diagenetic sulfurization of organic matter: A precursor-product relationship in Holocene sediments of the anoxic Cariaco Basin, Venezuela. Geochimica et Cosmochimica Acta 64, 1741-1751.

Williamson, C.E., 1995. What role does UV-B radiation play in freshwater ecosystems? Limnology and Oceanography 40, 386-392.

Wilson, M.A., 2004. Analysis of complex distributions of bacteriochlorophylls: Development and application of HPLC and LC-MS methods, Ph.D. Thesis. University of York.

Wilson, M.A., Hodgson, D.A., Keely, B.J., 2004a. Structural variations in derivatives of the bacteriochlorophylls of Chlorobiaceae: impact of stratigraphic resolution on depth profiles as revealed by methanolysis. Organic Geochemistry 35, 1299-1307.

Wilson, M.A., Airs, R.L., Atkinson, J.E., Keely, B.J., 2004b. Bacterioviridins: novel sedimentary chlorins providing evidence for oxidative processes affecting palaeobacterial communities. Organic Geochemistry 35, 199-202.

Wilson, M.A., Hodgson, D.A., Keely, B.J., 2005. Atmospheric pressure chemical ionisation liquid chromatography/multistage mass spectrometry for assignment of sedimentary bacteriochlorophyll derivatives. Rapid Communications in Mass Spectrometry 19, 38-46.

Wolman, Y., 1974. Protection of the Thiol Group. In: Patai, S. (Ed.) The Chemistry of the Thiol Group. Wiley & Sons, London, UK. pp. 669-684.

Woolley, P.S., Moir, A.J., Hester, R.E., Keely, B.J., 1998. A comparative study of the allomerization reaction of chlorophyll *a* and bacteriochlorophyll *a*. Journal of the Chemical Society-Perkin Transactions 2, 1833-1839.